Abstract

Title of Document: ACYCLIC CONGENERS OF CUCURBIT[N]URIL AND A RELATED MECHANISTIC STUDY ON THE CUCURBIT[N]URIL FORMING REACTIONS.

Da Ma, Doctor of Philosophy, 2010.

Directed By: Professor Lyle D. Isaacs,
Department of Chemistry and Biochemistry

Supramolecular chemistry has been a very important research area in the past several decades. In this research field, molecular containers, such as cyclodextrin, attracts special attention due to their wide applications both in academia and industry. Cucurbit[*n*]uril (CB[*n*]), as a new generation molecular container, has selective and tight binding towards lots of cations and neutral molecules. A homologous family of CB[*n*] has been discovered including CB[5]-CB[8], CB[10], iCB[*n*], ns-CB[10] and ns-CB[6]. CB[*n*] analogues and derivatives have also been developed. CB[*n*] still has several issues, such as low solubility in water, difficulty to be functionalized, and slow association and dissociation kinetics. This thesis describes efforts to address these issues by developing new CB[*n*] type molecular containers and carrying out mechanistic investigations. Three chapters are included in this thesis.

Chapter 1 is a literature review of molecular encapsulation and molecular container chemistry. We first introduced general concepts of molecular encapsulation

and present examples of molecular container, such as cyclodextrin. This is followed by an introduction to CB[*n*] molecular containers and their supramolecular chemistry.

Chapter 2 introduces new acyclic CB[*n*] congeners **II-5a** and **II-5b**. **II-5a** and **II-5b** are obtained from step-wise synthesis with reasonable yields. This step-wise synthetic route avoids difficult separation process. We measured the binding constants of **II-5a** towards a number of guests and found the binding affinity is usually comparable to CB[7]. The recognition property of **II-5a** is investigated in depth. We found that the length and functional groups of the guests greatly influence the binding affinity. Nevertheless, the charge and size of the guests do not have as a big influence on the binding constants as CB[7]. We discovered that the ionic strength of the buffer is critical for the binding constant. By comparing the recognition property of **II-5a** and **II-6**, it is discovered that the substituted o-xylyene walls are important for the tight binding compounds. **II-5a** and **II-5b** are new examples of CB[*n*] type molecular containers. They retain most of the good recognition property of CB[*n*] and have advantages compared to CB[*n*], including 1) aromatic walls that makes further functionalization possible; 2) acyclic structure that enables fast association and dissociation kinetics.

Chapter 3 describes the mechanistic study of CB[*n*] forming reactions. Another possible way to synthesize CB[*n*] molecular container is to use aldehydes instead of paraformaldehyde. But neither previous researchers nor our work has succeeded to make the aldehydes participating CB[*n*] forming reactions happen. Mechanistic investigation was carried out to explain why this reaction simply does not occur. We used **III-7** instead of glycoluril to avoid cyclization reactions. Several reasons are discovered: 1) side products are formed, such as **III-SP1** and **III-SP2**; 2) S-shape intermediates are

yielded, such as **III-15S**, **III-16S**, **III-17S** and **III-18S**, which are not able to continue the reaction to form macrocycles; 3) a small equilibrium constant for the chain grouth reaction. This study explains why aldehydes usually do not participate in CB[*n*] forming reactions. This work could also lead to the discovery of certain aldehydes that can form CB[*n*] type macrocycles.

Acyclic Congeners of Cucurbit[*n*]uril and a Related Mechanistic Study on the Cucurbit[*n*]uril Forming Reaction.

By

Da Ma

Dissertation submitted to the Faculty of the Graduate School of the
University of Maryland, College Park in partial fulfillment
of the requirements for the degree of
Doctor of Philosophy
2010

Advisory Committee:

Professor Lyle Isaacs, Chair
Professor Jeffery Davis
Professor Daniel Falvey
Professor Herman Sintim
Professor Sergei Sukharev

Dedication

To my parents, Minxing Ma and Jingxia Ding,

and my girlfriend Xiaoyu Sun

Acknowledgements

I would like to thank my Ph.D. advisor Lyle Isaacs for his guidance throughout my graduate studies. His knowledge, motivation and support have helped me a lot throughout my five year academic research.

I want to thank Dr. Simin Liu for teaching me all the essential skills to be an organic chemist. I want to appreciate Dr. Soumyadip Gosh, Dr. Regan Nally and Dr. Wei-Hao Huang for their role as caring seniors. I am grateful for their patient teaching and helpful advice.

It was my pleasure to work with supportive colleagues in the Isaacs lab. I want to express sincere gratitude to all of you. I especially want thank Jing Wu, Derick Lucas and James Wittenberg for their helpful discussion.

The supportive analytical instrumental staffs are very important for my academic success. I would like to thank Dr. Yiu-Fai Lam and Dr. Yinde Wang for their help with various NMR experiments. I want to appreciate Dr. Yue Li for Mass Spectroscopy supports. I also want to thank Peter Zavalij for his expert assistance with crystallography.

Finally, this accomplishment would have never been possible without the encouragement of my parents. Their support is the most essential to bring me all the way to this highest educational level.

Table of Contents

List of Tables

Chapter 1

List of Figures

Chapter 1

Chapter 2

List of Charts

Chapter 2

List of Schemes

Chapter 2

Chapter 3

Chapter 4

I. Chapter 1: Literature Review of Molecular Encapsulation

1.1 Introduction.

Cram, Lehn, and Pedersen have defined the area of supramolecular chemistry as a contemporary discipline with their pioneering work. Supramolecular chemistry is the discipline of chemistry which involves intermolecular interactions where non-covalent rather than covalent bonds are established between the interacting species, a majority of which are of the host-guest type. A variety of supramolecular host molecules, or molecular containers in another word, have been developed and well studied including crown ethers, cyclodextrin (CD), calixarene, and cucurbituril (CB[n]). Molecular containers often show selective recognition towards cation, anion and neutral guest molecules. Based on the molecular encapsulation principle, a lot of applications have been developed for molecular containers. CD has been one of the most widely used molecular containers. Its applications include drug delivery, chiral separation, and odor/scent control. CB[n], the new generation of molecular container, is well recognized for its tight and selective binding towards cations and neutral guests. The high affinity binding is critical for numerous biological applications. Its rigid structure of CB[*n*] and the formation of thermodynamically stable host-guest complexes have enabled its applications for molecular machine, reaction catalysis, drug delivery, and so on. Nevertheless, some weaknesses of CB[*n*] include poor solubility in water and slow kinetics of association and dissociation, which have stopped CB[*n*] from wider applications in the industry. And to date, it has been very hard to functionalize CB[n].

Accordingly, scientists have been developing alternate routes to get water soluble CB[n] analogues or derivatives.

1.2 Molecular Encapsulation.

Molecular encapsulation in supramolecular chemistry refers to the confinement of a guest molecule inside the cavity of a supramolecular host molecule. It is often referred to as host-guest chemistry. Its application has ranged from academic research to industrial production.

1.2.1 Early Examples of Molecular Encapsulation.

In 1967, Charles Pedersen synthesized crown ether.[1] In his report, he described the simple synthesis of 33 cyclic polyethers derived from aromatic vicinal diols and containing from 9 to 60 atoms including 3 to 20 oxygen atoms in the ring (some examples are given in Figure I-1, compound **I-1**-**I-5**). Many of these crown ethers containing five to ten oxygen atoms form stable complexes with some or all the cations of: Li^+, Na^+, NH_4^+, RNH_3^+, K^+, Rb^+, Cs^+, Ag^+, Au^+, Ca^{2+}, Sr^{2+}, Ba^{2+}, Cd^{2+}, Hg^+, Hg^{2+}, La^{3+}, Tl^+, Ce^{3+}, and Pb^{2+}. Many of these complexes were isolated in the crystalline form depending on the anion. They appear to be salt-polyether complexes formed by ion-dipole interaction between the cation and the electrostatically negatively charged oxygen atoms of the polyether ring. Since the discovery of crown ether, other molecular containers have also been synthesized and well studied, e.g. cyclodextrin, calixarene, and cucurbituril. Among them, cyclodextrin is the most important with regard to industrial applications.

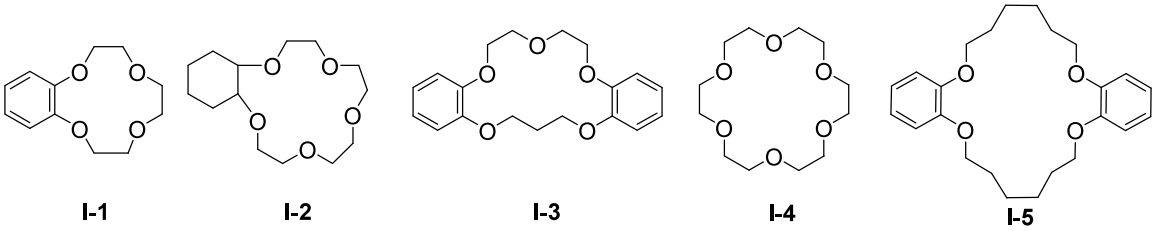

Figure I-1. Examples of crown ethers.

1.2.2 Cyclodextrin Molecular Container.

Cyclodextrin was first discovered in 1891 by Villiers.[2] Its structure was elucidated in 1948-1950.[3] French and Cramer intensively worked on the enzymic production of cyclodextrins and characterizing their true chemical and physical properties in the 1950s.[4,5] Cyclodextrins comprise a family of three well-known industrially produced major, as well as several rare, minor cyclic oligosaccharides. These three major cyclodextrins are crystalline, homogeneous, non-hygroscopic substances, which are torus-like macro-rings built up from glucopyranose units. The α-cyclodextrin comprises six glucopyranose units, β-CD comprises seven such units, and γ-CD comprises eight such units (Figure I-2). The shape of cyclodextrin is also displayed in Figure I-2. It has a hydrophobic cavity and hydrophilic portals and outer walls.

The slightly apolar CD cavity is occupied by water molecules in an aqueous solution. Guest molecules which are less polar than water can readily substitute these water molecules. Different host:guest ratios can been formed. But the most frequent one is 1:1, which is the essence of "molecular encapsulation".

Based upon molecular encapsulation, cyclodextrin has lots of applications. One of the most important applications is drug delivery. The primary purpose of drug delivery is to deliver drugs to the targeted site for a necessary amount and necessary period of time efficiently and precisely. Investigation proved that natural cyclodextrins do not exhibit toxicity.[6] Cyclodextrin and its derivatives usually are soluble in water. As a type of easily functionalized and bioadaptable molecular container, cyclodextrin is suitable for drug delivery applications.

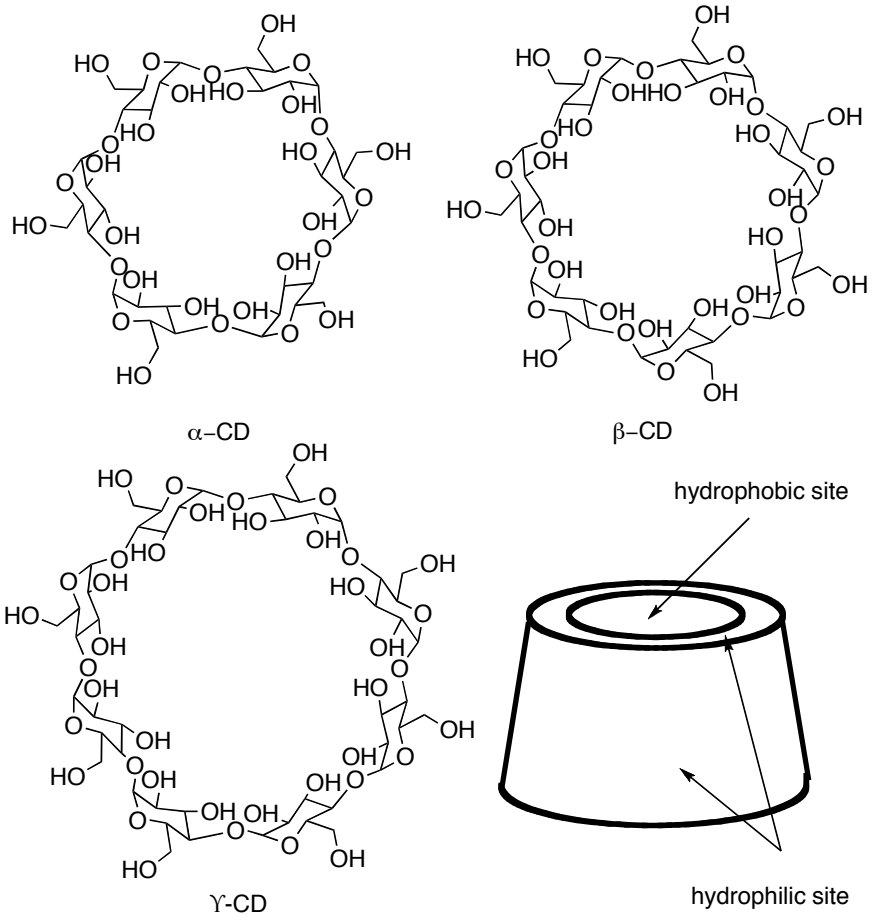

Figure I-2. Structures of cyclodextrins.

Numerous drug delivery applications with cyclodextrin are reported, including drug solubility enhancement,[7] drug stabilization,[8] drug absorption enhancement, alleviation of local and systemic toxicity of certain drugs, and cyclodextrin based drug delivery systems.

There are a good number of drugs prescribed in the market with a poor solubility in water. In order to formulate the drugs for injection, their solubility in water needs to be enhanced. Cyclodextrin and its derivatives are capable to solubilize drugs based on host-guest inclusion. The solubilization ability of cyclodextrin is quantitatively evaluated by the phase solubility method developed by Higuchi and Connors.[9] The phase solubility diagrams are classified as either type A or type B (Figure I-3). As for type A, a very soluble complex is formed and a complex of moderate solubility for type B. They can be further classified into subtypes A_L, A_P, A_N, B_S and B_I. To reach the maximum solubility enhancement, cyclodextrins were functionalized by introducing hydroxylalkyl groups or sulfonate groups to the backbone or forming branched cyclodextrins. The solubilizing effect of 2-hydroxyethyl-*β*-CD (**I-6**) and 2-hydroxypropyl-*β*-CD (**I-7**) with different degrees of substitution on poorly water-soluble drugs, such as hydrocortisone (**I-8**), digitoxin (**I-9**), diazepam (**I-10**), and indomethacin (**I-11**) was studied by Müller and Brauns.[7] Compared to their parent *β*-CD, which has a limited solubility and thus poor solubility enhancement capability, these two hydroxyalkylated *β*-CDs demonstrated the A_L-type diagram pattern with the guest solubility increasing linearly up to 10% (w/v) concentration of the hosts. By comparing the solubility enhancement capabilities of different degrees of substitution, researchers discovered that the degree of substitution markedly influences the solubilization. Sulfated cyclodextrins are another type of

functionalized CD for drug solubilization. But the sulfated cyclodextrin has a significantly weaker binding, because negative charges are surrounding the rims.[10] To avoid this problem, sulfoalkylated cyclodextrins were developed and studied. The study on the inclusion ability of sulfopropyl-*β*-CD (**I-12**) and sulfobutyl-*β*-CD (**I-13**) with different degrees of substitution towards testosterone (**I-14**) and progesterone (**I-15**) demonstrates sulfoalkylated cyclodextrins' tighter binding than *β*-CD.[11] Sulfobutyl-*β*-CD is reported to be a good solubilizer for various poorly water soluble drugs such as pilocarpine (**I-16**), cinnarizine (**I-17**), indomethcin, naproxen (**I-18**), warfarin (**I-19**), papaverin (**I-20**), thiabendazole (**I-21**), and miconazole (**I-22**).[12]

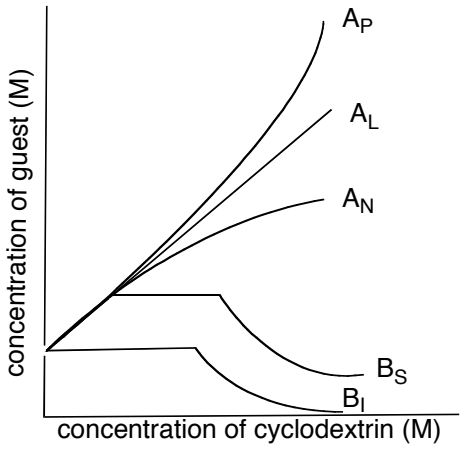

Figure I-3. Phase diagram showing different solubility behaviors.

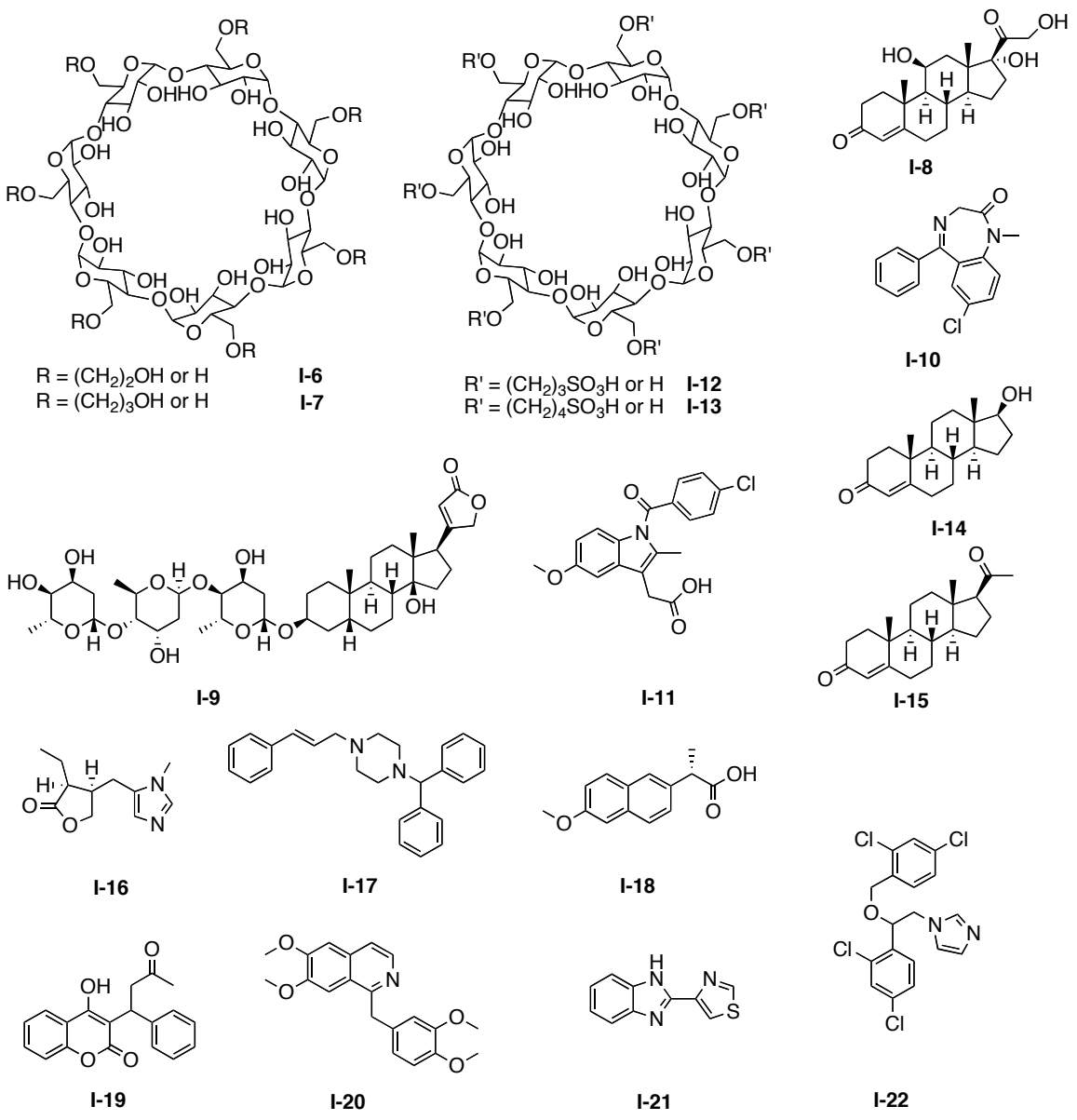

Figure I-4. Compounds for drug solubility enhancement.

Cyclodextrin's application to stabilize drugs is based upon the principle that CD is capable to accelerate or decelerate reactions occurring to the molecules encapsulated inside it. Cyclodextrins are used to stabilize digoxin (**I-23**),[8] one of the potent cardiac glycosides. Digoxin is susceptible to hydrolysis in acidic media. (Figure I-5) This degradation pathway yields digoxigenin, whose cardioactivity is only one-tenth of that of

digoxin. Research showed that the addition of cyclodextrins decelerates the acid-catalyzed hydrolysis of the glycoside bonds. In the absence of cyclodextrins, the hydrolysis rate constant is 0.17 h^{-1}. In the presence of α-CD, β-CD and γ-CD, the rate constants are 0.108, 0.002 and 0.025 h^{-1}, respectively.

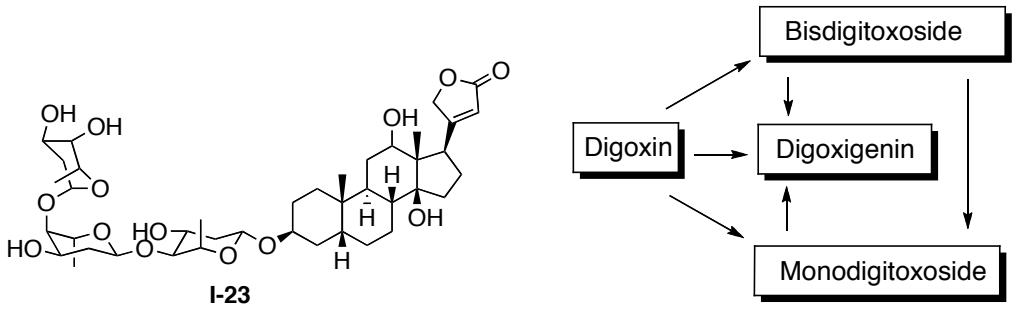

Figure I-5. Acid-catalyzed hydrolysis of the glycoside bonds in digoxin.

Cyclodextrin has a lot of applications even though it usually has a weak binding towards guests. CB[*n*] family, as a type of hosts with tight and selective binding towards lots of guests, is a good candidate for similar or novel applications. We will discuss this type of novel host molecules in the next chapter.

1.3 Cucurbituril (CB[n]) Molecular Container.

CB[*n*] is cyclic glycoluril oligomers with methylene bridges and a shape resembles a pumpkin. Since the discovery of CB[6] in 1981 by Mock and co-workers,[13] the CB[*n*] family has grown to homologues, including CB[5]-CB[8], CB[10] and nor-seco-CB[*n*], derivatives, congeners and analogues with various sizes, shapes and functional groups.

Their unique shapes, tight and selective bindings enable CB[*n*] to play a very important role in molecular recognition.

1.3.1 Introduction to Cucurbituril.

Behrend reported an insoluble polymeric material from the condensation of glycoluril and formaldehyde in concentrated HCl in the year of 1905.[14] And then 75 years later, in 1981, it was clarified that the polymeric material discovered by Behrend is actually cucurbit[6]uril, a macrocycle composed of six glycoluril (**I-24**) units and twelve methylene bridges.[13] At that time, CB[6] was the only cucurbituril detected by Mock. Later other CB[n] family members with different sizes including CB[5], CB[7] and CB[8] were discovered (Figure I-6).[15,16] Also, inverted CB[n] with the protons on one of the glycoluril units pointing into the cavity was discovered.[17] Recently, the largest CB[n] that has ever been discovered, CB[10],[18] was separated from CB[10]•CB[5].[19] The vast cavity of CB[10] (870 $Å^3$) enables it to host some big molecules, such as porphyrin. A mixture of these homologues is obtained from the condensation reaction of glycoluril and paraformaldehyde, followed by separation to yield pure products.

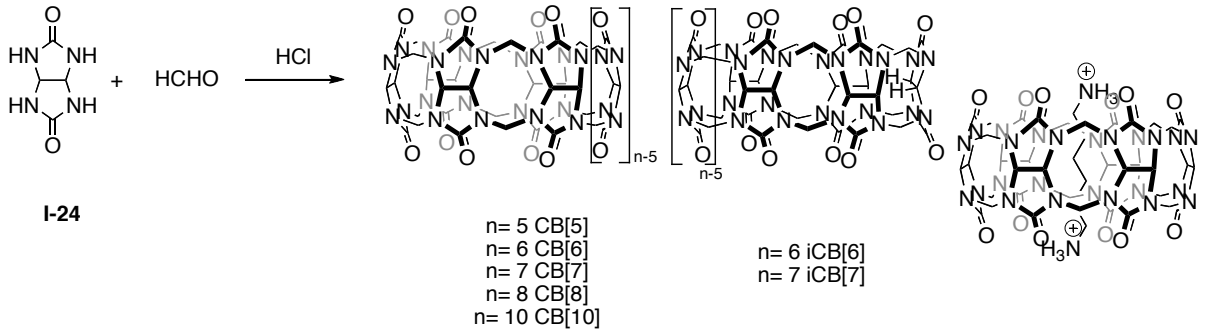

Figure I-6. Synthesis and structure of CB[*n*].

All the above CB[n]s are only varied in size. The recent outcome in the searching for new CB[n] has been the synthesis of CB[n] with different shapes. Basically obtained from a kinetically controlled reaction, bis-ns-CB[10] is a brand new type of CB[n], with two cavities, inside which two guests could be accommodated and influence each other.[20] As for bis-ns-CB[10], the size of cavities is comparable to that of CB[6] or CB[7]. Bis-ns-CB[10] has most of the binding profile same as CB[*n*]. It also could bind to larger guests considering the five glycoluril units composing each of the two cavities. Bis-ns-CB[10] displays a homotropic allostery based on a guest size induced preorganization mechanism. It could either expand or contract the cavity according to the size of the guest (**I-25**, Figure I-7).

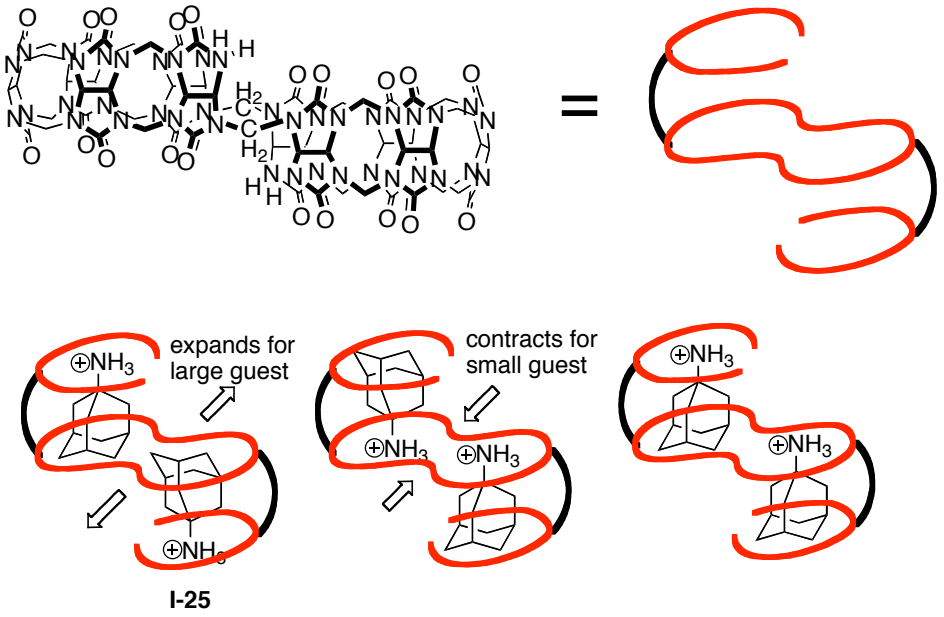

Figure I-7. Bis-ns-CB[10] and its size change responding to guest size.

Another novel CB[*n*] discovered recently is (±)-bis-ns-CB[6] (Figure I-8) which lacks one methylene bridge compared to CB[6].[21] It is synthesized by conducting the condensation reaction between glycoluril (1 eq) and paraformaldehyde (less than 2 eq.). As a racemic mixture of two enantiomers, researchers are able to use (±)-bis-ns-CB[6] to do enantio- and diastereoselective recognition inside its cavity. This chiral bis-ns-CB[6] undergoes moderately diastereoselective complexation with chiral amines including amino acids, amino alcohols and meso-diamine. It promises to greatly widen the scope of CB[*n*]'s application since it is able to create enantioselective molecular devices. From a similar reaction as chiral bis-ns-CB[6], an achiral ns-CB[6] (**I-26**, Figure I-8) was synthesized.[22] It lacks one methylene bridge compared to CB[6]. Treating it with *o*-phthalaldehyde under acidic conditions gives us a CB[*n*] derivative (**I-27**), which displays

diastereoselective recognition towards unsymmetrical guests. The back-folding of long chain alkanediammonium ions is also promoted by this new CB[*n*] derivative in water.

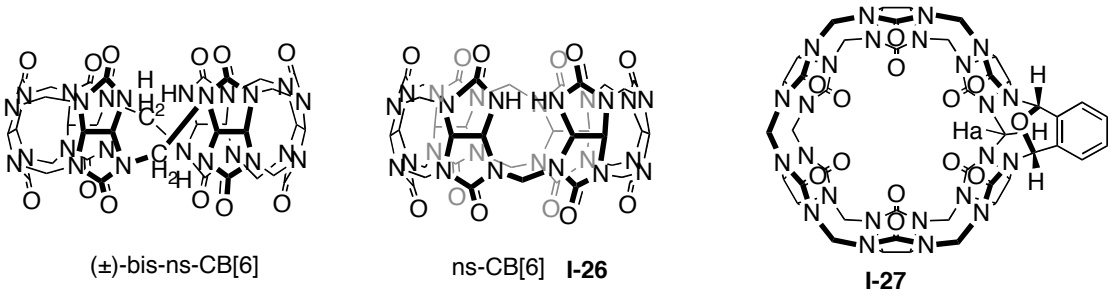

Figure I-8. Structures of (±)-bis-ns-CB[6] and ns-CB[6].

1.3.2 Cucurbituril Derivatives, Analogues and Acyclic Congeners.

Besides the CB[*n*] family, CB[*n*] analogues and derivatives also attract researchers' interest. CB[*n*] analogues and derivatives are prepared in order to alleviate the weakness of regular CB[*n*], including limited solubility in water and an inability to modify internal or external molecular surface of the CB[*n*] molecule. Researchers hope that by altering the shape and size of the cavity or providing different functional groups that directly interact with guests, the range of the potential CB[*n*] applications could be dramatically expanded. There have been numerous attempts to prepare CB[*n*] derivatives by using substituted glycoluril derivatives in CB[*n*] forming reactions. In 1992, Stoddart and co-workers reported the first characterized CB[*n*] derivative with the synthesis of Me_{10}CB[5] from dimethylglycoluril and formaldehyde under acidic conditions.[23] Since then, various CB[*n*] derivatives have been prepared from different pathways. One drawback is that

preferentially the smaller CB[*n*] derivatives are formed, usually CB[5] and CB[6] derivatives.

Another pathway to obtain CB[*n*] derivatives is by the direct functionalization of CB[5]-CB[8]. In 2003, Kim and co-workers reported the direct oxidation of CB[5]-CB[8] with $K_2S_2O_8$ in water to yield the perhydroxylated species $(HO)_{2n}$CB[*n*] (Figure I-9).[24] The good solubility of $(HO)_{12}$CB[6] in DMSO and DMF allows its subsequent derivatization. $(HO)_{2n}$CB[*n*] can be alkylated by treatment with allyl bromide to yield $(CH_2$=CHCH2O$)_{12}$CB[6]. The allylated compound $(CH_2$=CHCH2O$)_{12}$CB[6] is then treated with **I-28** in photochemical reaction to afford $(CH_3(CH_2)_4S(CH_2)_3O)_{12}$CB[6]. They demonstrate an approach to covalently anchor $(CH_2$=CHCH2O$)_{12}$CB[6] onto a patterned glass surface through the photochemical reaction. This CB[6] modified surface is capable to bind to fluorescent guest.

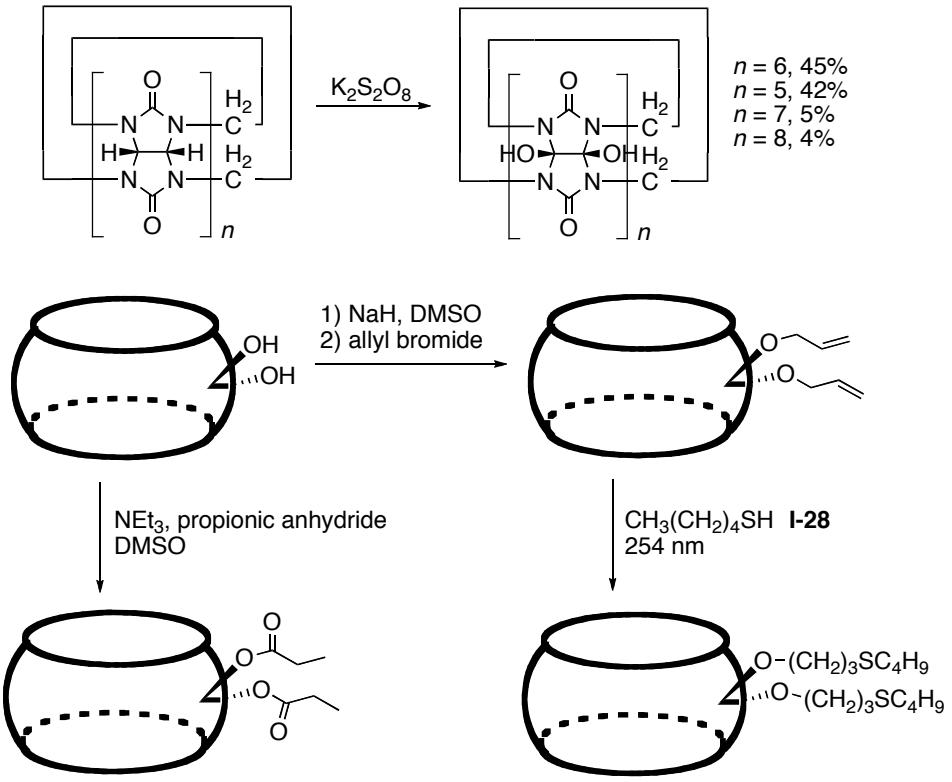

Figure I-9. Synthesis and functionalization of $(HO)_{2n}$CB[*n*].

Later, Kim and coworkers synthesized a modified amphiphilic CB[6] from the $(CH_2CHCH_2O)_{12}$CB[6] (Figure I-10a).[25] This amphiphilic CB[6] (**I-29**) is able to form vesicle. They found the modified CB[6] surface can form stable host-guest complex with FITC (fluorescein isothiocyanate) - spermine conjugate ligand. This structure was observed under a confocal microscope, which confirmed the accessibility of the host molecule in the vesicle membrane toward the spermine-based guest. This research provides a new noncovalent, modular approach to the modification of vesicle surfaces with CB[6] derivatives. The researchers then synthesized sugar-decorated vesicle from the amphiphilic CB[6] and thiourea linked α-mannose-spermidine conjugate. When they treated it with a solution of concanavalin A (ConA), a lectin with specificity toward α-

mannose, the aggregation occurred immediately. In contrast, no aggregation was observed when they mixed free ligand or vesicle decorated with a galactose-spermidine conjugate with ConA. This result illustrates the specific and multivalent interactions between the mannose-decorated vesicle and ConA.

In another application of functionalized CB[7], researchers succeeded to anchor modified CB[7] (**I-30**, Figure I-10b) on a gold solid surface.[26] Proteins were immobilized on this solid surface through noncovalent interaction of CB[7]-ferrocenemethylammonium (**I-31**) pair. They used glucose oxidase (GOx) as a model protein to detect glucose. This process was monitored by surface plasmon resonance (SPR) technique. They then utilized this modified gold surface as a glucose sensor and investigated it by cyclic voltammetry and glucose-concentration-dependent current measurements (Figure I-10c). It turned out to be no appreciable current in the absence of glucose and an increasing catalytic current with increasing glucose concentration, which suggested that this modified gold electrode can be used as a glucose sensor.

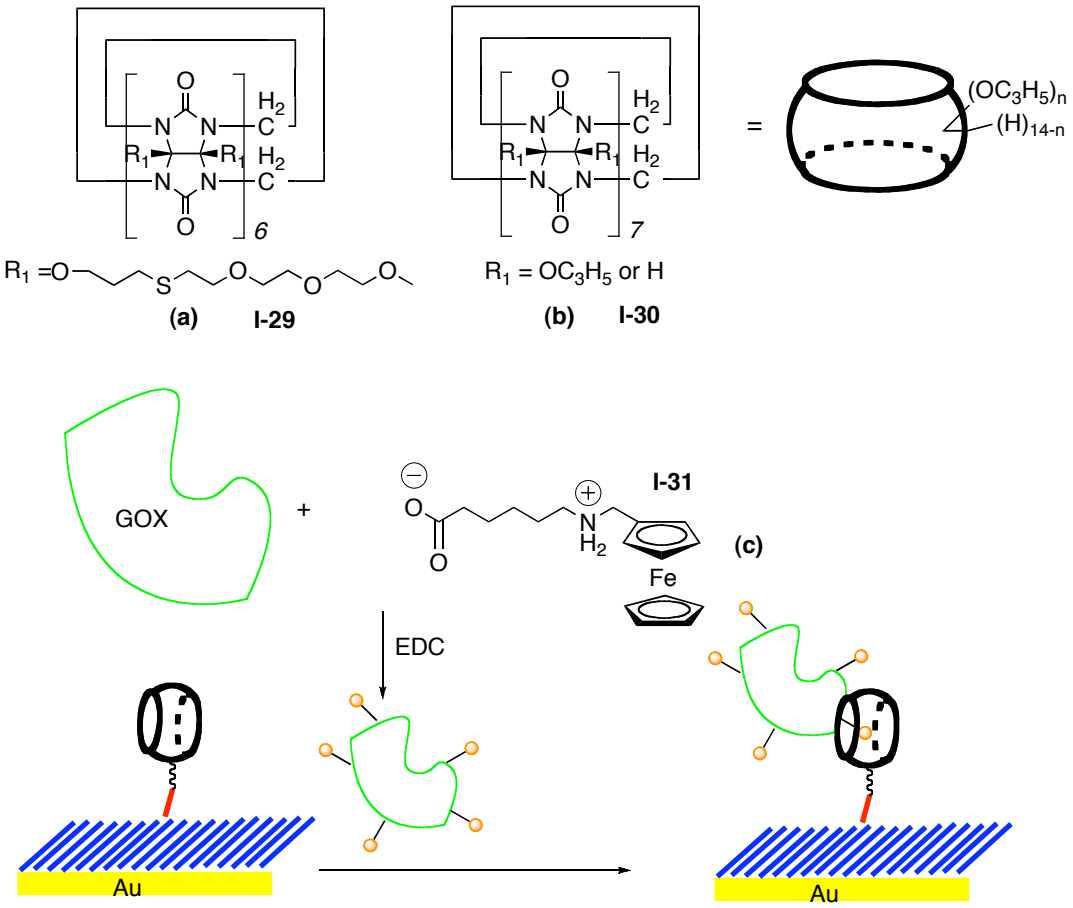

Figure I-10. Functionalized CB[*n*] and its application as bio-sensor.

Kim and co-workers even used the modified CB[6] ($C_8H_{17}S(CH_2)_3O)_{12}$CB[6], **I-32**)[27] to form ion channel (Figure I-11). In order to study the proton transport across membranes, large unilamellar vesicles were prepared from egg yolk L-α-phosphatidyl-choline (EYRC), cholesterol, and dicetyl phosphate with $C_8H_{17}S(CH_2)_3O)_{12}$CB[6]. A pH-sensitive dye 8-hydroxypyrene-1,3,6-trisulfonate (HPTS) was entrapped inside the vesicles to monitor the proton flux through the membranes. They were able to measure the proton flux by watching the fluorescence intensity of HPTS. They found that this novel artificial ion channel can transport proton and alkali metal ions across a lipid membrane with ion selectivity. Interestingly, this ion channel could be blocked by excess

amount of neurotransmitter acetylcholine, which forms a stable host-guest complex with CB[6] derivatives in water.

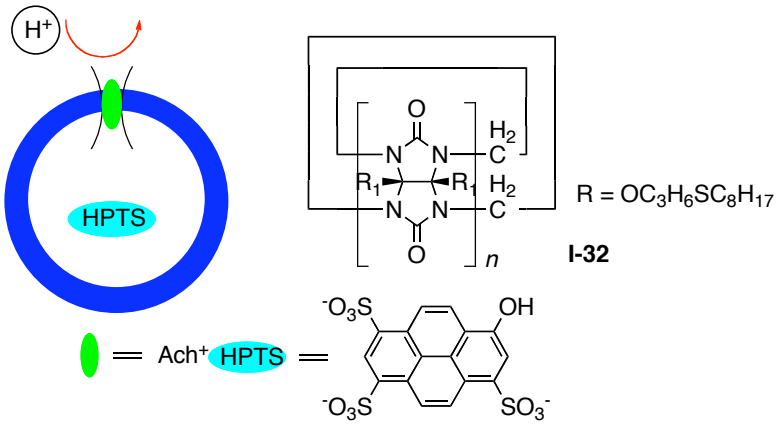

Figure I-11. Modified CB[*n*] as ion channel.

Although these results show very promising applications, the same significant issue was not solved in this direct functionalization, that is, only the smaller modified CB[*n*]s, CB[5] and CB[6], can be obtained with a good yield. It is still very hard to synthesize derivatives of the larger CB[*n*]s, which have larger cavities and more applications.

Cucurbituril analogues have also been synthesized. One of these new compounds was synthesized by Isaacs and co-workers.[28] They synthesized CB[6] analogues (**I-35**) in high yield from the cyclization reactions of bis(phthalhydrazide) (**I-33**) and glycoluril ether building blocks (**I-34**). These CB[*n*] analogues have noteworthy features including electrochemically, UV/Vis, and fluorescently active "walls", elongated shapes, and decent solubility in both organic and aqueous media. Another CB[*n*] analogue was prepared by Miyahara from the acid-catalyzed condensation reaction of ethyleneurea (**I-36**).[29] The product, hemicucurbituril (**I-37**), was obtained with a very high yield. It does not bind metal cations, but does retain the ability to bind towards small organic molecules

such as $HCONH_2$ and $HOCH_2CCH$. Similar to CB[*n*] derivatives, these CB[*n*] analogues' applications are limited by their relatively small cavities.

In order to further expand the scope of CB[*n*] family, researchers have been working on acyclic CB[*n*] congeners as well. Isaacs synthesized a novel acyclic CB[*n*] congener (**I-38**) with alternating glycoluril (**I-39**) and aromatic rings (**I-40**), and preorganized into the a,a,a,a-conformation required for molecular recognition.[30] It displays selective binding towards positively charged guests and competitive binding with alkali metals present in solution. But the binding affinity is weak compared to cyclic CB[*n*] (only 10^4 towards hexanediamine, compared to 10^6 for CB[6]), which might be due to shortage of enough glycoluril units. Recently, Sindelar prepared a glycoluril trimer (**I-44**) from the condensation reaction of glycoluril diether (**I-41**) with glycoluril bisether (**I-42**) or tetrakis hydroxyl methyl glycoluril (**I-43**).[31] This glycoluril trimer is able to encapsulate bispyridinium ethylene (**I-45**, $K_a = 8.4 \times 10^4\ M^{-1}$) and methylviologen (**I-46**, $K_a = 7.5 \times 10^4\ M^{-1}$) guests in the solid state and aqueous solution. This acyclic congener CB[*n*] with more glycoluril units still has only a weak or moderate binding towards positively charged guests. We hypothesize that the binding will be much stronger if we add more glycoluril units into the congener. The reason is more glycolurils will help form a preorgnized carbonyl portal, which is necessary to form a tight binding by ion-dipole interactions. From previous study, it shows that at least four glycoluril units are needed.

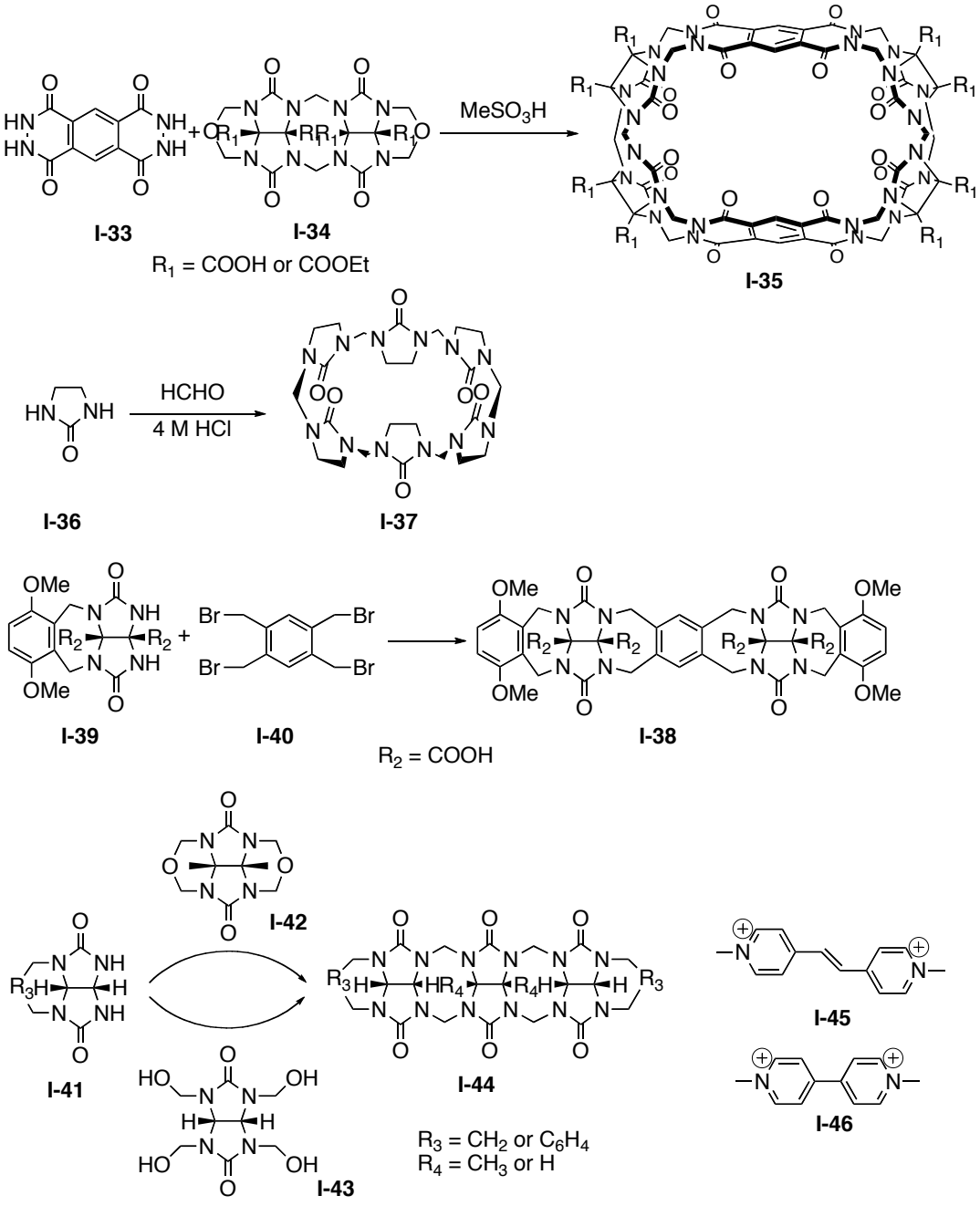

Figure I-12. Examples of CB[*n*] analogues and congeners.

1.3.3 Applications of Cucurbituril.

As a novel host with a tight and selective binding towards various guests, cucurbituril has lots of applications, such as molecular machines, catalysis and drug delivery.

1.3.3.1 Molecular Machines.

Examples of CB[*n*] molecular machines include molecular switches under chemical, photochemical and electrochemical controls.

An early example was a chemical controlled molecular switch based on CB[6] developed by Mock.[32] In his study, he developed a pseudo-rotaxane system of CB[6] and triamine (**I-47**, Figure I-13). CB[6] is able to shuttle along the guest, triamine, by changing the pH value.

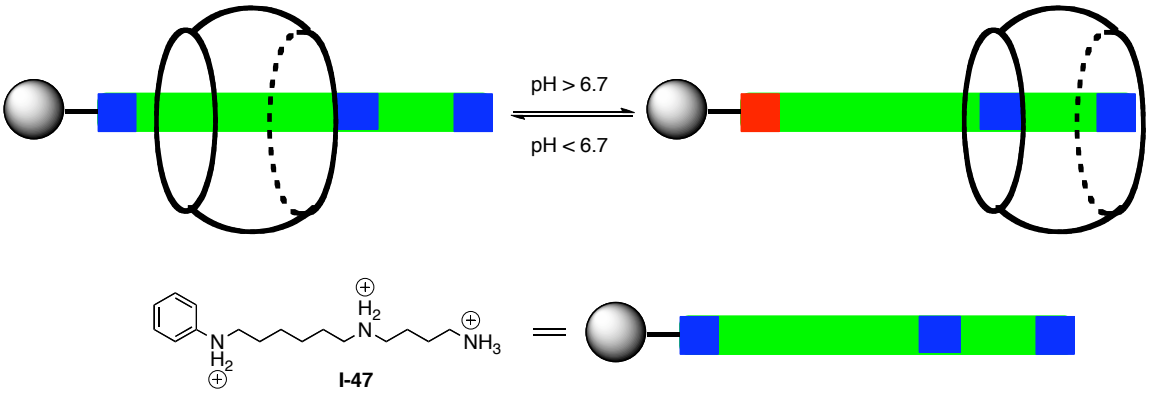

Figure I-13. Chemcially controlled molecular machine.

An example for electrochemically controlled molecular switch is the complex of CB[7] and methylviologen (MV, **I-46**), which was developed by Kim and co-workers.[33] CB[7] forms a stable 1:1 complex with MV^{2+} ($K_a = 2 \times 10^5\ M^{-1}$) and its reduced forms $MV^{+\bullet}$ ($K_a = 8.5 \times 10^4\ M^{-1}$) and MV^0 ($K_a = 2.5 \times 10^2\ M^{-1}$). A series of electrochemical study was carried out to demonstrate that 1) the dimerization of the cation radical $MV^{+\bullet}$ is

suppressed effectively by forming a stable complex with CB[7]; 2) direct electron transfer to and from the MV^{2+}-CB[7] complex is observed, which is rare in host-guest complexes.

Based upon the knowledge above, Kim utilized CB[8]'s larger cavity to accommodate two flat aromatic ring systems.[34] A novel [2]pseudorotaxane molecular machine based on the complex of CB[8] and dimeric viologen (**I-47**, Figure I-14) was synthesized. Dimeric viologen forms 1:1 host-guest complex with CB[8]. Similar to methyl viologen, it can go through electrochemical and photochemical process. By giving this complex an electrochemical or photochemical stimulus, the dimeric viologen can reversibly convert between dication and tetracation. The change of the electron density and charge leads to the folding and unfolding of the thread reversibly, which makes it a reversible molecular machine.

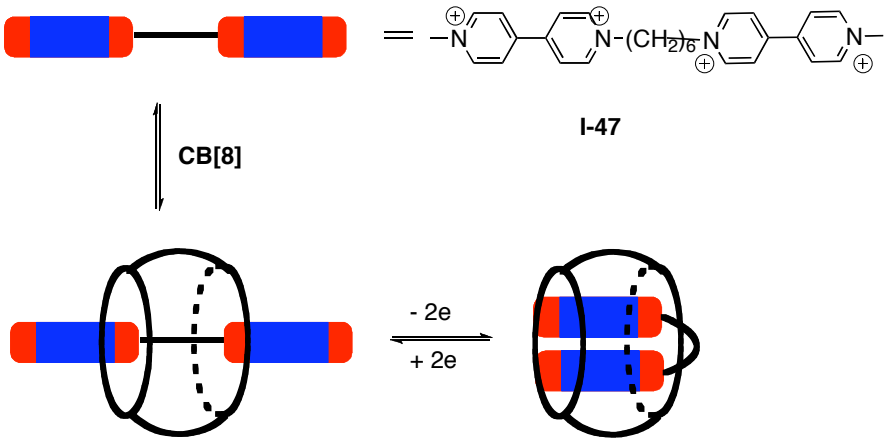

Figure I-14. Photochemically controlled molecular machine.

1.3.3.2 Catalysis.

Catalysis is very important in chemistry, since it increases the reaction rate. The mechanism of the catalysis could be very different depending on different reactions. As

for CB[*n*], it usually is that CB[*n*] encapsulate starting material molecules and thus bring them closer to each other.

Shortly after CB[6] was discovered and characterized, its application to catalyze chemical reactions was developed. Mock discovered that the dipolar cycloaddition between azide (**I-48**) and alkyne (**I-49**) was catalyzed by CB[6].[35] CB[6] accelerates this reaction by 5.5×10^4 fold and the reaction is highly regioselective, which makes this reaction a very elegant click reaction.

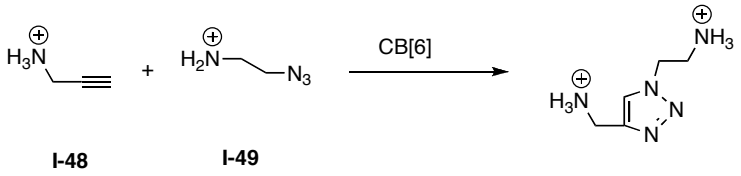

Figure I-15. Dipolar cycloaddition reaction catalyzed by CB[6].

Kim and co-workers developed a photoreaction based upon CB[8] (Figure I-16).[36] Two molecules of (*E*)-diaminostilbene dihydrochloride (**I-50**) would have [2+2] photoreaction. This photoreaction has a small reaction rate in the solution due to the large distance between reactant molecules. CB[8] could act as a catalyst for this reaction as a result of the formation of 1:2 host-guest complex. Inside the CB[8] cavity, (*E*)-diaminostilbene dihydrochloride molecules are brought to a very close distance, which leads to a much higher reaction rate (150 times higher). Also this CB[8] catalyzed photoreaction is stereoselective. The [2+2] photoreaction product has a high stereoselectivity (syn-anti ratio > 95:5) in the presence of CB[8].

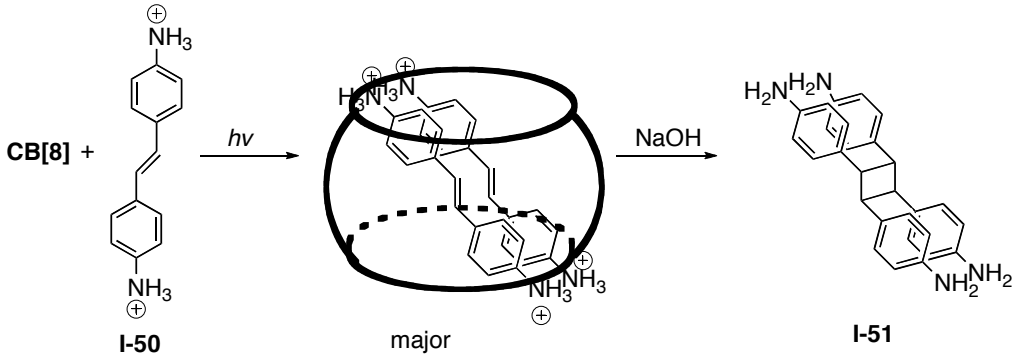

Figure I-16. [2+2] photoaddition reaction mediated by CB[8].

1.3.3.3 Drug Delivery

Drug delivery is a very important research topic in chemistry, biology and pharmacology. In order to improve the efficacy and safety of certain drugs, researchers use drug delivery technologies to modify drug release profile, absorption, distribution and elimination. As mentioned above, the cyclodextrin family has been widely used for drug delivery purposes. CB[*n*] family, especially CB[7], as a kind of macrocycles with high affinity and high selectivity towards various clinical drugs and reasonable solubility in water, is a very promising candidate for drug delivery. Recently, a number of reports have been made on CB[*n*]'s application for drug delivery purpose.

One example is reported by Nau and co-workers.[37] In their study, benzimidazoles were selected as drugs, including lansoprazole (**I-52**) and omeprazole (**I-53**), very important drugs that are prescribed worldwide to cure diseases related to the secretion of gastric acid, or in another word, proton-pump inhibitors. In order to study the complexation-induced pK_a shifts easily, chromophoric guest, thiabendazole (TBZ, **I-54**), was used in the research. Researchers found that the pK_a of TBZ was increased by as many as 4.0 units when it was bound to CB[7], the largest directly determined value so

far reported for an organic macrocyclic host. Proton-pump inhibitors have to convert to their active form, sulfonamide form (**I-55**), before they can react with cysteine residues of gastric (H^+-K^+)-ATPase and reduces the production of gastric acid (Figure I-17). But this activation process is usually slow. Also the sulfonamide form is unstable. It would go through dimerization and decomposition processes. By forming a 1:1 inclusion complex, CB[7] catalyzes the rapid and highly efficient formation of the active form of the drugs (sulfonamide form). Meanwhile, CB[7] stabilizes this sulfonamide form and thus the decomposition pathways are effectively suppressed. So CB[7] serves as a very useful agent to stabilize and activate proton-pump inhibitors.

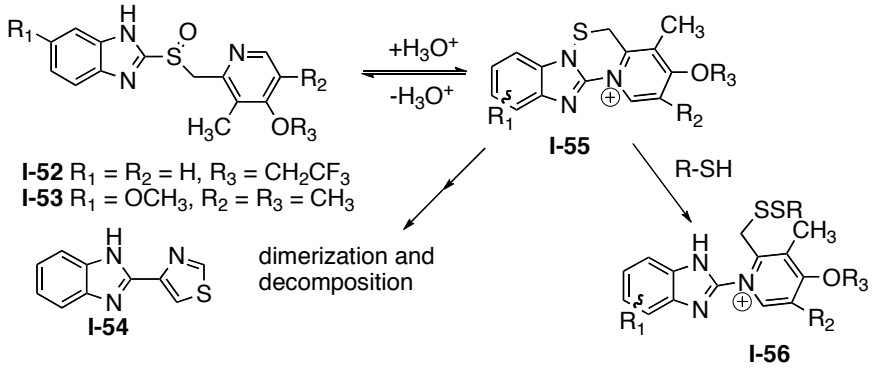

Figure I-17. Decomposition and reaction pathways of proton-pump inhibitor drugs.

Kim and his co-workers reported drug delivery research on functionalized CB[*n*], galactosylated CB[*n*] (Figure I-18).[38] The galactosylated CB[*n*] (**I-57**) used in their study is derived from CB[6] with 12 thioglucose groups on it. It can form a host-guest complex with dextran-spermine conjugate (**I-58**). The molar ratio of dextran-spermine conjugate and CB[*n*] residue can vary, such as 100:12 (Dex-spm-gCB-12) and 100:25 (Dex-spm-gCB-25). The complex of CB[*n*] and dextran-spermine conjugate is able to form a stable electrostatic complex with negatively charged pDNA, which enables it to achieve gene

transfection. The gene transfection efficacy of the vectors was studied in cultured cell systems. Researchers discovered that the transfection efficiency depends on N/P (nitrogen of spermine/phosphate of pDNA) ratio. And Dex-spm shows enhanced transfection efficiency only at N/P ratio as high as 5-7. This technology enables researchers to tailor the supramolecular entity very precisely with respect to overall transfection efficiency and target specificity by varying the spermine derivative conjugated to diverse templates and tagging different target specific ligands to CB[*n*].

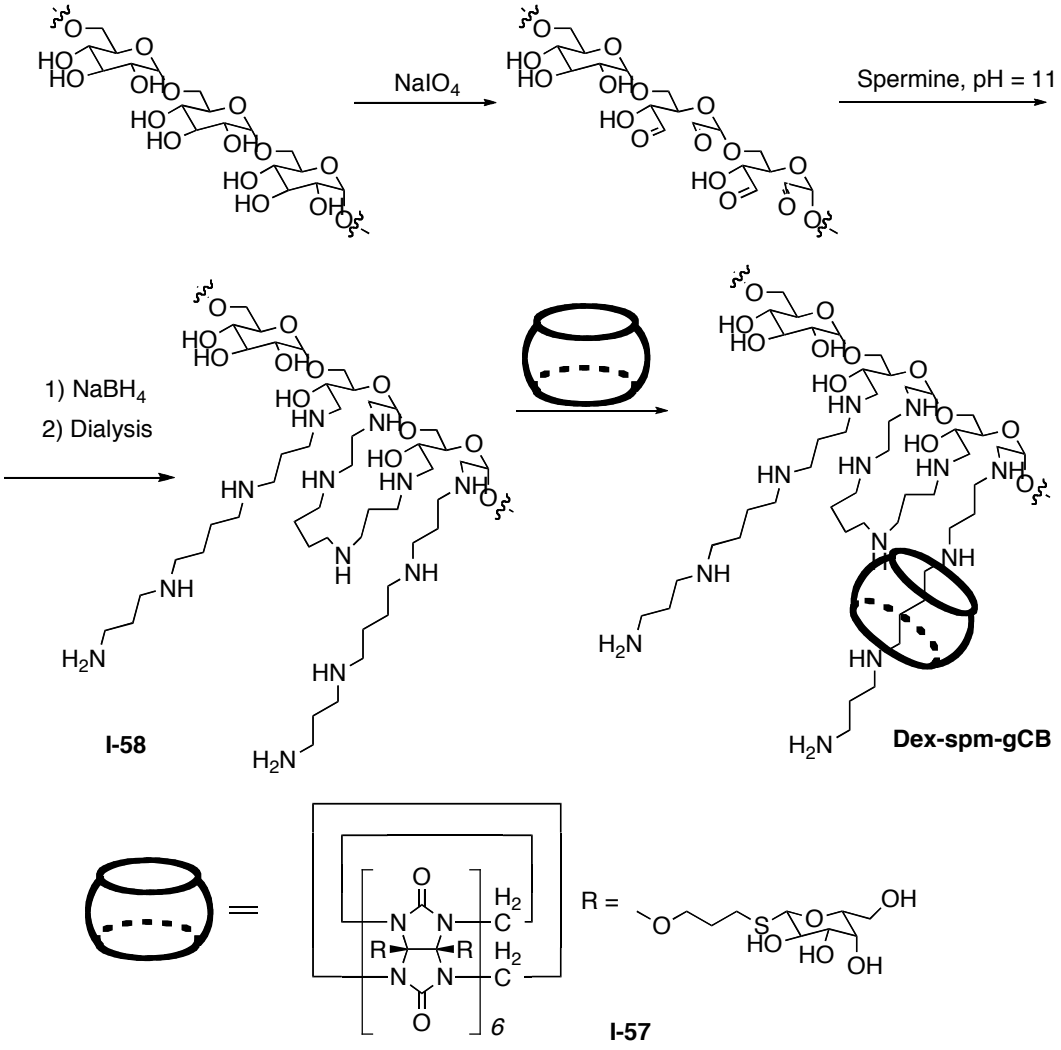

Figure I-18. Synthesis of Dex-spm-gCB conjugate.

Before CB[*n*] can be used for drug delivery purpose, researchers have to prove its safety in *vivo*. Nau and Day investigated CB[7] and CB[8]'s toxicity in *vitro* and in *vivo*.[39] After testing them in *vitro* on CHO-K1 cells and in *vivo* intravenous injection, as well as oral administration studies on mice, CB[7] and CB[8] are proved to have a very low toxicity. The mutually consistant IC_{50} and *MTD* values suggest that CB[7] is essentially nontoxic when applied in concentrations below 250 mg/kg tissue or body weight, or below concentrations of 0.5 mM. Briken and Isaacs recently studied the toxicity of several CB[*n*] and CB[*n*] type receptors on human cells, which also demonstrates very low toxicity.[40] These results suggest that CB[*n*]s are usually safe for drug delivery.

1.4 Summary.

Since its foundation, supramolecular chemistry has been developing into a very important research area both for academia and industry. Molecular encapsulation with cyclodextrin has already been proved to be a very useful technology. Meanwhile, applications of molecular encapsulation with cucurbituril are being developed currently. Significant progress has been achieved. But issues are still existing: 1) poor solubility of current CB[*n*] compared to cyclodextrin; 2) difficulty to functionalize CB[*n*] for more applications. This thesis will discuss the work that has been done to solve these problems by functionalizing CB[*n*]. Meanwhile, in order to develop new pathways to functionalized CB[*n*], the mechanism of CB[*n*] forming reaction is also investigated.

II. Chapter 2: New CB[*n*] Congeners with High Affinity.

2.1 Introduction.

As introduced in the Chapter 1, the cucurbit[*n*]uril (CB[*n*], n = 5, 6, 7, 8, 10) family of molecular containers are formed in a single step by the condensation of glycoluril with formaldehyde under strongly acidic conditions.[13,15,16,18] The key structural features of CB[*n*] molecular containers are the presence of a hydrophobic cavity guarded by two symmetry equivalent ureidyl carbonyl portals which constitute regions of high negative electrostatic potential.[41,42] As a consequence of these structural features CB[*n*] compounds bind to species which contain both hydrophobic chains and cationic groups. In a series of elegant papers throughout the 1980's Mock showed that CB[6] displays tight and highly selective binding interactions toward alkaneammonium and alkanediammonium ions in aqueous solution and used these properties to catalyze a 3+2 dipolar cycloaddition and construct an early example of a molecular switch.[43-45] Interest in the CB[*n*] family of molecular containers surged after the isolation of the larger CB[*n*] homologues which displayed even more interesting recognition properties. For example, the exceptionally high binding constants (K_a up to 10^{15} M^{-1}) displayed by CB[7][46-48] and the ability of CB[8] and CB[10] to bind two guests simultaneously has resulted in the a number of intriguing applications including the preparation of molecular machines,[49] chemical sensors, stationary phases for chromatographic separations and affinity capture, supramolecular polymers, supramolecular catalysis, and drug delivery vehicles.[37,41,42,50-72]

Despite the range of applications demonstrated for members of the CB[n] family, a number of issues have not been fully resolved that currently limit an even wider application of the CB[n] family.[73] The first issue is the generally poor solubility characteristics of CB[6], CB[8], and CB[10] (< 100 μM) in D_2O. A second, related issue is that the preparation of CB[*n*] derivatives especially those with enhanced solubility is challenging, particularly for the higher CB[*n*] homologues (n = 7, 8, 10).[24] A final issue involves the dynamics of the formation and dissociation of CB[n] complexes. Because of their narrow ureidyl carbonyl portals, CB[*n*] compounds exhibit constrictive binding.[74-78] In constrictive binding processes, large barriers to dissociation and sometimes association exist which translates in kinetics of dissociation and association that are slow on the laboratory time scale. Obviously, slow kinetics can be a limitation in many applications.

Over the past decade we have been using mechanistic insights to guide us toward synthetic approaches that alleviate some of these limitations. In one line of inquiry we have used glycoluril surrogates to prepare CB[*n*] analogues with built-in fluorescent walls.[28,73,79] In a second line of inquiry we have starved the CB[*n*] forming reaction of formaldehyde and isolated acyclic glycoluril oligomers and a number of macrocyclic CB[*n*]-type compounds lacking one or more bridging CH_2-groups (known as *nor-seco*-CB[*n*]).[20-22,80,81] In a third line of inquiry we have appended *o*-xylylene walls to glycoluril dimers and related systems and delineated the recognition properties (e.g. enantiomeric self-recognition, heterochiral recognition, and self-sorting) of the resultant acyclic CB[*n*] congeners.[82-84] Recently, Sindelar [20,22,80] has reported the synthesis and recognition properties of a glycoluril trimer capped with *o*-xylylene rings.[85] Throughout these studies we have found that any structural change that compromised the highly electrostatically

negative ureidyl carbonyl portals decreased the affinity of host toward guest. In this paper we continue the third line of inquiry by preparing hosts **II-5a** and **II-5b** which comprise a methylene bridged glycoluril tetramer capped with two substituted *o*-xylylene rings and studying their recognition properties toward various ammonium ions in water.

2.2 Results and Discussion.

This results and discussion section is organized as follows. First, we describe the design and synthesis of acyclic CB[*n*] congeners **II-5a** and **II-5b**. Second, we discuss their conformational properties, x-ray crystal structures, and verify the absence of self-association of hosts **II-5a** and **II-5b**. Third, we use a combination of direct and competitive UV/Vis spectroscopy and ^{1}H NMR spectroscopy to study the strength and geometrical details of the host-guest complexes of hosts **II-5a** and **II-5b**. Lastly, we discuss the trends in the tabulated values of K_a that give insights into the behavior of **II-5a** and **II-5b**.

2.2.1 Design and Synthesis of Acyclic CB[n] Congeners II-5a and II-5b.

Hosts **II-5a** and **II-5b** are composed of a central methylene brided glycoluril tetramer that is capped by two *o*-xylylene rings. The substituents (e.g. H and Ph or Me) on the central methylene bridged glycoluril tetramer all point away from the cavity which preorganizes the oligomer into the C-shaped configuration required for binding. The bridging *o*-xylylene units are substituted with OCH_2CO_2H groups which were expected

to enable the synthetic route, enhance the solubility of **II-5a** and **II-5b**, and potentially enhance the binding affinity toward ammonium ions due to additional electrostatic (e.g. carboxylate•ammonium) interactions. The synthesis of the acyclic CB[*n*] congeners follows a building block approach (Scheme II-1). First, glycoluril bis(cyclic ethers) **II-1a** or **II-1b**[86,87] are reacted with C-shaped dimer **II-2C**[81,88] in $MeSO_3H$ at 50 ˚C to yield tetramer bis(cyclic ethers) **II-3a** (35%) and **II-3b** (53%) in moderate yield. Compound **II-3b** was reacted with hydroquinone in refluxing TFA to install the HO-substituted *o*-xylylene walls to yield **II-4**. Compound **II-4** was then reacted with ethyl bromoacetate to yield an intermediate ester which was directly hydrolyzed to yield host **II-5b**. For the synthesis of **II-5a** we allowed **II-3a** to react with $(EtO_2CCH_2O)_2C_6H_4$ under acidic conditions (TFA, Ac_2O) to yield an intermediate ester which was directly hydrolyzed to yield **II-5a** in moderate yield (32%). As a control compound to study the influence of the substituted *o*-xylylene walls we decided to prepare methylene bridged glycoluril tetramer **II-6**. Heating **II-3a** with 3,5-dimethylphenol as a formaldehyde scavenger[73] in refluxing TFA delivered **II-6** in 45% yield.

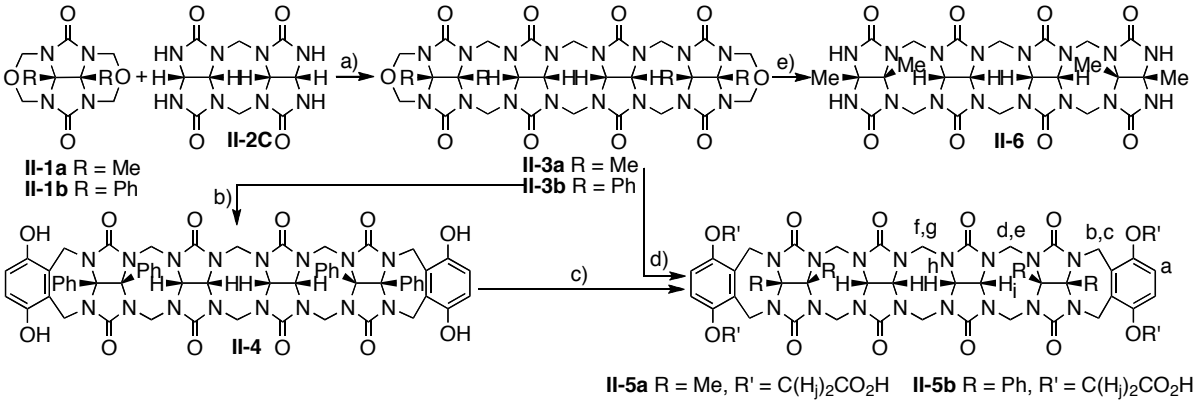

Scheme II-1. Synthesis of Acyclic CB[*n*] Congeners **II-5a** and **II-5b** and tetramer **II-6**. Conditions: a) $MeSO_3H$, 50 ˚C, b) hydroquinone, TFA, reflux, c) $BrCH_2CO_2Et$, K_2CO_3,

CH_3CN, reflux then LiOH, MeOH / H_2O, 70 ˚C then conc. HCl, d) $(EtO_2CCH_2O)_2C_6H_4$, TFA, Ac_2O, reflux then LiOH, MeOH / H_2O, 70 ˚C then conc. HCl, e) 3,5-dimethylphenol, TFA, reflux.

2.2.2 Conformational Properties of II-5a and II-5b.

The chemical structures of **II-5a** and **II-5b** greatly limit the conformational degrees of freedom of the system. For example, the fused bicyclic glycoluril ring system are conformationally locked. Similarly, the eight-membered rings that connect the glycolurils together by methylene bridges adopt the crown conformation which minimizes 1,5-diaxial interactions between substitutents on the convex face of the glycoluril rings.[89,90] Finally, the seven membered ring (7-MR) that connects the terminal substituted *o*-xylylene rings to the glycolurils has the potential to adopt two conformations (anti: *o*-xylylene ring oriented toward the cavity with 7-MR in chair conformation; syn: *o*-xylylene ring oriented away from the cavity with 7-MR in boat conformation). On the basis of previous studies by Nolte[91-93] and our group[30] we anticipated a preference for the anti-conformation (*vide infra*, Figure II-1a). In this manner, the 15 fused rings of **II-5a** and **II-5b** were designed to prefer a single conformation that preorganizes these acyclic hosts toward guest binding. Macrocyclization is not necessary.

2.2.3 X-ray Crystal Structures of Host II-5b and Complexes II-5b•II-20 and II-5a•II-25.

We were fortunate to obtain single crystals of **II-5b** in its uncomplexed form (Figure II-1a). As expected based on the precedent described above, **II-5b** assumes a C-shaped conformation that defines a hydrophobic cavity. There are several interesting aspects of the structure of **II-5b** that deserve comment. First, although the 15 fused rings effectively limit the conformation of the molecule to a C-shape, **II-5b** is able to undergo out-of-plane twisting. Figure II-1a shows that the substituted *o*-xylylene tips are skewed with respect to one another with one residing above the mean plane of the compound and the other below. This out-of-plane skewing results in an overall helical shape of **II-5b** and therefore **II-5b** assumes a chiral conformation in the crystal. Within the crystal of **II-5b** there are equal amounts of the two enantiomeric forms of **II-5b**. Second, the OCH_2CO_2H groups on the *o*-xylylene rings are oriented roughly parallel to the cavity. In the neutral form of **II-5b** present in the crystal, the CO_2H groups form intramolecular H-bonds back to the ureidyl C=O portal of **II-5b** as expected on the basis of its highly negative electrostatic potential. Third, although the chemical structure of **II-5b** contains six units (e.g. four glycolurils and two *o*-xylylene rings) the cavity of **II-5b** appears to be larger than that of CB[6]. To quantify this effect we consider the distance between the quaternary (PhC) carbon atoms on opposite sides of **II-5b** and CB[*n*]. The relevant distances for **II-5b** are 11.91 and 12.60Å. Comparable values for CB[5] are 8.48 and 7.60, for CB[6] are 10.05 and 10.05, for CB[7] are 10.74 and 11.37 Å, and for CB[8] are 11.47 and 12.54. By this measure, the curvature of the methylene bridged glycoluril tetramer subunit of **II-5b** is most similar to that of CB[8]. However, the 7-MR adopt a chair-like conformation that projects the connected substituted *o*-xylylene rings into the cavity of **II-5b** at a sharper angle than is observed for CB[6] – CB[8]. In this manner it

appears that **II-5b** contains structural regions that resemble CB[8] and other regions that are similar to smaller CB[*n*].

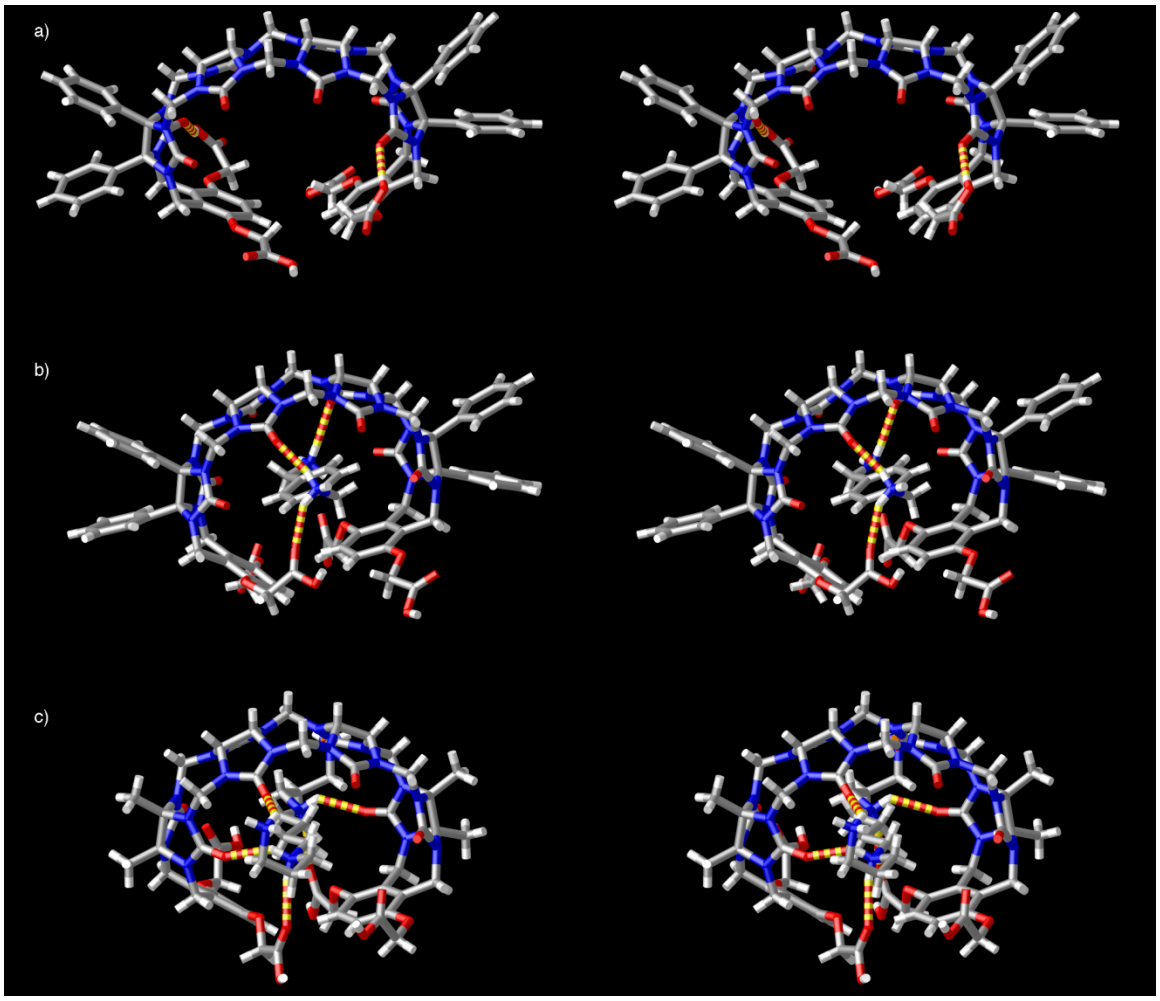

Figure II-1. Cross-eyed stereoviews of the x-ray crystal structures of: a) **II-5b**, b) **II-5b•II-20**, and c) **II-5a•II-25**. Color code: C, gray; H, white; N, blue; O, red; H-bonds, red-yellow striped.

Figure II-1b shows a stereoview of the x-ray crystal structure of **II-5b•II-20**. In this structure, **II-20** is bound within the cavity of **II-5b** and is held in place by two ureidyl

C=O•••HN H-bonds and one carboxylic acid C=O•••HN H-bond. Host **II-5b** undergoes a structural change that decreases the size of the host cavity in the **II-5b•II-20** complex. This structural change is reflected in the decreased distance between the opposing quaternary PhC carbon atoms (11.44 and 11.85 Å). In addition, one of the terminal *o*-xylylene rings of **II-5b** engages in an offset stacking interaction (mean plane separation = 3.45 Å; centroid-centroid distance = 3.74 Å) with the aromatic ring of guest **II-20**. Figure II-1c shows a stereoview of the x-ray crystal structure of **II-5a•II-25**. Spermine **II-25** is bound within the cavity of **II-5a** by virtue of four H-bonds between the central NH2 groups of **II-25** and the ureidyl C=O groups and the carboxylic acid groups of **II-25**. In addition, each of the terminal $N(CH_2)NH_3^+$ groups folds back and form an additional H-bonds to the C=O portal of **II-5a**. In total the **II-5a•II-25** complex benefits from six H-bonds. One of the interesting structural features of the **II-5a•II-25** complex is the pronounced out-of-plane skewing of the terminal *o*-xylylene rings. This geometrical feature places the CH_2-groups of the central butylene linker within the shielding region of the adjacent aromatic ring which is reflected in the large upfield shifts observed for H_m and H_n in the ^1H NMR spectrum of the **II-5a•II-25** complex (*vide infra*). Overall, hosts **II-5a** and **II-5b** exhibit a substantial ability to respond to the structural characteristics of the guest.

2.2.4 Hosts II-5a, II-5b, and II-6 Do Not Undergo Self-Association.

In our previous studies self-association has been an important and in some cases dominant mode of interaction.[58] Therefore, before proceeding to study the host-guest

recognition properties of **II-5a**, **II-5b**, and **II-6** we wanted to rule out the possibility of self-association in water. For this purpose we performed ^{1}H NMR dilution experiments (Supporting Information) and do not observe any changes in chemical shift over the 60 μM to 1.52 mM range of concentration. These results indicate that **II-5a**, **II-5b**, and **II-6** do not undergo self-association which allows us to study their host-guest recognition properties free of these effects.

2.2.5 Binding Studies Between Hosts II-5a, II-5b, and II-6 and Guests II-7 – II-32.

This section describes the non-covalent interaction between the hosts and guests **II-7** – **II-30** (Chart II-1) by several different methods.

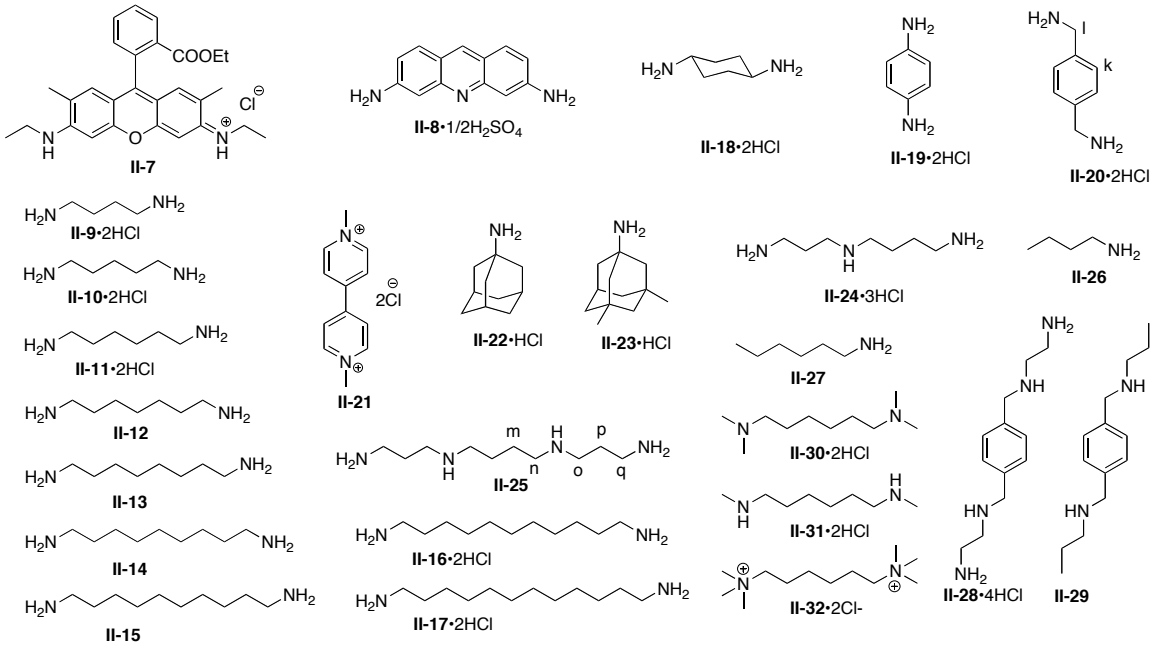

Chart II-1. Chemical structures of guests used in this study.

^{1}H NMR Investigations of the Binding Interactions. Initially, we used ^{1}H NMR to study the interaction between **II-5b** and **II-20.** Figure II-2a-c shows the ^{1}H NMR spectra recorded for **II-5b**, **II-20**, and for an equimolar mixture of **II-5b** and **II-20**. The protons on the aromatic ring of **II-20** undergo a substantial upfield shift in the presence of **II-5b** which suggests that **II-20** is bound within the cavity of **II-5b** which is corroborated by the x-ray crystal structure of **II-5b•II-20** (Figure II-1b). When **II-5b** and **II-20** are mixed at a 1:2 stoichiometry we observe resonances for free **II-21** and complexed **II-21** which establishes that the dynamics of exchange are slow on the chemical shift time-scale. Attempts to perform ^{1}H NMR titration experiments to determine values of K_a were unsuccessful because they exceeded those that can be determined accurately ($K_a < 10^5$ M^{-1}) by this technique.[94] Figure II-2d-f shows the ^{1}H NMR recorded for **II-5a**, spermine **II-25**, and an equimolar mixture of **II-5a** and **II-25**. In this case the pattern of upfield shift of the resonances for guest **II-26** suggests that the central diaminobutane linker of **II-25** is bound within the central cavity of **II-5a** with the $N(CH_2)_3NH_3^+$ arms extending past the ureidyl C=O portals of **II-5a**. This interpretation is supported by the x-ray crystal structure of the **II-5a• II-26** shown in Figure II-1c and discussed below.

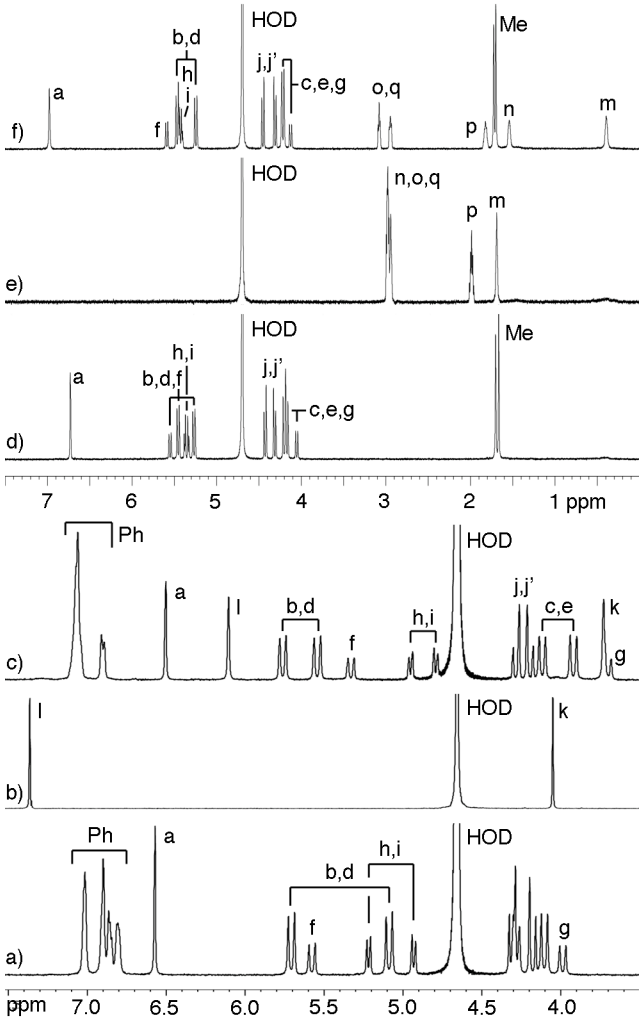

Figure II-2. ^{1}H NMR spectra recorded for: a) **II-5b**, b) **II-20**, and c) an equimolar mixture of **II-5b** and **II-20** (400 MHz, RT, 25 mM sodium phosphate buffered D_2O, pH 7.4) and d) **II-5b**, e) **II-25**, f) an equimolar mixture of **II-5b** and **II-25** (600 MHz, RT, 25 mM sodium phosphate buffered D_2O, pH 7.4)

Direct UV/Vis Titrations. Because the values of K_a for the interaction between **II-5a** and **II-20** were inaccessible by ^{1}H NMR titrations we decided to resort to competitive UV/Vis binding assays. We used competitive UV/Vis binding assays rather than the competitive

^{1}H NMR binding method used by us earlier[46] because most of the complexes of **II-5a** display fast exchange kinetics on the chemical shift time scale. We found that dye **II-7** (Rhodamine 6G) binds to **II-5a** and undergoes changes in its UV/Vis spectrum. Figure II-3a shows the UV/Vis spectra recorded when a fixed concentration of **II-7** (9.23 μM) was titrated with **II-5a** (0 – 49 μM). The UV/Vis spectra show large changes at 520 and 550 nm and the presence of an isosbestic point at 533 nm which allowed us to conclude that **II-5a** and **II-7** undergo clean formation of the **II-5a•II-7** complex. Figure 3b shows a plot of UV/Vis absorbance at 520 nm versus the concentration of **II-5a** which can be fitted to a 1:1 binding model to determine the stability of the **II-5a•II-7** complex (K_a = $2.1 \pm 0.1 \times 10^5$ M^{-1}). With this value of K_a in hand it is possible to measure K_a values for weaker binding guests by competitive indicator displacement assays.[95,96]

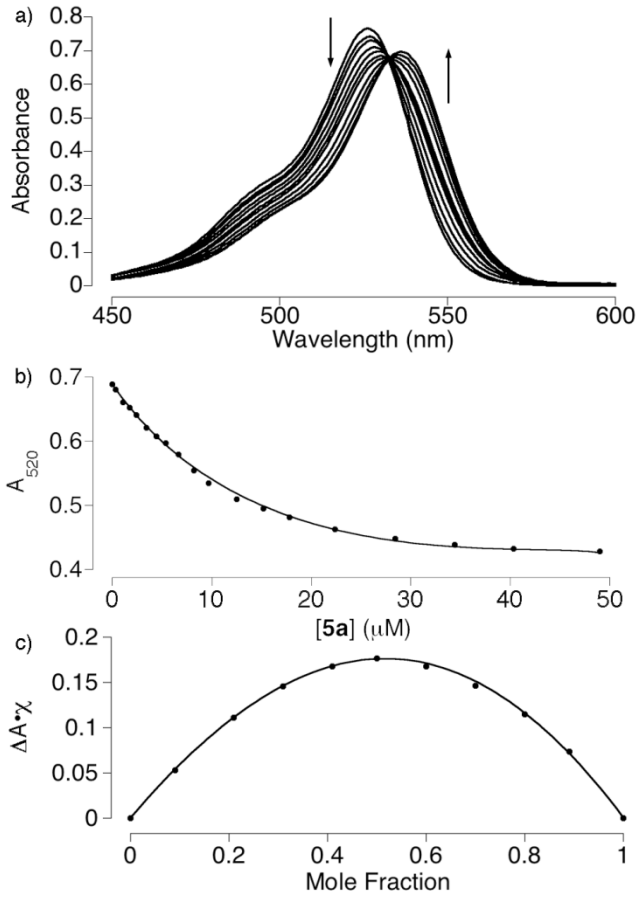

Figure II-3. a) UV/Vis spectra obtained during the titration of a fixed concentration of **II-5a** (9.23 μM) with **7** (0 – 49 μM), b) Plot of absorbance versus [**II-7**] used to determine the value of K_a by non-linear least squares fitting, c) Job plot ([**II-5a**] + [**II-7**] = 1.5 mM) of mole fraction of **II-5a** versus $\Delta A \times \chi$.

UV/Vis Indicator Displacement Assays. In indicator displacement assays, a complex is formed between a host and an indicator that undergoes an UV/Vis change upon complexation. Upon addition of a competitive binding guest, the indicator is released resulting in a UV/Vis spectral change. Based on a knowledge of the concentrations employed and the value of K_a for either the host•indicator complex or the host•guest

interaction it is possible to calculate the unknown K_a. We used this strategy with dyes (indicators) **II-7** and **II-8** to determine the values of K_a for the complexes between host **II-5a** and guests **II-9**–**II-30** (Table II-1). We first used the competition between non-UV/Vis active guest butylammonium ion **II-26** and rhodamine G (**II-7)** to determine the stability of the **II-5a•II-26** complex ($K_a = 1.4 \pm 0.1 \times 10^5$ M^{-1}). Subsequently we performed an indicator displacement assay between **II-5a**, UV/Vis active acridine dye **II-8**, and **II-26** which allowed us to determine the value of K_a for the **II-5a•II-8** complex ($K_a = 7.2 \pm 0.4 \times 10^8$ M^{-1}). We then measured the values of K_a for the remaining complexes of **II-5a** by indicator displacement assays using the **II-5a•II-8** complex (Table II-1). The data from the UV/Vis competition assays and their analysis to extract the K_a values are given in the supporting information section of this chapter. Table II-1 also presents the literature values of the binding constants for a subset of these guests toward CB[6][45] and CB[7].[46]

		K_a (M^{-1})	
Guests	Host **II-5a**	CB[6][a)]	CB[7][b)]
II-7	$2.1 \pm 0.1 \times 10^5$		
II-8	$7.2 \pm 0.4 \times 10^8$		
II-9	$1.4 \pm 0.1 \times 10^6$	1.5×10^5	
II-10	$2.8 \pm 0.3 \times 10^7$	2.4×10^6	
II-11	$1.6 \pm 0.1 \times 10^8$	2.8×10^6	$9.0 \pm 1.4 \times 10^7$
II-12	$1.4 \pm 0.1 \times 10^8$	4.3×10^4	
II-13	$3.6 \pm 0.4 \times 10^8$	9.1×10^3	
II-14	$2.2 \pm 0.2 \times 10^8$	4.8×10^2	
II-15	$2.0 \pm 0.2 \times 10^8$	1.0×10^2	
II-16	$7.2 \pm 0.7 \times 10^7$		
II-17	$3.2 \pm 0.3 \times 10^7$		
II-18	$4.3 \pm 0.4 \times 10^7$		$2.3 \pm 0.4 \times 10^7$
II-19	$7.1 \pm 0.8 \times 10^5$		$2.1 \pm 0.3 \times 10^6$
II-20	$6.8 \pm 0.9 \times 10^8$		$1.8 \pm 0.3 \times 10^9$
II-21	$4.0 \pm 0.4 \times 10^8$		$1.3 \pm 0.2 \times 10^7$
II-22	$3.5 \pm 0.4 \times 10^6$		$4.2 \pm 1.0 \times 10^{11}$
II-23	$4.8 \pm 0.5 \times 10^5$		$2.5 \pm 0.4 \times 10^4$

II-24	$2.6 \pm 0.4 \times 10^7$	1.4×10^6
II-25	$4.5 \pm 0.4 \times 10^8$	1.3×10^7
II-26	$1.4 \pm 0.1 \times 10^5$	1.0×10^5
II-27	$1.4 \pm 0.1 \times 10^6$	2.2×10^3
II-28	$3.6 \pm 0.5 \times 10^9$	
II-29	$2.0 \pm 0.2 \times 10^9$	
II-30	$9.8 \pm 0.9 \times 10^7$	9.1×10^3
II-31	$3.1 \pm 0.4 \times 10^8$	1.7×10^6
II-32	$1.4 \pm 0.2 \times 10^8$	

(a) Measured in H_2O/85% HCO_2H (1:1),[44] b) Measured in 50 mM NaOAc buffer,pH 4.74.[45]

Table II-1. Binding constants (K_a) for the interaction of **II-5a** and various guests.

2.2.6 Trends in the Values of K_a Between Host II-5a and Guests. The values of K_a given in Table II-1 allow us to make comparisons between various guests that shed light on the overall binding properties of **II-5a** compared other CB[*n*].

Influence of Chain Length. One of the best studied phenomena in the binding properties of the CB[*n*] family is the influence of guest length on the binding affinity of alkanediammonium ions. For the relatively rigid host CB[6] a maximum binding affinity is seen for pentanediammonium and hexanediammonium ions **II-10** and **II-11** with greatly reduced affinity toward longer and shorter diammonium ions.[45] Figure II-4 shows a plot of binding affinity of **II-5a** and CB[6] toward diammonium ions **II-9** – **II-17** as a function of chain length. Several trends in this data are worth noting. First, host **II-5a** binds more tightly to many of these alkanediammonium ions than CB[6] does. These higher binding constants may reflect: 1) that the larger hydrophobic cavity of **II-5a** (relative to CB[6]) provides a larger hydrophobic driving force toward complexation, and/or 2) the energetic contributions of the interaction between the CO_2^- arms of host **II-**

5a and the diammonium guest (*vide infra*). Second, host **II-5a** appears to be less sensitive to changes in length than CB[6]; host **II-5a** is less selective than CB[6] and binds **II-11** – **II-15** with high affinity ($K_a > 10^8\ M^{-1}$). We believe this lower selectivity is due to the structural flexibility of host **II-5a** relative to CB[6]. For example, when host **II-5a** adopts a skewed (helical) conformation the distance between its ureidyl C=O portals also change. It is well known that the ureidyl C=O portals of CB[n] provide a significant portion of the driving force for the binding of ammonium ions by ion-dipole / H-bonding interactions. Similarly, host **II-5a** is acyclic which allows it to increase its cavity size by flexing its pairs of CH_2-bridges. This process allows **II-5a** to accommodate longer guests perhaps by folding the hydrophobic chain of the guest inside the host.[22,97]

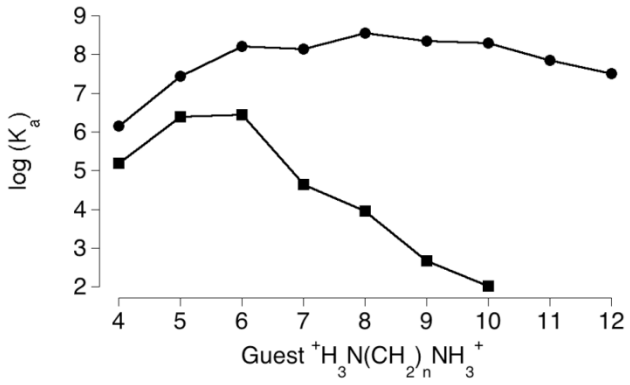

Figure II-4. Plot of log (K_a) versus chain length for the interaction between alkanediammonium ions (**II-9** – **II-17**) and hosts **II-5a** (•) or CB[6] (■).

*Binding Capacity of **II-5a**.* Based on the analysis of the x-ray structure of **II-5a** (Figure II-1) and the ability of **II-5a** to bind the longer diammonium ions tightly (e.g.

decanediammonium ion **II-15**) we anticipated that host **II-5a** would be able to complex larger guests that typically only bind to the more spacious hosts CB[7] and CB[8]. For this purpose, we studied the binding affinity of **II-5a** toward guests **II-18** – **II-23** which display a range of guest sizes. For example, CB[6] binds to the smaller guests **II-19** and **II-20**, CB[7] can accommodate slightly larger guests **II-18**, **II-21**, and **II-22**, and CB[8] is able to bind tightly even to dimethyl adamantaneammonium ion **II-23**.[46] In contrast, host **II-5a** forms complexes with all six size probe guests **II-18** – **II-23** albeit with differences in affinity. For example, host **II-5a** binds relatively weakly to the smallest (**II-19**, $K_a = 7.1 \times 10^5$ M^{-1}) and largest (**II-23**, $K_a = 4.8 \times 10^5$ M^{-1}) guests in this series. The intermediate sized guests **II-18**, **II-20**, and **II-21** are all bound more tightly by **II-5a**. These higher levels of affinity may be due to a better size match between the cavity of host **II-5a** and guests **II-18**, **II-20**, and **II-21**, the possibility of-interactions between guests **II-20** or **II-21** and the substituted *o*-xylylene walls of host **II-5a**, or a combination of these factors. In combination these results suggest that the effective cavity volume of **II-5a** is similar to or slightly larger than that of CB[7] (V = 272 $Å^3$).[42] It is worth noting that the affinity of **II-5a** toward several of these size probe guests (**II-18**, **II-21**, and **II-23**) exceeds the K_a values measured toward CB[7] (Table II-1). In contrast, the affinity of CB[7] toward its best guests (**II-20** and **II-22**) is greater than that measured toward **II-5a**. These results reinforce our belief that the flexibility of **II-5a** makes it a more general purpose high affinity but modest selectivity host in water.

Effect of the Number of Ammonium Groups. In his pioneering work Mock demonstrated that the addition of ammonium groups to guests for CB[6] generally resulted in a 10 – 1000-fold increase in binding affinity[45] which also holds for other CB[*n*]. For example,

spermine **II-25** (K_a = 1.3 × 10^7 M^{-1}) binds ≈ 10-fold stronger to CB[6] than spermidine **II-24** (K_a = 1.4 × 10^6 M^{-1}), which in turn binds ≈ 10-fold stronger to CB[6] than butanediammonium ion (**II-9**, K_a = 1.5 × 10^5 M^{-1}) does. The values of K_a contained in Table II-1 allow us to ascertain whether similar trends hold for **II-5a**. For example, butylammonium ion (**II-26**, K_a = 1.4 × 10^5 M^{-1}) binds 10-fold weaker to **II-5a** than butanediammonium ion (**II-9**, K_a = 1.4 × 10^6 M^{-1}) does. Similarly, hexylammonium ion (**II-27**, K_a = 1.4 × 10^6 M^{-1}) binds ≈ 100-fold weaker to **II-5a** than hexanediammonium ion (**II-11**, K_a = 1.6 × 10^8 M^{-1}). Related trends (5-fold increase in K_a per ammonium group) can be seen when comparing the binding of butanediammonium ion (**II-9**, K_a = 1.4 × 10^5 M^{-1}) with triammonium ion spermidine **II-24** (K_a = 2.6 × 10^7 M^{-1}) and tetraammonium ion spermine **II-25** (K_a = 4.5 × 10^8 M^{-1}). Acyclic CB[n] congener **II-5a** displays similar gains in Ka as a result of additional ammonium groups as CB[6] does.

Effect of the Degree of Alkylation of the Ammonium Ion. The affinity of CB[6] toward alkanediammonium ions is dramatically effected by the degree of alkylation of the N-atoms. For example, CB[6] binds tightly to hexanediammonium ion **II-11** (K_a = 2.8 × 10^6 M^{-1}) and N,N'-dimethylhexanediammonium ion **II-31** (K_a = 1.7 × 10^6 M^{-1}) but binds only weakly to N,N,N',N'-tetramethylhexanediammonium ion **II-30** (K_a = 9.1 × 10^3 M^{-1}). This effect can be explained based on the geometry of the CB[6]•**II-11** complex which displays two N-H•••O=C H-bonds per portal. Accordingly, each ammonium ion can have two C-subsitutents and 2 H-atoms and still assume this ideal geometry; addition of a third C-subsitutent (e.g. **II-30**) results in severe steric interactions between host and guest. The affinity of **II-5a** toward **II-11** (K_a = 1.8 × 10^8 M^{-1}), **II-31** (K_a = 3.1 × 10^8 M^{-1}), **II-30** (K_a = 9.8 × 10^7 M^{-1}), **II-32** (K_a = 1.4 × 10^8 M^{-1}) does not follow a similar trend.

The comparable affinities of **II-5a** toward **II-11**, **II-31**, **II-30**, and **II-32** suggests that the flexibility of **II-5a** allows it to compensate for the loss of N-H•••O=C H-bonds by an increased hydrophobic driving force for the inclusion of the additional alkyl groups in the cavity of **II-5a**.

Effect of the Concentration of Buffer Used. It is well known from CB[n] supramolecular chemistry that the presence of metal cations in solution reduces their apparent binding affinity toward guests due to competitive binding at the electrostatically negative ureidyl C=O lined portals.[30,78,98-100] We hypothesized that the ureidyl C=O portals of acyclic CB[n] congeners **II-5a** and **II-5b** which are shaped by four contiguous glycoluril units should also bind to metal cations and thereby reduce their affinity toward guests. Accordingly, we measured the affinity of rhodamine 6G (**II-7**) toward **II-5b** by direct UV/Vis titration in sodium phosphate buffer (pH 7.4) at different concentrations. Figure II-5 shows a plot of K_a versus phosphate concentration. As the concentration of sodium phosphate is increased the log Ka value undergoes a steady decrease as expected based on competitive binding of Na^+ for the C=O portals of **II-5b**. This analysis indicates that the ureidyl C=O portal of host **II-5b** retains this essential feature of the CB[n] family which supports our description of **II-5a** and **II-5b** as acyclic CB[n] congeners.

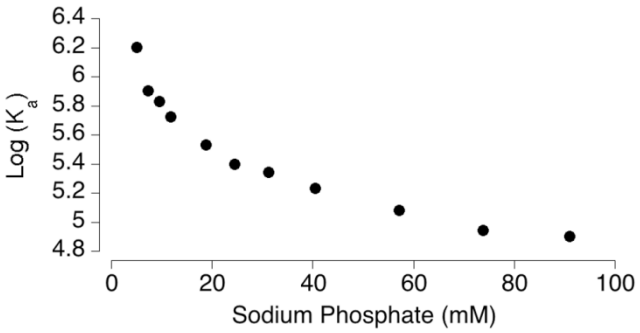

Figure II-5. Plot of log K_a versus the concentration of sodium phosphate buffer (H_2O, pH 7.4) for the formation of the **II-5b•II-7** complex.

Contribution of the substituted o-xylylene walls to the binding. Based on the excellent binding affinity of **II-5a** toward the aromatic guests **II-8**, **II-20**, **II-21**, **II-28**, and **II-29** and the x-ray structure of **II-5b•II-20** (Figure II-1b) we suspected that interactions between the substituted *o*-xylylene walls of **II-5a** and the aromatic rings of the guest might be an important driving force in the recognition behavior of host **II-5a**. Accordingly, we prepared compound **6** which lacks the substituted *o*-xylylene walls of **II-5a**. We measured the value of K_a for the interaction between **II-6** and hexanediammonium ion (**II-11**, $K_a = 5.6 \pm 0.4 \times 10^3$ M^{-1}) or *p*-xylenediammonium ion (**II-20**, $K_a = 1.5 \pm 0.1 \times 10^4$ M^{-1}) by direct ^1H NMR titrations (Supporting Information). These K_a values are greater than substantially smaller than the corresponding values for the interaction of **II-5a** with **II-11** ($K_a = 1.6 \pm 0.1 \times 10^8$ M^{-1}) and **II-20** ($K_a = 6.8 \pm 0.9 \times 10^8$ M^{-1}). This indicates that the substituted *o*-xylylene walls of **II-5a** do contribute substantially to the overall binding behavior of **II-5a**. The fact that reduction in affinity for aliphatic **II-11** (2.8×10^4-fold) is comparable to that of aromatic **II-20** (4.5×10^4-

fold) suggests that the aromatic walls do not participate in strong specific interactions but instead probably enhance binding by defining a structured environment from which water can be released upon binding. To ascertain the potential contributions of carboxylate-ammonium ion electrostatic interactions on the recognition behavior of **II-5a** we compared its binding toward **II-28** and **II-29**. Both **II-28** and **II-29** are derivatives of *p*-xylylene diamine; **II-29** contains two $CH_2CH_2CH_3$ arms whereas **II-28** contains two $CH_2CH_2NH_3^+$ arms. We specifically chose the two carbon linkers to prevent backfolding of the $CH_2CH_2NH_3^+$ arms to the ureidyl C=O portals of **II-5a** and potentially promote carboxylate-ammonium ion electrostatic interactions in the **II-5a•II-28** complex. Experimentally, we find that the binding constants measured for **II-5a•II-28** and **II-5a•II-29** are quite similar which suggests that carboxylate•ammonium ion electrostatic interactions do not play a large role in the recognition behavior of **II-6** and **II-5a**.

2.3 Conclusions.

In summary, we have presented the synthesis of acyclic CB[*n*] congeners **II-5a** and **II-5b** that contain four contiguous methylene bridged glycoluril units. Despite the acyclic nature of **II-5a** and **II-5b** the 15 fused rings effectively pre-organizes **II-5a** and **II-5b** into a C-shape required for binding. By a combination of direct UV/Vis titrations along with indicator displacement assays we determined the values of K_a for the interaction of **II-5a** with a variety of guest compounds (**II-7** – **II-32**). We find that **II-5a** acts as a high affinity host – just like CB[*n*] – with binding constants in the 10^5 – 10^9 M^{-1} range. The cavity volume of host **II-5a** is comparable to that of CB[7]. Unlike CB[*n*],

II-5a displays only moderate levels of selectivity based on guest length and the degree of alkylation of the N-atoms of the ammonium ion guests. We attribute this lower selectivity to the conformational changes of the host that occur upon formation of the host•guest complexes. Similar to CB[*n*], the binding affinity of **II-5a** toward its guests increases by a factor of 10 – 1000 as the number of ammonium ions in the guests is increased (e.g. **II-9** vs. **II-24** vs. **II-25**) whereas the affinity is reduced as the concentration of metal cations in the buffer increases due to competitive binding at the ureidyl C=O portals.

To date, three major issues for the use of CB[*n*] compounds in practical applications have been: 1) their generally poor solubility in aqueous solution, 2) challenges for their selective functionalization, and 3) the relatively slow uptake and release rates of guests due to the constrictive binding nature of the CB[*n*] cavity. The acyclic CB[*n*] congeners presented in this paper were prepared by convergent building block routes and feature terminal *o*-xylylene rings that are readily functionalized and endowed with carboxylic acid groups that increase solubility in aqueous solution. By virtue of its fused ring acyclic structure **II-5a** is both preorganized for ammonium ion binding and capable of fast uptake and release of its guests. Macrocyclization is not necessary to achieve high affinity interactions between acyclic CB[*n*] congeners and ammonium ion guests. The availability of acyclic CB[*n*] congeners that can be readily functionalized while maintaining the outstanding recognition properties of the CB[*n*] family promises their future use in a variety of applications including chemical sensing, controlled release or sequestration, and as a component of molecular machines.

2.4 Experimental Section.

General Experimental. Starting materials were purchased from commercial suppliers and were used without further purification. Compounds **II-1a**, **II-1b**, **II-2C**, **II-28** and **II-29** were prepared according to literature procedures.[81,86,87,101,102] Melting points were measured on a Meltemp apparatus in open capillary tubes and are uncorrected. TLC analysis was performed using pre-coated plastic plates from Merck. IR spectra were recorded on a JASCO FT/IR 4100 spectrometer and are reported in cm^{-1}. NMR spectra were measured on a Bruker DRX-400 instrument operating at 400 MHz for ^{1}H and 100 MHz for ^{13}C. Mass spectrometry was performed using a JEOL AccuTOF electrospray instrument (ESI).

Compound **II-3a**: To a mixture of **II-2C** (7.42 g, 24.0 mmol) in anhydrous $MeSO_3H$ (55 mL), **II-1a** (24.46 g, 96.2 mmol) was added. The mixture was stirred and heated at 50 ºC for 3 h. The reaction mixture was poured into water (700 mL). After filtration, the crude solid was dried in high vacuum. The crude solid was recrystallized from TFA (15 mL) and water (45 mL) to yield **II-3a** as a white solid (6.60 g, 8.45 mmol, 35%). M.p. > 227 ºC (decomposed). IR (ATR, cm^{-1}):1714s, 1456m, 1314m, 1223s, 1177s, 1079m, 960m, 920m, 857m, 799s, 757m, 668m. ^{1}H NMR (400 MHz, DMSO-d^6): 5.64 (d, J = 14.0, 2H), 5.50 (d, J = 15.1, 4H), 5.50 (d, J = 11.0, 2H), 5.37 (d, 1 J = 8.6, 2H), 5.25 (d, J = 11.0, 2H), 5.12 (d, J = 11.7, 4H), 4.78 (d, J =11.0, 4H), 4.20 (d, J = 14.8, 4H), 4.16 (d, J = 12.5, 2H), 1.72 (d, J = 69.6, 12H). ^{13}C NMR (100 MHz, TFA, 1, 4-dioxane as internal reference): δ 157.0, 156.6, 78.5, 74.5, 71.2, 71.0, 70.6, 52.3, 48.1, 15.5, 14.4. MS (ESI): m/z 781 ($[M + H]^+$).

Compound **II-3b:** A mixture of **II-2C** (0.920 g, 3.00 mmol) and **II-2b** (2.61 g, 6.90 mmol) in $MeSO_3H$ (10 mL) was stirred at room temperature for 20 min. Then the mixture was stirred and heated at 50 ^oC for 4 hours. The reaction mixture was poured into MeOH (500 mL). After filtration, the crude solid was dried in high vacuum. The crude solid was recrystallized from TFA (25 mL) and water (25 mL) to yield **II-3b** as a white solid (1.700 g, 1.65 mmol, 53%). M. P. >350 °C. TLC ($MeCN/H_2O$, 4:1) R_f 0.47. IR (cm^{-1}): 3450w, 1722s, 1445m, 1362m, 1314m, 1198s. ^{1}H-NMR (400 MHz, DMSO-d_6): 7.14-6.95 (m, 20H), , 5.82 (d, J = 15.2, 4H), 5.68 (d, J = 14.2, 2H), 5.38 (d, J = 10.8, 4H), 5.20 (d, J = 10.2, 2H), 5.03 (d, J = 8.4, 2H), 4.30 (d, J = 10.8, 4H), 4.08 (d, J = 14.2, 2H), 4.05 (d, J = 15.2, 4H) ^{13}C NMR (100 MHz, TFA, 1, 4-dioxane as internal reference): δ 159.6, 157.5, 130.7, 130.3, 129.6, 128.9, 128.3, 128.2, 127.4, 87.8, 81.9, 72.3, 72.0, 71.6, 53.2, 50.6. MS (ESI): *m/z* 1029 ($[M + H]^+$).

Compound **II-4:** A mixture of **II-3b** (4.18 g, 4.06 mmol) and hydroquinone (7.15 g, 65.0 mmol) in TFA (60 mL) was heated at reflux for 10 hours. The solvent was removed by rotary evaporation. The solid was washed twice with MeOH (2 × 70 mL) and then hot DMSO (15 mL). The solid was obtained by filtration and dried under high vacuum to yield **II-4** as a white solid (2.90 g, 2.39 mmol, 59%). M. P. >350 °C (decomposed). IR (cm^{-1}): 3400w, 1722s, 1448s, 1194s. ^{1}H-NMR (400 MHz, DMSO-d_6): 8.70 (s, 4H), 7.09-6.77 (m, 24H), 6.53 (s, 4H), 5.77 (d, J = 14.4, 4H), 5.54 (d, J = 15.2, 2H), 5.32 (d, J = 15.8, 4H), 5.10 (d, J = 8.0, 2H), 4.89 (d, J = 8.0, 2H), 3.96 (d, J = 14.0, 2H), 3.88 (d, J = 14.4, 4H), 3.72 (d, J = 15.5, 4H). ^{13}C NMR (100 MHz, TFA, 1, 4-dioxane as internal reference): δ. 159.4, 156.6, 146.2, 130.1, 130.0, 129.7, 129.0, 128.8, 128.0, 127.1, 125.1, 118.7, 88.0, 87.1, 72.0, 71.4, 50.3, 37.5, 35.9. MS (ESI): *m/z* 1213 ($[M + H]^+$).

Compound **II-5a:** To a mixture of **II-5a** (6.56 g, 8.36 mmol) and **II-4** (17.9 g, 66.9 mmol) in TFA (40 mL), Ac_2O (6.30 mL, 66.9 mmol) was added. The mixture was heated at reflux for 2 h. The solvent was removed by rotary evaporation. The solid was washed twice with diethyl ether (2 × 200 mL). Filtration and drying on high vacuum gave a white solid. This white solid was mixed with LiOH (1.70 g, 70.8 mmol) and dissolved in MeOH and water (1:1, v/v, 400 mL). The mixture was heated at 80 ˚C for 15 h. The solvent was removed by rotary evaporation. The crude solid was dissolved in water (60 mL) and treated with conc. HCl (14 mL). The solid was obtained by filtration, dried on high vacuum and then recrystallized with TFA (40 mL) and water (120 mL) to yield **II-5a** as a white solid (3.2 g, 2.65 mmol, 32%). M.p. > 310 ˚C (dec.). IR (ATR, cm^{-1}): 1707s, 1477m, 1313m, 1200m, 964m, 785s. ^{1}H NMR (400 MHz, DMSO-d^6): 6.74 (s, 4H), 5.56 (d, J = 14.8, 2H), 5.46 (d, J = 14.8, 4H), 5.35 (d, J = 9.6, 2H), 5.25 (d, J = 15.6, 4H), 5.24 (d, J = 9.6, 2H), 4.65 (m, 8H), 4.13 (d, J = 15.6, 4H), 4.03 (d, J = 14.8, 4H), 4.03 (d, J = 14.8, 2H), 1.65 (s, 6H), 1.63 (s, 6H). ^{13}C NMR (100 MHz, TFA, DMSO-d^6 as internal reference): δ 175.7, 157.0, 156.6, 149.5, 127.4, 113.7, 79.9, 78.3, 72.0, 71.4, 65.8, 53.2, 48.4, 35.0, 15.1, 14.3. HR-MS (ESI): *m/z* 1197.3548 ($[M + H]^+$), calculated 1197.3622.

Compound **II-5b:** A mixture of **II-4b** (2.90 g, 2.39 mmol), ethyl bromoacetate (3.20 g, 19.1 mmol) and anhydrous K_2CO_3 (6.62 g, 48.0 mmol) in MeCN (300 mL) was heated at reflux for 10 hrs. Solvent was removed under reduced pressure. Crude product was extracted with acetone (70 mL×3). After the solvent was removed with rotary evaporation, the crude product was washed with ethyl acetate (15 mL) to yield a white solid. And then this white solid was mixed with LiOH (0.400 g, 16.7 mmol) and

dissolved in MeOH and water mixture (1:1, v/v, 120 mL). The mixture was heated at 80 ^{o}C for 15 hrs. Solvent was removed with rotovapory evaporation. The crude solid was treated with water (60 mL) and conc. HCl (1.6 mL, 19.2 mmol) and then filtered to yield **II-5b** as a white solid (1.7 g, 1.2 mmol, 50%). M.p. > 248 ˚C (dec.). IR (ATR, cm^{-1}): 1713s, 1462s, 1380m, 1315m, 1224s, 1196s, 1094m, 971s, 863m, 801m, 696m. ^{1}H NMR (400 MHz, D_2O): 7.02-6.81 (m, 20H), 6.57 (s, 4H), 5.71 (d, *J* = 16.0, 4H), 5.58 (d, *J* = 15.2, 2H), 5.21 (d, *J* = 8.8, 2H), 5.09 (d, *J* = 15.2, 4H), 4.93 (d, *J* =8.8, 2H), 4.31 (d, *J* = 15.6, 4H), 4.28 (d, *J* = 15.2, 4H), 4.18 (d, *J* = 15.6, 4H), 4.10 (d, *J* = 16.0, 4H), 3.99 (d, *J* = 15.2, 2H). ^{13}C NMR (100 MHz, TFA, 1, 4-dioxane as internal reference): δ 173.7, 157.5, 155.0, 148.0, 128.3, 128.04, 127.3, 127.1, 126.3, 126.1, 125.4, 125.3, 112.4, 86.3, 85.3, 70.6, 69.6, 64.2, 52.2, 48.5, 35.3. HR-MS (ESI): *m/z* 1445.4252 ([M + H]$^{+}$), calculated 1445.4248.

Compound **II-6**: A mixture of **II-3a** (3.95 g, 5.06 mmol) and 3, 5-dimethyl phenol (2.50 g, 20.5 mmol) in TFA (10 mL) was heated at reflux for 1 h. The solvent was removed with rotovapory evaporation. The crude solid was washed with MeOH (50 mL). The product was extracted with conc. HCl (150 mL) to yield **II-6** as a white solid (1.5 g, 2.25 mmol, 45%). M.p. > 281 ºC (decomposed). IR (ATR, cm^{-1}): 1711s, 1455s, 1376m, 1221s, 1073m, 972m, 797s, 757m, 667m. ^{1}H NMR (400 MHz, D_2O): 5.65 (d, *J* = 15.5, 2H), 5.50 (d, *J* = 15.9, 4H), 5.42 (s, 4H), 4.15 (d, *J* = 16.6, 6H), 1.56 (s, 6H), 1.39 (s, 6H). ^{13}C NMR (100 MHz, 35% DCl): δ 155.8, 154.1, 79.3, 73.3, 68.0, 67.6, 49.4, 45.5, 18.6, 13.1. MS (ESI): *m/z* 697 ([M + H]$^{+}$).

2.5 Supporting Information

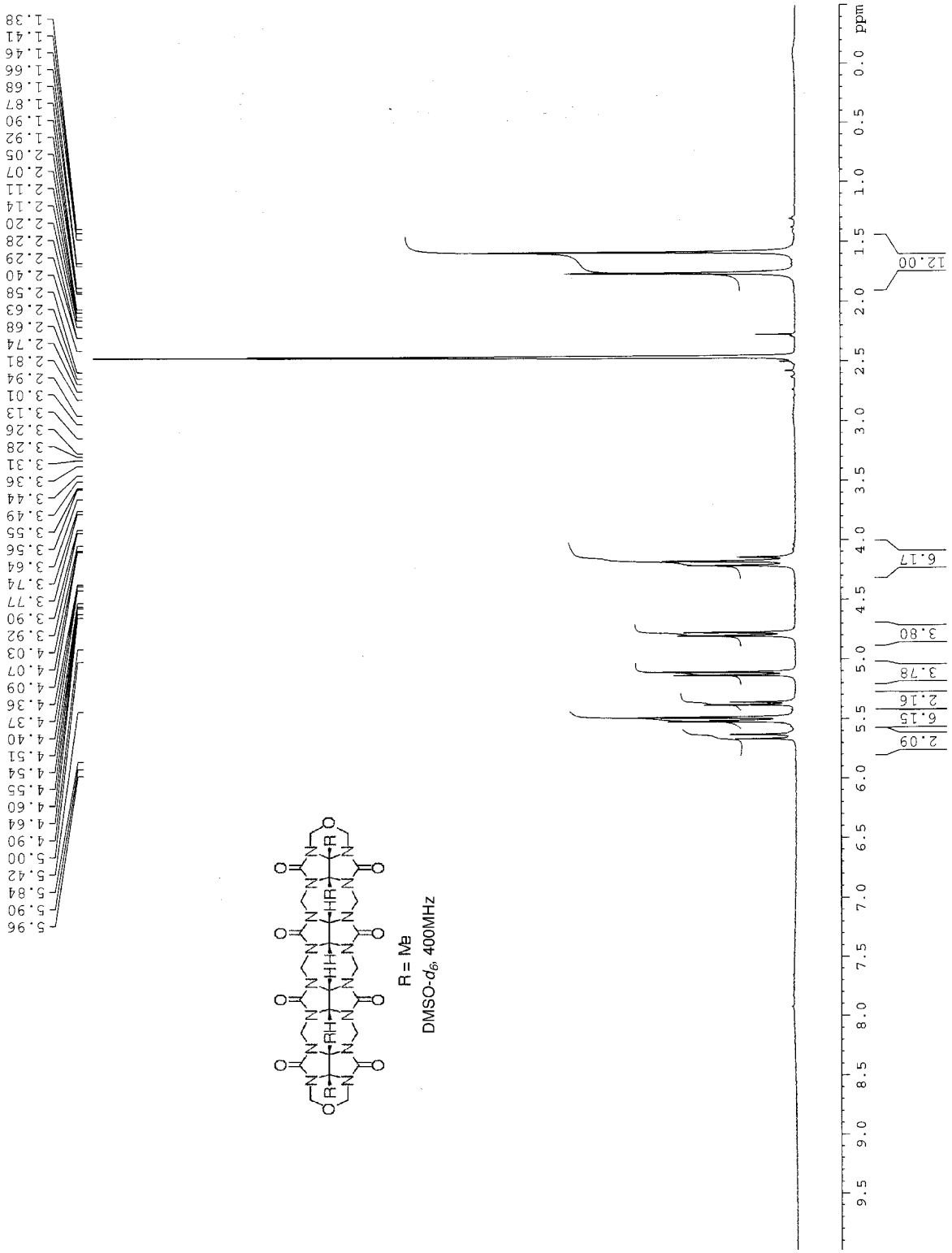

Figure II-S1. ^{1}H NMR spectrum (400 MHz, DMSO-d_6) recorded for **II-3a**.

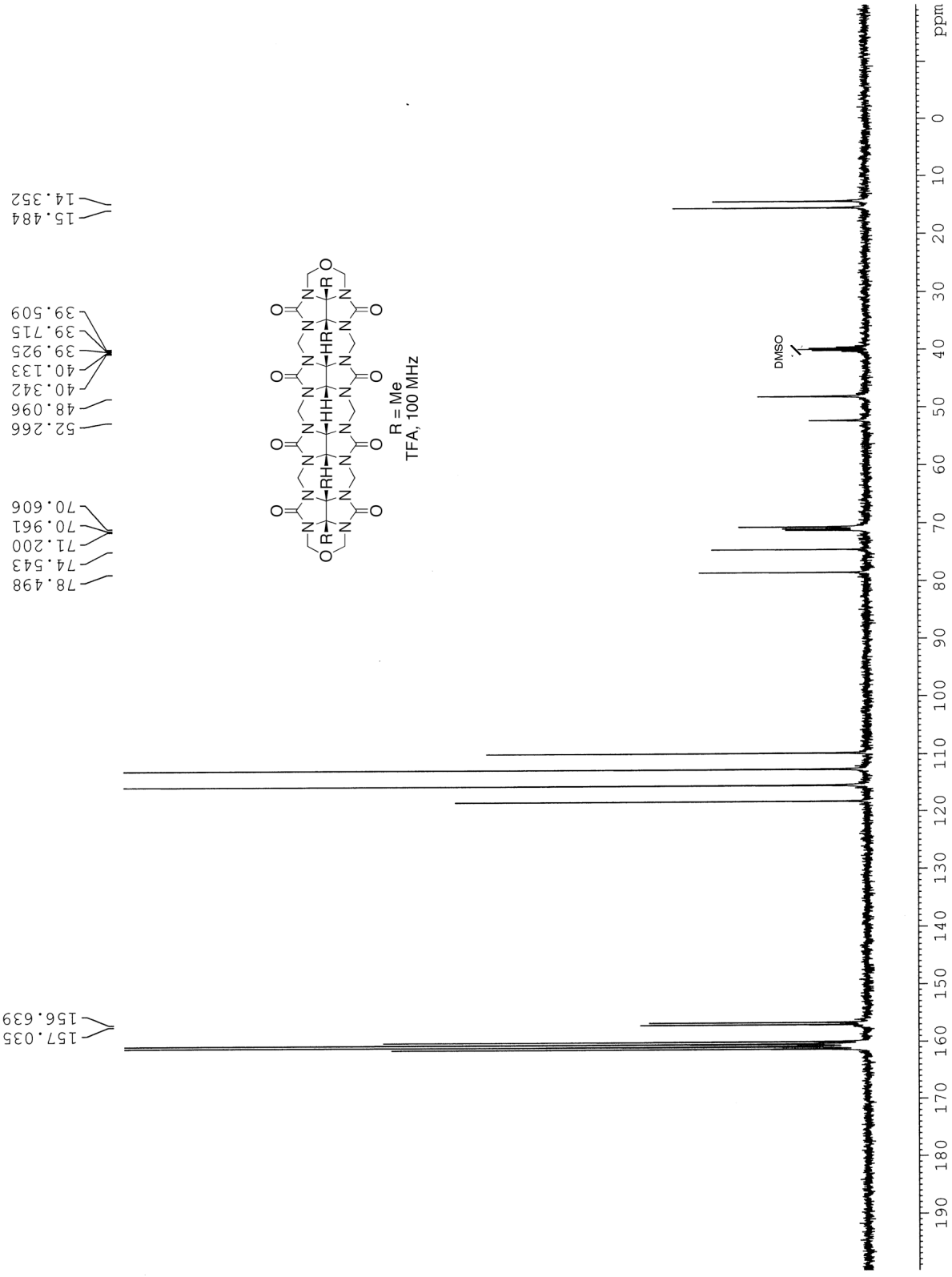

Figure II-S2. ^{13}C NMR spectrum (100 MHz, TFA, DMSO-d_6 as internal reference) recorded for **II-3a**.

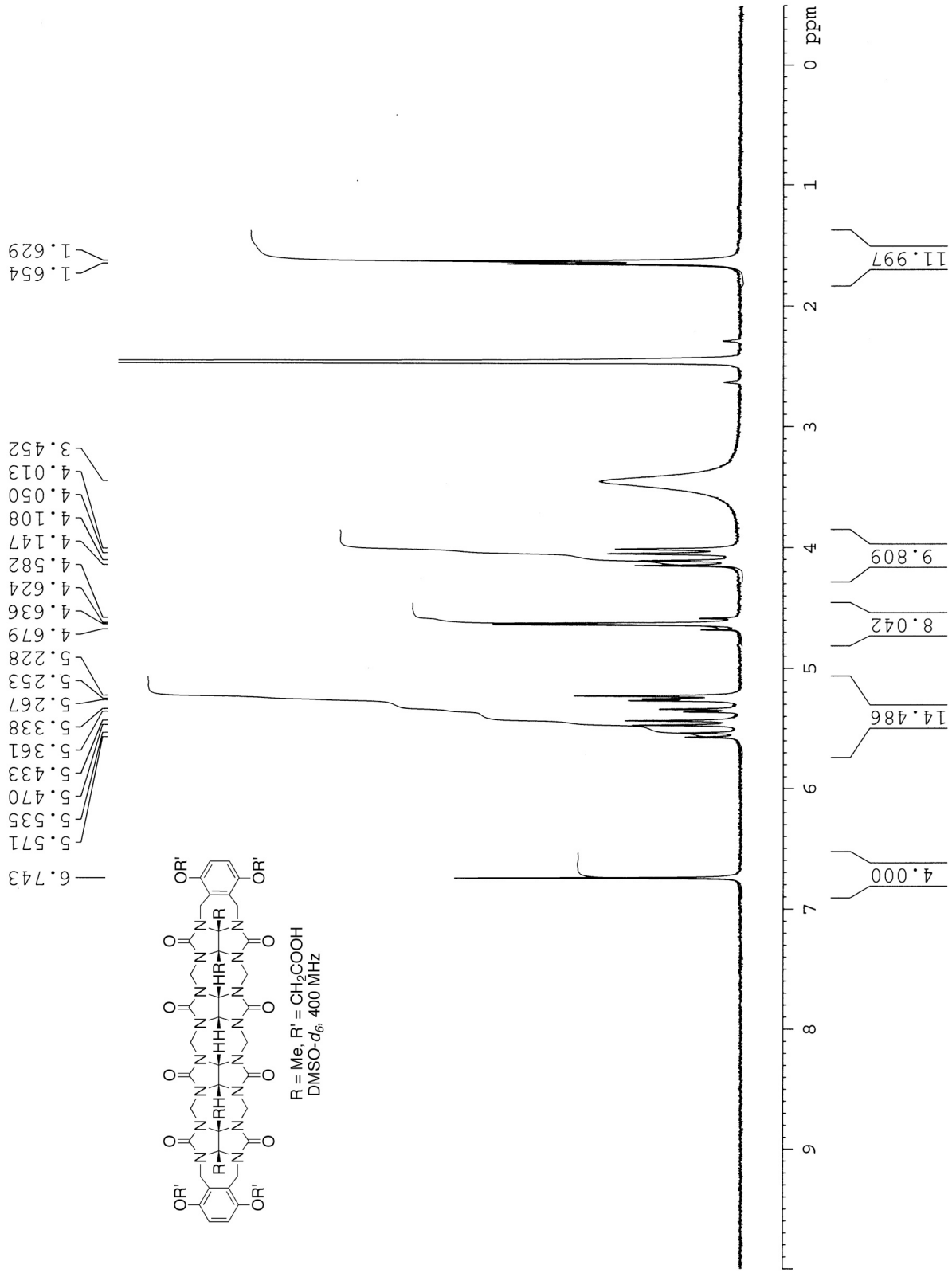

Figure II-S3. ^{1}H NMR spectrum (400 MHz, DMSO-d_6) recorded for **II-5a**

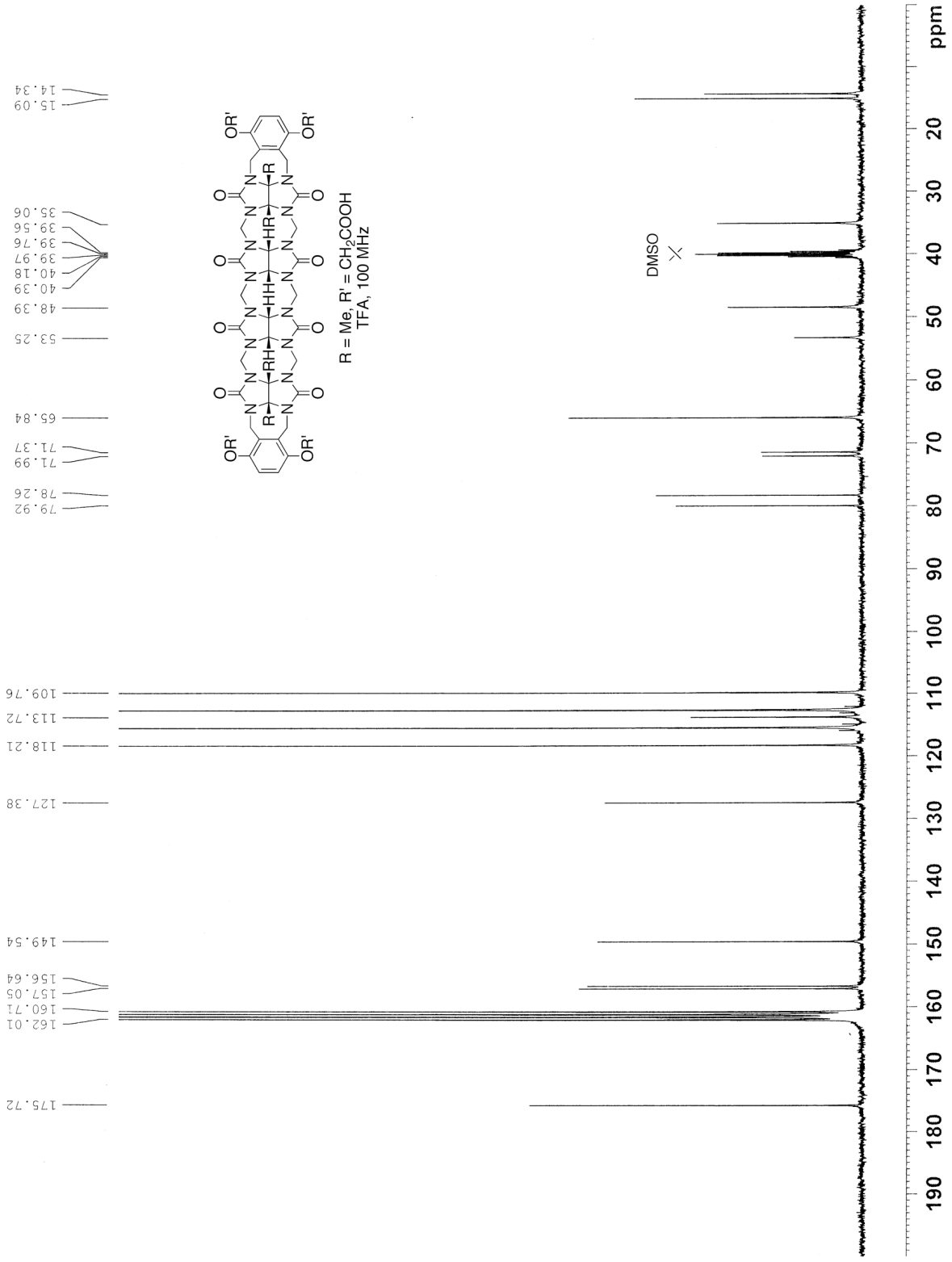

Figure II-S4. ^{13}C NMR spectrum (100 MHz, TFA, DMSO-d_6 as internal reference) recorded for **II-5a**.

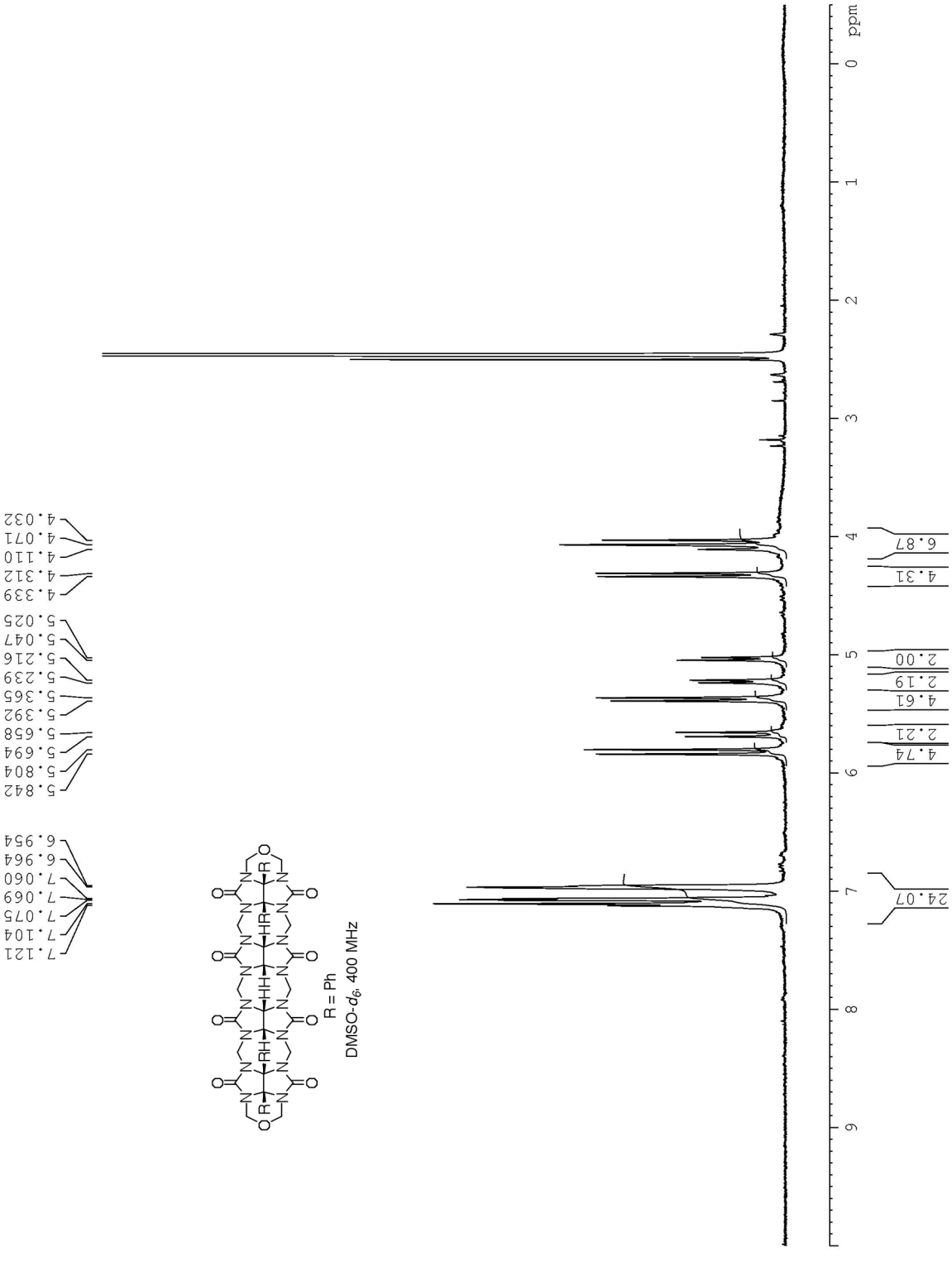

Figure II-S5. ^{1}H NMR spectrum (400 MHz, DMSO-d_6) recorded for **II-3b**.

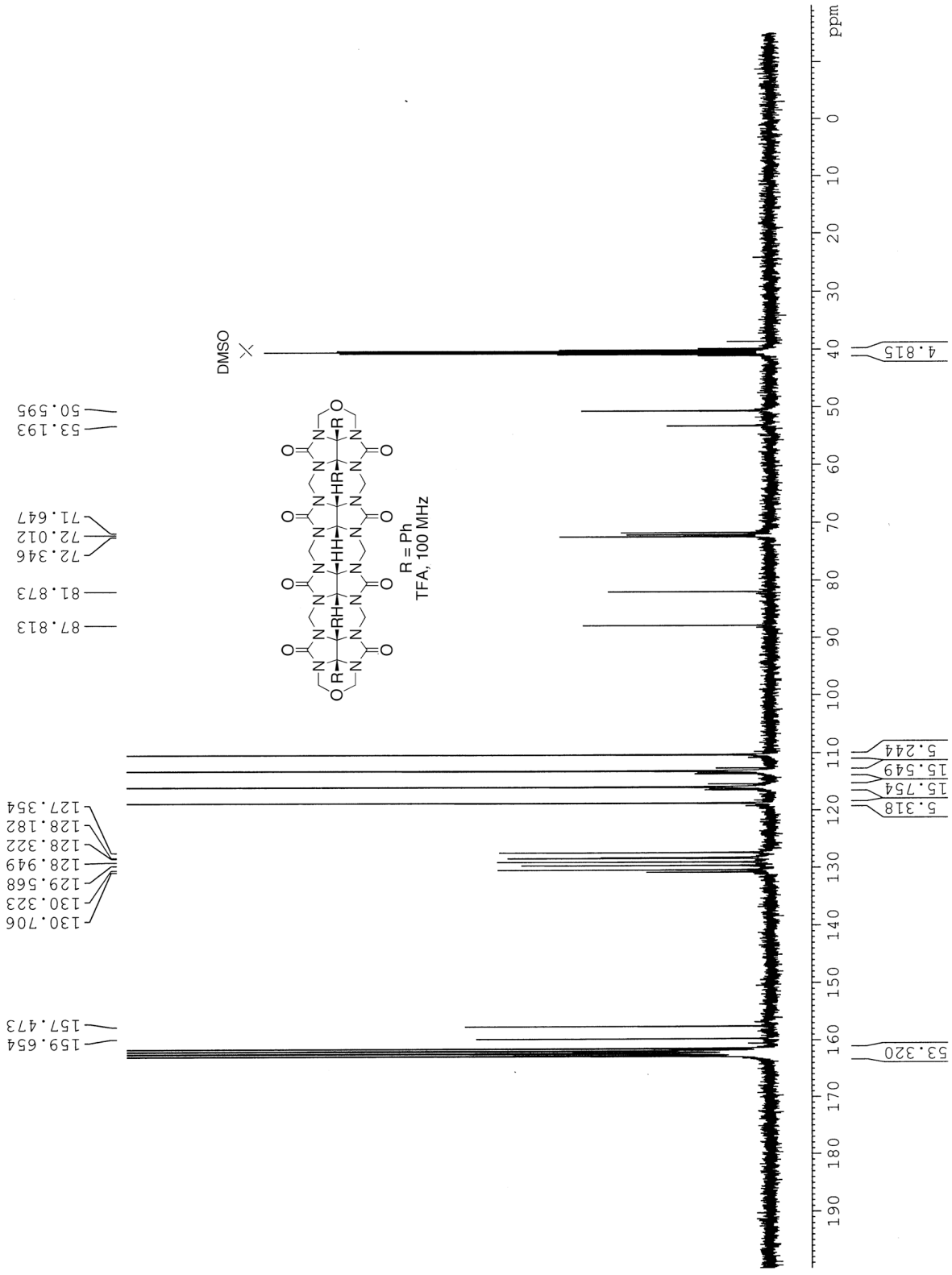

Figure II-S6. ^{13}C NMR spectrum (100 MHz, TFA, DMSO-d_6 as internal reference) recorded for **II-3b**.

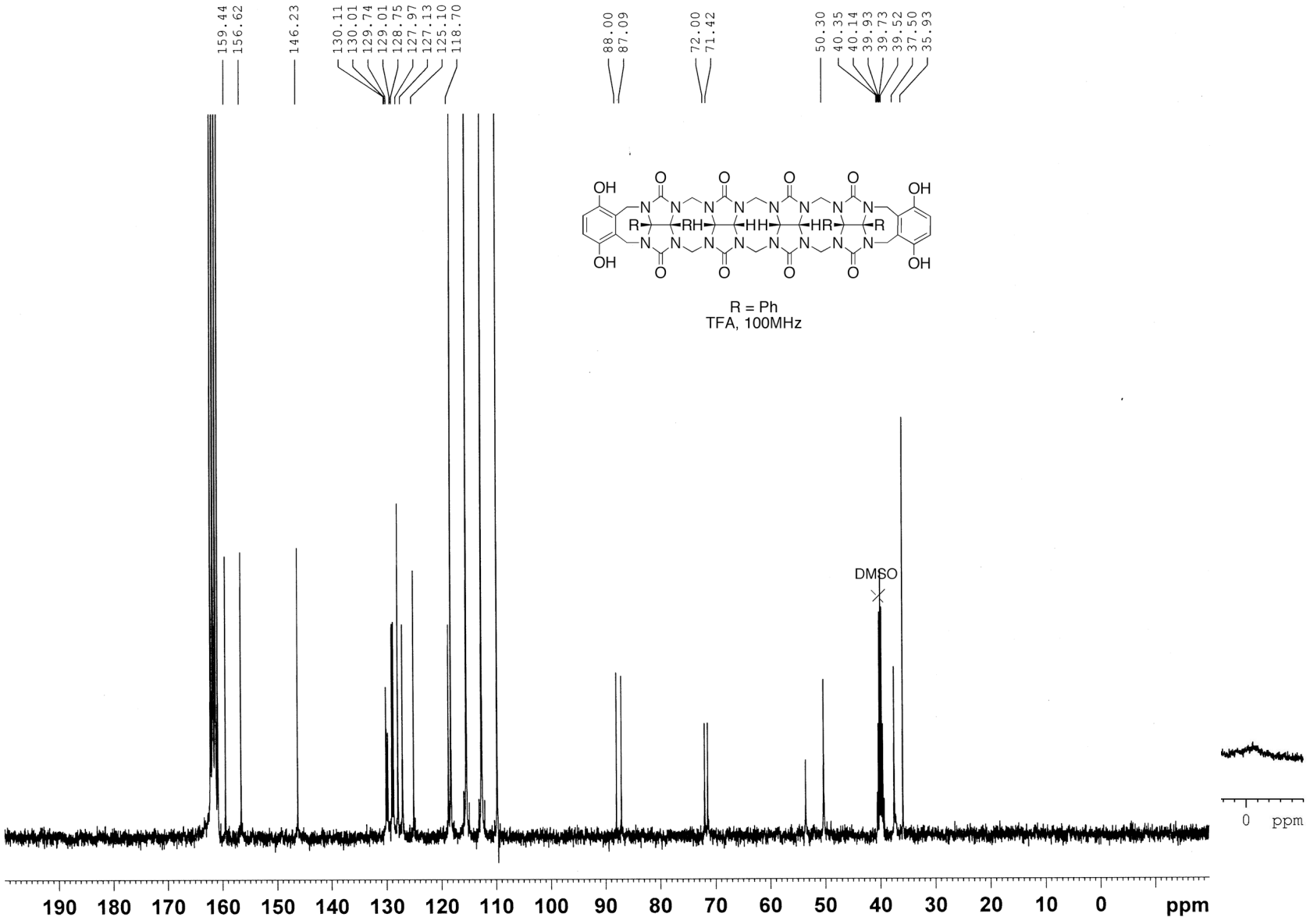
159.44
156.62
146.23
130.11
130.01
129.74
129.01
128.75
127.97
127.13
125.10
118.70
88.00
87.09
72.00
71.42
50.30
40.35
40.14
39.93
39.73
39.52
37.50
35.93
OH
OH
OH
OH
R
RH
HH
HR
R
R = Ph
TFA, 100MHz
DMSO
0 ppm
190 180 170 160 150 140 130 120 110 100 90 80 70 60 50 40 30 20 10 0 ppm

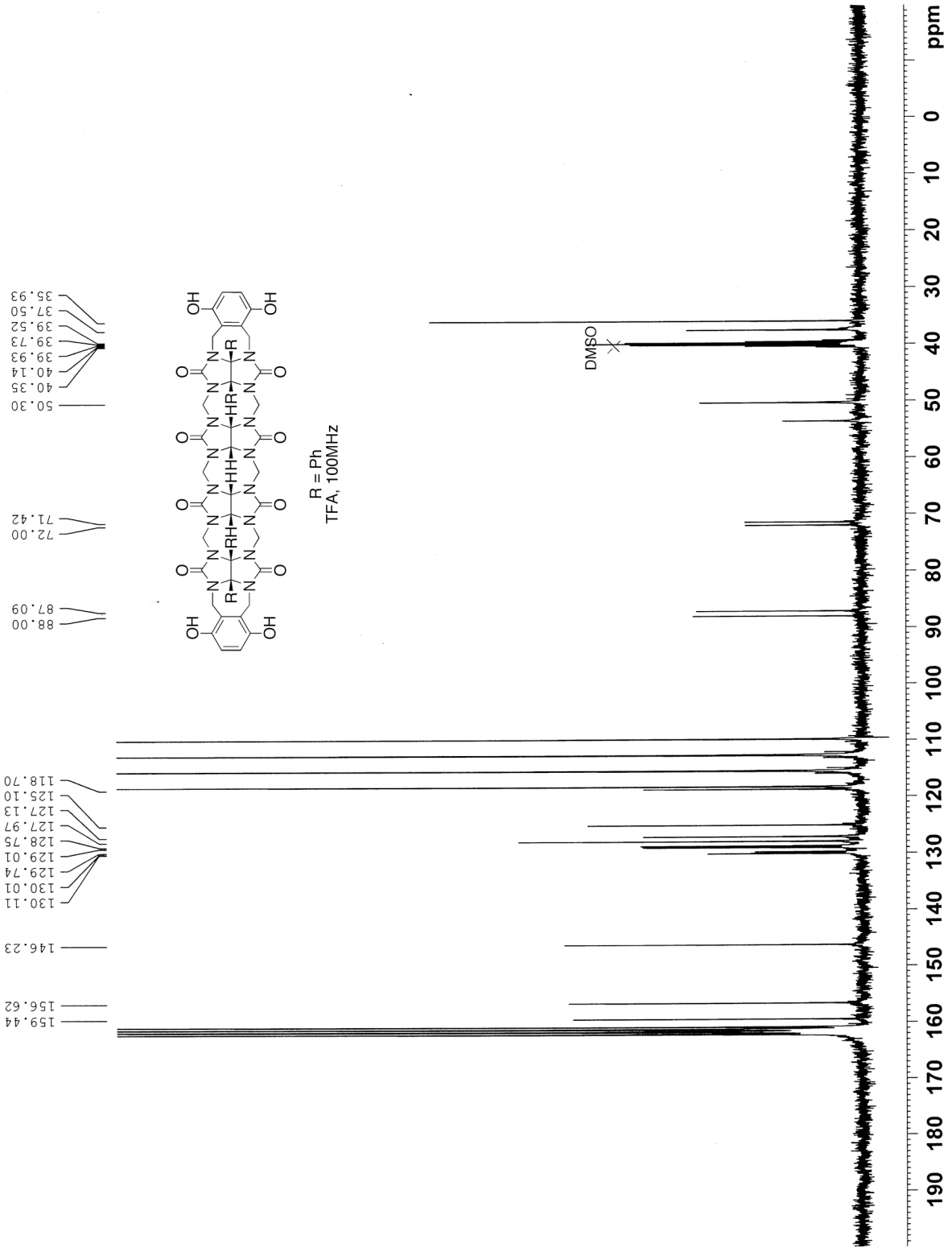

Figure II-S8. ^{13}C NMR spectrum (100 MHz, TFA, DMSO-d_6 as internal reference) recorded for **II-4b**.

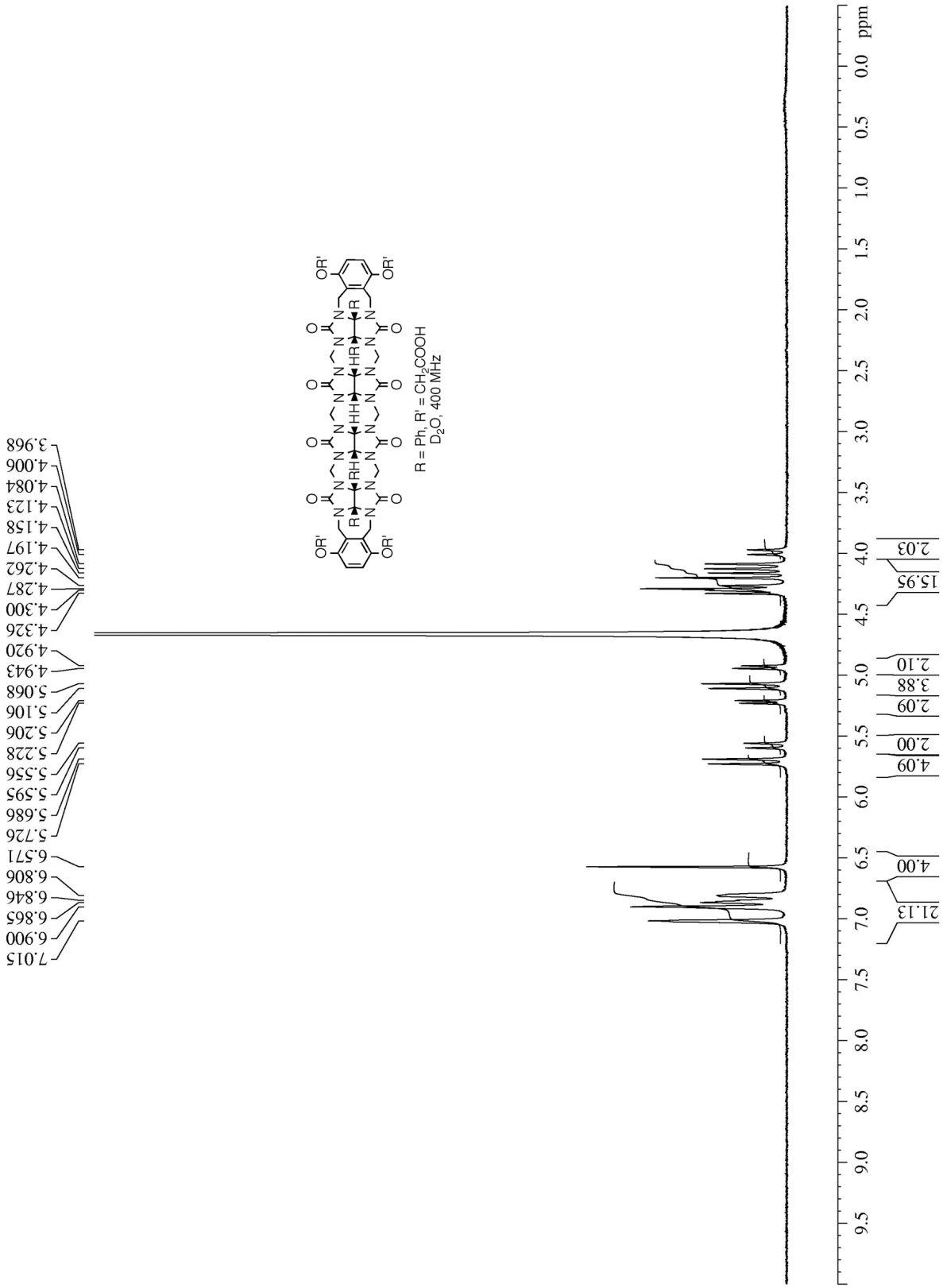

Figure II-S9. ^{1}H NMR spectrum (400 MHz, D_2O) recorded for **II-5b**.

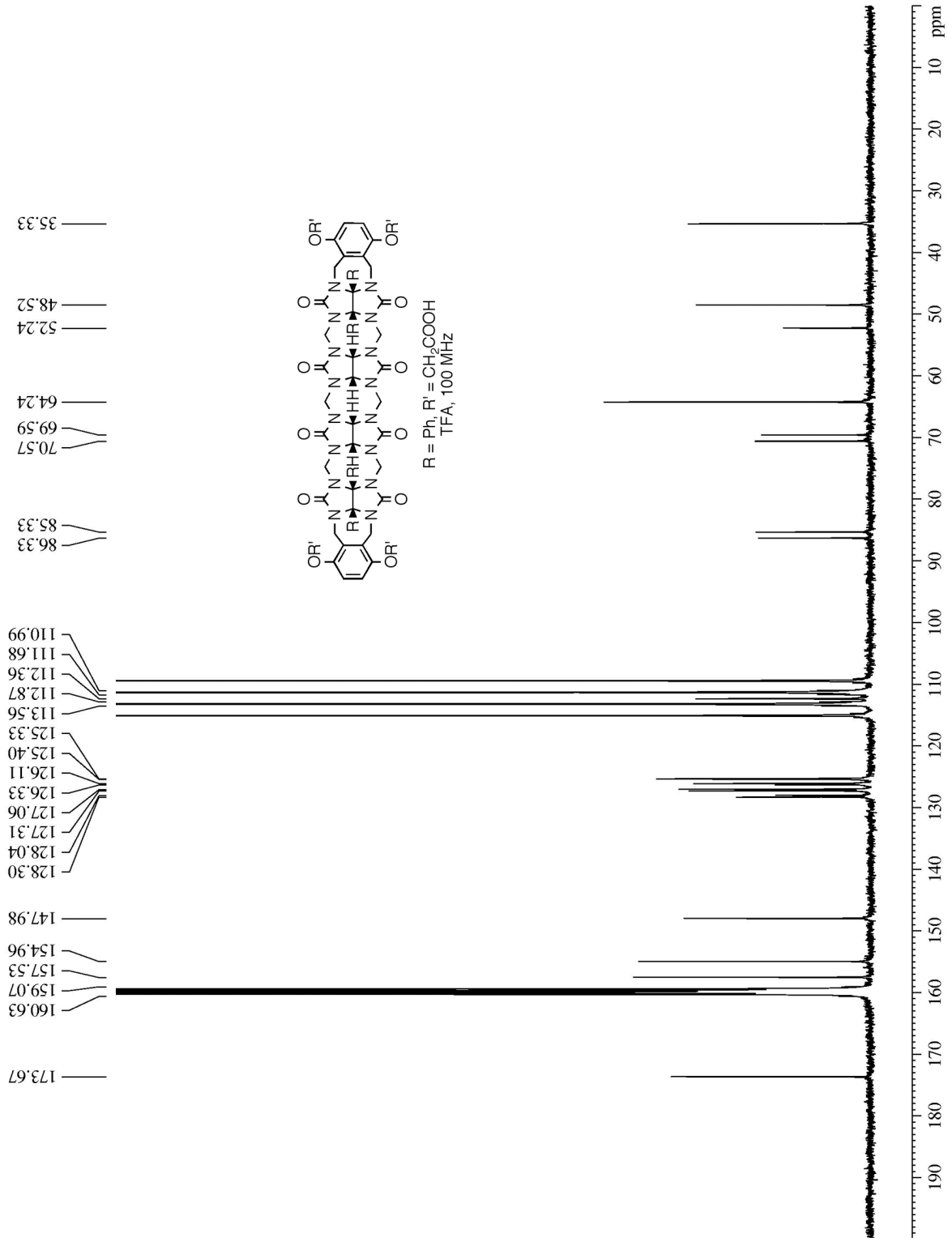

Figure II-S10. ^{13}C NMR spectraum (100 MHz, TFA, 1, 4-dioxane as internal reference) recorded for **II-5b**.

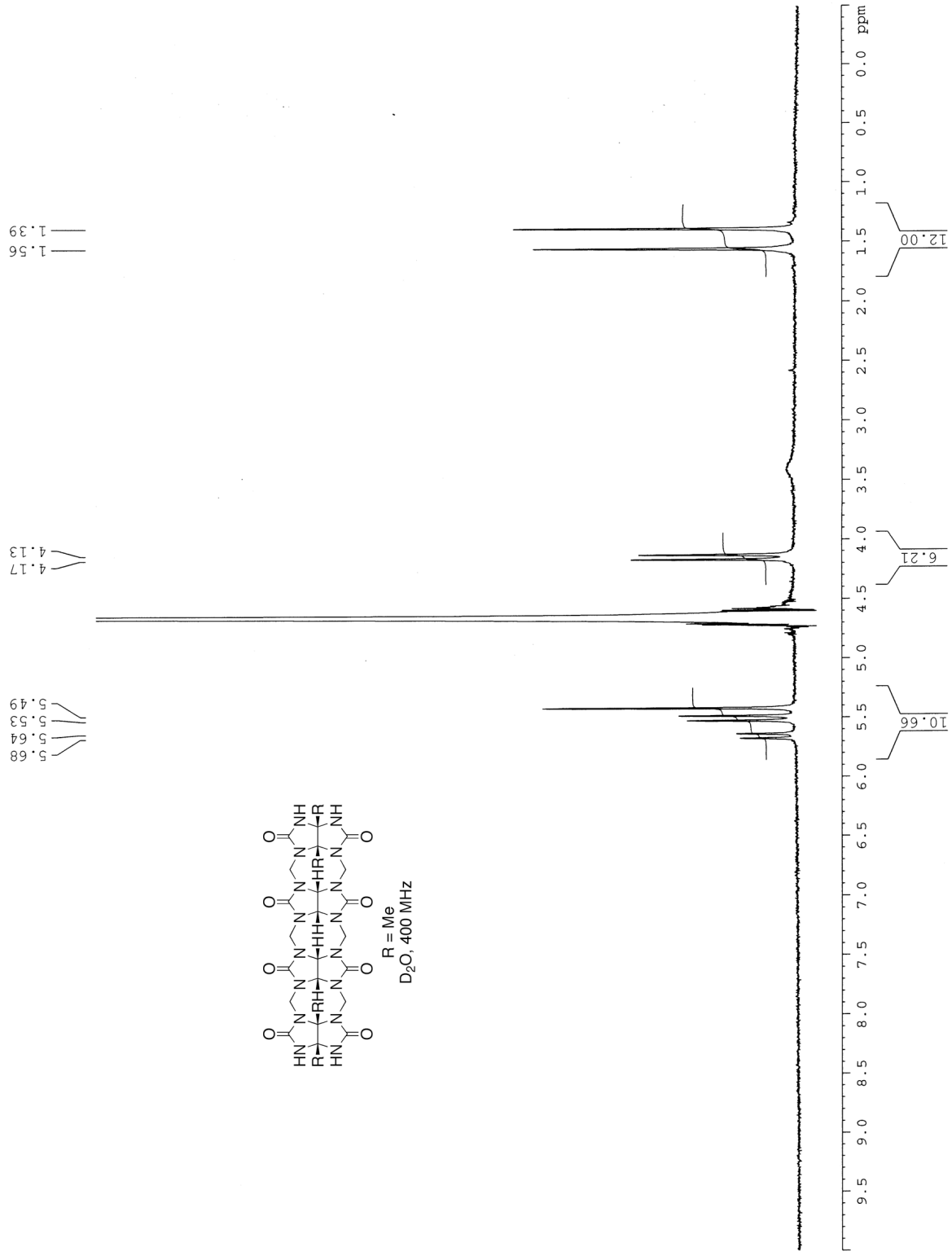

Figure II-S11. ^{1}H NMR spectrum (400 MHz, D_2O) recorded for **II-6**.

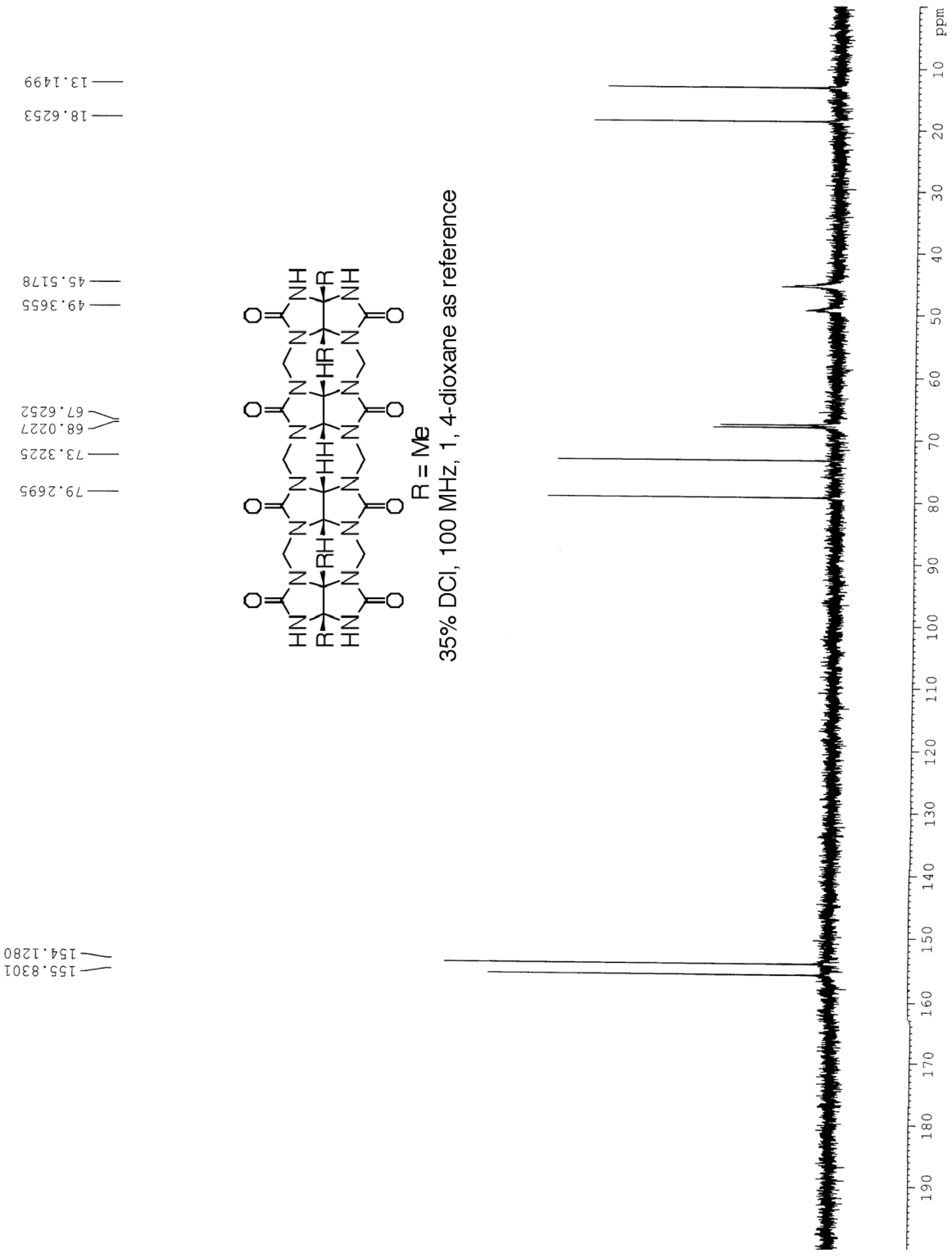

Figure II-S12. ^{13}C NMR spectrum (100 MHz, 35% DCl, 1, 4-dioxane as internal reference) recorded for **II-6**.

Determination of binding constants:

1:1 Binding Models Used in Scientist.

All calculations were performed on a personal computer running Scientist.

Models used to calculate the binding constant of dyes and **II-5a** or **II-5b**.

// Micromath Scientist Model File

// 1:1 Host:Guest binding model

//This model assumes the guest concentration is fixed and host concentration is varied IndVars: ConcHostTot

DepVars: SpectroscopicSignal

Params: Ka, ConcGuestTot, SpectroscopicSignalMin, SpectroscopicSignalMax

Ka = ConcHostGuest/(ConcHostFree*ConcGuestFree)

ConcHostTot=ConcHostFree + ConcHostGuest

ConcGuestTot=ConcGuestFree + ConcHostGuest

SpectroscopicSignal = SpectroscopicSignalMin + (SpectroscopicSignalMax - SpectroscopicSignalMin) * (ConcHostGuest/ConcGuestTot)

//Constraints

0 < ConcHostFree < ConcHostTot

0 < Ka

0 < ConcGuestFree < ConcGuestTot

0 < ConcHostGuest < ConcHostTot

Models used to calculate the binding constant of guests and **II-5a** or **II-5b** using displacement assay.

// MicroMath Scientist Model File

IndVars: ConcAntot

DepVars: Absorb

Params: ConcHtot, ConcGtot, Khg, Kha, AbsorbMax, AbsorbMin

Khg = ConcHG / (ConcH * ConcG)

Kha = ConcHAn / (ConcH * ConcAn)

Absorb = AbsorbMin + (AbsorbMax-AbsorbMin)*(ConcHG/ConcGtot)

ConcHtot = ConcH + ConcHG + ConcHAn

ConcGtot = ConcHG + ConcG

ConcAntot = ConcAn + ConcHAn

0 < ConcHG < ConcHtot

0 < ConcH < ConcHtot

0 < ConcG < ConcGtot

0 < ConcAn < ConcAntot

***

Models used to calculate the binding constant of guests **II-11** and **II-20** with host **II-6** using NMR titration.

// Micromath Scientist Model File

// 1:1 Host:Guest binding model for NMR

//This model assumes the guest concentration is fixed and host concentration is varied

IndVars: ConcHostTot

DepVars: Deltaobs

Params: Ka, ConcGuestTot, Deltasat, Deltazero

Ka = ConcHostGuest/(ConcHostFree*ConcGuestFree)

ConcHostTot=ConcHostFree + ConcHostGuest

ConcGuestTot=ConcGuestFree + ConcHostGuest

Deltaobs = Deltazero + (Deltasat - Deltazero) * (ConcHostGuest/ConcGuestTot)

//Constraints

0 < ConcHostFree < ConcHostTot

0 < Ka

0 < ConcGuestFree < ConcGuestTot

0 < ConcHostGuest < ConcHostTot

***

(A)

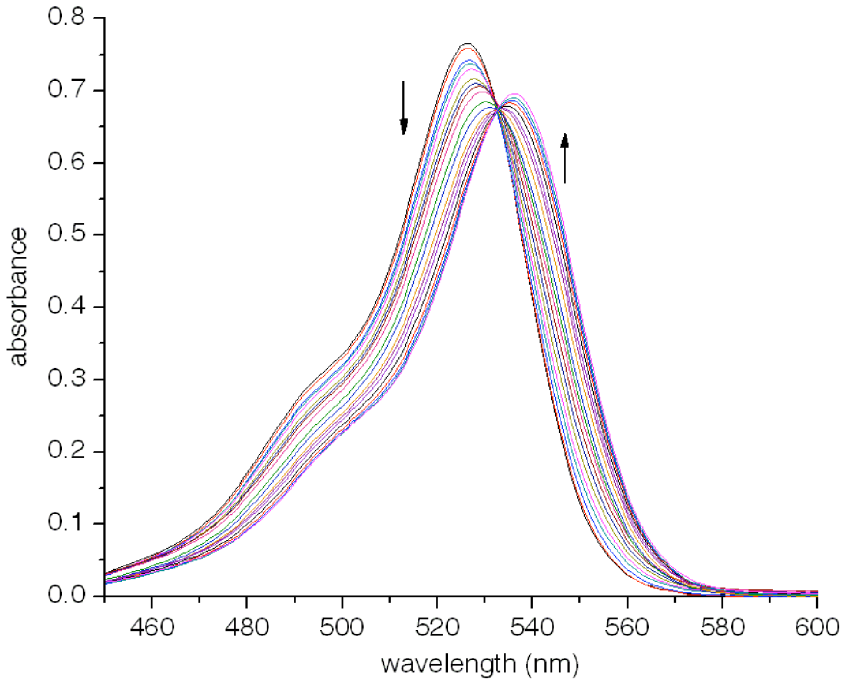

(B)

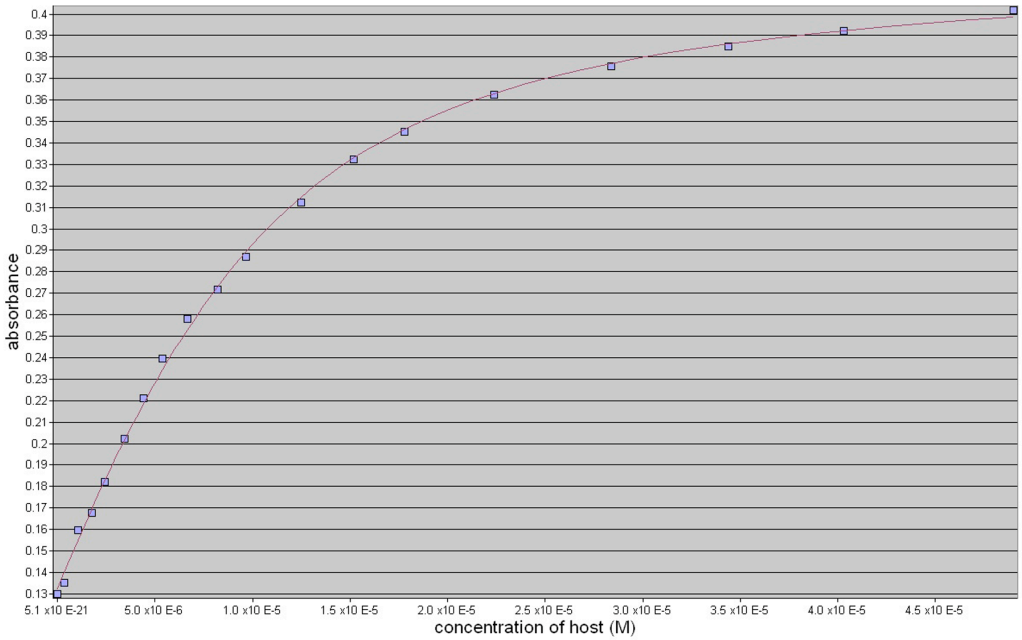

Figure II-S13. (A) UV/Vis spectra from the titration of dye **II-7** (9.23 µM) with **II-5a** (0 – 48 µM) in 20 mM NaH_2PO_4 buffer (pH 7.4); (B) plot of the ΔA_{550} as a function of **II-5a** concentration. The solid line represents the best non-linear fit of the data to a 1:1 binding model ($K_a = 2.1 \pm 0.1 \times 10^5\ M^{-1}$).

(A)

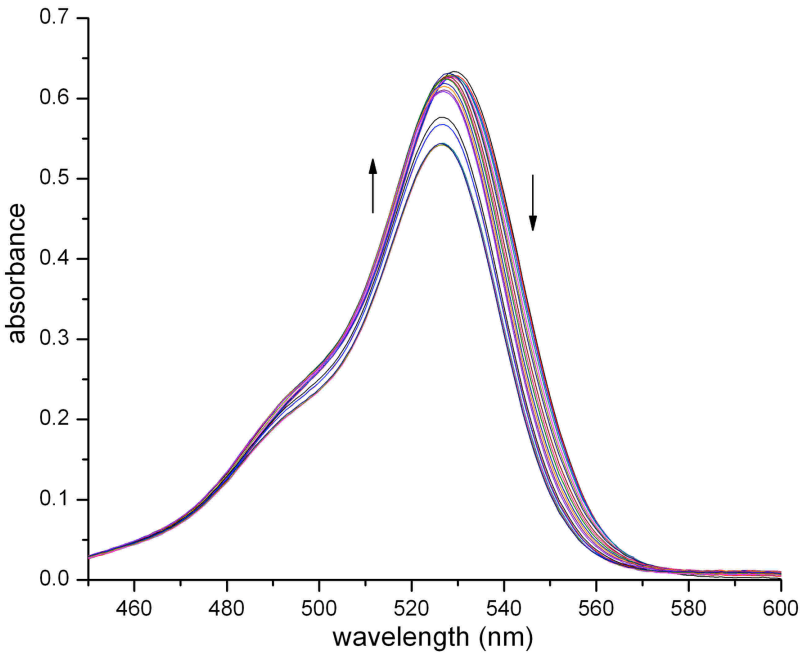

(B)

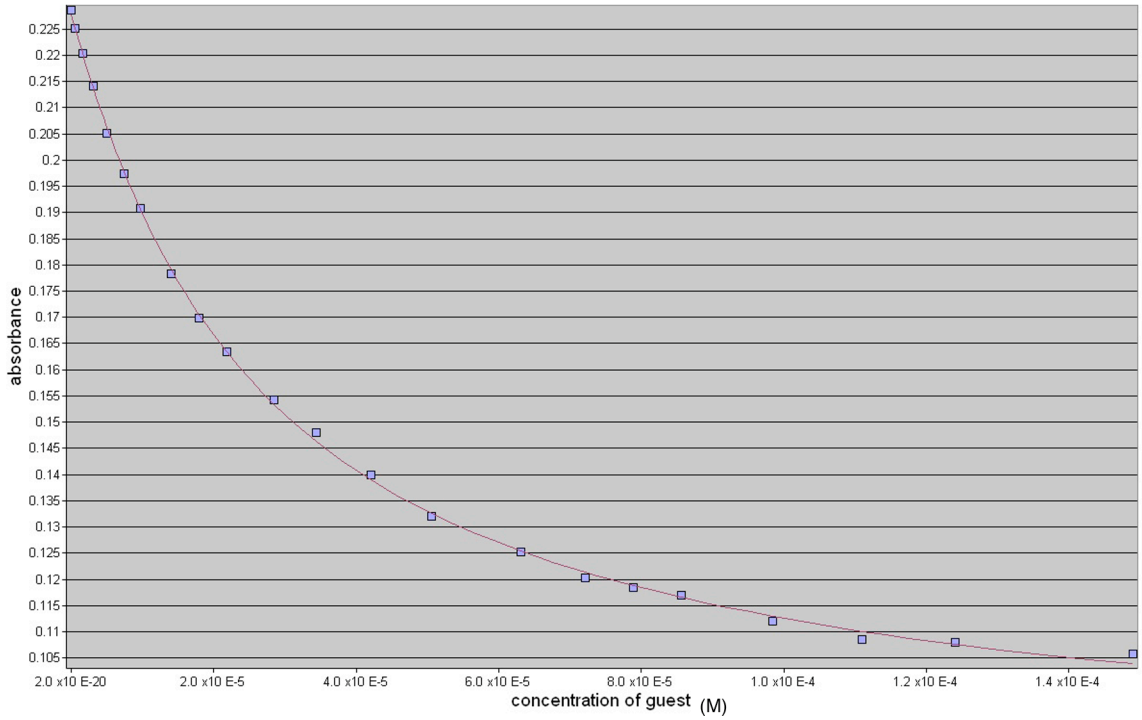

Figure II-S14. Displacement titration of a solution of dye **II-7** (9.23 μM) and **II-5a** (7.28 μM) solution with **II-26** (0 – 0.15 mM) (20 mM NaH_2PO_4 buffer, pH 7.4): (A) spectral change, (B) Non-linear fitting plot of absorbance *versus* concentration for the displacement titration of **II-26** with Scientist^{TM}. K_a was evaluated as $1.4 \pm 0.1 \times 10^5\ M^{-1}$.

(A)

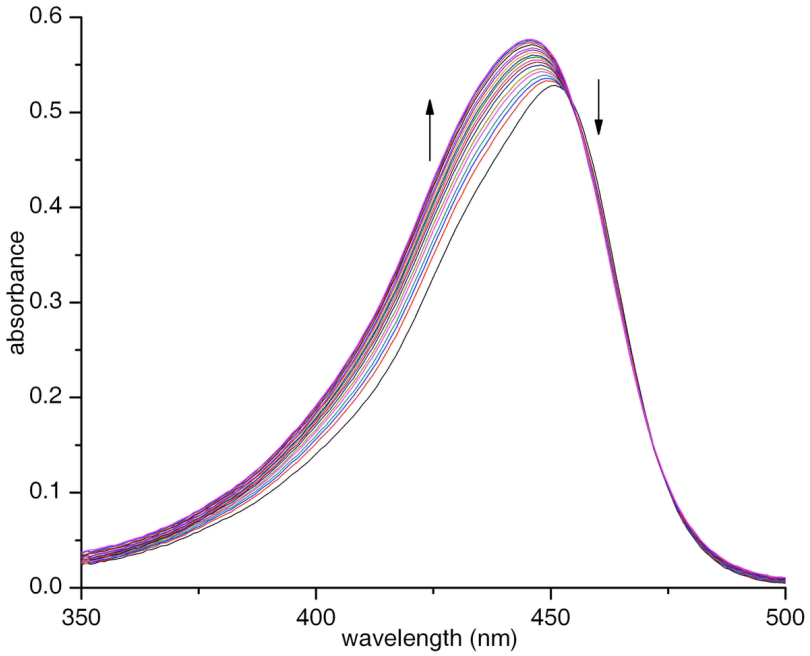

(B)

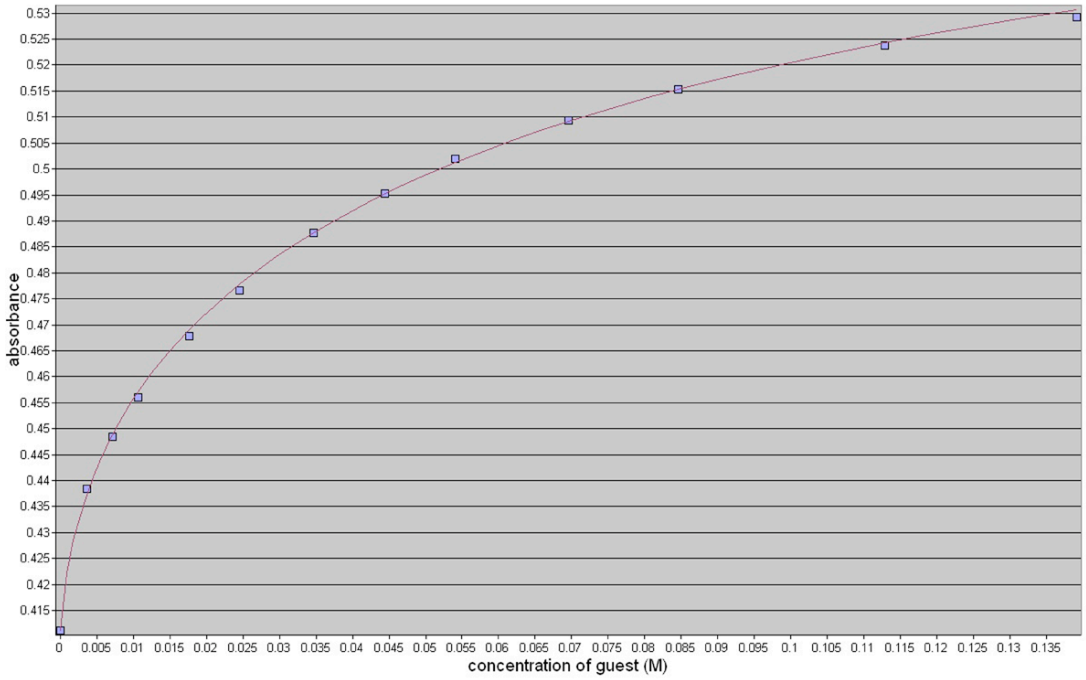

Figure II-S15. Displacement titration of a solution of dye **II-8** (18.62 μM) and **II-5a** (17.04 μM) solution with **II-26** (0 – 0.14 M) (20 mM NaH_2PO_4 buffer, pH 7.4): (A) spectral change, (B) Non-linear fitting plot of absorbance *versus* concentration for the displacement titration of **II-26** with Scientist^{TM}. K_a was evaluated as $7.2 \pm 0.4 \times 10^8\ M^{-1}$.

(A)

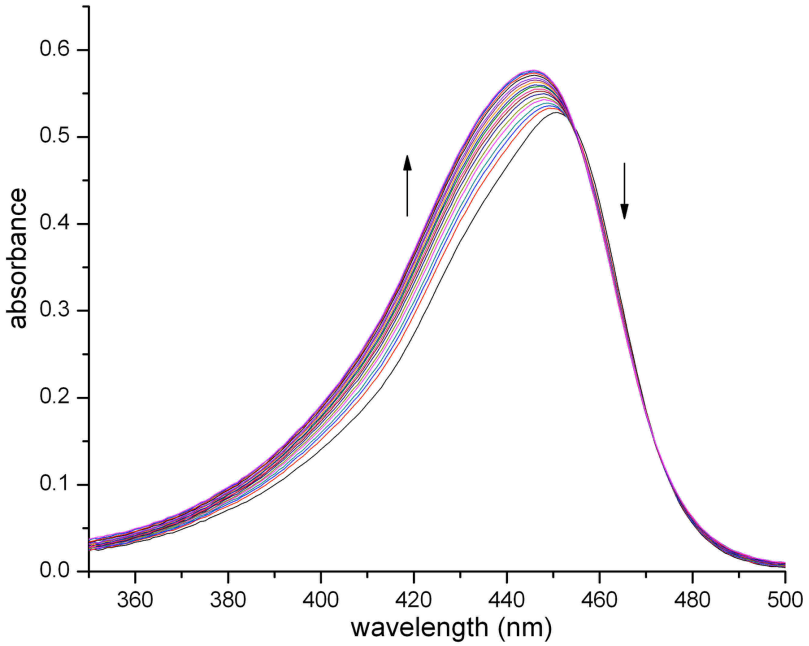

(B)

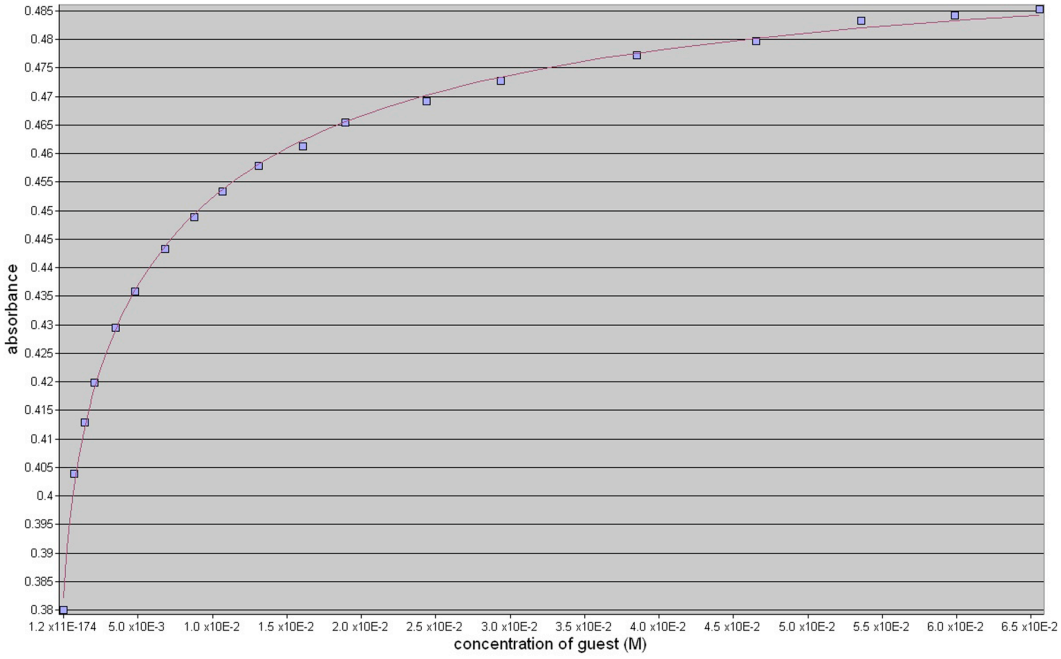

Figure II-S16. Displacement titration of a solution of dye **II-8** (17.77 μM) and **II-5a** (13.16 μM) solution with **II-9** (0 - 65 mM) (20 mM NaH_2PO_4 buffer, pH 7.4): (A) spectral change, (B) Non-linear fitting plot of absorbance *versus* concentration for the displacement titration of **II-9** with Scientist^{TM}. K_a was evaluated as $1.4 \pm 0.1 \times 10^6\ M^{-1}$.

(A)

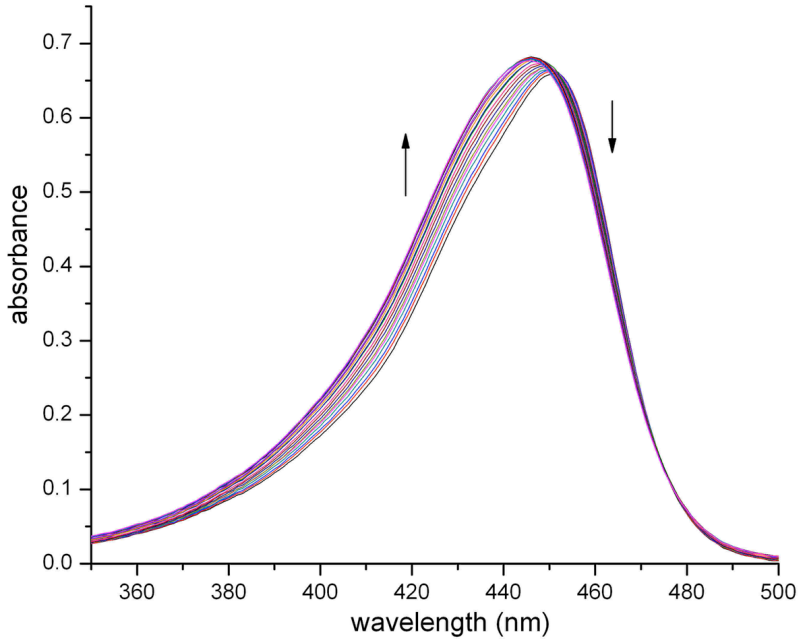

(B)

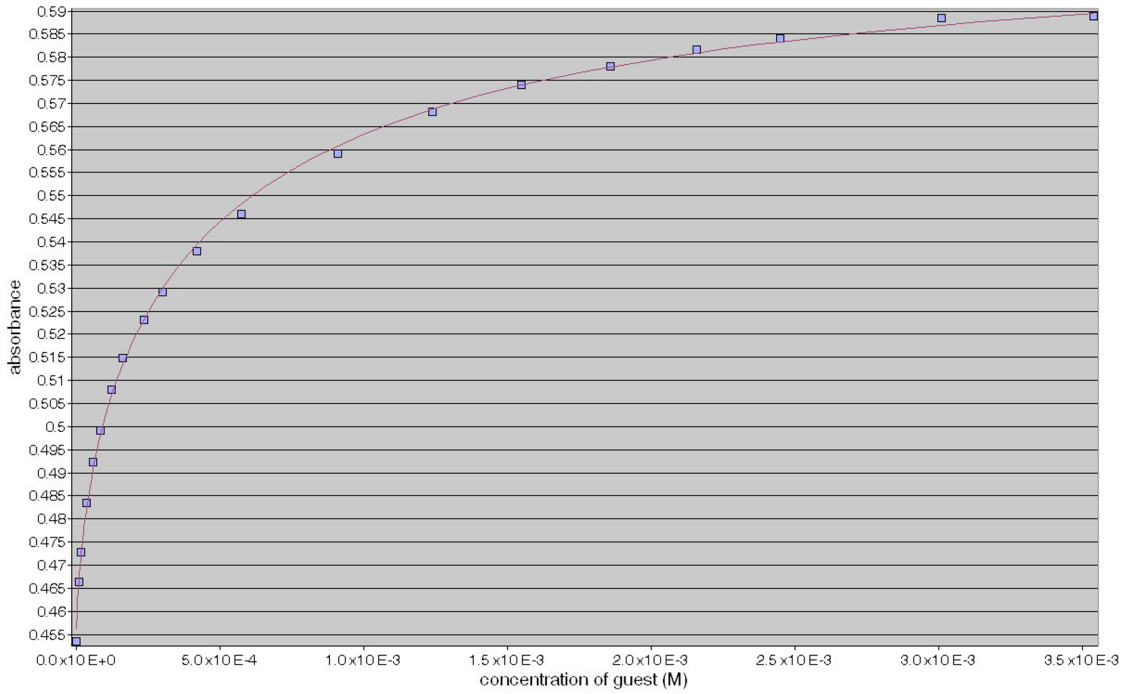

Figure II-S17. Displacement titration of a solution of dye **II-8** (21.75 μM) and **II-5a** (18.83 μM) solution with **II-10** (0 – 3.6 mM) (20 mM NaH_2PO_4 buffer, pH 7.4): (A) spectral change, (B) Non-linear fitting plot of absorbance *versus* concentration for the displacement titration of **II-10** with Scientist^{TM}. K_a was evaluated as $2.8 \pm 0.3 \times 10^7$ M^{-1}.

(A)

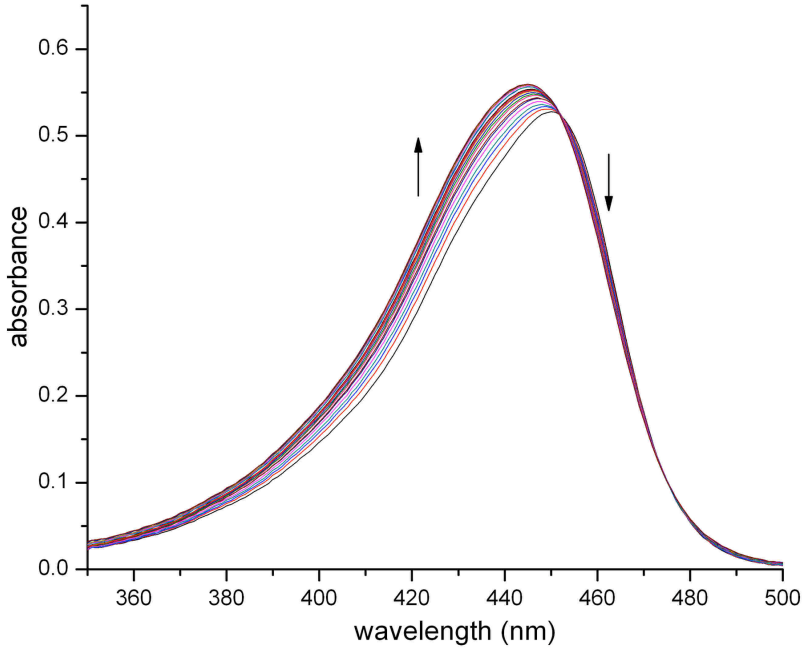

(B)

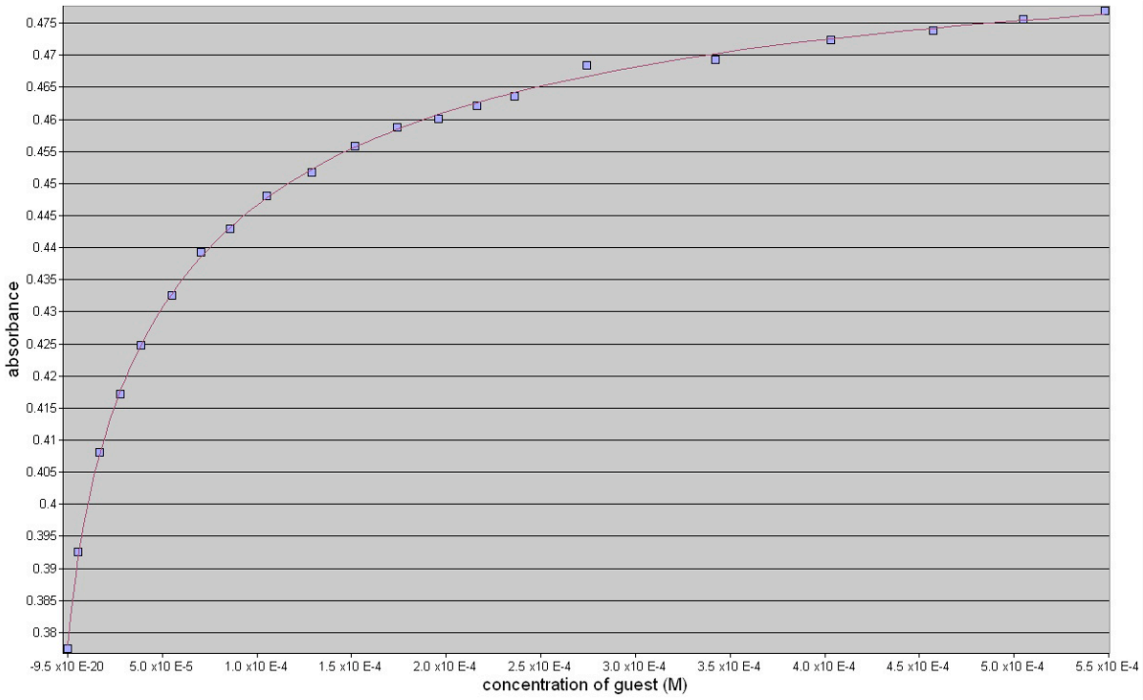

Figure II-S18. Displacement titration of a solution of dye **II-8** (17.77 μM) and **II-5a** (13.16 μM) solution with **II-11** (0 - 550 μM) (20 mM NaH_2PO_4 buffer, pH 7.4): (A) spectral change, (B) Non-linear fitting plot of absorbance *versus* concentration for the displacement titration of **II-11** with Scientist^{TM}. K_a was evaluated as $1.6 \pm 0.1 \times 10^8$ M^{-1}.

(A)

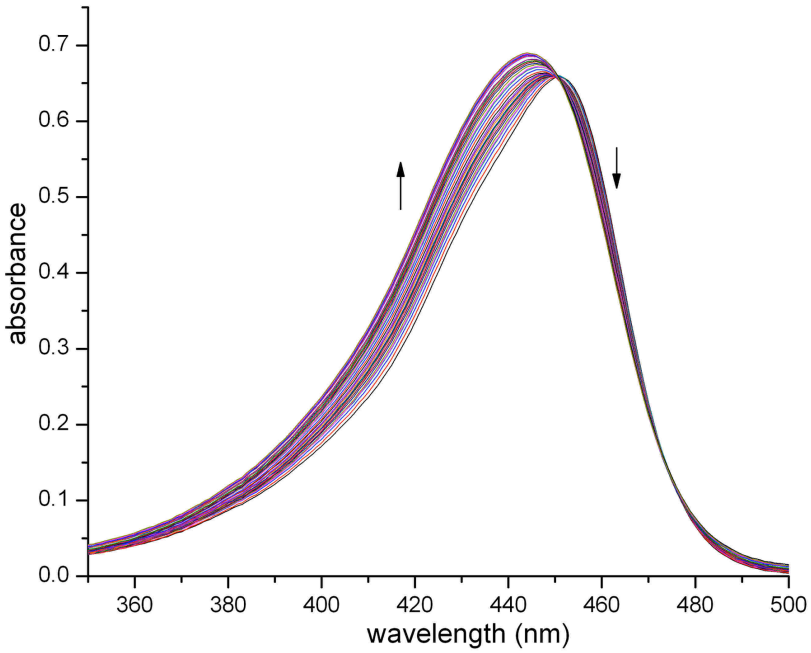

(B)

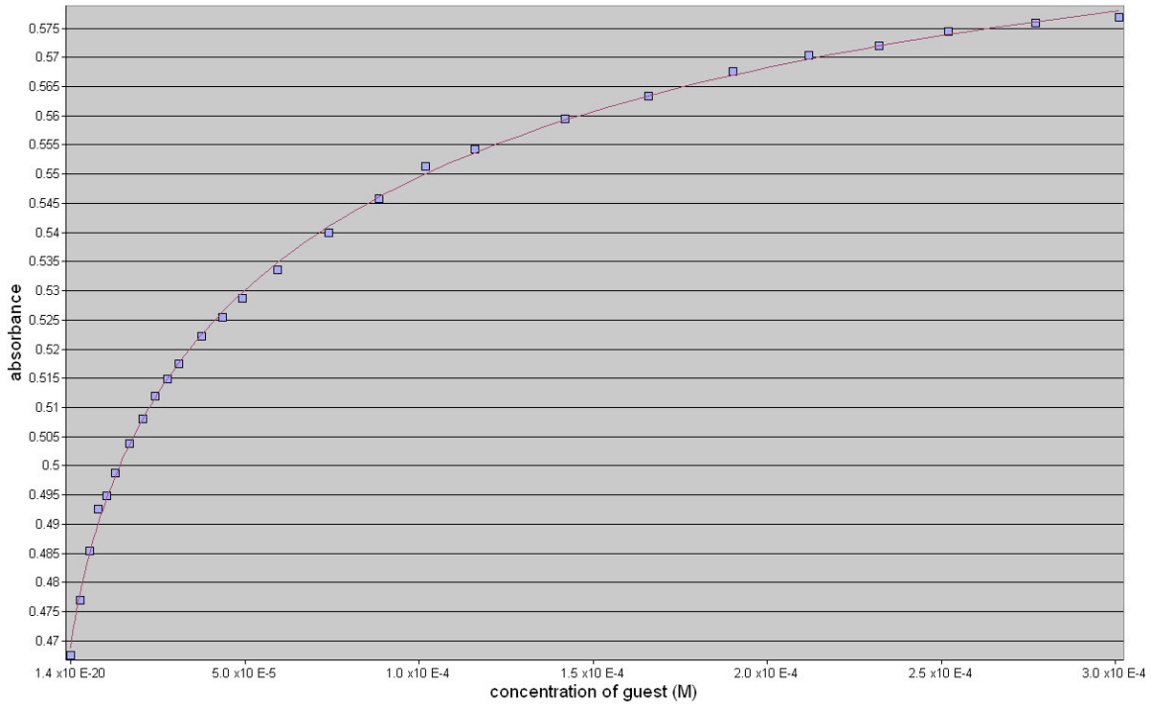

Figure II-S19. Displacement titration of a solution of dye **II-8** (21.75 μM) and **II-5a** (18.82 μM) solution with **II-12** (0 - 305 μM) (20 mM NaH_2PO_4 buffer, pH 7.4): (A) spectral change, (B) Non-linear fitting plot of absorbance *versus* concentration for the displacement titration of **II-12** with Scientist^{TM}. K_a was evaluated as $1.4 \pm 0.1 \times 10^8$ M^{-1}.

(A)

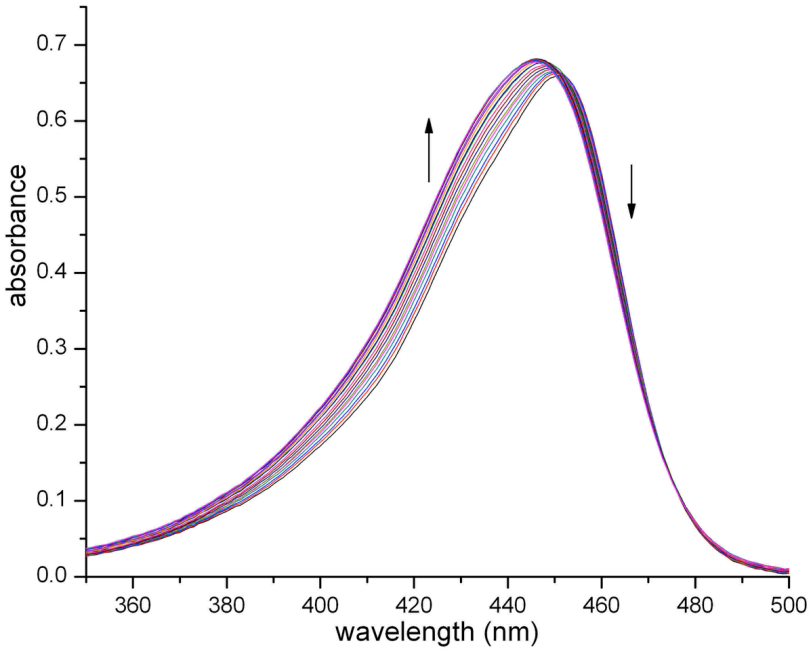

(B)

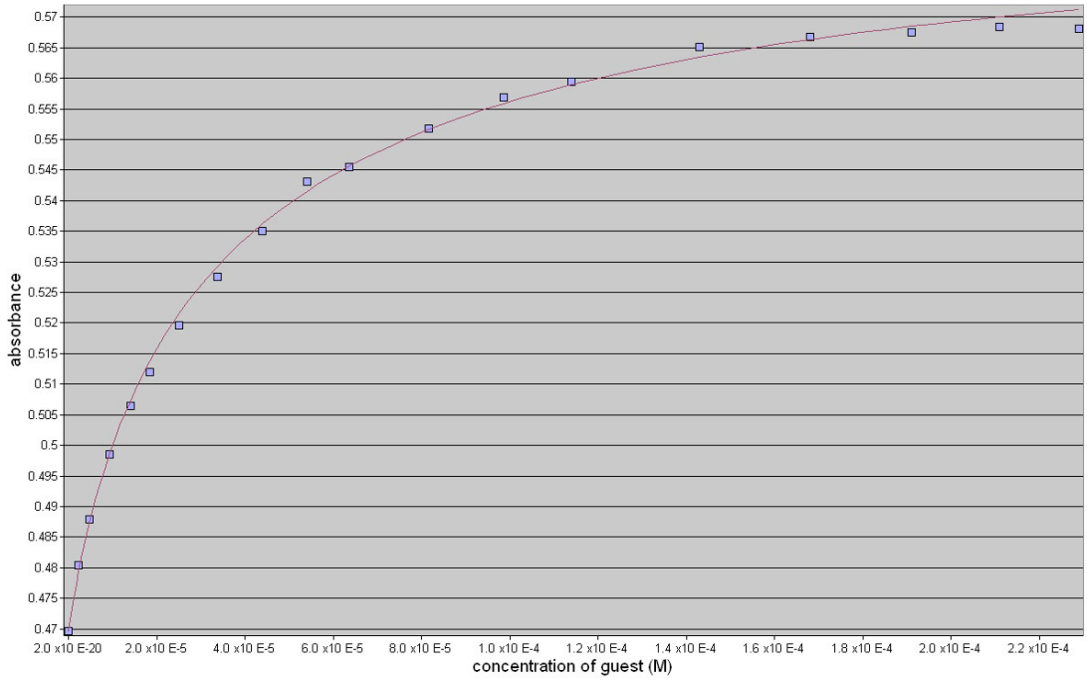

Figure II-S20. Displacement titration of a solution of dye **II-8** (21.75 μM) and **II-5a** (18.83 μM) solution with **II-13** (0 - 230 μM) (20 mM NaH_2PO_4 buffer, pH 7.4): (A) spectral change, (B) Non-linear fitting plot of absorbance *versus* concentration for the displacement titration of **II-13** with Scientist^{TM}. K_a was evaluated as $3.6 \pm 0.4 \times 10^8$ M^{-1}.

(A)

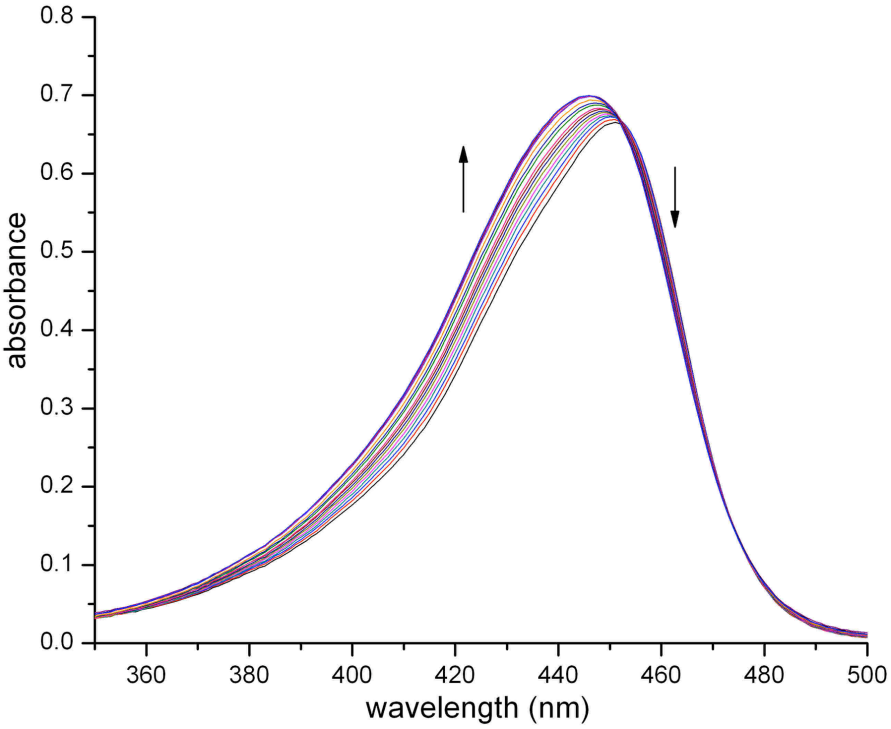

(B)

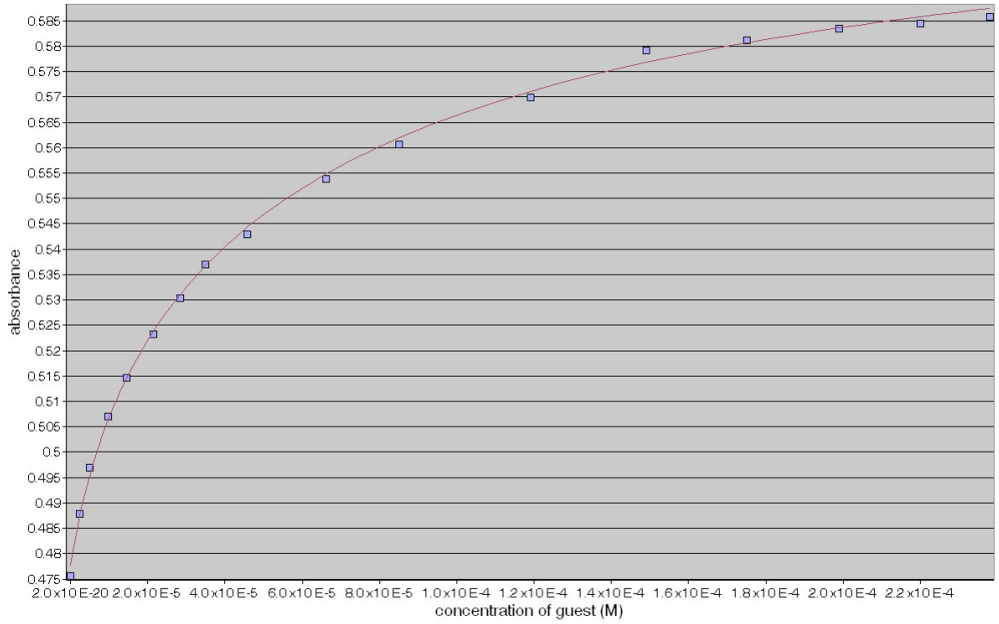

Figure II-S21. Displacement titration of a solution of dye **II-8** (21.75 μM) and **II-5a** (18.83 μM) solution with **II-14** (0 - 230 μM) (20 mM NaH_2PO_4 buffer, pH 7.4): (A) spectral change, (B) Non-linear fitting plot of absorbance *versus* concentration for the displacement titration of **II-14** with Scientist^{TM}. K_a was evaluated as $2.2 \pm 0.2 \times 10^8$ M^{-1}.

(A)

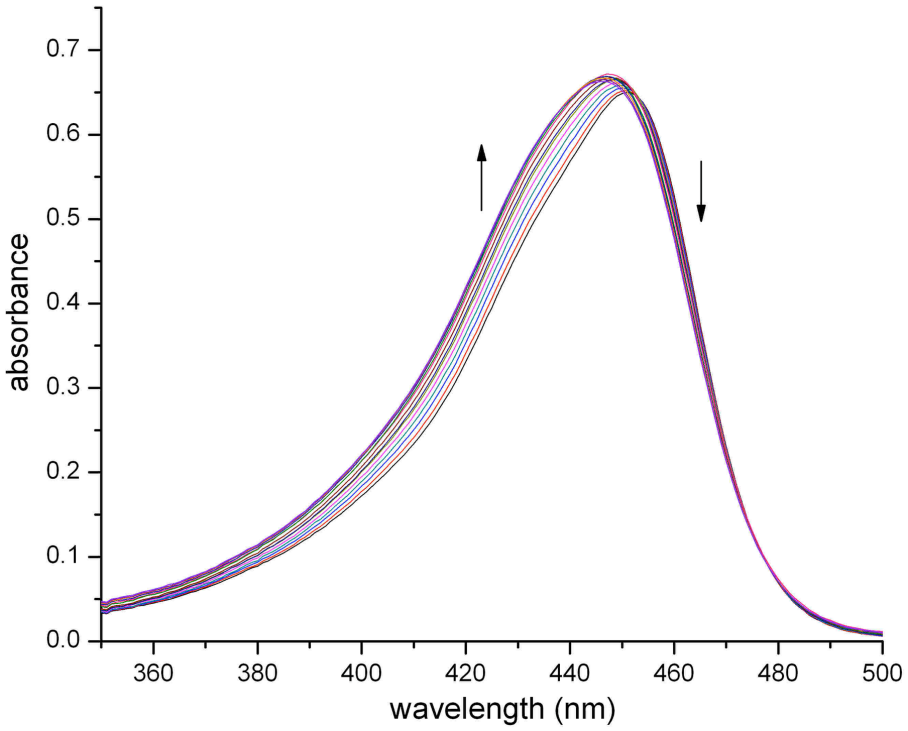

(B)

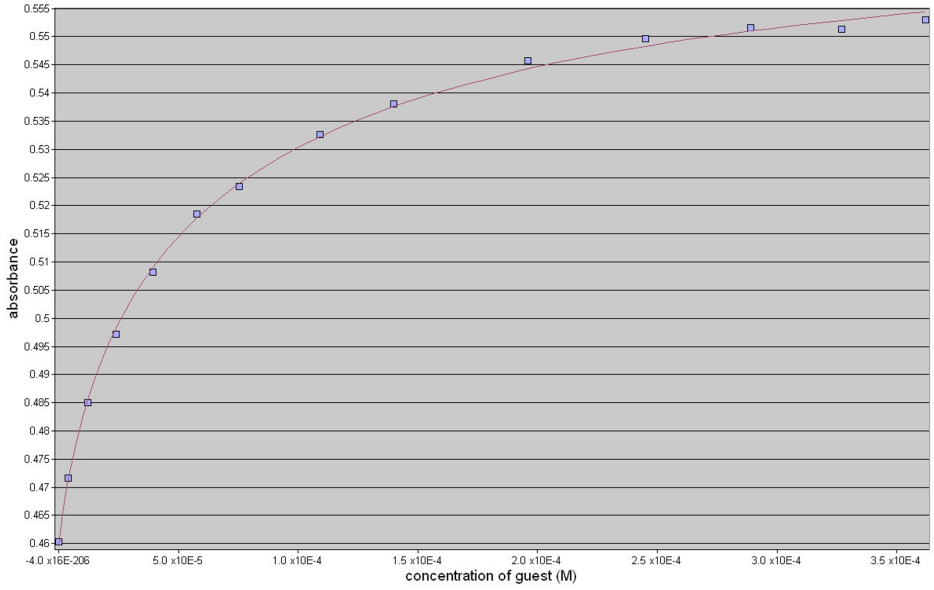

Figure II-S22. Displacement titration of a solution of dye **II-8** (21.75 μM) and **II-5a** (18.83 μM) solution with **II-15** (0 - 365 μM) (20 mM NaH_2PO_4 buffer, pH 7.4): (A) spectral change, (B) Non-linear fitting plot of absorbance *versus* concentration for the displacement titration of **II-15** with Scientist^{TM}. K_a was evaluated as $2.0 \pm 0.2 \times 10^8$ M^{-1}.

(A)

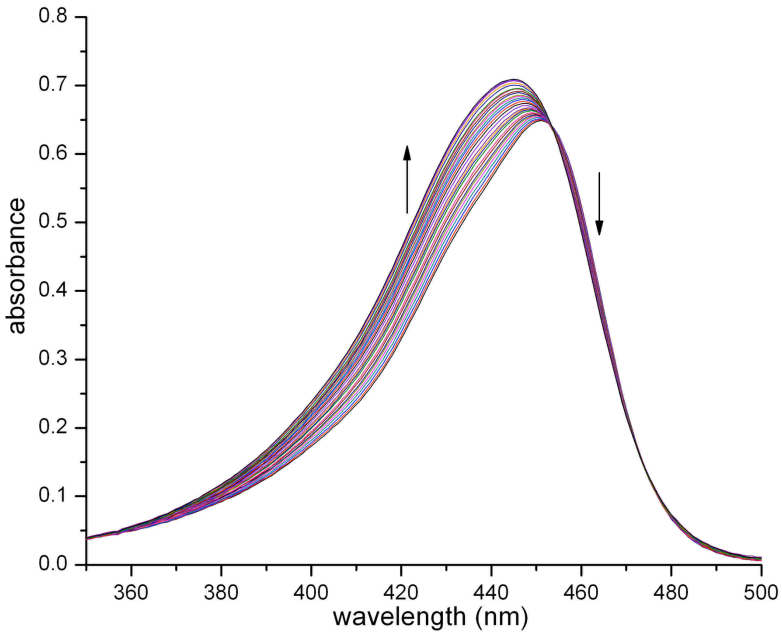

(B)

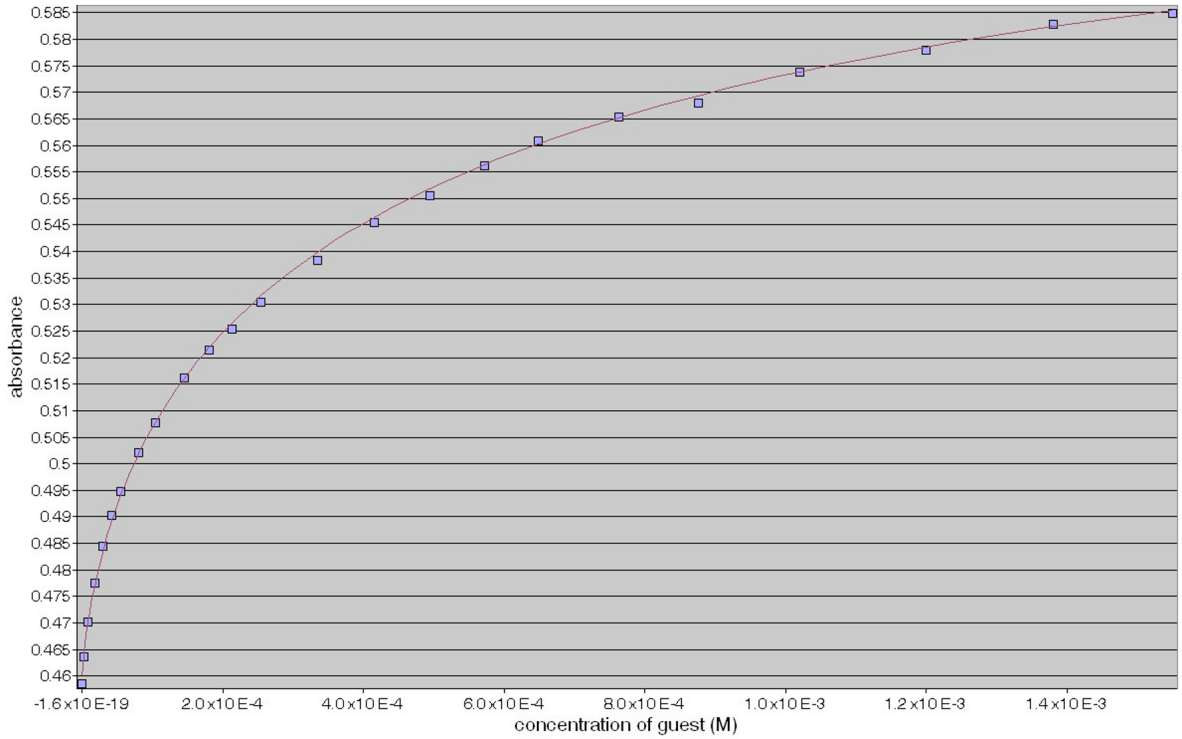

Figure II-S23. Displacement titration of a solution of dye **II-8** (21.75 μM) and **II-5a** (18.83 μM) solution with **II-16** (0 – 1.55 mM) (20 mM NaH_2PO_4 buffer, pH 7.4): (A) spectral change, (B) Non-linear fitting plot of absorbance *versus* concentration for the displacement titration of **II-16** with Scientist^{TM}. K_a was evaluated as $7.2 \pm 0.7 \times 10^7$ M^{-1}.

(A)

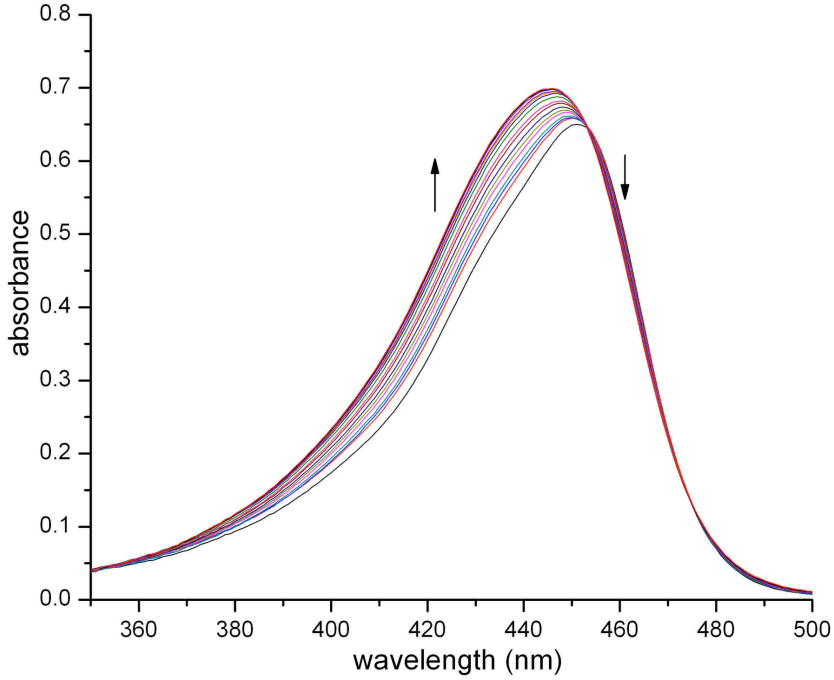

(B)

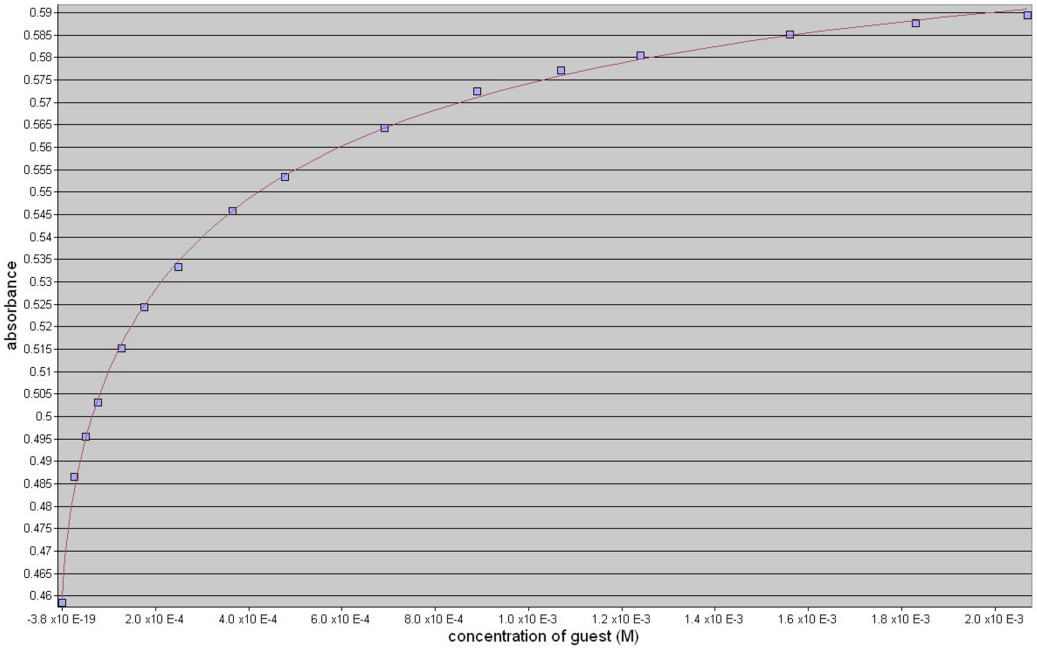

Figure II-S24. Displacement titration of a solution of dye **II-8** (21.75 μM) and **II-5a** (18.83 μM) solution with **II-17** (0 – 2.1 mM) (20 mM NaH_2PO_4 buffer, pH 7.4): (A) spectral change, (B) Non-linear fitting plot of absorbance *versus* concentration for the displacement titration of **II-17** with Scientist^{TM}. K_a was evaluated as $3.2 \pm 0.3 \times 10^7$ M^{-1}.

(A)

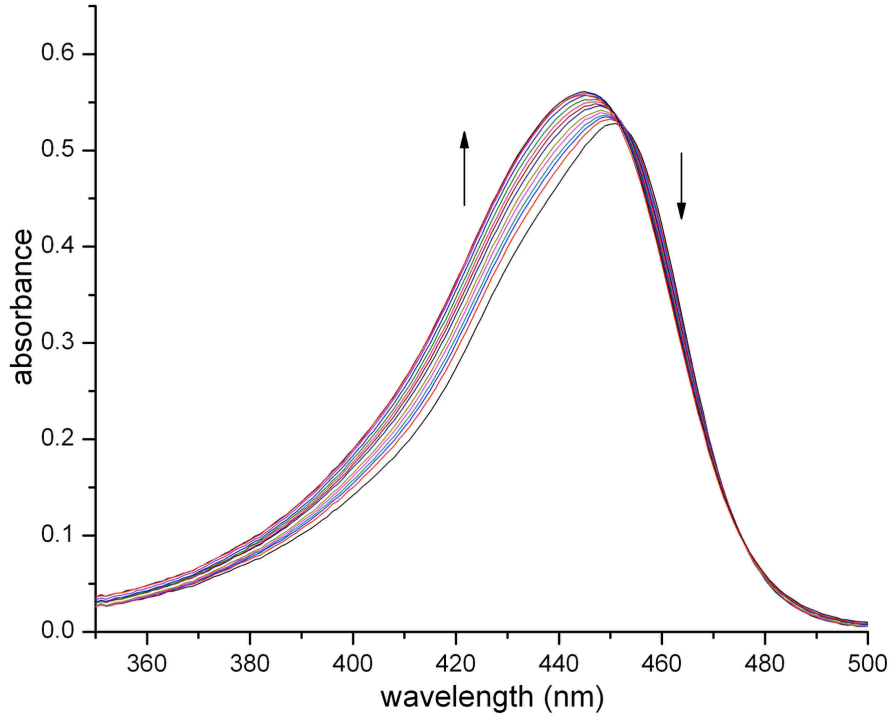

(B)

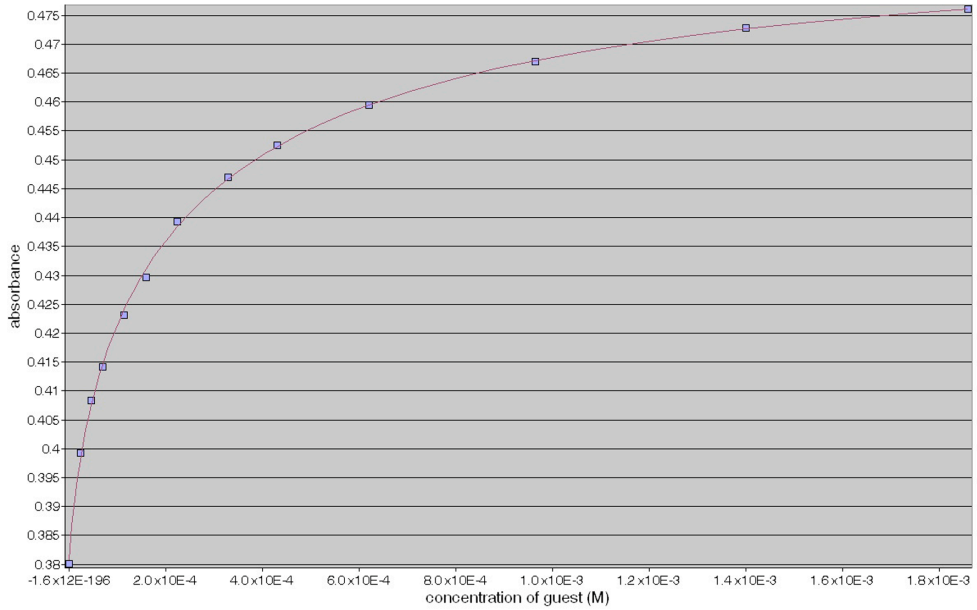

Figure II-S25. Displacement titration of a solution of dye **II-8** (17.77 μM) and **II-5a** (13.16 μM) solution with **II-18** (0 – 1.85 mM) (20 mM NaH_2PO_4 buffer, pH 7.4): (A) spectral change, (B) Non-linear fitting plot of absorbance *versus* concentration for the displacement titration of **II-18** with Scientist^{TM}. K_a was evaluated as $4.3 \pm 0.4 \times 10^7$ M^{-1}.

(A)

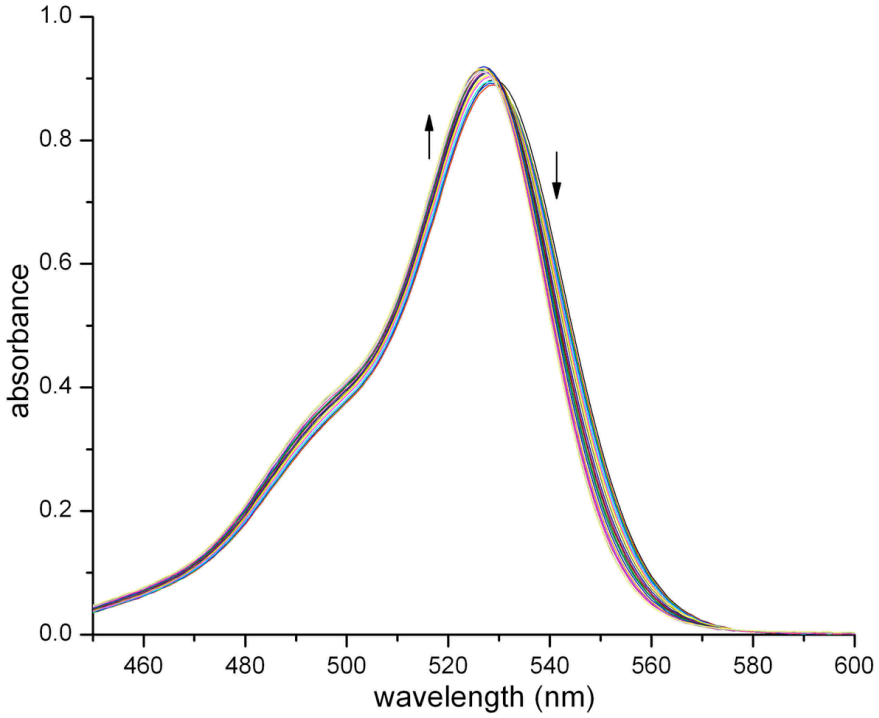

(B)

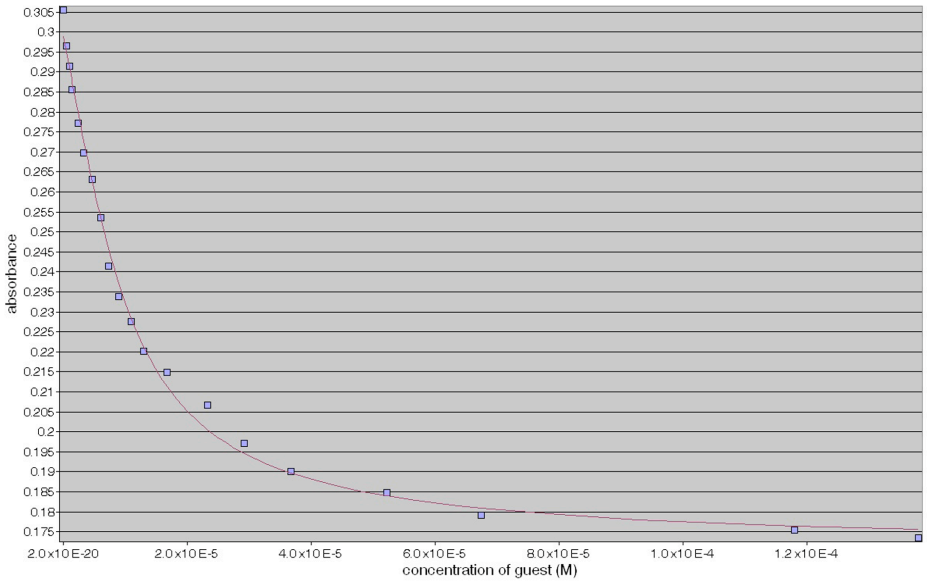

Figure II-S26. Displacement titration of a solution of dye **II-7** (8.32 μM) and **II-5a** (9.09 μM) solution with **II-19** (0 - 140 μM) (20 mM NaH_2PO_4 buffer, pH 7.4): (A) spectral change, (B) Non-linear fitting plot of absorbance *versus* concentration for the displacement titration of **II-19** with Scientist^{TM}. K_a was evaluated as $7.1 \pm 0.8 \times 10^5$ M^{-1}.

(A)

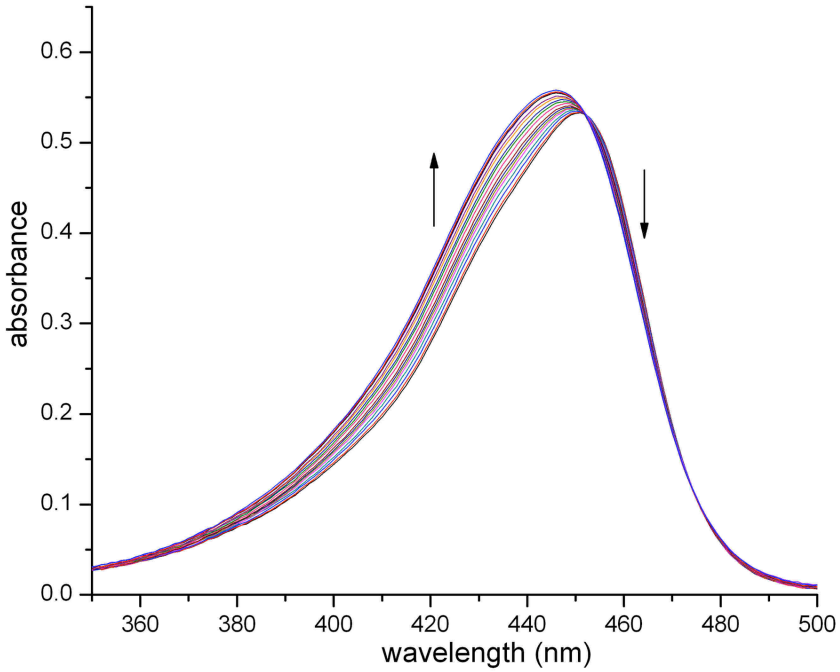

(B)

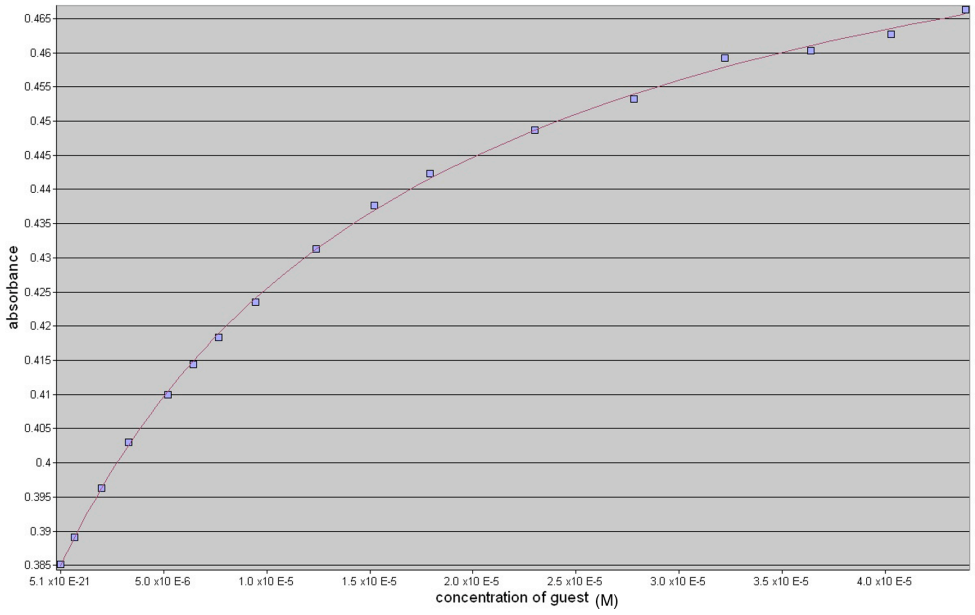

Figure II-S27. Displacement titration of a solution of dye **II-8** (17.77 μM) and **II-5a** (13.16 μM) solution with **II-20** (0 - 45 μM) (20 mM NaH_2PO_4 buffer, pH 7.4): (A) spectral change, (B) Non-linear fitting plot of absorbance *versus* concentration for the displacement titration of **II-20** with Scientist^{TM}. K_a was evaluated as $6.8 \pm 0.9 \times 10^8$ M^{-1}.

(A)

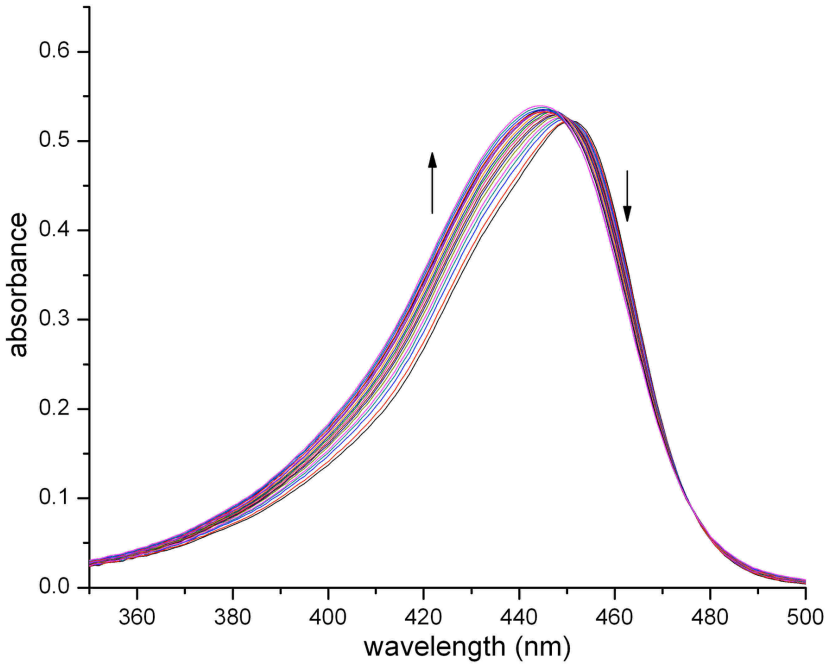

(B)

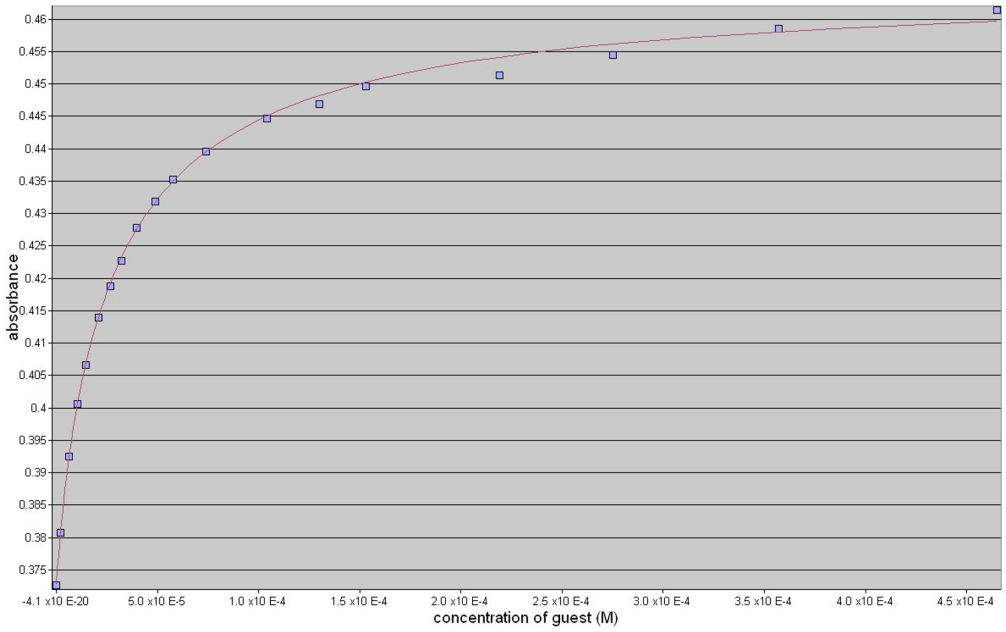

Figure II-S28. Displacement titration of a solution of dye **II-8** (17.77 μM) and **II-5a** (13.16 μM) solution with **II-21** (0 - 460 μM) (20 mM NaH_2PO_4 buffer, pH 7.4): (A) spectral change, (B) Non-linear fitting plot of absorbance *versus* concentration for the displacement titration of **II-21** with Scientist^{TM}. K_a was evaluated as $4.0 \pm 0.4 \times 10^8$ M^{-1}.

(A)

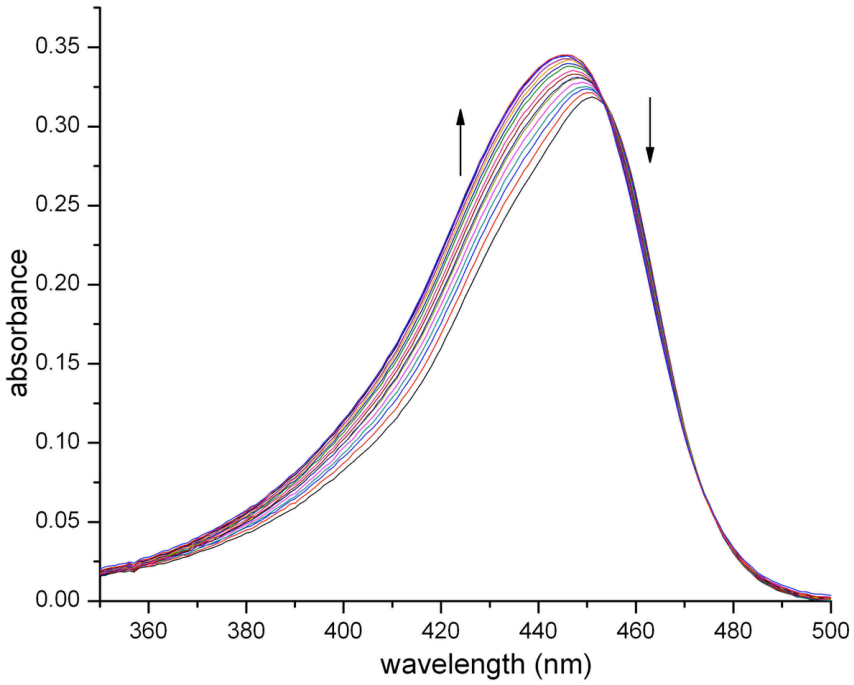

(B)

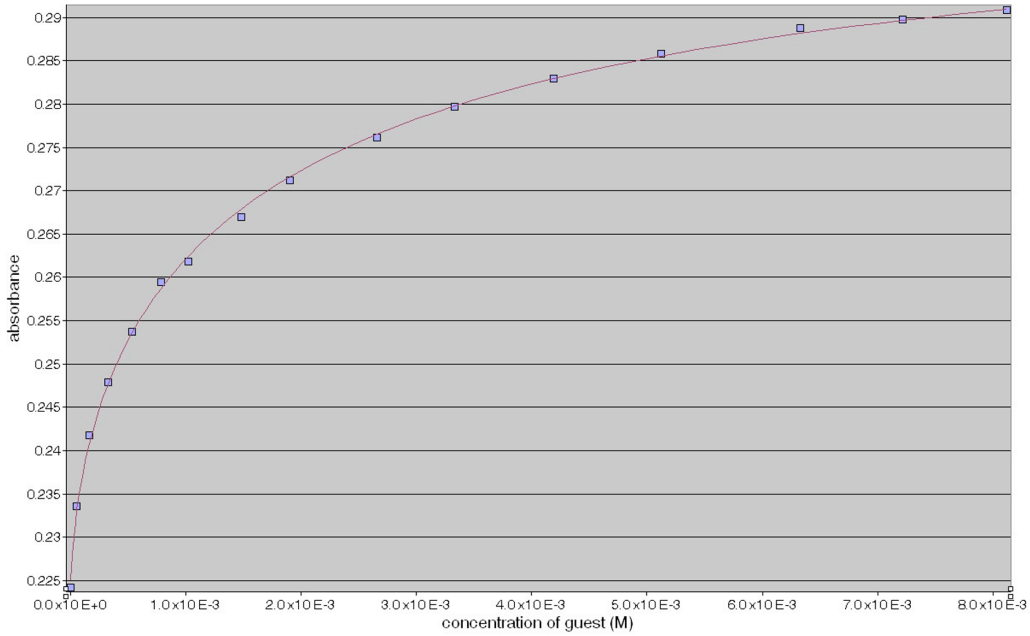

Figure II-S29. Displacement titration of a solution of dye **II-8** (10.87 μM) and **II-5a** (9.41 μM) solution with **II-22** (0 – 8.2 mM) (20 mM NaH_2PO_4 buffer, pH 7.4): (A) spectral change, (B) Non-linear fitting plot of absorbance *versus* concentration for the displacement titration of **II-22** with Scientist^{TM}. K_a was evaluated as $3.5 \pm 0.4 \times 10^6$ M^{-1}.

(A)

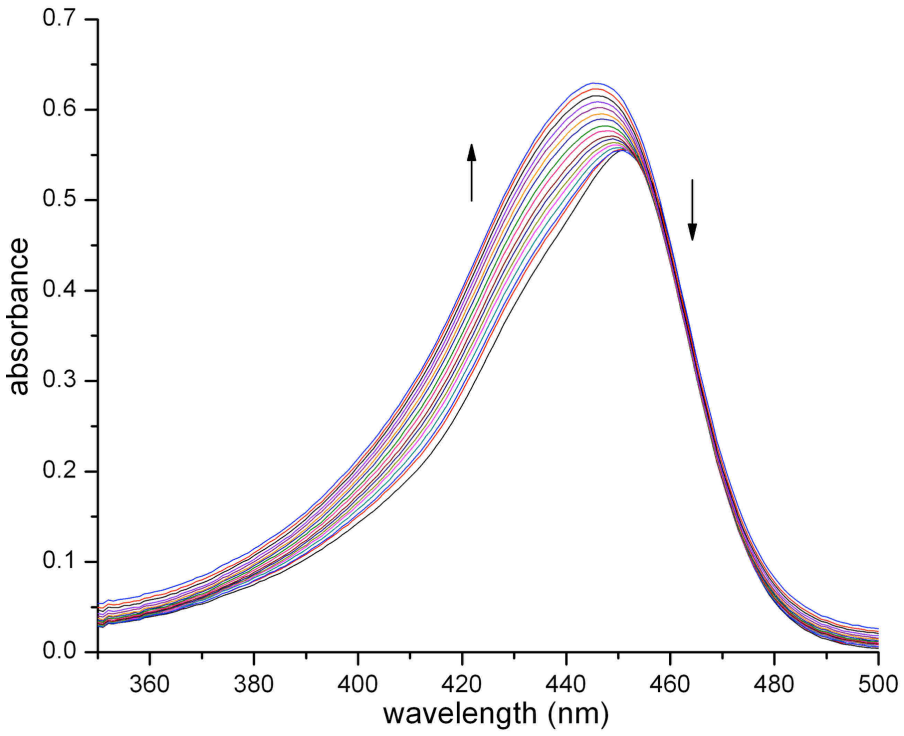

(B)

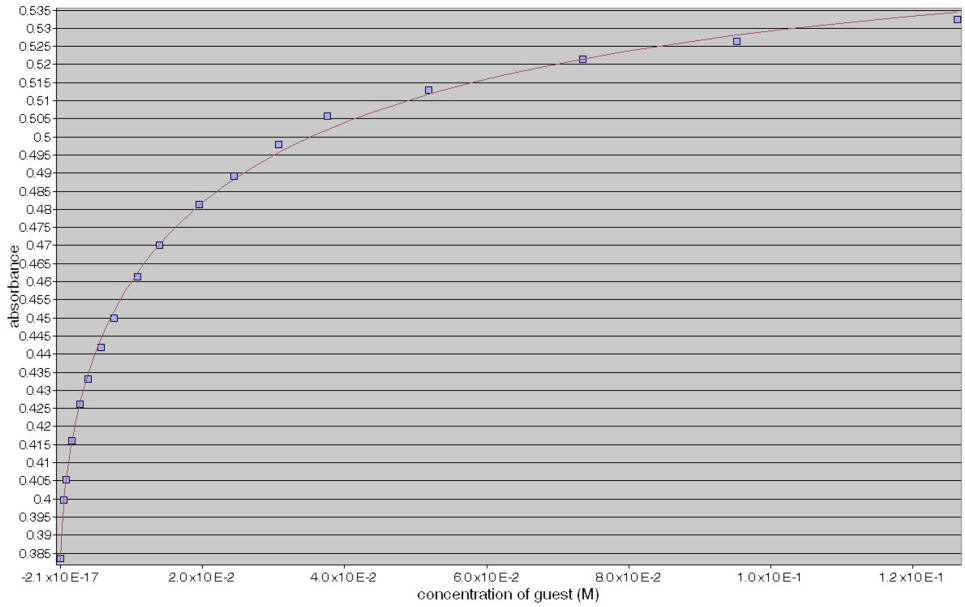

Figure II-S30. Displacement titration of a solution of dye **II-8** (18.62 μM) and **II-5a** (17.04 μM) solution with **II-23** (0 – 0.12 M) (20 mM NaH_2PO_4 buffer, pH 7.4): (A) spectral change, (B) Non-linear fitting plot of absorbance *versus* concentration for the displacement titration of **II-23** with Scientist^{TM}. K_a was evaluated as $4.8 \pm 0.5 \times 10^5$ M^{-1}.

(A)

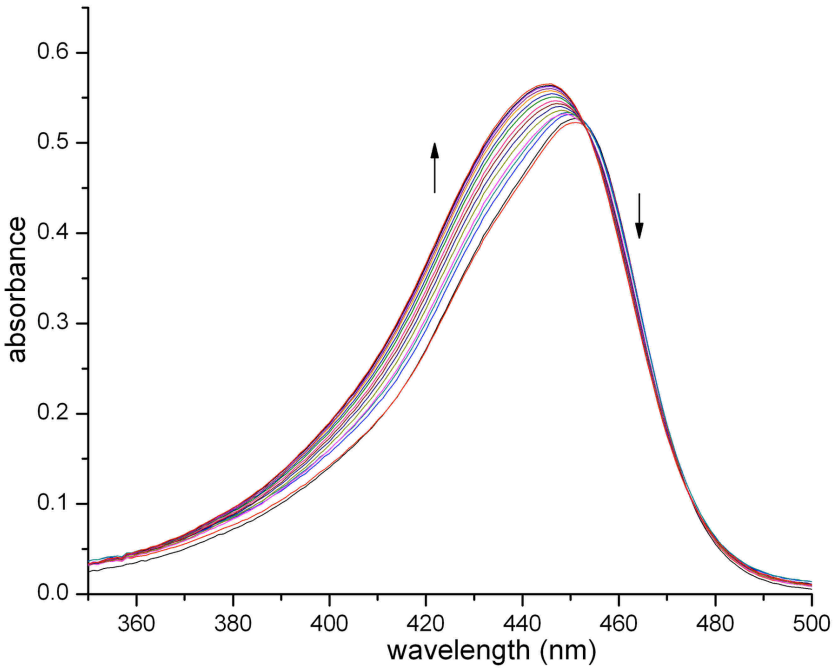

(B)

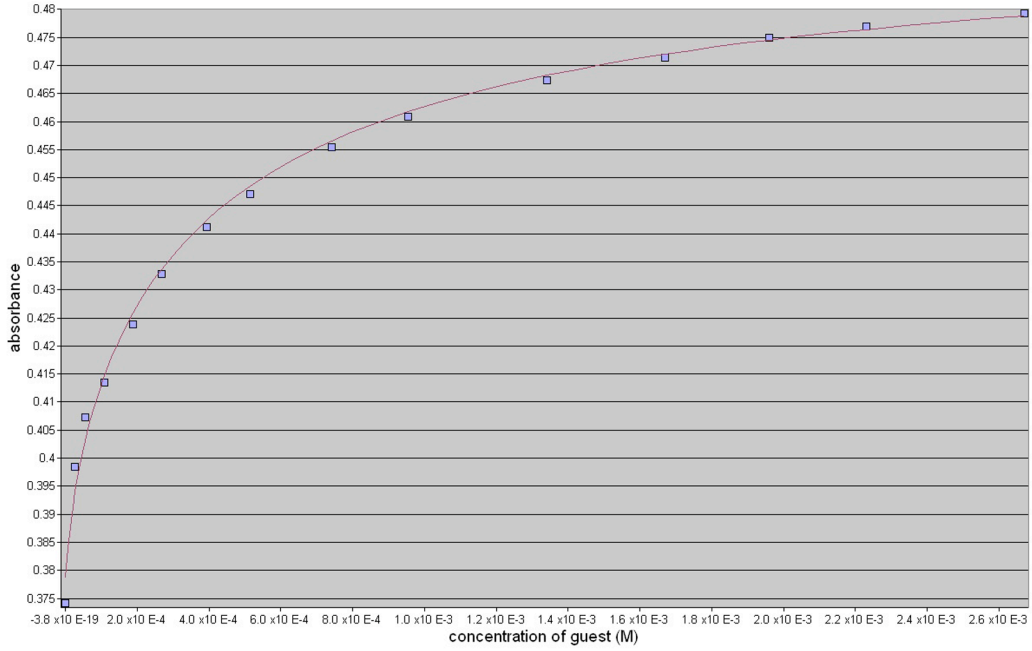

Figure II-S31. Displacement titration of a solution of dye **II-8** (17.77 μM) and **II-5a** (13.16 μM) solution with **II-24** (0 – 2.7 mM) (20 mM NaH_2PO_4 buffer, pH 7.4): (A) spectral change, (B) Non-linear fitting plot of absorbance *versus* concentration for the displacement titration of **II-24** with Scientist^{TM}. K_a was evaluated as $2.6 \pm 0.4 \times 10^7$ M^{-1}.

(A)

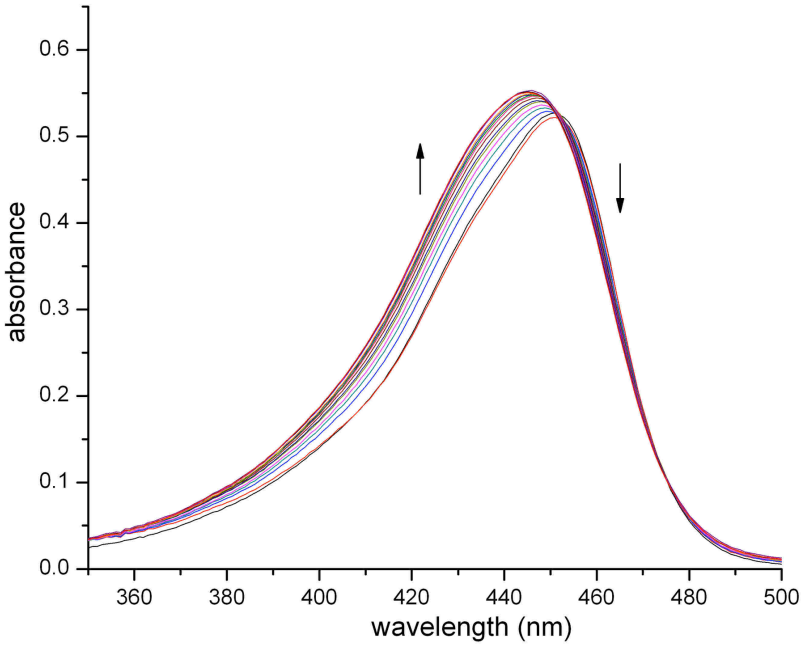

(B)

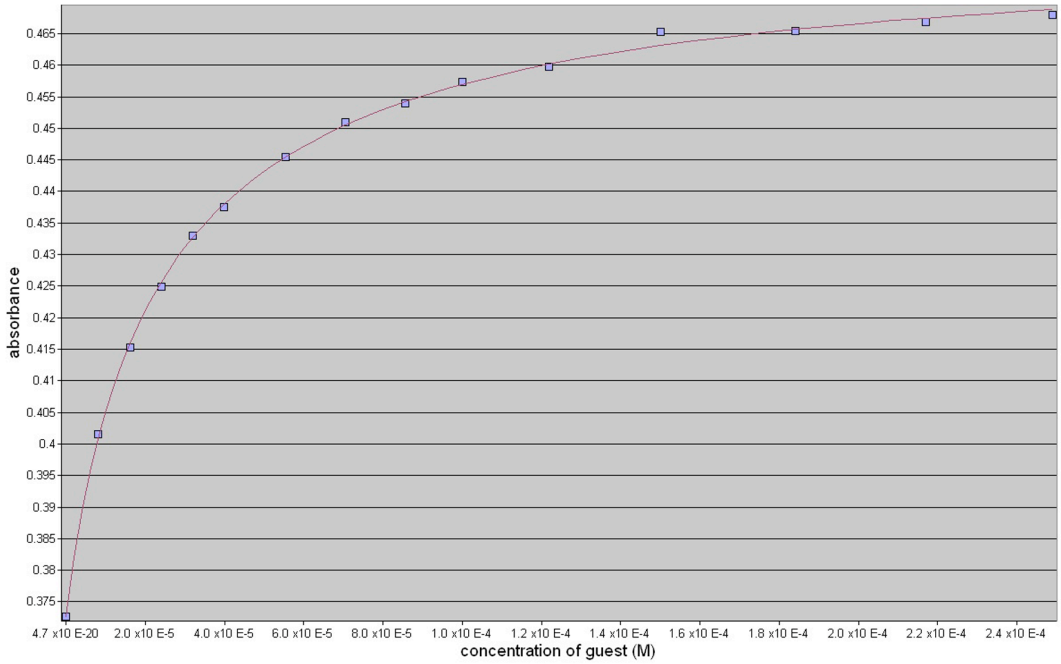

Figure II-S32. Displacement titration of a solution of dye **II-8** (17.77 μM) and **II-5a** (13.16 μM) solution with **II-25** (0 - 250 μM) (20 mM NaH_2PO_4 buffer, pH 7.4): (A) spectral change, (B) Non-linear fitting plot of absorbance *versus* concentration for the displacement titration of **II-25** with Scientist^{TM}. K_a was evaluated as $4.5 \pm 0.4 \times 10^8$ M^{-1}.

(A)

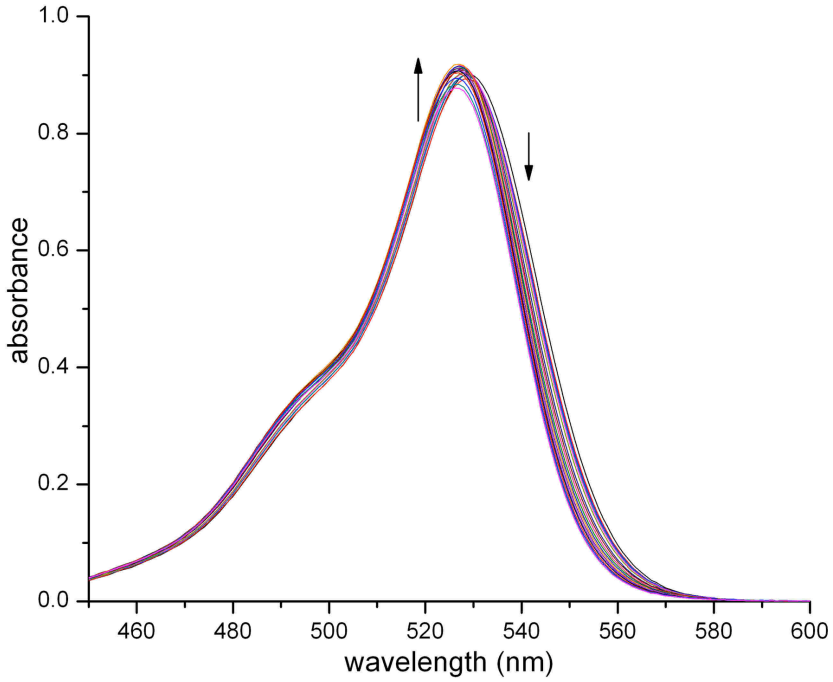

(B)

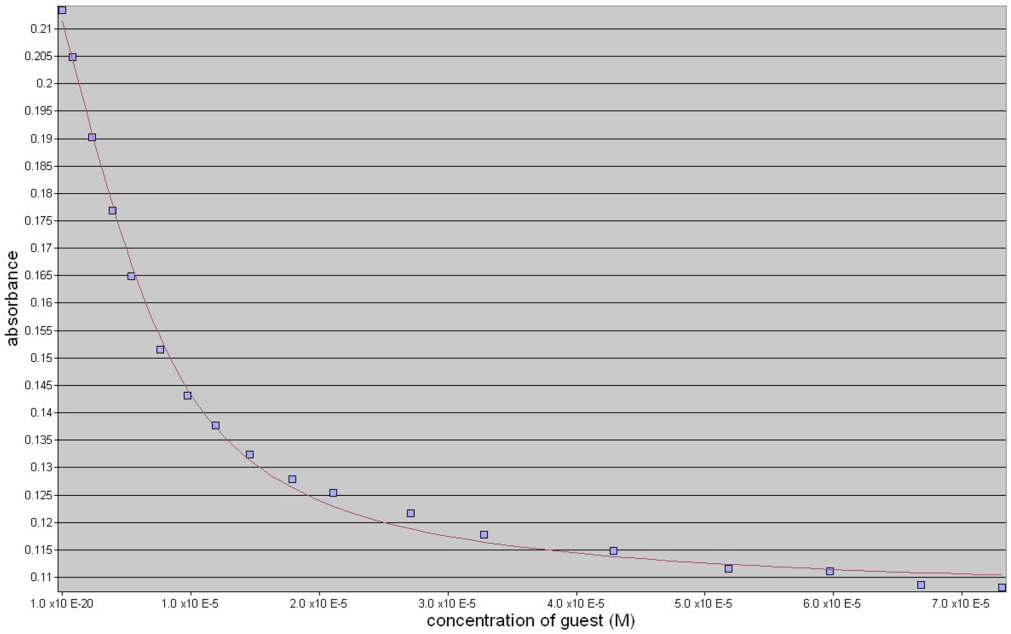

Figure II-S33. Displacement titration of a solution of dye **II-7** (9.23 μM) and **II-5a** (7.28 μM) solution with **II-27** (0 - 73 μM) (20 mM NaH_2PO_4 buffer, pH 7.4): (A) spectral change, (B) Non-linear fitting plot of absorbance *versus* concentration for the displacement titration of **II-27** with Scientist^{TM}. K_a was evaluated as $1.4 \pm 0.1 \times 10^6$ M^{-1}.

(A)

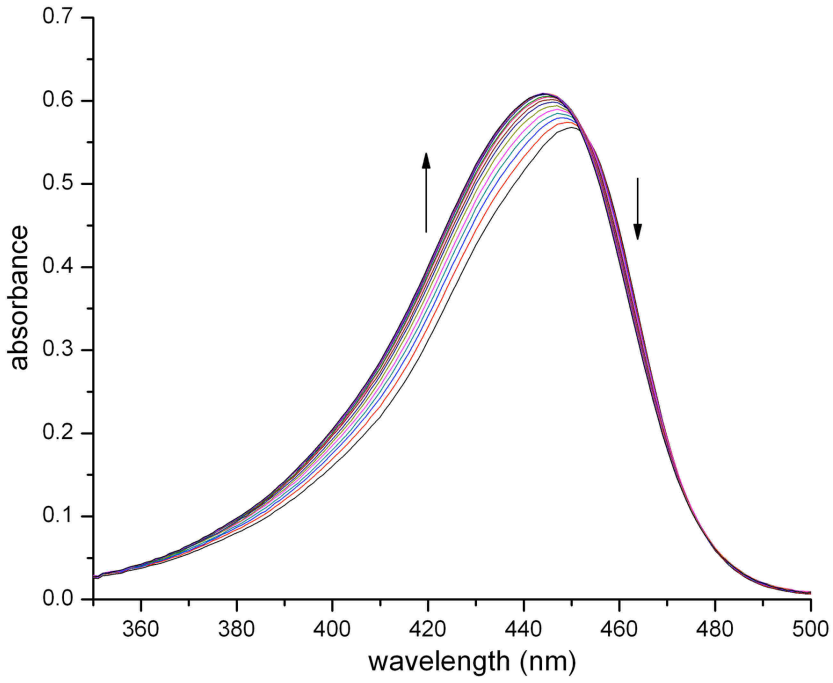

(B)

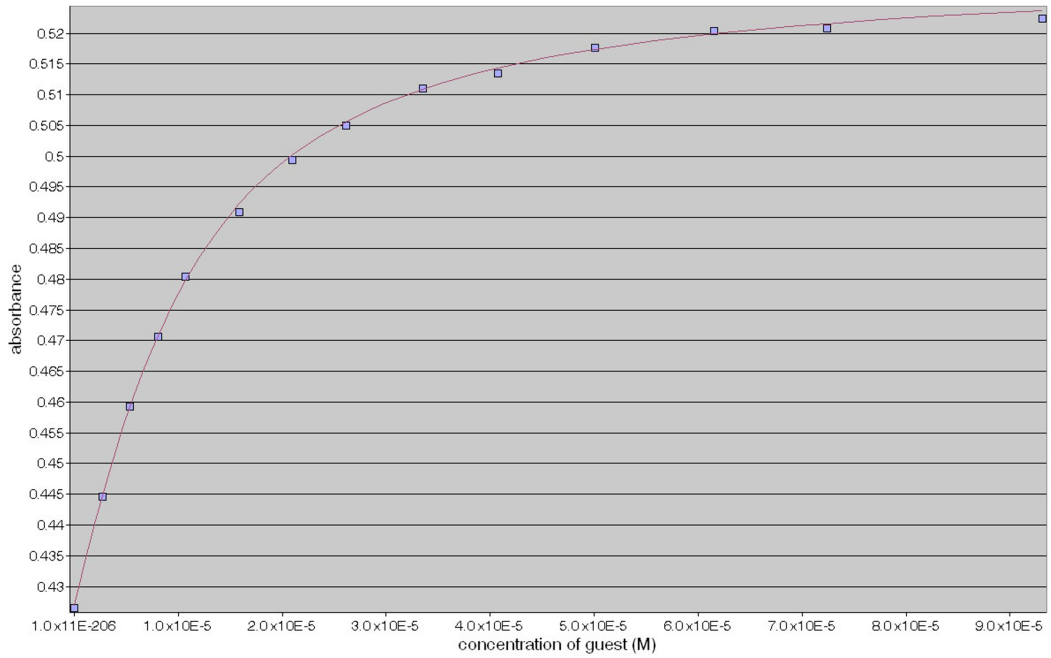

Figure II-S34. Displacement titration of a solution of dye **II-8** (17.96 μM) and **II-5a** (12.28 μM) solution with **II-29** (0 - 93 μM) (20 mM NaH_2PO_4 buffer, pH 7.4): (A) spectral change, (B) Non-linear fitting plot of absorbance *versus* concentration for the displacement titration of **II-29** with Scientist^{TM}. K_a was evaluated as $2.0 \pm 0.2 \times 10^9$ M^{-1}.

(A)

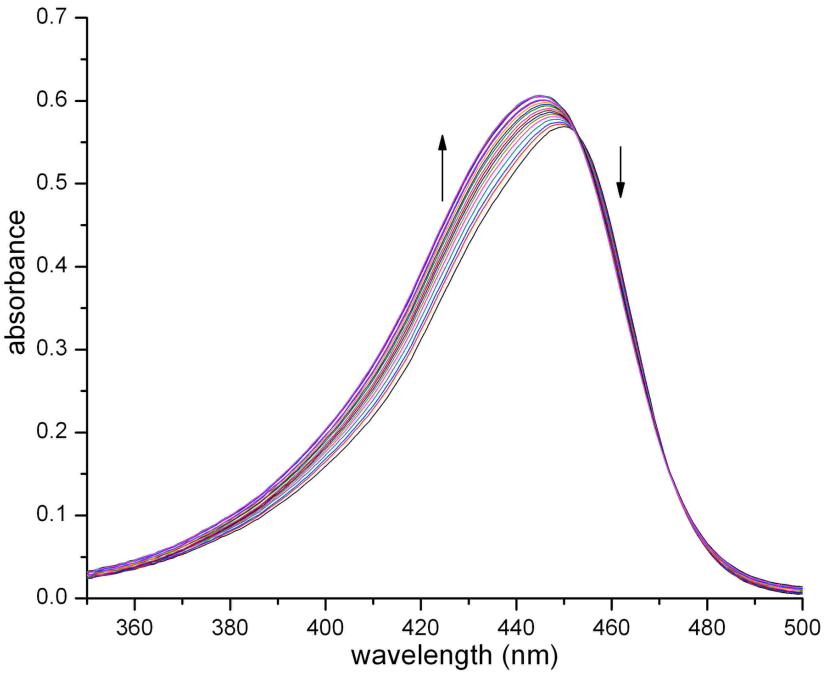

(B)

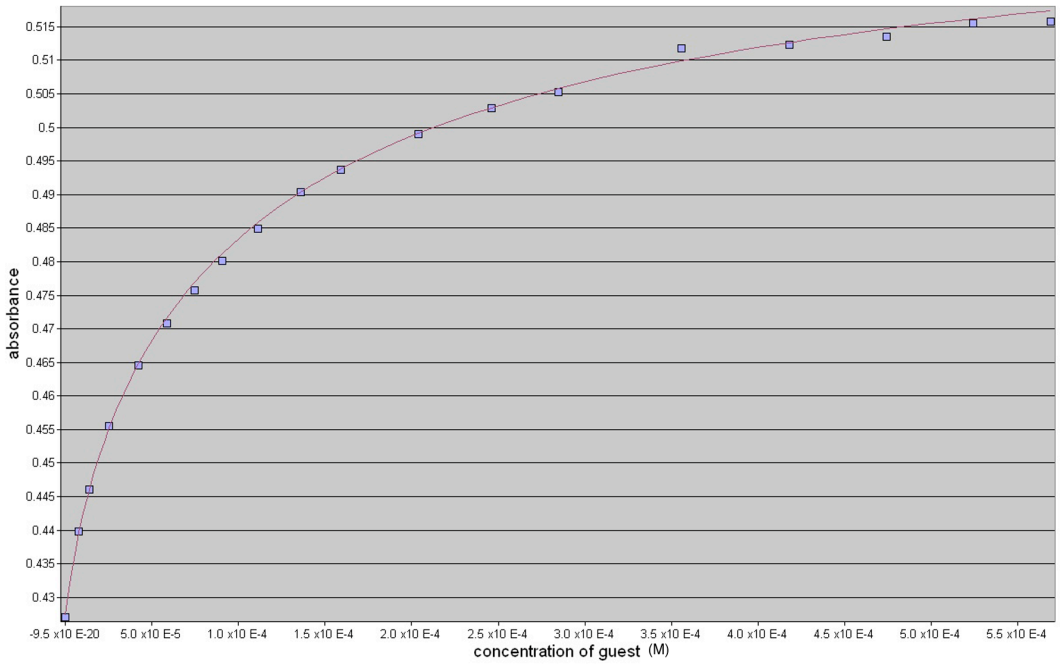

Figure II-S35. Displacement titration of a solution of dye **II-8** (17.77 μM) and **II-5a** (13.16 μM) solution with **II-30** (0 - 570 μM) (20 mM NaH_2PO_4 buffer, pH 7.4): (A) spectral change, (B) Non-linear fitting plot of absorbance *versus* concentration for the displacement titration of **II-30** with Scientist^{TM}. K_a was evaluated as $9.8 \pm 0.9 \times 10^7$ M^{-1}.

Sample Determination of K_{rel} for the Competition Between II-20 and II-28 for II-5a. We use equation 1 to determine K_{rel} for the interaction of **II-20** and **II-28** for **II-5a**. For this purpose, we prepared a solution containing **II-5a** (1.44 mM), **II-20** (3.48 mM), **II-28** (1.92 mM) and reference (1, 3, 5-benzene tricarboxylic acid, 0.88 mM) and allowed it to reach equilibrium (Figure XX). Next, we determined the concentration of **II-5a• II-28** by integration of the appropriate resonances in the ^{1}H NMR spectrum compared to reference (Figure II-S36: **II-5a• II-28**: 5.97 ppm; reference: 8.23 ppm). Using the concentration and the mass balance expression (equation 2) allowed us to calculate [**II-28**]$_{free}$ = 1.00 mM and [**II-5a• II-28**] = 0.918 mM. Equation 3

is then used to calculate [**II-5a• II-20**] (0.518 mM) using the known value of **II-5a• II-28**. Lastly, equation 4 is used to calculate [**II-20**]$_{free}$ (2.96 mM) using the known value of [**II-5a • II-21**].

$$K_{rel} = ([\textbf{II-5a• II-28}][\ \textbf{II-20}]_{free}) / ([\textbf{II-5a• II-20}][\ \textbf{II-28}]_{free}) \quad (1)$$

$$[\textbf{II-28}]_{Total} = 1.92\ mM = [\textbf{II-28}]_{free} + [\textbf{II-5a• II-28}] \quad (2)$$

$$[\textbf{II-5a}]_{Total} = 1.44\ mM = [\textbf{II-5a• II-28}] + [\textbf{II-5a• II-20}] \quad (3)$$

$$[\textbf{II-20}]_{Total} = 3.48\ mM = [\textbf{II-20}]_{free} + [\textbf{II-5a • II-20}] \quad (4)$$

Substitution of the values of [**II-5a• II-28**], [**II-28**]$_{free}$, [**II-5a• II-20**], and [**II-20**]$_{free}$ into equation 1 gave K_{rel} = 5.25. These determinations were done in triplicate from independently prepared stock solutions and the average values were used in the calculations of K_a and the error analysis shown below.

In preparing the solutions for the above determinations we used a small excess of **II-28** (to ensure there is no free **II-5a**) and a large excess of **II-20**; under those conditions the errors in [**II-21**]$_{free}$, [**II-28**]$_{free}$ are small and both [**II-28**] and [**II-5a• II-28**] are kept in a good range for accurate measurement of their ratio by ^{1}H NMR.

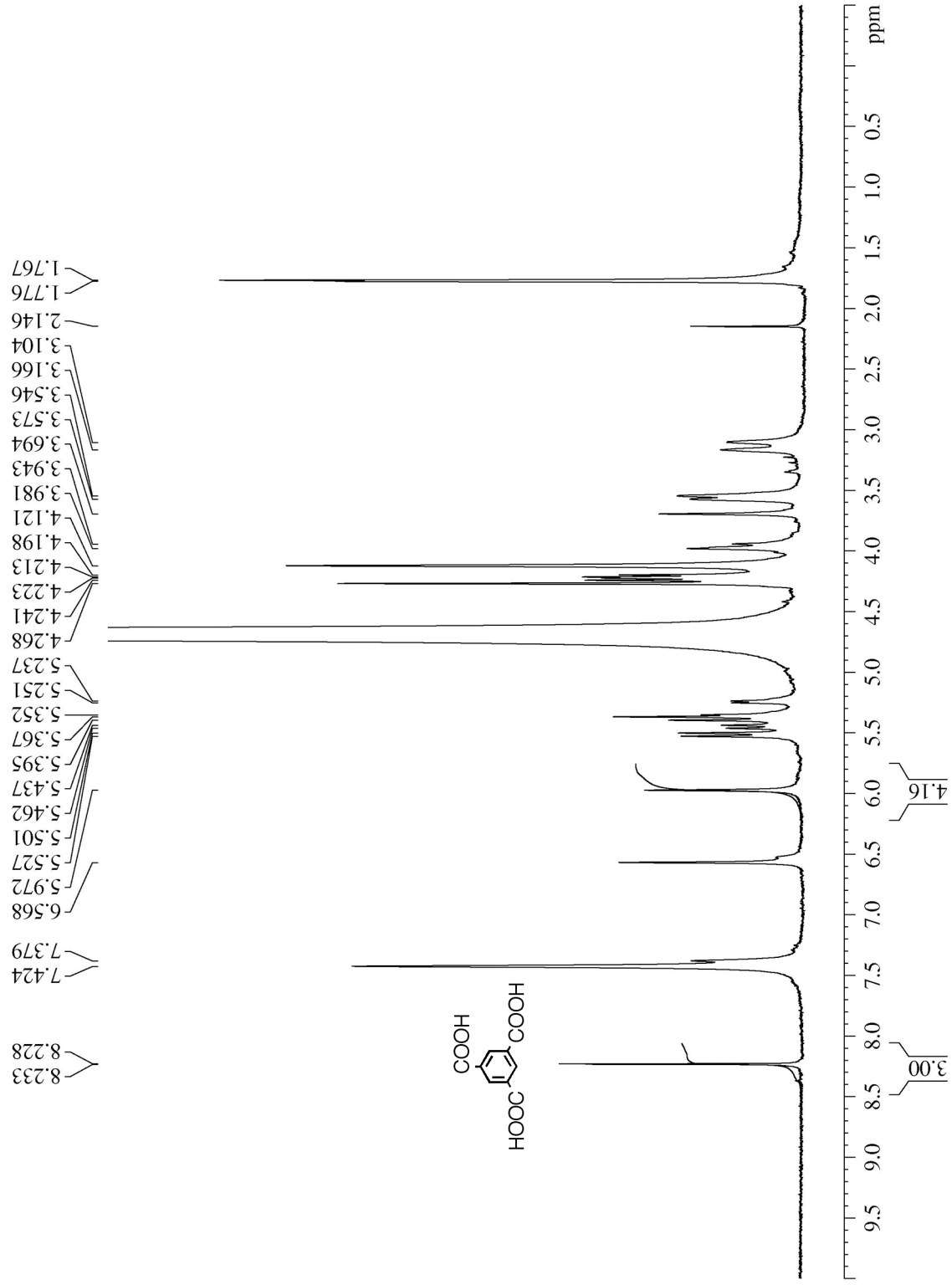

Figure II-S36. ^{1}H NMR spectrum (400 MHz, 20 mM sodium phosphate buffer, pD = 7.4) recorded for a solution of **II-5a** (1.44 mM), **II-20** (3.48 mM), **II-28** (1.92 mM) and reference benzene-1, 3, 5-tricarboxylic acid (0.88 mM).

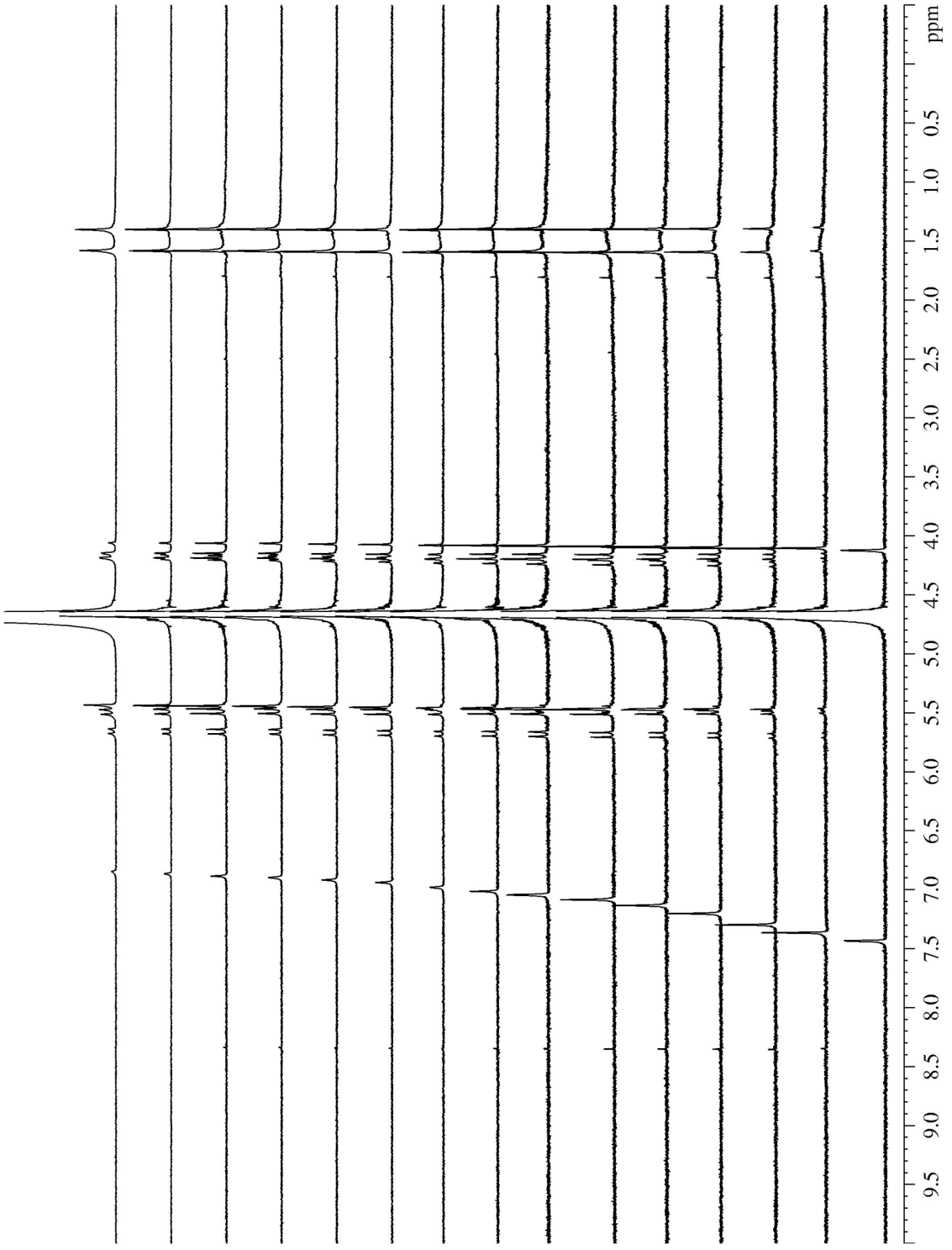

Figure II-S37. ^{1}H NMR spectra (400 MHz, 20 mM sodium phosphate buffer, pD = 7.4) recorded for a solution of **II-20** (162 μM) and **6** of variable concentrations (0 – 0.65 mM).

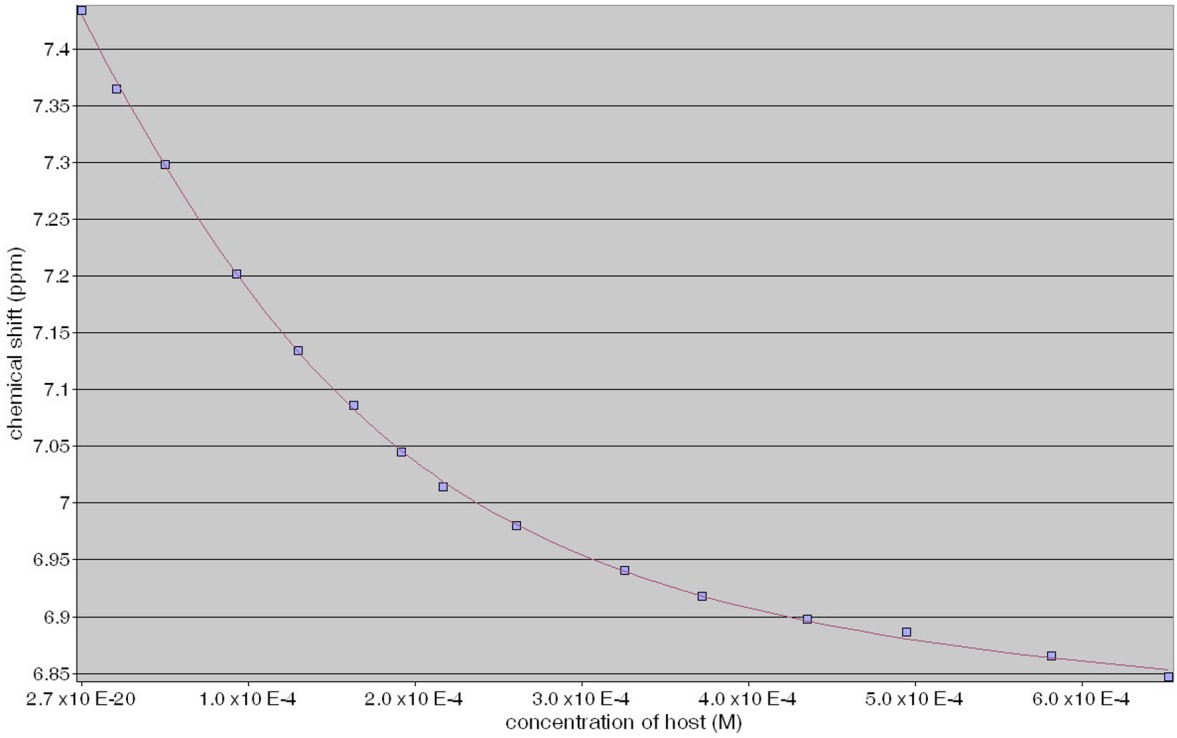

Figure II-S38. Plot of the chemical shift of **II-20** as a function of **II-6** concentration. The solid line represents the best non-linear fitting of the data to a 1:1 binding model (K_a = $1.5 \pm 0.1 \times 10^4$ M^{-1}).

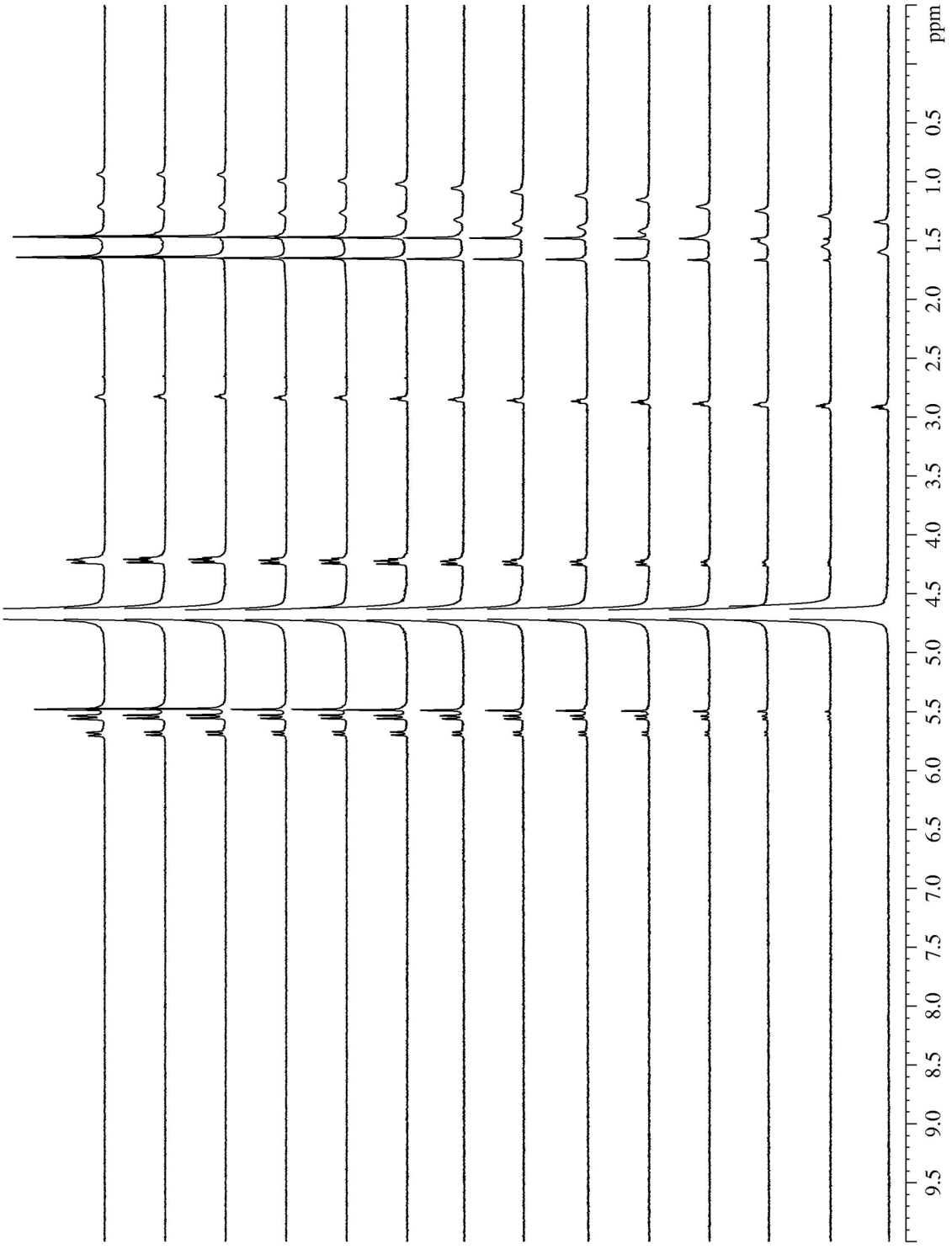

Figure II-S39. ^{1}H NMR spectra (400 MHz, 20 mM sodium phosphate buffer, pD = 7.4) recorded for a solution of **II-11** (197 μM) and **II-6** of variable concentrations (0 – 0.71 mM).

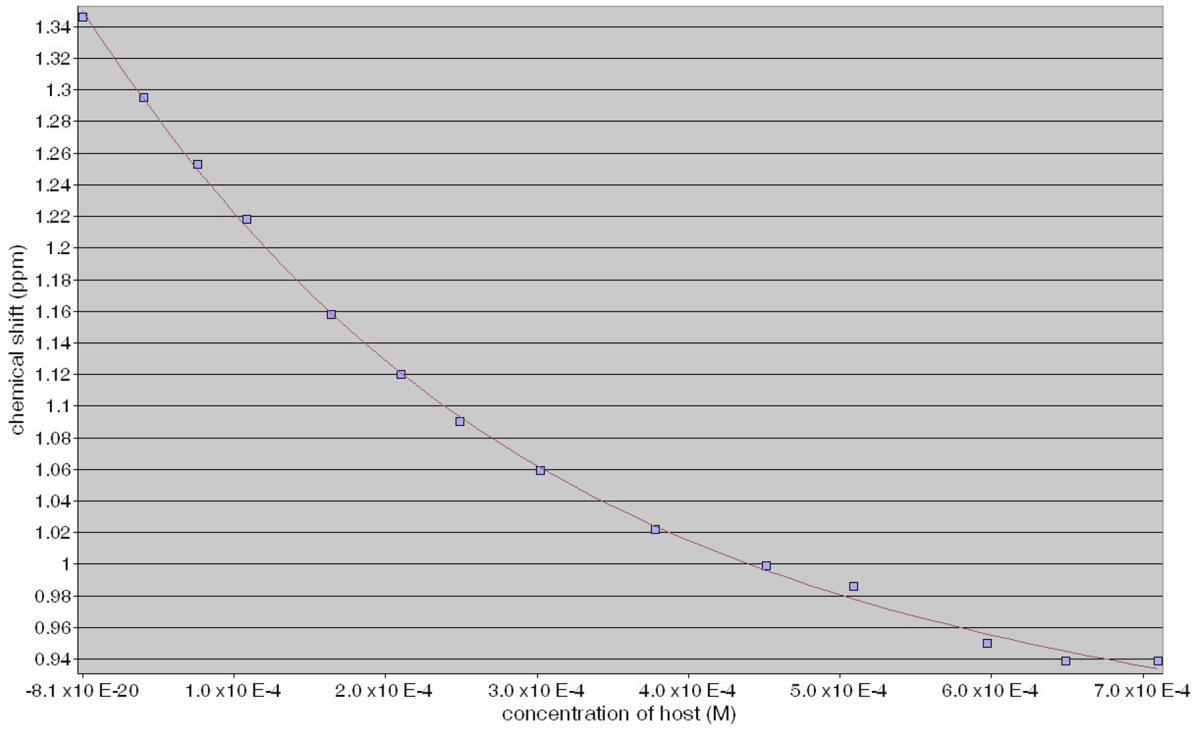

Figure II-S40. Plot of the chemical shift of **II-11** as a function of **II-6** concentration. The solid line represents the best non-linear fitting of the data to a 1:1 binding model ($K_a = 5.6 \pm 0.4 \times 10^3\ M^{-1}$).

(A)

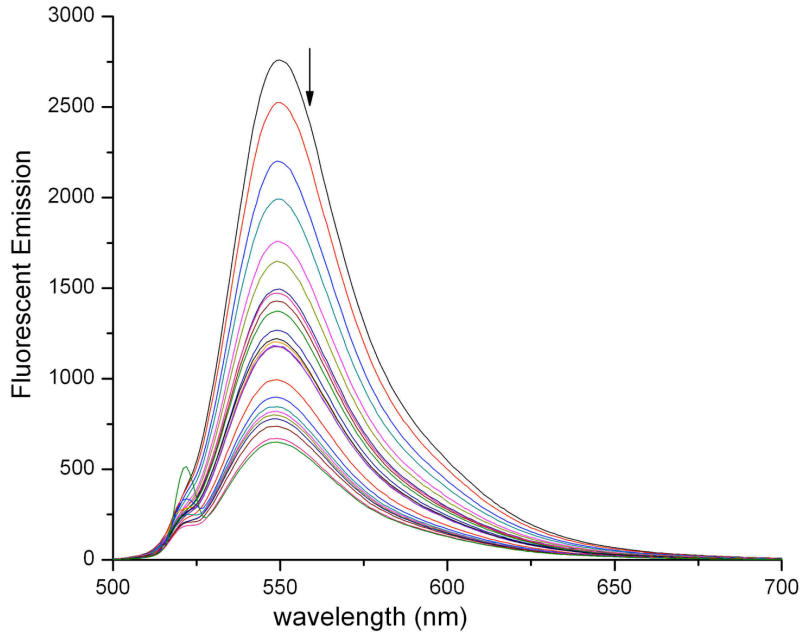

(B)

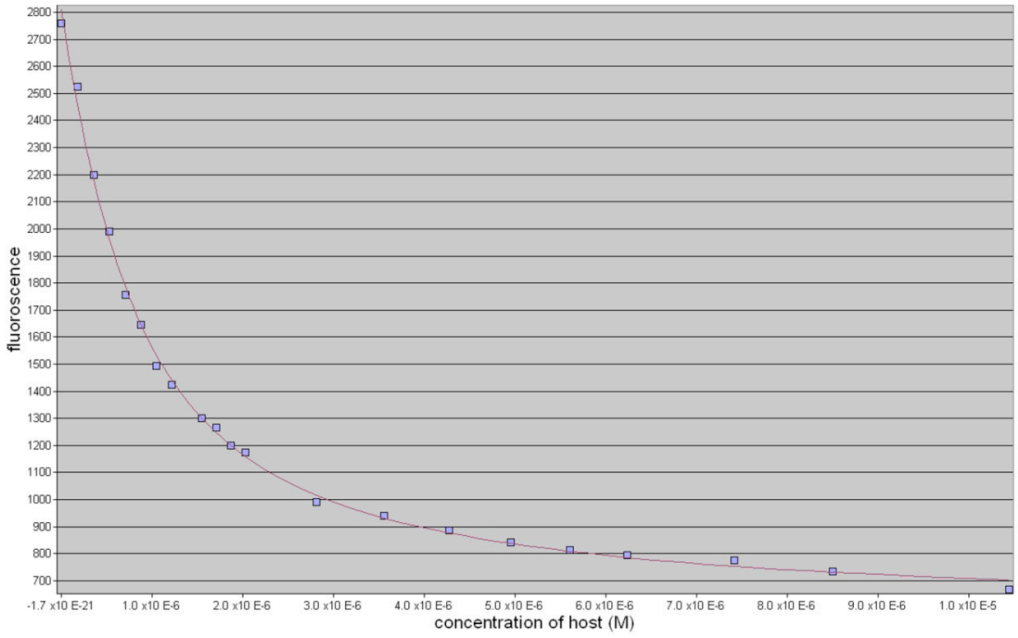

Figure II-S41. (A) Fluorescence spectra from the titration of dye **II-7** (0.42 μM) with **II-5b** (0 – 10 μM) in 5 mM NaH_2PO_4 buffer (pH 7.4), excited at 520 nm and emission at 550 nm; (B) plot of the ΔA_{550} as a function of **II-5b** concentration. The solid line represents the best non-linear fit of the data to a 1:1 binding model ($K_a = 1.6 \pm 0.1 \times 10^6$ M^{-1}).

(A)

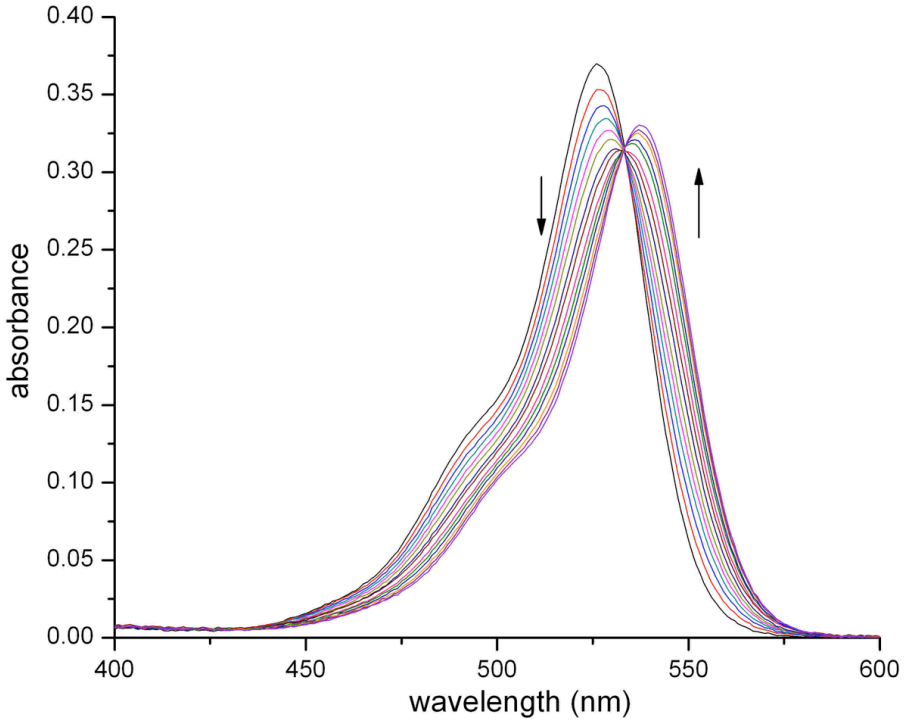

(B)

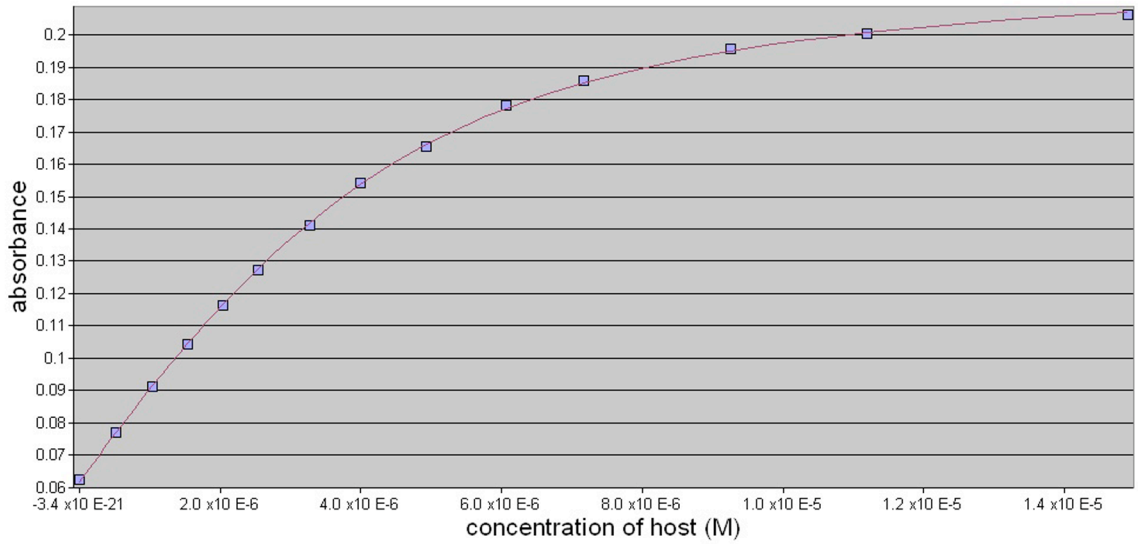

Figure II-S42. (A) UV/Vis spectra from the titration of dye **II-7** (4.14 μM) with **II-5b** (0 – 15 μM) in 7.24 mM NaH_2PO_4 buffer (pH 7.4); (B) plot of the ΔA_{550} as a function of **II-5b** concentration. The solid line represents the best non-linear fit of the data to a 1:1 binding model ($K_a = 8.0 \pm 0.4 \times 10^5\ M^{-1}$).

(A)

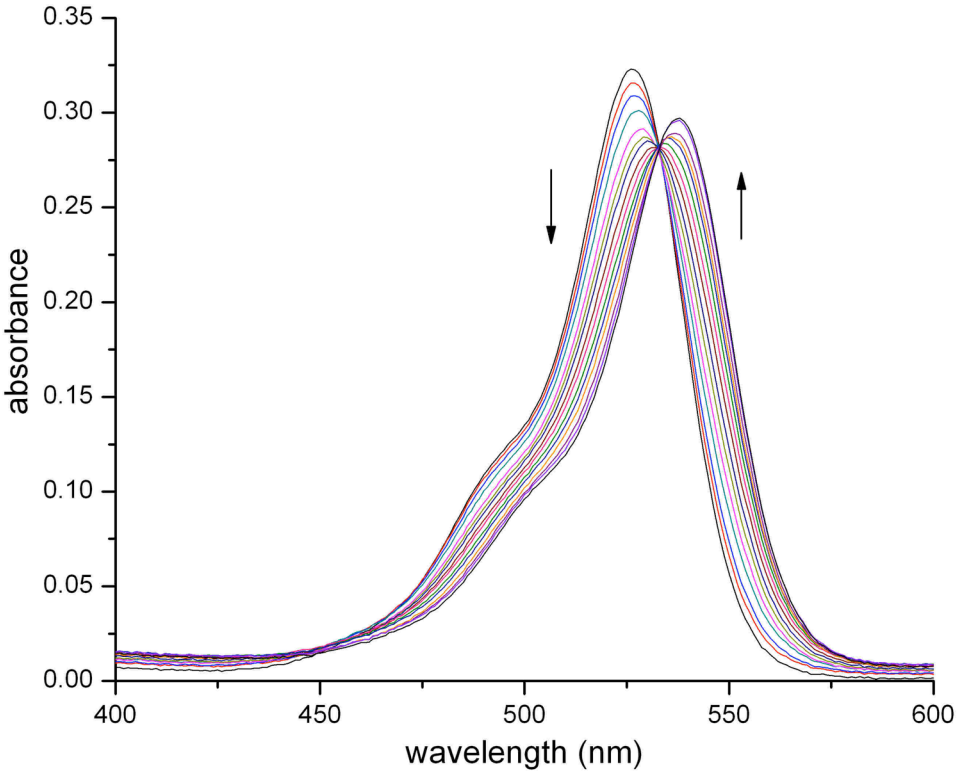

(B)

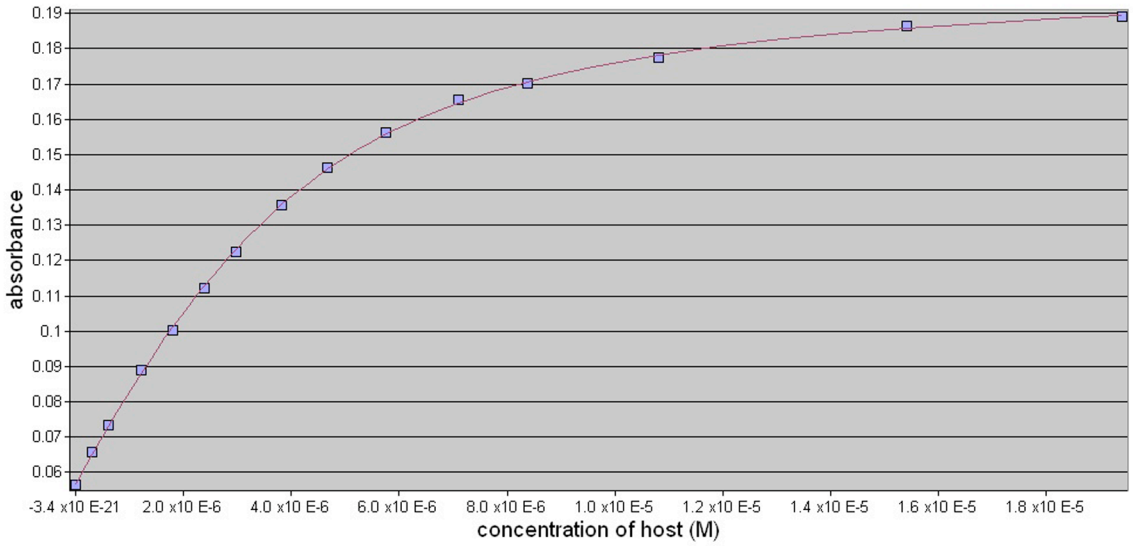

Figure II-S43. (A) UV/Vis spectra from the titration of dye **II-7** (3.74 µM) with **II-5b** (0 – 19 µM) in 9.52 mM NaH_2PO_4 buffer (pH 7.4); (B) plot of the ΔA_{550} as a function of **II-5b** concentration. The solid line represents the best non-linear fit of the data to a 1:1 binding model ($K_a = 6.8 \pm 0.2 \times 10^5\ M^{-1}$).

(A)

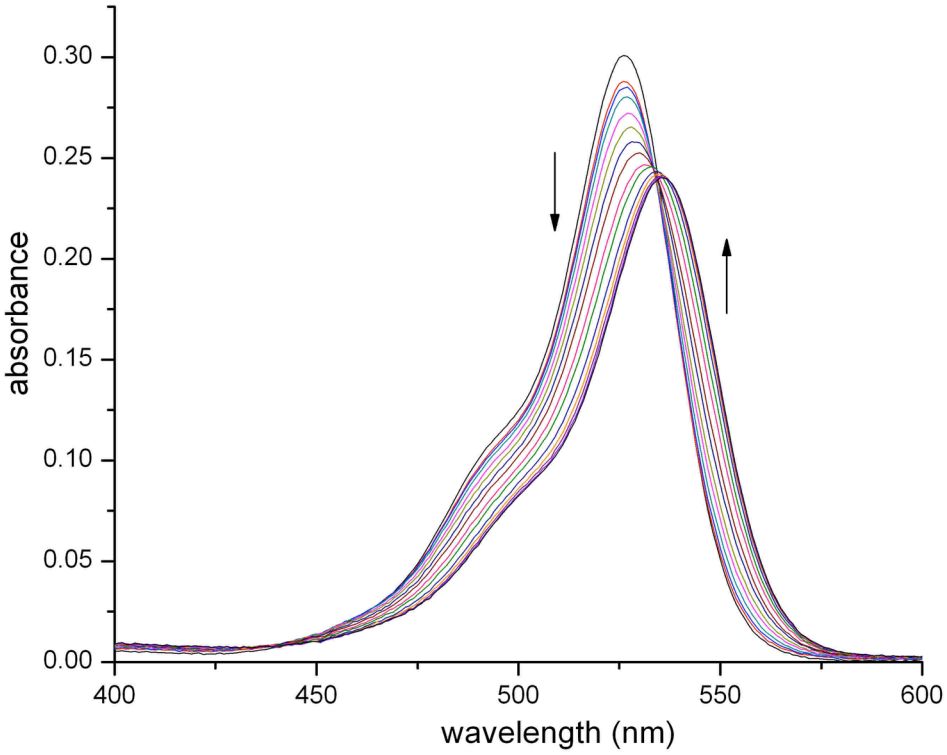

(B)

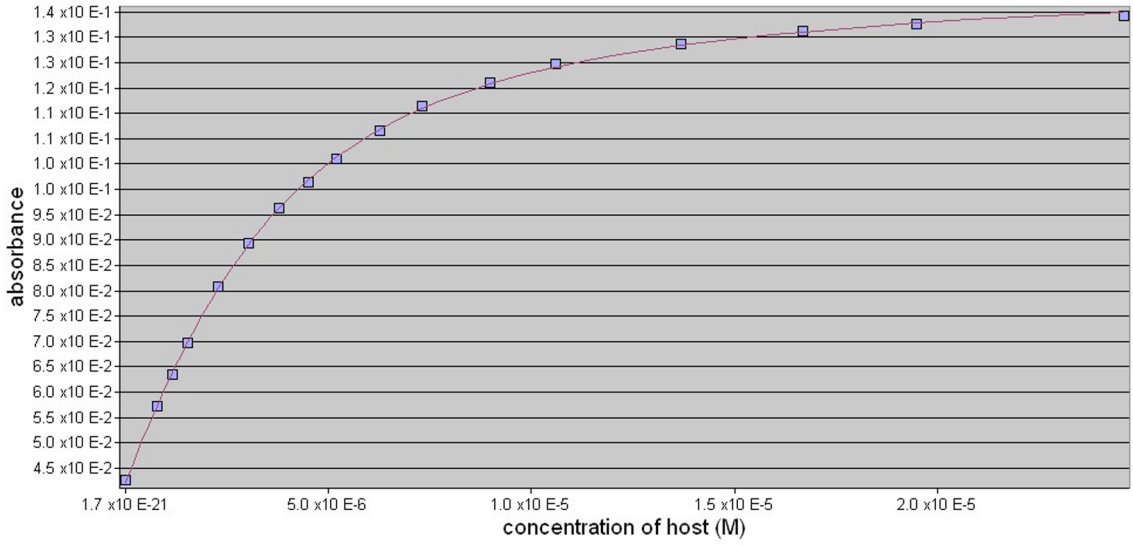

Figure II-S44. (A) UV/Vis spectra from the titration of dye **7** (3.01 μM) with **II-5b** (0 – 25 μM) in 11.83 mM NaH_2PO_4 buffer (pH 7.4); (B) plot of the ΔA_{550} as a function of **II-5b** concentration. The solid line represents the best non-linear fit of the data to a 1:1 binding model ($K_a = 5.3 \pm 0.1 \times 10^5\ M^{-1}$).

(A)

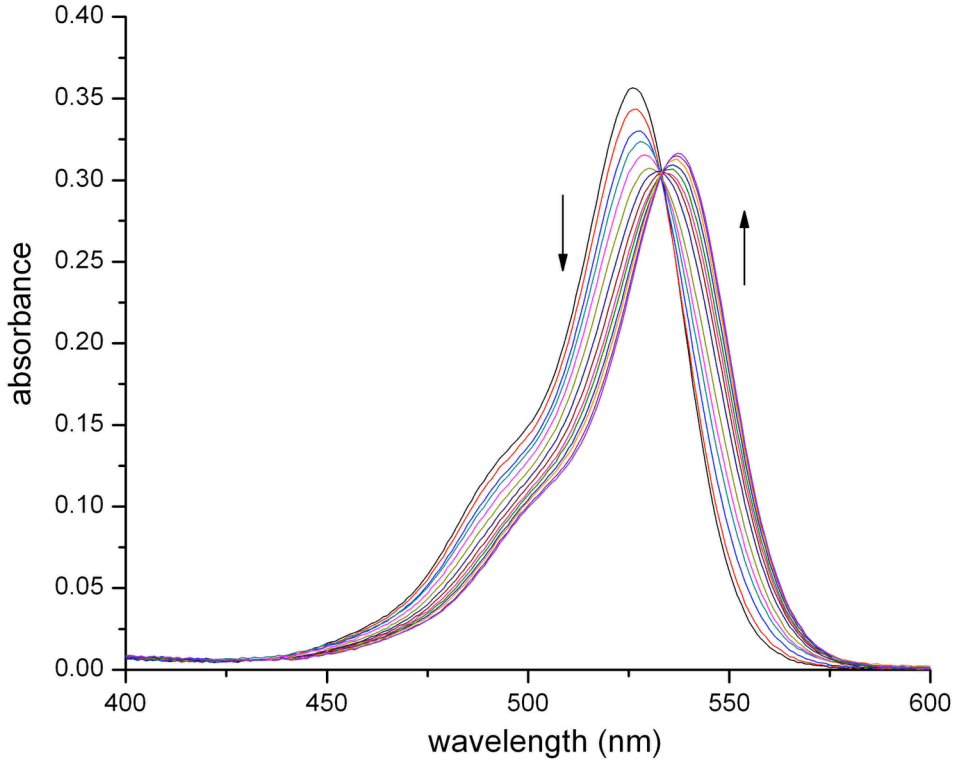

(B)

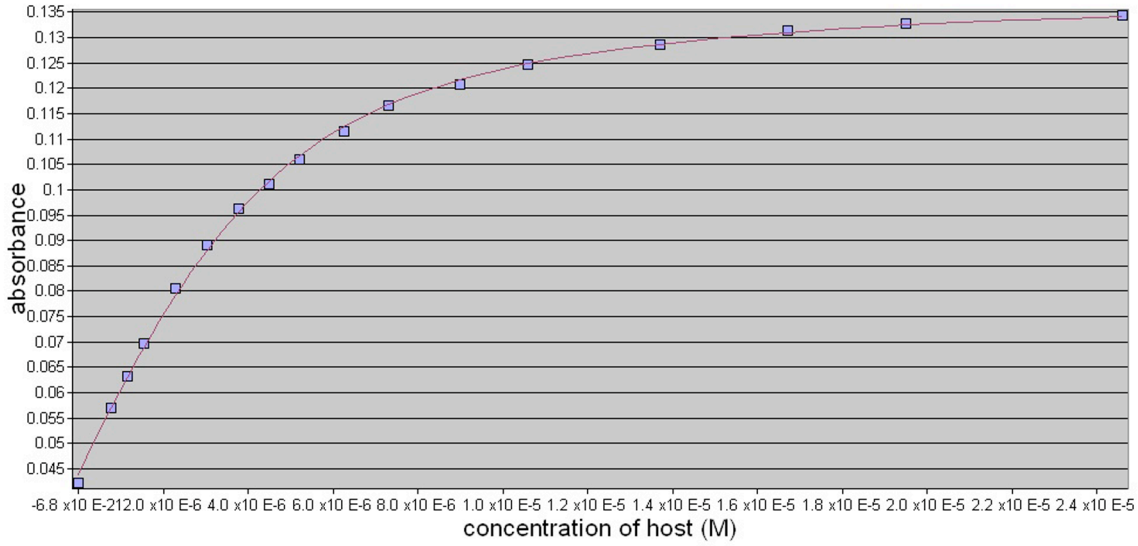

Figure II-S45. (A) UV/Vis spectra from the titration of dye **II-7** (4.15 μM) with **II-5b** (0 – 25 μM) in 18.81 mM NaH_2PO_4 buffer (pH 7.4); (B) plot of the ΔA_{550} as a function of **II-5b** concentration. The solid line represents the best non-linear fit of the data to a 1:1 binding model ($K_a = 3.4 \pm 0.1 \times 10^5\ M^{-1}$).

(A)

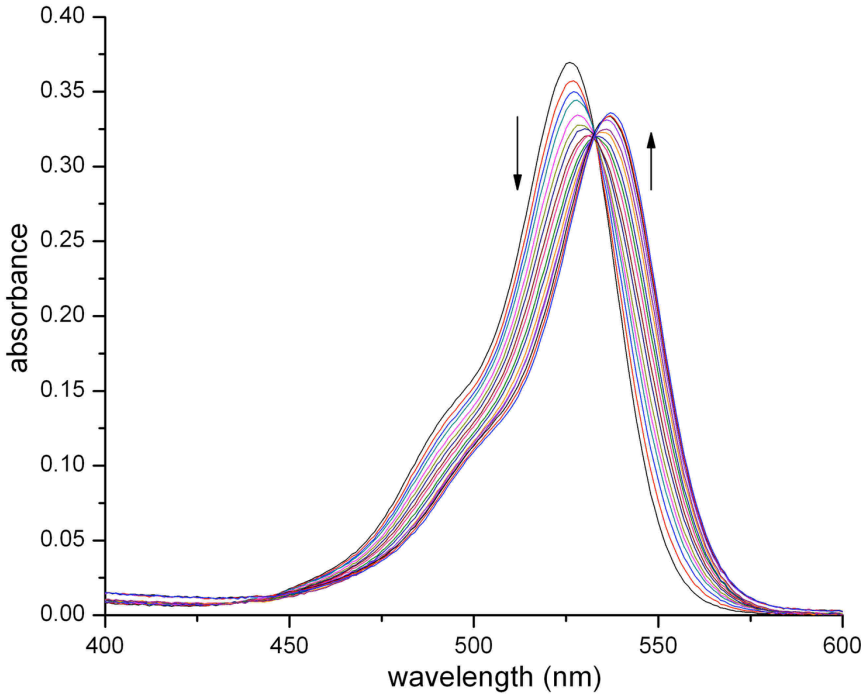

(B)

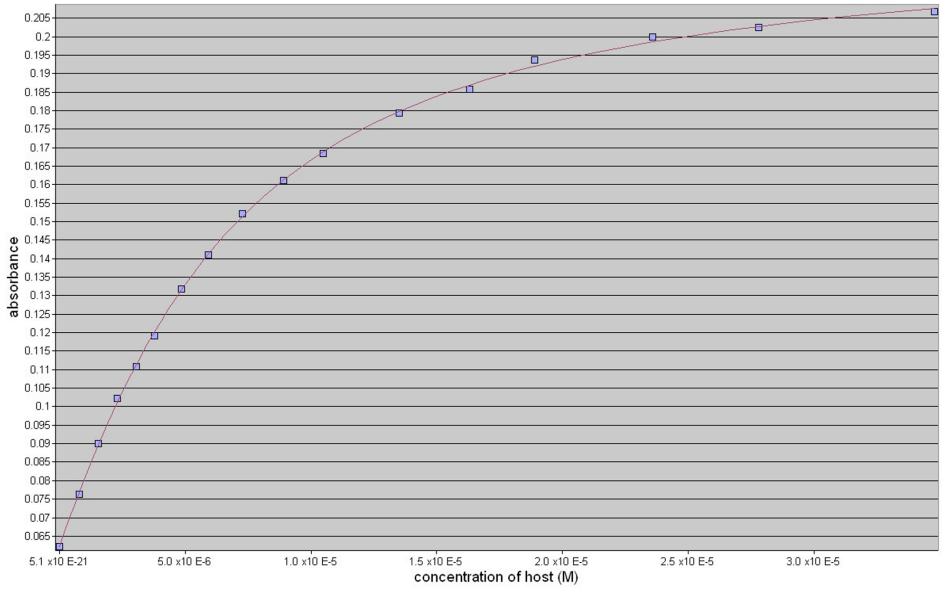

Figure II-S46. (A) UV/Vis spectra from the titration of dye **II-7** (3.28 μM) with **II-5b** (0 – 35 μM) in 24.52 mM NaH_2PO_4 buffer (pH 7.4); (B) plot of the ΔA_{550} as a function of **II-5b** concentration. The solid line represents the best non-linear fit of the data to a 1:1 binding model ($K_a = 2.5 \pm 0.1 \times 10^5\ M^{-1}$).

(A)

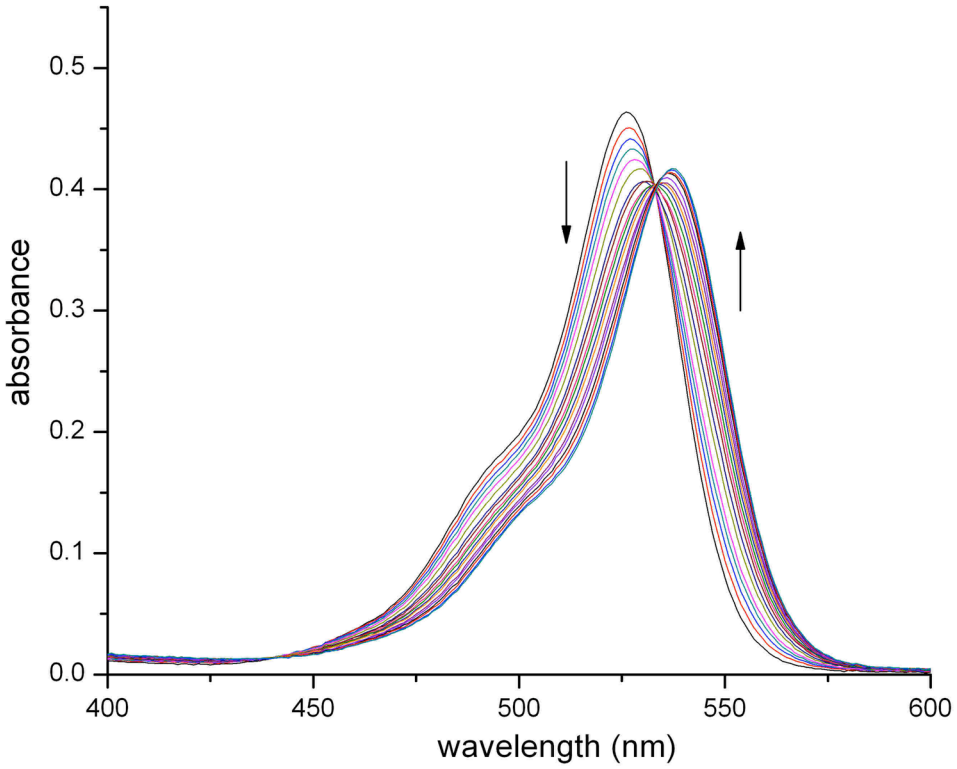

(B)

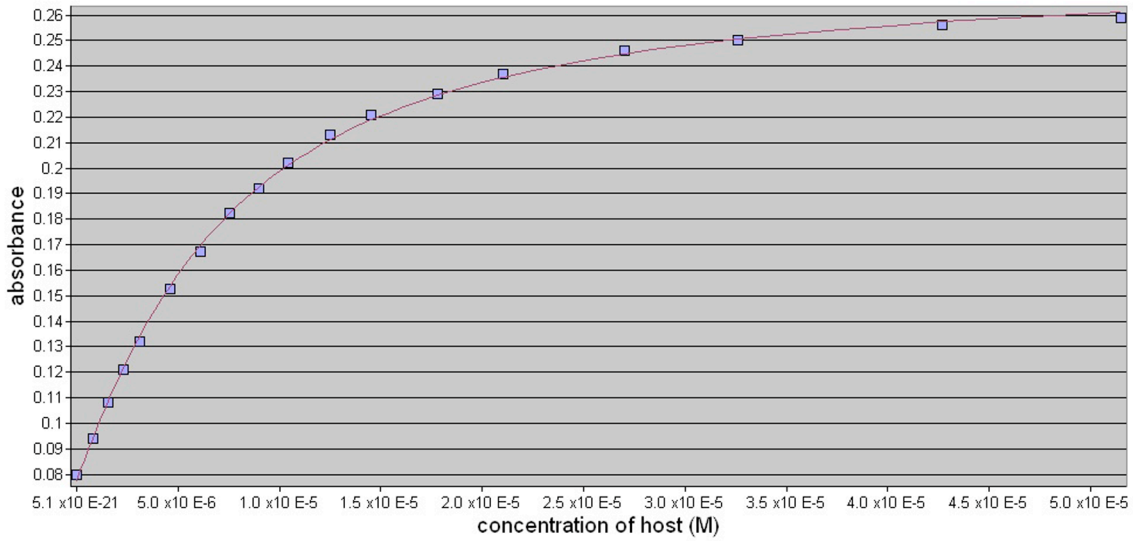

Figure II-S47. (A) UV/Vis spectra from the titration of dye **II-7** (4.16 µM) with **II-5b** (0 – 52 µM) in 31.27 mM NaH_2PO_4 buffer (pH 7.4); (B) plot of the ΔA_{550} as a function of **II-5b** concentration. The solid line represents the best non-linear fit of the data to a 1:1 binding model ($K_a = 2.2 \pm 0.1 \times 10^5\ M^{-1}$)

(A)

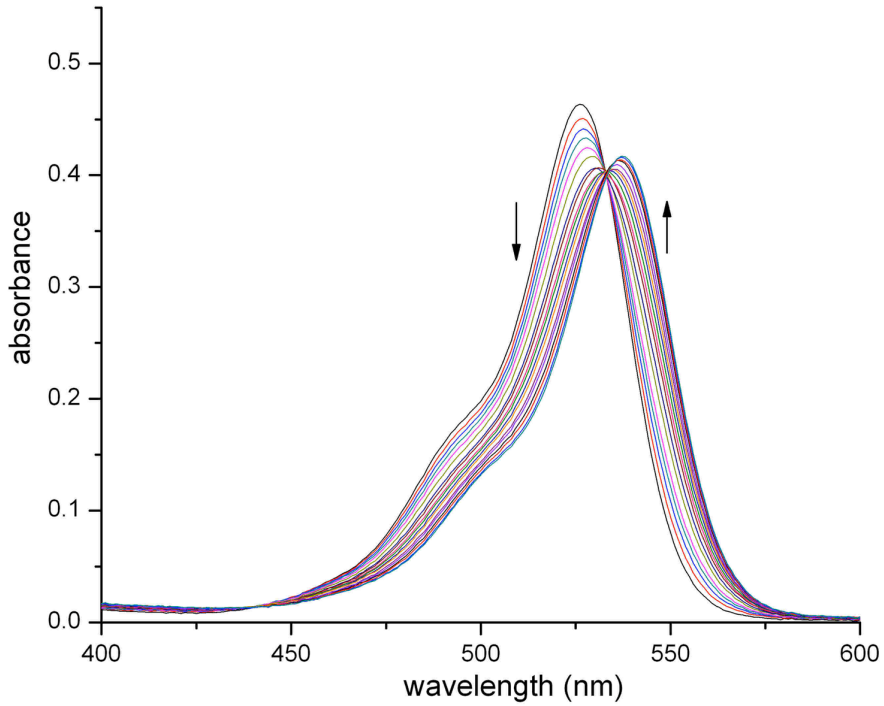

(B)

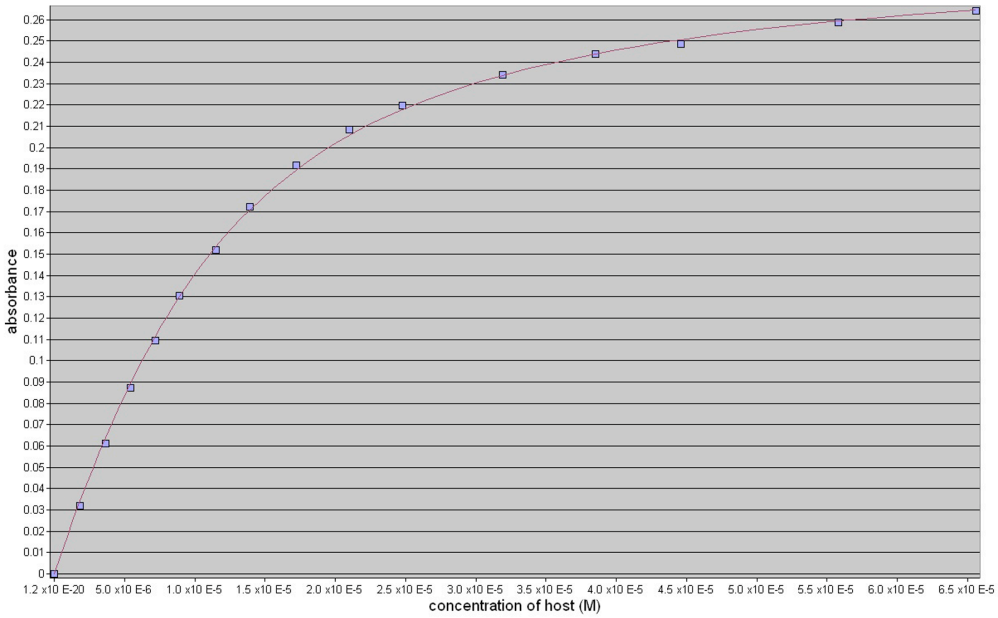

Figure II-S48. (A) UV/Vis spectra from the titration of dye **II-7** (8.58 μM) with **II-5b** (0 – 65 μM) in 40.44 mM NaH_2PO_4 buffer (pH 7.4); (B) plot of the ΔA_{550} as a function of **II-5b** concentration. The solid line represents the best non-linear fit of the data to a 1:1 binding model ($K_a = 1.7 \pm 0.1 \times 10^5\ M^{-1}$).

(A)

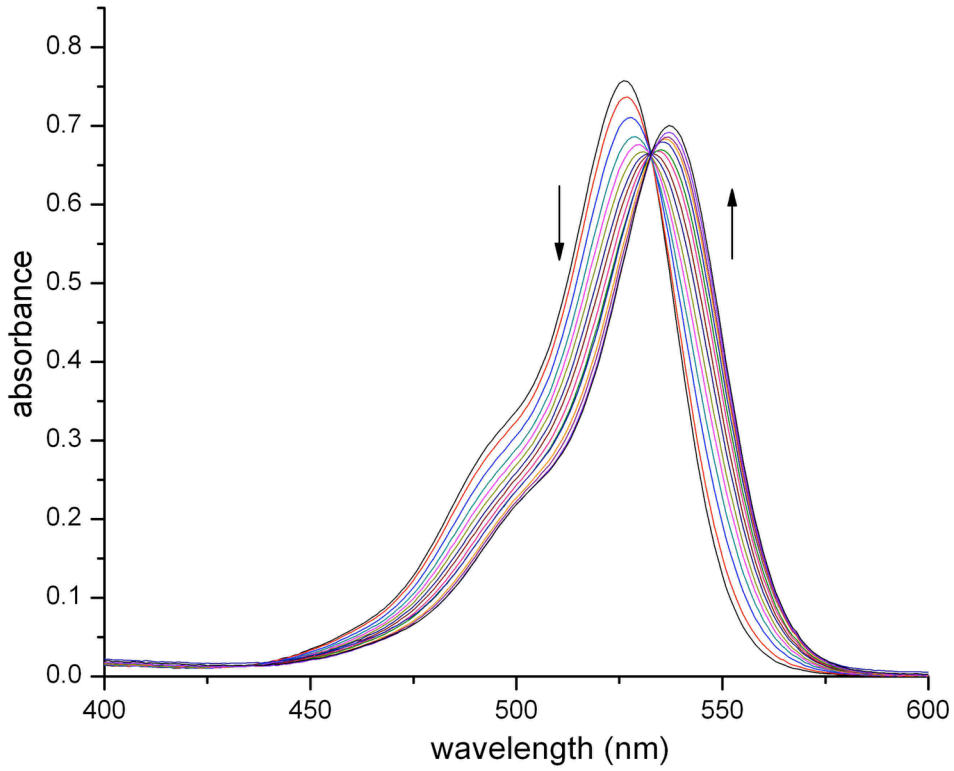

(B)

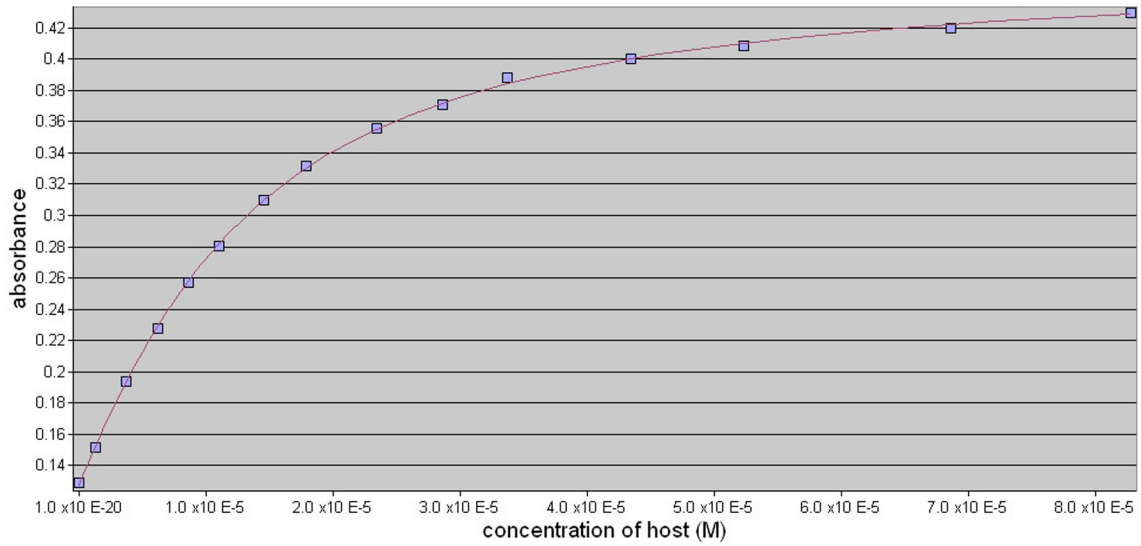

Figure II-S49. (A) UV/Vis spectra from the titration of dye **II-7** (8.52 μM) with **II-5b** (0 – 82 μM) in 57.16 mM NaH_2PO_4 buffer (pH 7.4); (B) plot of the ΔA_{550} as a function of **II-5b** concentration. The solid line represents the best non-linear fit of the data to a 1:1 binding model ($K_a = 1.2 \pm 0.1 \times 10^5\ M^{-1}$).

(A)

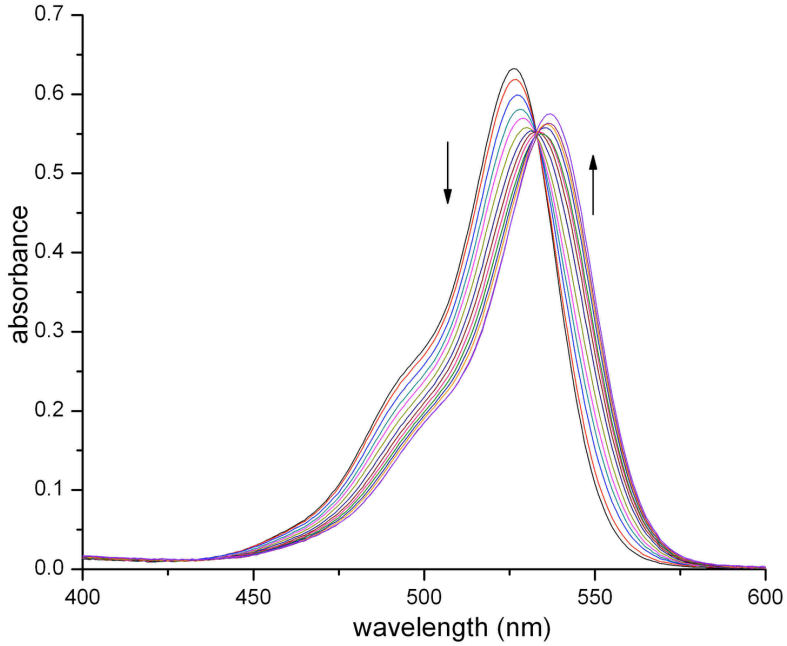

(B)

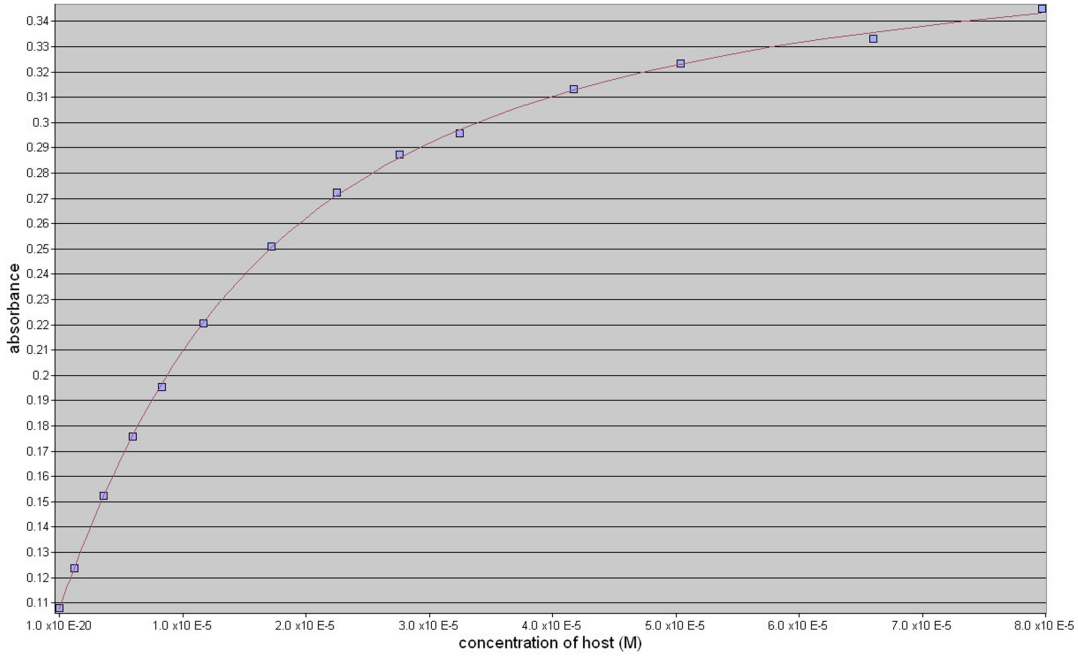

Figure II-S50. (A) UV/Vis spectra from the titration of dye **II-7** (7.45 μM) with **II-5b** (0 – 80 μM) in 73.8 mM NaH_2PO_4 buffer (pH 7.4); (B) plot of the ΔA_{550} as a function of **II-5b** concentration. The solid line represents the best non-linear fit of the data to a 1:1 binding model ($K_a = 8.8 \pm 0.2 \times 10^4\ M^{-1}$).

(A)

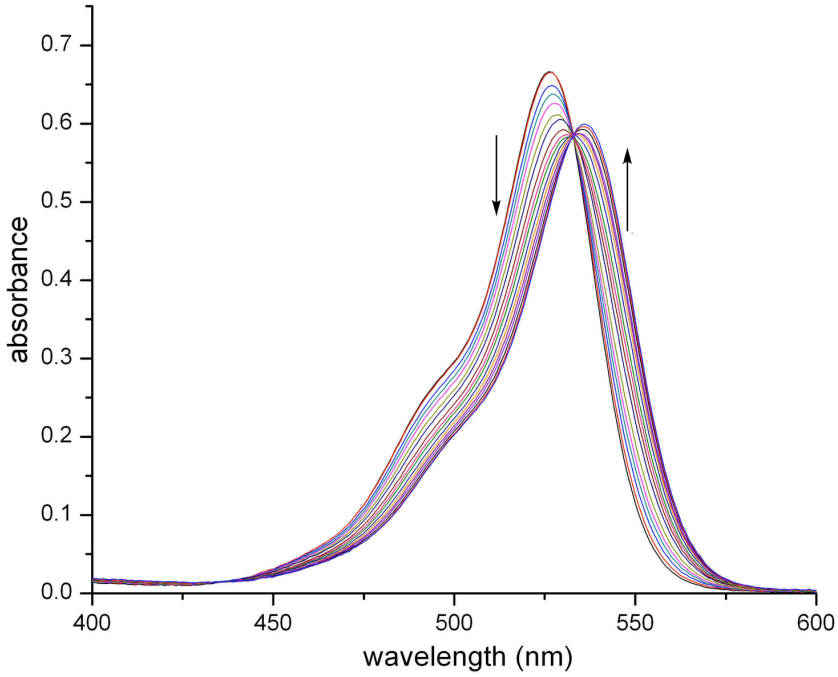

(B)

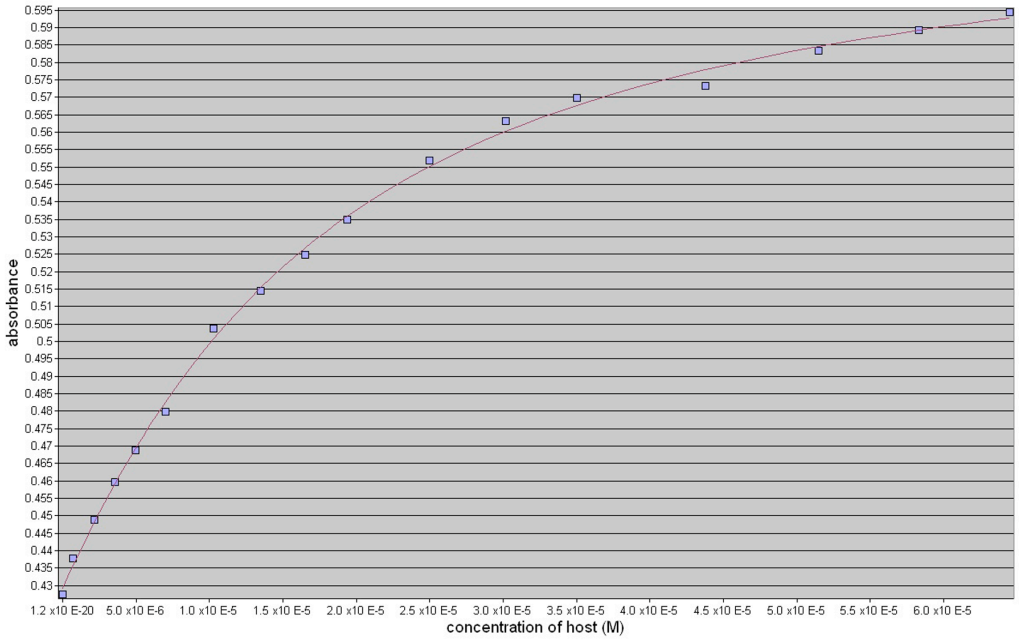

Figure II-S51. (A) UV/Vis spectra from the titration of dye **II-7** (9.88 µM) with **II-5b** (0 – 64 µM) in 91 mM NaH_2PO_4 buffer (pH 7.4); (B) plot of the ΔA_{550} as a function of **II-5b** concentration. The solid line represents the best non-linear fit of the data to a 1:1 binding model ($K_a = 8.0 \pm 0.5 \times 10^4\ M^{-1}$)

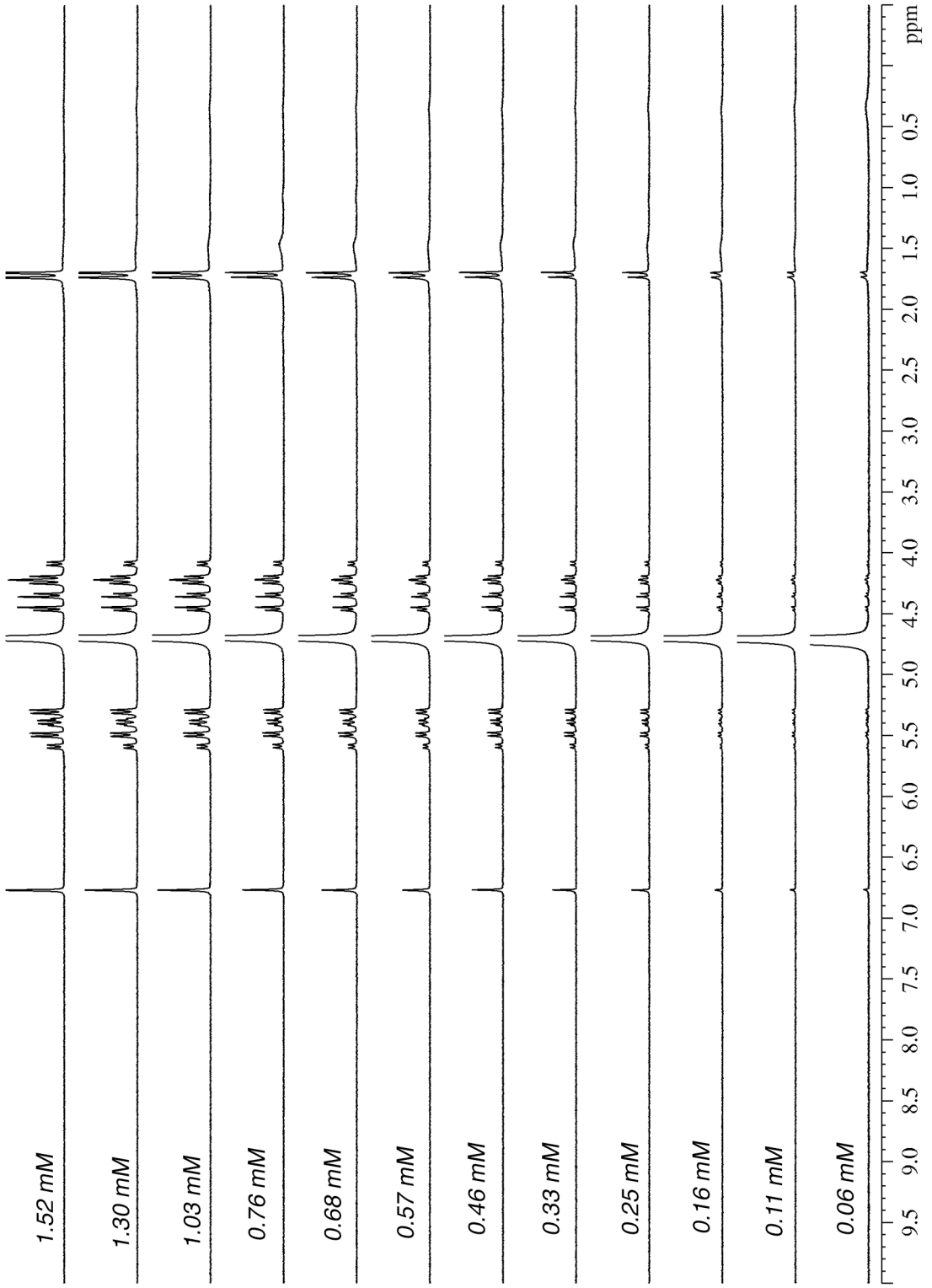

Figure II-S52. ^{1}H NMR spectra (400 MHz, 20 mM sodium phosphate buffer, pD = 7.4) recorded for self-association experiment of **II-5a**.

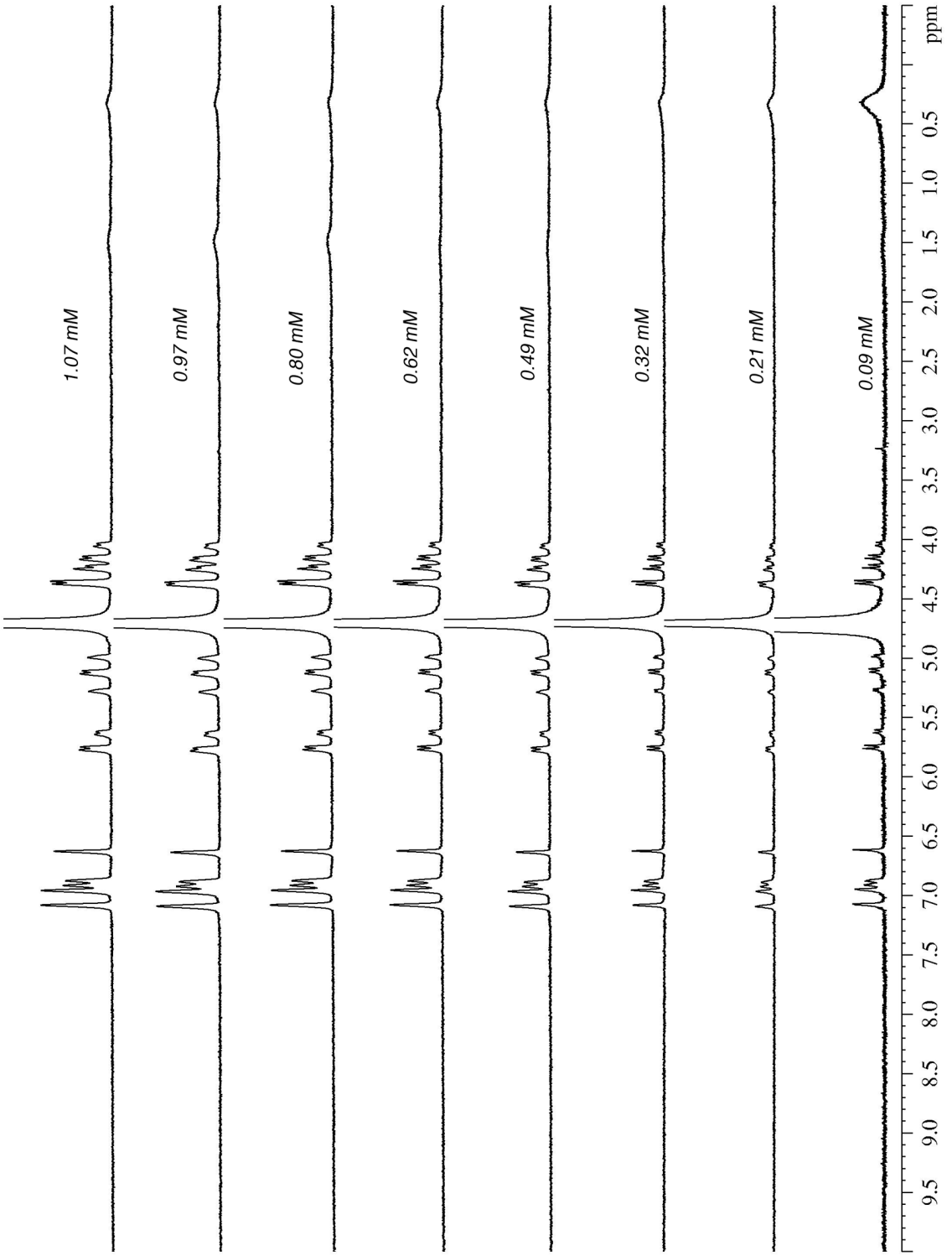

Figure II-S53. ^{1}H NMR spectra (400 MHz, 20 mM sodium phosphate buffer, pD = 7.4) recorded for self-association experiment of **II-5b**.

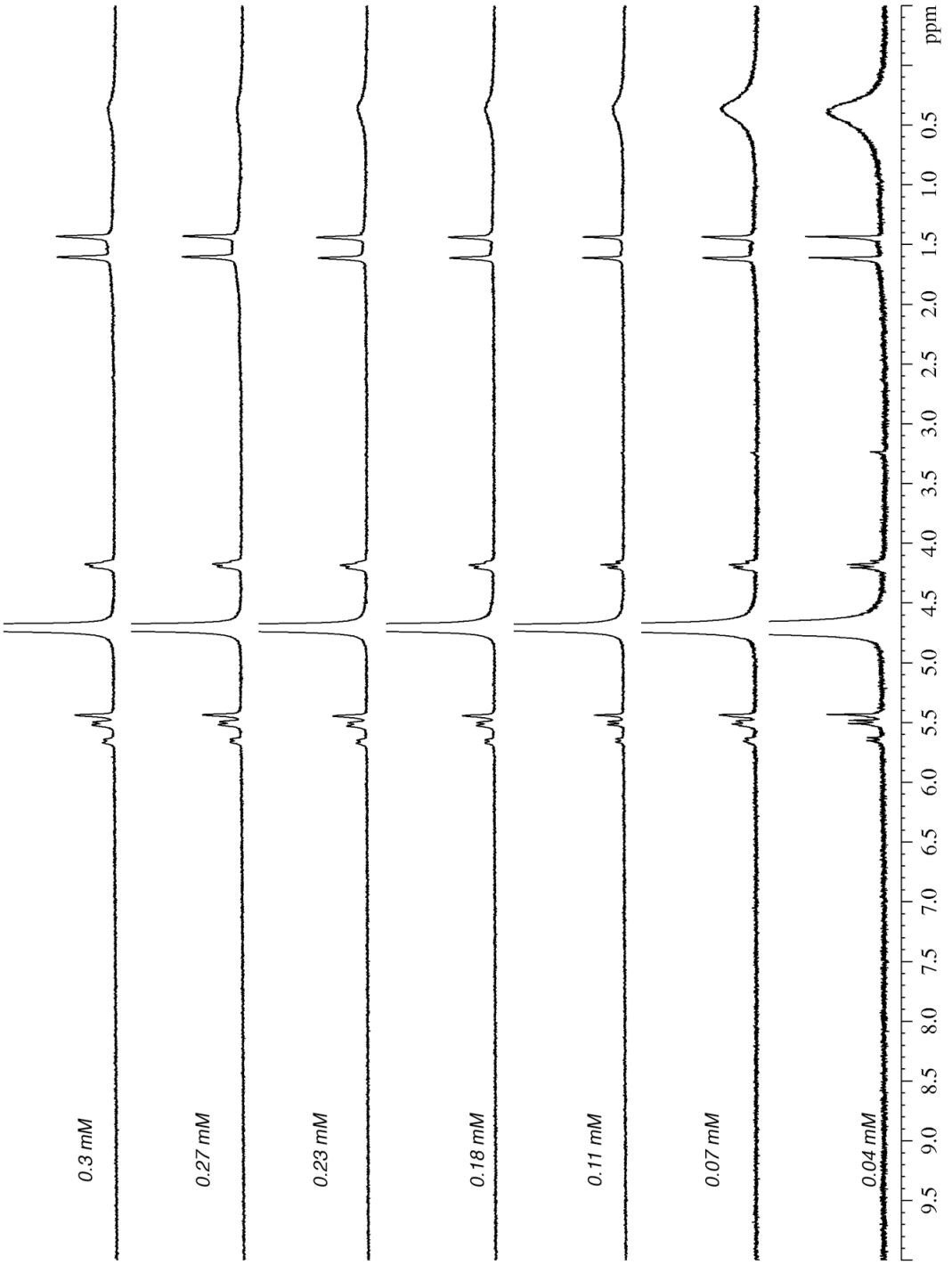

Figure II-S54. ^{1}H NMR spectra (400 MHz, 20 mM sodium phosphate buffer, pD = 7.4) recorded for self-association experiment of **II-6**.

III. Chapter 3. Why Aldehydes Usually Do Not Participate in CB[*n*] Forming Reactions.

3.1 Introduction.

In 1981 Mock and co-workers disclosed that the condensation reaction of glycoluril (**III-1**$_H$) with formaldehyde under strongly acidic conditions delivers cucurbit[6]uril (CB[6]) in high yield (Scheme III-1).[13] In a series of elegant papers throughout the 1980's, Mock established that CB[6] is a truly remarkable host with the ability to bind to alkaneammonium ions with high affinity and selectivity,[44,45,74] to act as a bead in a pH switchable molecular shuttle,[32] and even to accelerate the click reaction between certain acetylenes and azides.[35,43] Around the turn of the millenium, the groups of Kim and Day reported that the condensation of glycoluril (1 equiv. generally > 1 M) with formaldehyde (2 equiv.) under milder conditions (e.g. conc. HCl, 100 °C) results in the formation of a homologous series of cucurbit[n]uril (CB[*n*]; n = 5, 6, 7, 8, 10) hosts.[15,18,19] In the intervening years, the supramolecular chemistry of the larger CB[n] homologues (CB[7] and CB[8]) have been shown to be particularly exciting with applications ranging from molecular machines, chemical sensors, solid phases for sequestration and chromatography, and drug delivery vehicles. [37,41,42,50-70,103]

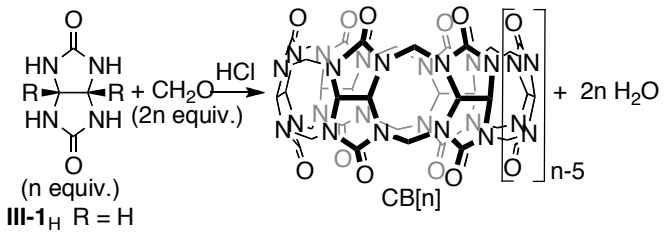

Scheme III-1. Synthesis of CB[*n*].

As a result of these exciting recognition properties, a number of groups have been interested in the synthesis of CB[*n*] derivatives with new structures and tailor-made properties (e.g. enhanced solubility). For this purpose, a number of synthetic strategies have been investigated (Scheme III-2).[23,104] For example, the condensation reaction between a few substituted glycolurils (**III-1**$_R$) and formaldehyde was shown to give R_{10}CB[5] and R_{12}CB[6] compounds (Scheme III-2a). Cy_5CB[5] and Cy_6CB[6] have enhanced solubility in organic solvents and can be used in the formation of ion-selective electrodes.[104] Unfortunately, the self-condensation of a single glycoluril derivative (e.g. **III-1**$_{Me}$) does not yield any substituted CB[7] or CB[8] presumably due to steric interactions between substituents that increase as the size of the ring increases.[90] To address this concern a number of researchers have performed the condensation between two different glycolurils and have been able to isolate partially substituted CB[*n*] (Scheme III-2b).[88,90,105,106] For example, the condensation of **1**$_H$ and **1**$_{Ph}$ resulted in the formation of Ph_2CB[6].[105] Other research groups have developed building block strategies[31,73] based on condensation between glycoluril monomers and glycoluril oligomers.[88] For example, the group of Tao demonstrated the condensation between glycoluril dimer **III-2C** and bis(cyclic ether) **III-1**$_{Me}$BCE yields Me_4CB[6] (Scheme 2c).[88] Perhaps the most useful method for the synthesis of CB[*n*] derivatives involves the direct functionalization of preformed CB[*n*] (n = 5, 6).[24] For example, Kim's group has described the perhydroxylation of CB[*n*] (n = 5, 6) to yield $(HO)_{2n}$CB[*n*] (n = 5, 6)[107] which is amenable to further functionalization reactions (Scheme III-2d) which allows the properties of CB[6] derivatives to be tailored toward specific applications.[103]

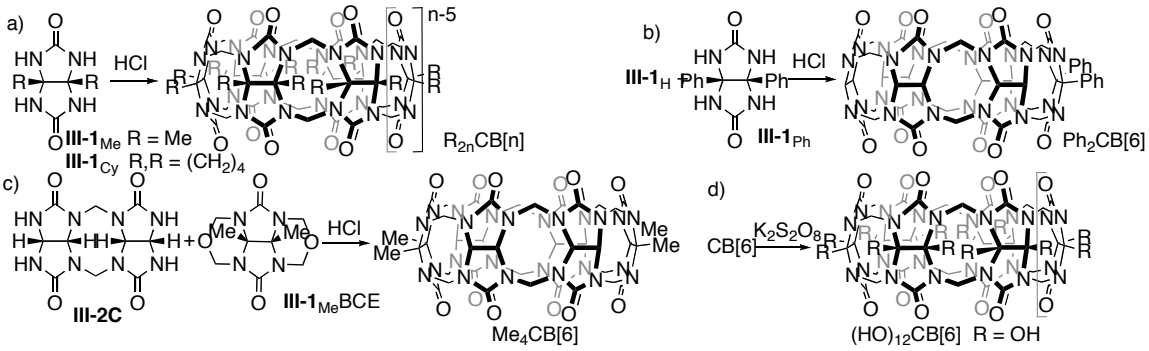

Scheme III-2. Synthesis of substituted CB[6] compounds.

All of the methods described above involve the use of glycoluril derivatives or the functionalization of the convex face of the glycoluril ring system. Is it possible to expand the scope of the CB[*n*] forming reaction beyond formaldehyde (Scheme III-2d)? Although this question has been posed and attempted experimentally by several researchers, the reasons behind the failure of such synthetic routes have remained unclear to date.[103] In this paper, we address this question and delineate two of the reasons why aldehydes do not generally participate in CB[*n*] forming reactions.

3.2 Results and Discussion.

This results and discussion section is organized as follows. First, we present a summary of a portion of the mechanism of CB[*n*] formation proceeding *via* oligomers **III-2** – **III-6** which is relevant to the use of aldehydes in CB[*n*] forming reactions. Next, we present the unsuccessful attempts to react glycolurils with mono-aldehydes followed by the successful synthesis of several S-shaped glycoluril dimers from glycolurils and *o*-

phthalaldehyde. We use the results of these experiments along with product resubmission experiments to explain why aldehydes do not generally participate in CB[*n*] forming reactions.

3.2.1 Mechanism of CB[n] Formation.

The Isaacs group has been heavily involved in the elucidation of the mechanism of CB[*n*] formation.[73,81,108,109] This section presents an overview of portions of the mechanism of CB[*n*] formation (Scheme III-3) that are relevant to our discussion of the use of aldehydes in CB[n] forming reactions. Initially, glycoluril **III-1**$_{H}$ undergoes condensation with formaldehyde to yield a mixture of C-shaped and S-shaped glycoluril dimers (**III-2C** and **III-2S**). Diastereomers **III-2C** and **III-2S** differ in the relative orientation of the pairs of methine H-atoms on the convex face of each equivalent of glycoluril. Previously, we studied the equilibrium between the C-shaped and S-shaped forms using end-capped derivatives of **III-1**$_{COOEt}$ and established a large (> 95:5) thermodynamic preference for the C-shaped form.[108] Subsequently, the **III-2C** may grow to yield trimer (**III-3**), tetramer (**III-4**), pentamer (**III-5**), hexamer (**III-6**), and higher oligomers by the stepwise addition of **III-1**$_{H}$. When the oligomer is long enough (e.g. **III-5** or **III-6**) addition of 1 equivalent of formaldehyde yields *nor-seco*-CB[n] which then goes on to yield CB[*n*] by addition of a final equivalent of formaldehyde. The Isaacs group has previously isolated *ns*-CB[6] and demonstrated its conversion to CB[6] by product resubmission experiments.[22] It is also possible for oligomers (e.g. **III-3** or **III-5**) to condense by a step-growth process (not shown) to yield *nor-seco*-CB[n] with double

cavity (bis-*ns*-CB[10]) or even chiral ((±)-*ns*-CB[6]) structures.[20,21] Please note that in the depicted mechanism (Scheme III-3) oligomers **III-2** – **III-6** are connected by equilibrium arrows which reflect the reversibility of these steps. At this time no quantitative information is available regarding the equilibrium constants for any of these steps. In contrast, Day has demonstrated by product resubmission experiments that the final conversion to CB[6] is an irreversible step and is indicted as such in Scheme 3.[16] Another fact worth noting is that CB[*n*] formation is a condensation reaction and that one molecule of H_2O is produced (highlighted in aqua) for each molecule of CH_2O that is consumed. Two factors that are critical in the successful formation of CB[6] from $\mathbf{1}_H$ and CH_2O are: 1) that the equilibrium between **III-1**$_H$ + CH_2O and **III-2S** / **III-2C** + H_2O favors the dimers, and 2) that the equilibrium between S-shaped (e.g. **III-2S**) and C-shaped (e.g. **III-2C**) diastereomers greatly favors the C-shaped forms.

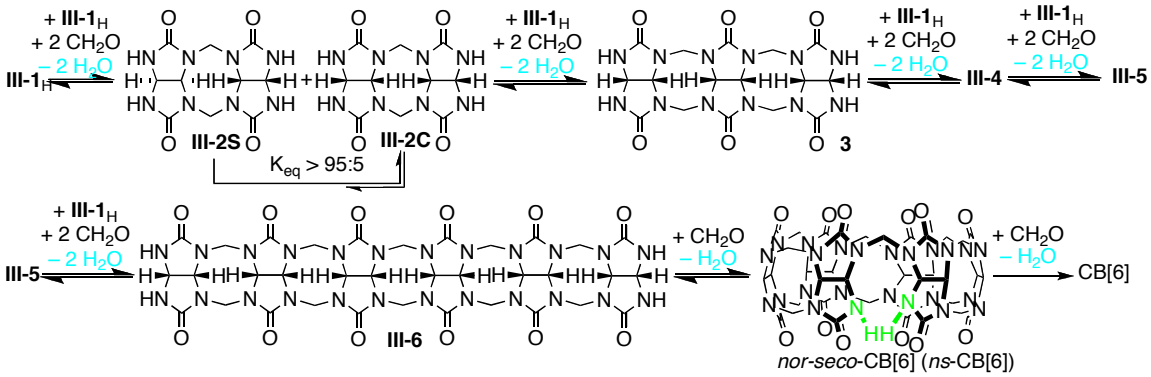

Scheme III-3. Portion of the mechanism of CB[*n*] formation.

3.2.2 Reactions Between Capped Glycoluril 7 and Some Aldehydes Do Not Yield Dimeric Products.

As described above it is critical that the equilibrium between **III-1**$_H$ + formaldehyde and **III-2C** / **III-2S** + H_2O favors products for a successful CB[*n*] forming reaction. We wondered whether this fundamental step of the mechanism of CB[*n*] formation would still favor products when aldehydes are used instead of formaldehyde. To address this question we decided to use capped glycoluril derivative **III-7** in place of **III-1**$_H$ to limit the complexity of the reaction to the formation of dimers.[110-112] Scheme III-4 shows the theoretical reaction between **III-7** and an aldehyde to yield dimers comprising two equivalents of **III-7** and two equivalents of aldehyde. Similar to the condensation of **III-1**$_H$ and formaldehyde described above (Scheme III-3), there are two sets of diastereomers (C-shaped: **III-9a** – **III-9c** and S-shaped: **III-9d** – **III-9e**) that differ in the orientation of the H-atoms on the convex face of the glycoluril ring system. In addition, the use of an aldehyde generates two new stereogenic centers each of which could conceivably adopt two possible configurations. In total, five possible diastereomers could be formed (Scheme III-4).

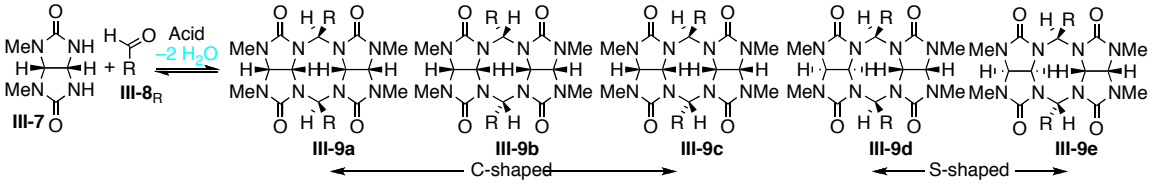

Scheme III-4. Possible products from condensation of **III-7** and an aldehyde.

First, we investigated the reaction between **III-7** (100 mM) and benzaldehyde (**III-8**$_{Ph}$, 100 mM) in conc. DCl at 70 °C. Analysis of the ^{1}H NMR spectrum of the crude reaction mixture showed consumption of starting materials **III-7** and **III-8**$_{Ph}$ but

resonances corresponding to the formation of **III-9** were not observed. Based on this result we surmised that benzaldehyde and **III-7** are not sufficiently reactive (e.g. starting materials are favored under normal concentrations) and that eventually **III-7** and **III-8**$_{Ph}$ undergo decomposition reactions instead. To be certain that this observation was not due to the particular experimental conditions we conducted several additional sets of experiments. In one set of experiments we varied the concentrations of **III-7** and **III-8**$_{Ph}$ (1 mM – 1 M) and still did not observe any dimer formation by ^{1}H NMR. In a second set of experiments we varied the temperature (70 ˚C, 50 ˚C, and room temperature) and followed the reaction by ^{1}H NMR. Once again we could not detect the formation of dimers. Given that the reaction between **III-7** and an aldehyde is a condensation reaction that leads to the formation of H_2O as byproduct we decided to conduct the reaction under anhydrous (CF_3CO_2H) rather than aqueous (conc. HCl) conditions. We hoped that the use of CF_3CO_2H as solvent would favor the formation of dimer as a consequence of Le Chatelier's principle. Unfortunately, similar to the reactions in HCl as solvent we did not observe the formation of any dimeric products. In many of the reactions between **III-7** and **III-8**$_{Ph}$ we observed the formation of hydantoin side product **III-SP1** in low yield (Scheme III-5a). This result is consistent with the known tendency of glycolurils to undergo transformation into hydantoins[110,113] followed by condensation with **III-8**$_{Ph}$. Similar attempted dimerization reactions were conducted between **III-7** and acetaldehyde (**III-8**$_{Me}$), pivaldehyde (**III-8**$_{t\text{-}Bu}$), and acrolein (**III-8**$_{CH=CH2}$). In these cases ^{1}H NMR showed the loss of the resonances due to the starting aldehyde, but no resonances that could be attributed to dimer **III-9** were observed.

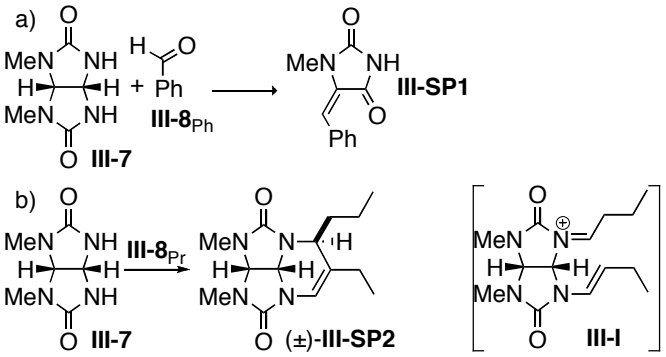

Scheme III-5. Reactions between **III-7** and a) benzaldehyde and b) butanal.

We also conducted the reaction between **III-7** (1 M) and **III-8**$_{Pr}$ (1 M) in TFA at 50 ˚C (Scheme III-5b). Once again, we did not observe the formation of dimer, but in this case we were able to isolate (±)-**III-SP2** in 67% yield.[114] Compound (±)-**III-SP2** is an N-acyl enamine that forms from 1 equivalent of **III-7** and 2 equivalents of **III-8**$_{Pr}$. We believe that (±)-**III-SP2** probably forms results from intramolecular enamine-iminium ion condensation of intermediate **III-I**. The isolation of (±)-**III-SP2** provides strong evidence that aldehydes do react with glycoluril NH groups under acidic conditions but that other factors may divert the reaction away from the formation of methylene bridged glycoluril dimers that are required for CB[*n*] formation.

3.2.3 Reaction Between ns-CB[6] and Phthaldehyde.

Our lack of success in the reactions described in the previous section was somewhat surprising to us given that we previously reported that the reaction between *ns*-CB[6] and *o*-phthaldehyde (**III-11**) delivers CB[6] derivative **III-10** (Scheme III-6).[22]

Compound **III-10** is somewhat unusual in that it contains an N-C-O-C-N bridge rather than the standard N-C-N connection typical of CB[*n*] reactions. Despite this idiosyncrasy it was clear that **III-11** – probably facilitated by the entropic advantage provided by using a dialdehyde – was sufficiently reactive to participate in a CB[*n*] forming reaction. Accordingly, we wondered whether phthaldehyde **III-11** would be reactive toward glycolurils and glycoluril oligomers and provide a new route toward the formation of CB[*n*] derivatives.

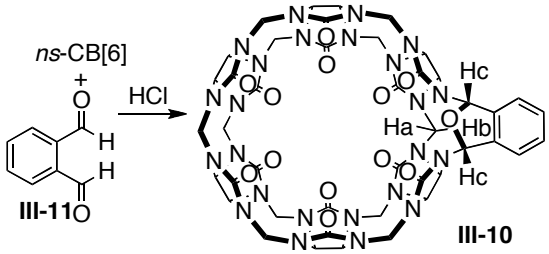

Scheme III-6. Synthesis of **III-10**.

3.2.4 Reaction Between Glycolurils and Phthaldehyde III-11.

Given our interest in the development of building block strategies[28,73] for the construction of CB[*n*] derivatives and analogues we wondered whether **III-11** would participate in such reactions. First, we decided to conduct the reaction between glycoluril dimer **III-2C** (3 equiv.) and **III-11** (3 equiv.) in the hopes of creating a CB[6] derivative. This experiment was conducted in CF_3CO_2H rather than HCl because **III-2C** is nicely soluble in CF_3CO_2H. Contrary to expectation, we observed the formation of tetramer **III-12S** (Scheme III-7a) whose structure was established by spectroscopic methods and also by x-ray crystallography (Figure III-1a). Minor resonances were observed in the crude

^{1}H NMR which may correspond to diastereomers **III-12Ca** and **III-12Cb**. The formation of **III-12S** was very interesting to us for a number of reasons. First, phthaldehyde **III-11** displayed a more normal reactivity in which the *o*-xylylene ring acts as bridge between the 1,5-positions of the newly formed 8-membered ring. Second, even though the condensation of two molecules of **III-2C** and one molecule of **III-11** could, in theory, yield three diastereomers (**III-12S**, **III-12Ca**, and **III-12Cb**) we observe the dominant formation of **III-12S**. Next, we examined the reaction between phthaldehyde **III-11** and glycoluril **III-1**$_H$ or capped glycolurils **III-7**, **III-13**, and **III-14**. In all cases, we observed the dominant formation of a single product (**III-15S** – **III-18S**) with an S-shaped geometry (Scheme III-7b – 7e). We were fortunate to obtain single crystals of **III-12S**, **III-16S**, and **III-17S** and solve their structures (Figure III-1). Figure 1a shows the x-ray crystal structure of **III-12S** which illustrates the overall S-shape of the oligomer due to the relative orientation of the methine C-H groups on the convex face of two equivalents of building block **III-2C** within **III-12S**. Figure 1b shows the x-ray crystal structure of **III-16S** which adopts a very similar geometry. In this case solvating MeOH molecules within the crystal form O-H•••O=C H-bonds to the ureidyl carbonyls of **III-16S**. Compound **III-17S** also displays a similar overall geometry in the crystal (Figure III-1c), but in this case the bridging *o*-xylylene rings of two adjacent molecules of **III-17S** in the crystal undergo π–π stacking interactions.

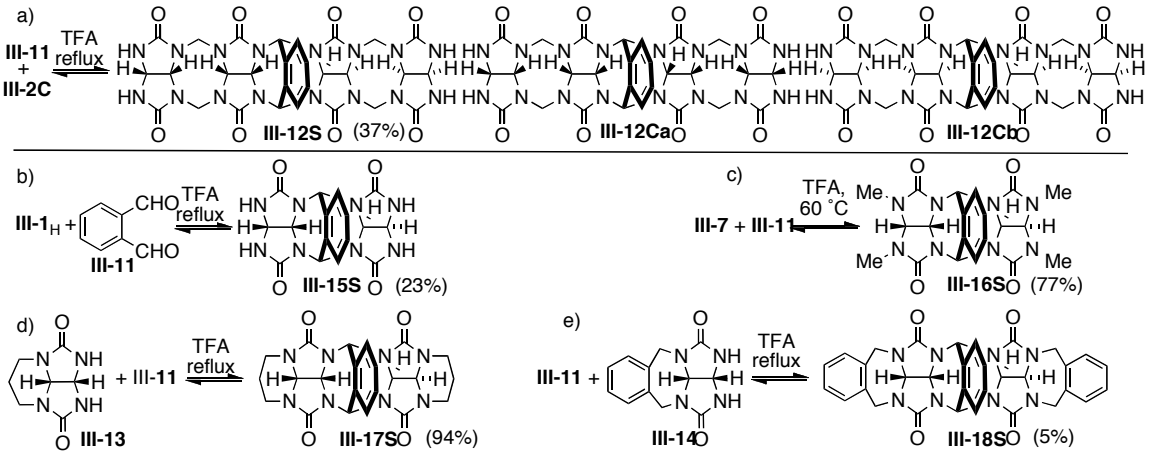

Scheme III-7. Synthesis of dimers and tetramers from glycolurils and phthaldehyde **III-11**.

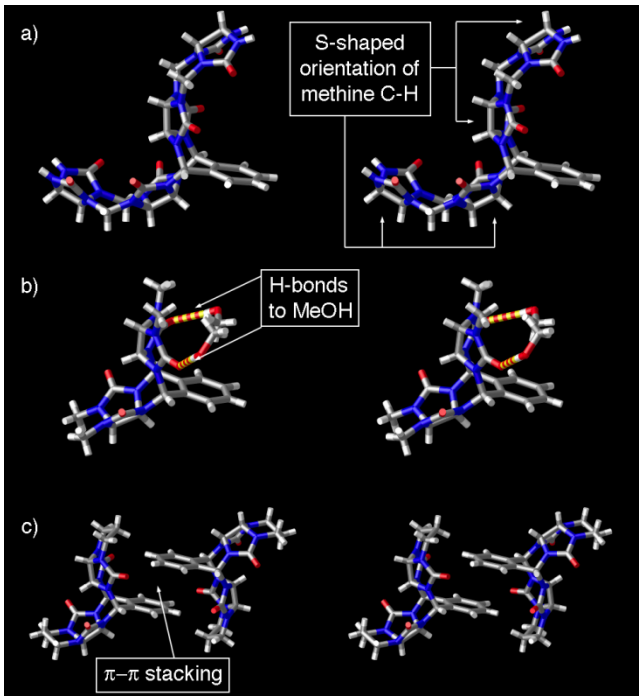

Figure III-1. Cross-eyed stereoviews of the x-ray crystal structures of: a) **III-12S**, b) **III-16S**, and c) **III-17S** rendered with CrystalMaker™. Color code: C, grey; H, white; N, blue; O, red; H-bonds, red-yellow striped.

The formation of the S-shaped diastereomers **III-12S** and **III-15S – III-18S** is of high relevance toward the use of **III-11** or aldehydes in CB[*n*] forming reactions. The formation of S-shaped subunits prevents the reactive NH tips of the oligomers from being close enough in space to undergo macrocyclization reactions. For this reason the use of **III-11** in CB[*n*] forming reactions is unlikely to be successful. We surmise that the reaction between *ns*-CB[6] and **III-11** is successful because *ns*-CB[6] is preorganized into the C-shape needed for macrocyclization before reaction with **III-11**.

3.2.5 Why Do the S-shaped Diastereomers Predominate?

The results described above and supported further below by product resubmission experiments establish that the S-shaped diastereomers **III-12S** and **III-15S – III-18S** are more stable than the corresponding C-shaped diastereomers. More importantly, why do the S-shaped forms predominate in this case? An examination of the x-ray crystal structure of **III-2C**[81] and the MMFF94s energy minimized structures of **III-16S**, **III-16Ca**, and **III-16Cb** (Figure III-2) gives some insights. The central 8-membered ring of **III-2C** exists in the crown-conformation (Figure III-2a).[115-118] Introduction of the bridging *o*-xylylene ring in **III-12** and **III-15 – III-18** results in the formation of two new seven membered rings (7-MR). It is well known that 7-MR prefer the chair conformation over the boat conformation. In the case of **III-16S** one of the two 7-MR adopts the chair

conformation whereas the other adopts the boat form. For **III-16Cb** both of these new 7-MR adopt the chair conformation whereas for **III-16Ca** both adopt the boat conformation. This analysis predicts that **III-16Cb** should be the most stable diastereomer followed by **III-16S** and finally **III-16Ca** which is contrary to the observed dominant formation of **III-16S**. Accordingly, we calculated the relative heats of formation of **III-16S**, **III-16Cb**, and **III-16Ca** of the MMFF94s minimized conformers using the PM3 method and found that theory predicts that **III-16S** is 2.21 kcal mol^{-1} more stable than **III-16Cb** (chair-chair) and 11.29 kcal mol^{-1} more stable than **III-16Ca** (boat-boat). We believe that unfavorable H•••H non-bonded interactions (2.01Å)[119] between H-atoms on adjacent glycoluril rings (Figure III-2c) destabilize **III-16Cb**. On the basis of this analysis, it becomes clear that the conformational preferences of the newly forming 8-MR and 7-MR control the diastereomer (e.g. S-shaped or C-shaped) that is formed. For a CB[*n*] derivative forming reactions to proceed smoothly it is critical that the equilibrium between S-shaped and C-shaped forms greatly favors the C-shaped form.

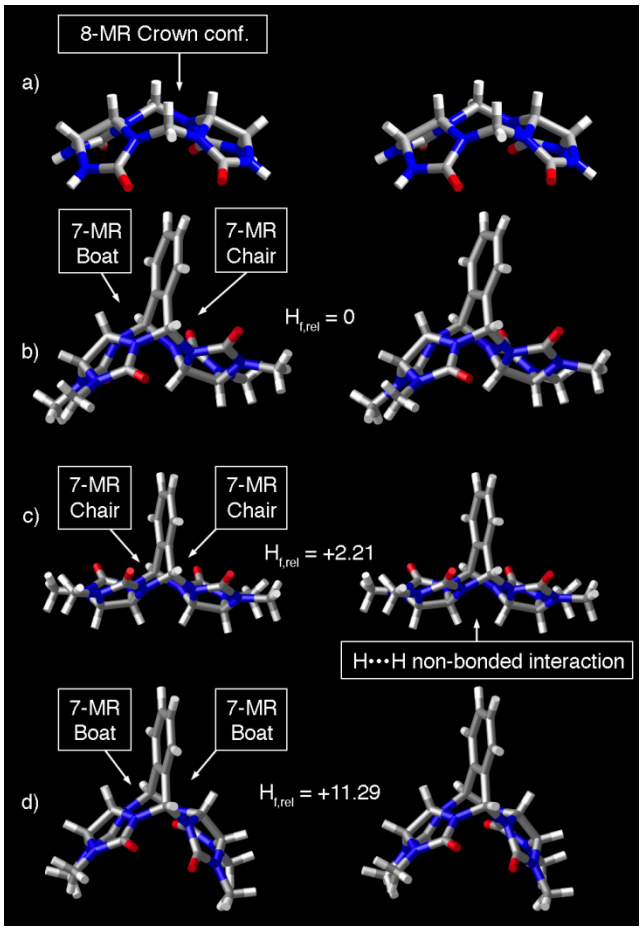

Figure III-2. Stereoscopic representations of the x-ray crystal structure of a) **III-2C** and the MMFF94s minimized geometries of b) **III-16S**, c) **III-16Cb**, and d) **III-16Ca**. Color code: C, grey; H, white; N, blue; O, red. The quoted relative heats of formation (kcal mol^{-1}) were obtained from PM3 calculations.

3.2.6 Product Resubmission Experiments.

In combination, the synthetic and theoretical studies described above strongly suggested that the S-shaped diastereomers **III-12S** and **III-15S** – **III-18S** were thermodynamically more stable than the C-shaped diastereomers. In previous model

system studies of the equilibrium between S-shaped and C-shaped methylene bridged glycoluril dimers we used product resubmission experiments to transform the S-shaped diastereomers into the C-shaped forms.[108] We decided to attempt similar experiments with **III-16S**. Accordingly, we monitored the composition of a solution of **III-16S** (12.5 mM) in 5% DCl at room temperature and observed a decrease in the concentration of **III-16S** over several days and somewhat surprisingly an increase in the concentration of glycoluril monomer **III-7** (Figure III-3a). No ^{1}H NMR resonances were detected that would indicate the formation of C-shaped diastereomers **III-16Ca** or **III-16Cb** which is in accord with the PM3 calculation described above. The observation of the mixture of S-shaped dimer **III-16S** and glycoluril monomer **III-7** suggested to us that the equilibrium constant for the conversion of **III-7** and **III-11** into **III-16S** and H_2O might be small due to the decreased reactivity of **III-11** relative to formaldehyde. To further verify this hypothesis, we dissolved **III-16S** in 5% DCl at room temperature at different concentrations (50 mM, 12.5 mM, 3.8 mM, and 1 mM) and followed the decrease in the mole fraction of **III-16S** by ^{1}H NMR spectroscopy (Figure III-3b). We also followed the formation of **III-16S** from equimolar mixtures of glycoluril monomer **III-7** and phthaldehyde **III-11** under identical conditions (Figure III-3a). Figure III-3 shows two important trends. First, both the formation and fragmentation of **III-16S** plateau at comparable mole fractions of **III-16S**. Second, as the concentration increases from 1 mM to 50 mM we observe an increase in the mole fraction of **III-16S** at the plateau level. Both of these observations suggest that the conversion of **III-7** and **III-11** into **III-16S** and H_2O is an equilibrium process with a modest equilibrium constant. In sharp contrast to the reaction between glycolurils and formaldehyde which greatly favors products over

starting materials over a range of conditions, the use of less reactive phthalaldehyde **III-11** results in only partial dimerization in the 1 – 50 mM concentration regime. We infer that the lack of observed reactivity between **III-7** and benzaldehyde probably reflects an even lower equilibrium constant that cannot be accessed over the concentration range employed (up to 1 M).

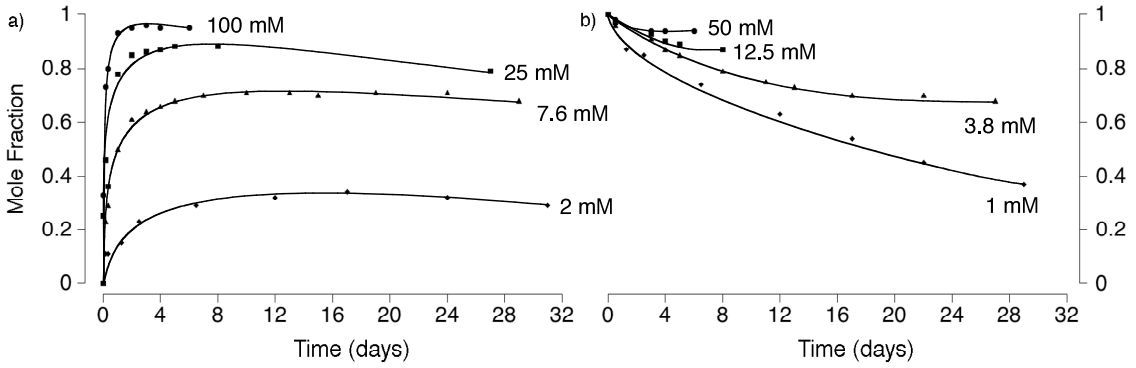

Figure III-3. Plots of mole fraction of **III-16S** versus time for the a) formation and b) fragmentation of **III-16S**. Conditions: 5% DCl in D_2O, room temperature. The solid lines are intended merely as guides for the eye.

3.2.7 Equilibrium and Reversibility of Formaldehyde Based Dimers.

The previous section demonstrated that the formation of glycoluril dimer **III-16S** from **III-7** and phthaldehyde **III-11** is a reversible process with the mole fraction of **III-16S** experiencing large changes over the 1 – 100 mM range. As further evidence of the relevance of this behavior to CB[*n*] forming reactions similar experiments were performed on the transformation of **III-7** and formaldehyde into **III-19C** (Scheme III-8) previously reported by the Sindelar group.[112] Given the higher reactivity of formaldehyde

than aldehydes we anticipated that we would need to resort to higher temperatures to entropically favor monomer **III-7**. Figure III-4a shows a plot of mole fraction of **III-19C** versus time obtained during the formation of **III-19C** (5% DCl, 70 ˚C) at three different concentrations. In all three cases we observe an initial increase in the mole fraction of **III-19C** followed by a maximum and finally a decrease. At higher concentrations the mole fraction reaches a higher maximal value and decreases more slowly after this maximum is reached. As a complementary experiment we dissolved **III-19C** in 5% DCl at 70 ˚C and followed the fragmentation of **III-19C** by ^{1}H NMR as a function of time (Figure III-4b). At higher concentrations of **III-19C** the mole fraction of **III-19C** decreases more slowly. We interpret this behavior as being indicative of two competing processes: 1) equilibrium between **III-7** and dimer **III-19C**, and 2) chemical decomposition of glycoluril monomer **III-7**. We performed identical experiments at 50 ˚C in 5% DCl (Figure III-4c and III-4d) and observe clearer plateau regions which indicates lower levels of side reactions (e.g. decomposition) relative to monomer-dimer equilibrium at this temperature.

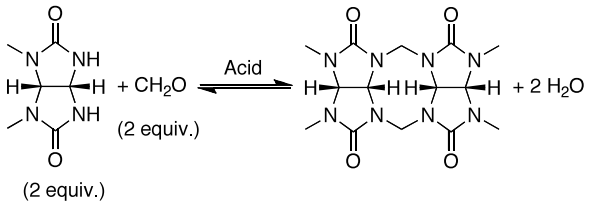

Scheme III-8. Formation of C-shaped glycoluril dimer **III-19C**.

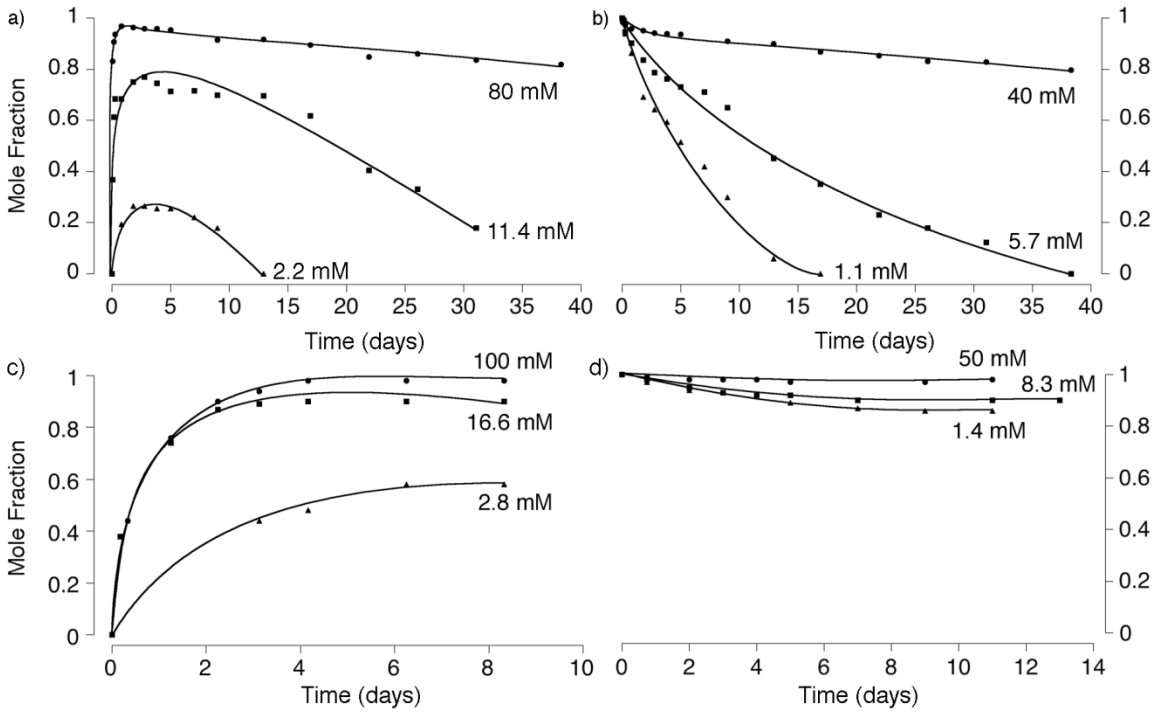

Figure III-4. Plots of mole fraction of **III-19C** versus time for the a) formation, b) fragmentation of **III-19C** (5% DCl in D_2O, 70 ˚C), c) formation, and d) fragmentation of **III-19C** (5% DCl in D_2O, 50 ˚C). The solid lines are intended merely as guides for the eye.

3.3 Conclusions.

We have shown that glycolurils react with a dialdehyde (*o*-phthaldehyde) to deliver S-shaped glycoluril dimers **III-15S** – **III-18S** and tetramer **III-12S**. We established that S-shaped compounds **III-12S** and **III-15S** – **III-18S** are thermodynamically preferred over the C-shaped diastereomers and trace this preference to the conformational biases of the newly formed benzo bicyclo[3.3.2]octane ring system. The presence of S-shaped segments in glycoluril oligomers hinders macrocyclization to CB[*n*]-type compounds by

holding the reactive NH groups far apart in space. Accordingly, the observation of the dominant formation of S-shaped dimers in the reaction between glycolurils and **III-11** provides one reason for the inability of *o*-phthalaldehyde and possibly other aldehydes to participate in CB[*n*] forming reactions. The side products observed in the reaction between **III-7** and aldehydes **III-8**$_{Ph}$ and **III-8**$_{Pr}$ illustrates two alternative reaction pathways (hydantoin formation and enamine-iminium ion cyclization) that become viable when less reactive aldehydes are used.

We used product resubmission experiments to provide evidence for an equilibrium between dimer **III-16S** and monomer **III-7** that responds to changes in concentration over the 1 – 50 mM range. This indicates that the equilibrium constant for dimer formation with *o*-phthalaldehyde is modest and that high concentrations of starting materials are needed to drive the reaction toward completion. In contrast to the results obtained with *o*-phthalaldehyde, we did not observe any reaction between benzaldehyde and glycoluril **7** under the range of concentrations (1 mM – 1 M) employed. We interpret this result as meaning that the reactivity of aldehydes toward glycolurils is even lower (lower equilibrium constant) than that of *o*-phthalaldehyde **III-11**. Given that concentrations of 50 mM are needed to drive the reaction with *o*-phthalaldehyde **III-11** to completion perhaps it is not surprising that mono-aldehydes do not react with glycolurils at concentrations up to 1 M. Accordingly, these results point toward poor reactivity (low equilibrium constant) as a second reason for the inability of aldehydes to participate in CB[*n*] forming reactions.

The delineation of two of the reasons why aldehydes do not generally participate in CB[*n*] forming reactions – the critical importance of the S- to C-shaped equilibrium and the magnitude of the equilibrium constant for chain growth – is important because it suggests methods to overcome these limitations in the future. When it is possible to introduce functionality onto the bridging CH_2-groups of CB[*n*] we expect that the range of applications (e.g. targeted drug delivery, affinity chromatography, and sensing arrays) to which CB[*n*] derivatives[103] can be applied will expand.

3.4 Experimental Section.

General experimental details have been reported previously.[69,112] Starting materials were obtained from commercial suppliers and used without further purification. Compounds **III-2C**, **III-7**, **III-13**, and **III-14** were prepared by the literature procedures.[81,112] Compound **III-SP1** has been reported in the literature previously.[114]

Compound III-12S. Compound **III-2C** (498 mg, 1.62 mmol) was dissolved in a mixture of TFA and water (19:1, v:v, 6 mL) and *o*-phthaldiadehyde (108 mg, 0.81 mmol) was added. The mixture was heated at 70 ˚C for 3 hours. The solution was then poured into MeOH (150 mL). The precipitate was filtered to yield the crude product (580 mg). The crude solid was stirred in a mixture of formic acid and water (1:2, v:v, 120 mL) 30 minutes. The filtrate was concentrated under reduced pressure and then poured into MeOH (200 mL). After filtration and drying, the precipitate was further purified by recrystallization from TFA and water (4:1, v:v, 20 mL) to yield **III-12S** as a white solid

(216 mg, 0.30 mmol, 37%). M.p. 350 ˚C (dec.). IR (ATR, cm^{-1}): 3450w, 1715s, 1445s, 1318m, 1228s, 1185s. ^{1}H NMR (400 MHz, DMSO-d_6): 7.71 (s, 2H), 7.61 (s, 2H), 7.60-7.55 (m, 2H), 7.45-7.40 (m, 2H), 6.46 (s, 2H), 5.56 (d, J = 14.6 Hz, 2H), 5.54 (d, J = 6.8 Hz, 1H), 5.42 (d, J = 14.6 Hz, 2H), 5.41 (d, J = 8.6 Hz, 1H), 5.30 (d, J = 8.6 Hz, 1H), 5.23 (d, J = 8.6 Hz, 1H), 5.13 (d, J = 8.6 Hz, 1H), 5.10 (d, J = 8.6 Hz, 1H). 4.79 (d, J = 8.6 Hz, 1H), 4.16 (d, J = 14.6 Hz, 2H), 4.06 (d, J = 14.6 Hz, 2H). ^{13}C NMR (100 MHz, TFA, external DMSO reference): δ 158.6, 158.5, 154.5, 153.8, 130.1, 129.6, 127.8, 72.5, 72.3, 69.0, 68.5, 63.7, 61.7, 61.5, 61.3, 49.5, 49.1 (Only 17 of the 18 expected resonances were observed). MS (ESI): m/z 715 ($[M + H]^+$). HR-MS (ESI^+): m/z 715.2220, calc. for $C_{28}H_{27}N_{16}O_8$ 715.2198. X-ray crystal structure.

Compound III-16S. Compound **III-7** (300 mg, 1.76 mmol) was dissolved in TFA (7 mL) and *o*-phthaldialdehyde **III-11** (120 mg, 0.89 mmol) was added. The mixture was stirred and heated at 60 ˚C for 3 hours. The solvent was removed under reduced pressure. The crude mixture was recrystallized from MeOH to yield **III-16S** as a white crystalline solid (300 mg, 0.68 mmol, 77%). M.p. 322 ˚C (dec.). TLC ($CHCl_3$/MeOH 6:1) R_f 0.28. IR (ATR, cm^{-1}): 3493w, 3003w, 2933w, 1692s, 1482s, 1405s, 1380s, 1203s, 1036s. ^{1}H NMR (400 MHz, $CDCl_3$): 7.50-7.45 (m, 2H), 7.40-7.35 (m, 2H), 6.59 (s, 2H), 5.34 (d, J = 7.9 Hz, 1H), 4.93 (d, J = 8.4 Hz, 1H), 4.85 (d, J = 7.9 Hz, 1H), 4.84 (d, J = 8.4 Hz, 1H), 3.01 (s, 6H), 2.84 (s, 6H). ^{13}C NMR (100 MHz, $CDCl_3$): d 155.2, 155.2, 134.2, 130.0, 129.2, 71.2, 71.1, 64.9, 64.3, 62.3, 30.2, 29.8. MS (ESI): m/z 439 ($[M + H]^+$). HR-MS (ESI^+): m/z 439.1818, calc. for $C_{20}H_{23}N_8O_4$ 439.1842. X-ray crystal structure.

3.5 Supporting Information

Compound III-SP1. A solution of **III-7** (102 mg, 0.60 mmol) and **III-8**$_{Ph}$ (64 mg, 0.60 mmol) in TFA (0.60 mL) was heated at 70 ˚C for 4 d. The solvent was removed by rotary evaporation. The crude solid was dissolved in $CHCl_3$ (1 mL) and washed with water (2 mL). The organic layer was evaporated with reduced pressure and the solid was recrystallized from ethanol (1 mL) to yield **III-SP1** as a white solid (12 mg, 10%). The spectroscopic data match that reported in the literature.

Compound III- (±)-SP2. To a solution of **III-7** (102 mg, 0.60 mmol) in TFA (0.6 mL), **III-8**$_{Pr}$ (43 mg, 0.60 mmol) was added. The solution was heated at 50 ˚C for 24 h. The solvent was removed by rotary evaporation. The crude solid was washed with $CHCl_3$ (3 mL). After filtration, the filtrate was concentrated under reduced pressure and then further purified by column chromatography (SiO_2, 20:1, CH_2Cl_2/CH_3OH, v:v) to yield a waxy yellow solid (56 mg, 67%). TLC (CH_2Cl_2/CH_3OH, 20:1, v:v) R_f = 0.12. IR (KBr): 3400m, 2961s, 2874m, 1708s, 1465s, 1411s, 1351m, 1233s, 1172m, 1107m, 1034m, 820m, 790m, 755m. ^{1}H NMR (400 MHz, $CDCl_3$): 6.42 (s, 1H), 5.18 (d, J = 7.4, 1H), 5.03 (d, J = 7.4, 1H), 4.20 (d, J = 8.0, 1H), 3.01 (s, 3H), 2.98 (s, 3H), 2.15-2.00 (m, 2H), 1.75-1.70 (m, 1H), 1.50-1.35 (m, 3H), 1.05 (t, J = 7.4, 3H), 0.97 (t, J = 7.0, 3H). ^{13}C NMR (150 MHz, $CDCl_3$): 158.5, 156.2, 122.7, 116.5, 71.8, 60.8, 51.9, 35.2, 30.1, 29.9, 24.5, 19.0, 13.7, 12.1. MS (ESI): *m/z* 279 ($[M + H]^+$). HR-MS (ESI): $[M + H]^+$ = 279.1829, calc. for $C_{14}H_{23}N_4O_2$ 279.1821.

Compound III-15S. Compound **III-1**$_H$ (450 mg, 3.17 mmol) was dissolved in TFA (5 mL) and *o*-phthaldialdehyde **III-11** (210 mg, 1.57 mmol) was added. The mixture was

stirred and heated at 70 ˚C for 24 hours. The solvent was removed under reduced pressure. The crude solid was washed with MeOH (10 mL) and then centrifuged to obtain a brown solid. The crude brown solid was further purified by recrystallization from water H_2O twice to yield **5** as a yellow powder (136 mg, 0.35 mmol, 23%). M.p. 302 ˚C (dec.). IR (ATR, cm^{-1}): 3266w, 1699s, 1426m, 1346m, 1212m, 1094m. ^1H NMR (400 MHz, DMSO-d_6): 7.96 (s, 2H), 7.63 (s, 2H), 7.55-7.45 (m, 2H), 7.45-7.35 (m, 2H), 6.29 (s, 2H), 5.30-5.20 (m, 2H), 5.18 (d, J = 8.4 Hz, 1H), 4.77 (d, J = 8.4 Hz, 1H). ^{13}C NMR (100 MHz, DMSO-d_6): d 156.4, 156.3, 135.1, 129.5, 129.0, 67.9, 65.6, 63.5, 59.4, 59.3. MS (ESI): *m/z* 383 ($[M + H]^+$). HR-MS (ESI^+): *m/z* 383.1226, calc. for $C_{16}H_{15}N_8O_4$ 383.1216.

Compound III-17S. A mixture of **III-13** (300 mg, 1.6 mmol) and *o*-phthaldialdehyde **III-11** (110 mg, 0.8 mmol) in TFA (7 mL) was refluxed under nitrogen for 4 hours. The solvent was removed under reduced pressure and the crude product was recrystallized from methanol to yield **III-17S** (360 mg, 94%). M.p. > 300 ˚C (dec.). TLC ($CHCl_3$/MeOH 7:1) R_f 0.27. IR (KBr, cm^{-1}): 2947w, 1709s, 1466s, 1444s, 1385m, 1358m, 1246s, 1163w, 1101m. ^1H NMR (300 MHz, $CDCl_3$): 7.56-7.52 (m, 2H), 7.43-7.39 (m, 2H), 6.50 (s, 2H), 5.18 (d, J = 7.76, 2H), 5.14 (s, 2H), 4.82 (d, J = 7.76, 2H), 4.19-4.13 (m, 2H), 3.95-3.90 (m, 2H), 3.17-3.07 (m, 2H), 3.02-2.92 (m, 2H), 1.64-1.48 (m, 2H), 1.31-1.19 (m, 2H). ^{13}C NMR (75 MHz, DMSO-d_6): 154.8, 154.2, 134.9, 129.4, 129.3, 67.3, 65.2, 64.3, 63.5, 63.3, 59.7, 62.5, 38.4, 38.3, 23.2, 22.9, 22.8. HRMS (ESI^+) *m/z* calcd for $[C_{22}H_{23}N_8O_4 + H]^+$ 463.1842 found 463.1841.

Compound III-18S. A mixture of *o*-xylyleneglycoluril **III-14** (300 mg, 1.2 mmol) and *o*-phthaldialdehyde **III-11** (80 mg, 0.6 mmol) in TFA (7 mL) was refluxed under nitrogen

for 4 h. After cooling down white solid precipitated from the solution and was collected by filtration, washed with water and dried under vacuum (19 mg, 5%). The content of **III-18S** in the crude reaction mixture is >50% based on NMR integration. M.p. > 300 ˚C (dec.). IR (KBr, cm^{-1}): 2970w, 1728s, 1685s, 1498s, 1344w, 1321w, 1250m, 1176w, 1097w. ^{1}H NMR (300 MHz, DMSO-d_6): 7.51-7.49 (m, 2 H), 7.37-7.32 (m, 4H), 7.30-7.27 (m, 2H), 7.15-7.08 (m, 4H), 6.30 (s, 2H), 5.68 (d, J = 7.9, 1H), 5.47 (d, J = 7.6, 1H), 4.78 (d, J = 7.9, 1H), 4.70 (d, J = 15.5, 2H), 4.63 (d, J = 15.5, 2H), 4.46 (d, 1H), 4.43 (m, 4H). ^{13}C NMR (75 MHz, DMSO-d_6): 153.7, 153.6, 137.5, 137.3, 134.6, 129.6, 129.4, 129.2, 129.1, 127.7, 127.5, 68.4, 68.1, 64.7, 63.8, 61.1, 45.2, 45.1. HRMS (ESI^+) *m/z* calcd for $[C_{32}H_{27}N_8O_4 + H]^+$ 587.2155 found 587.2138.

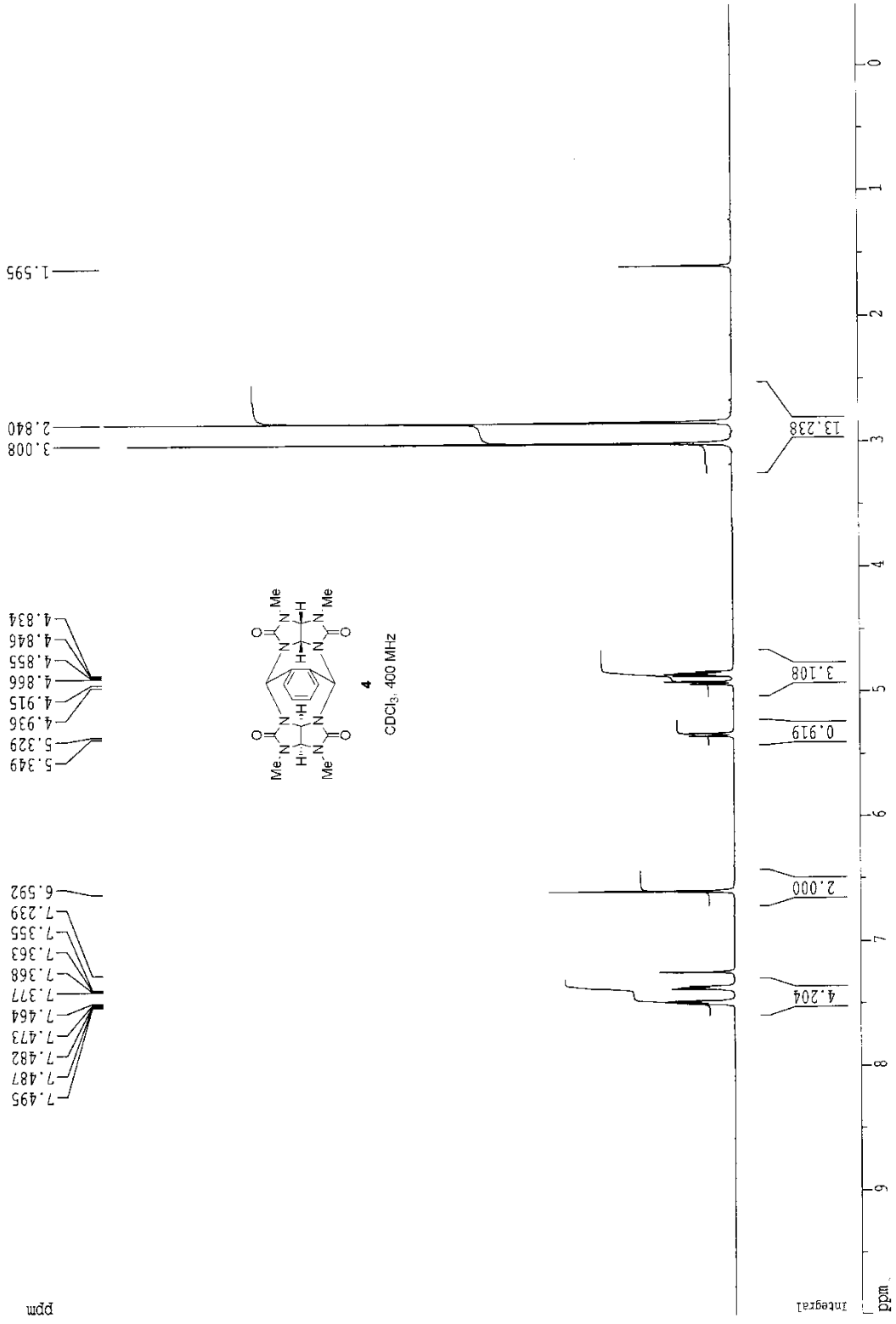

Figure III-S1. ^{1}H NMR spectra (400 MHz, $CDCl_3$) recorded for **III-16S**.

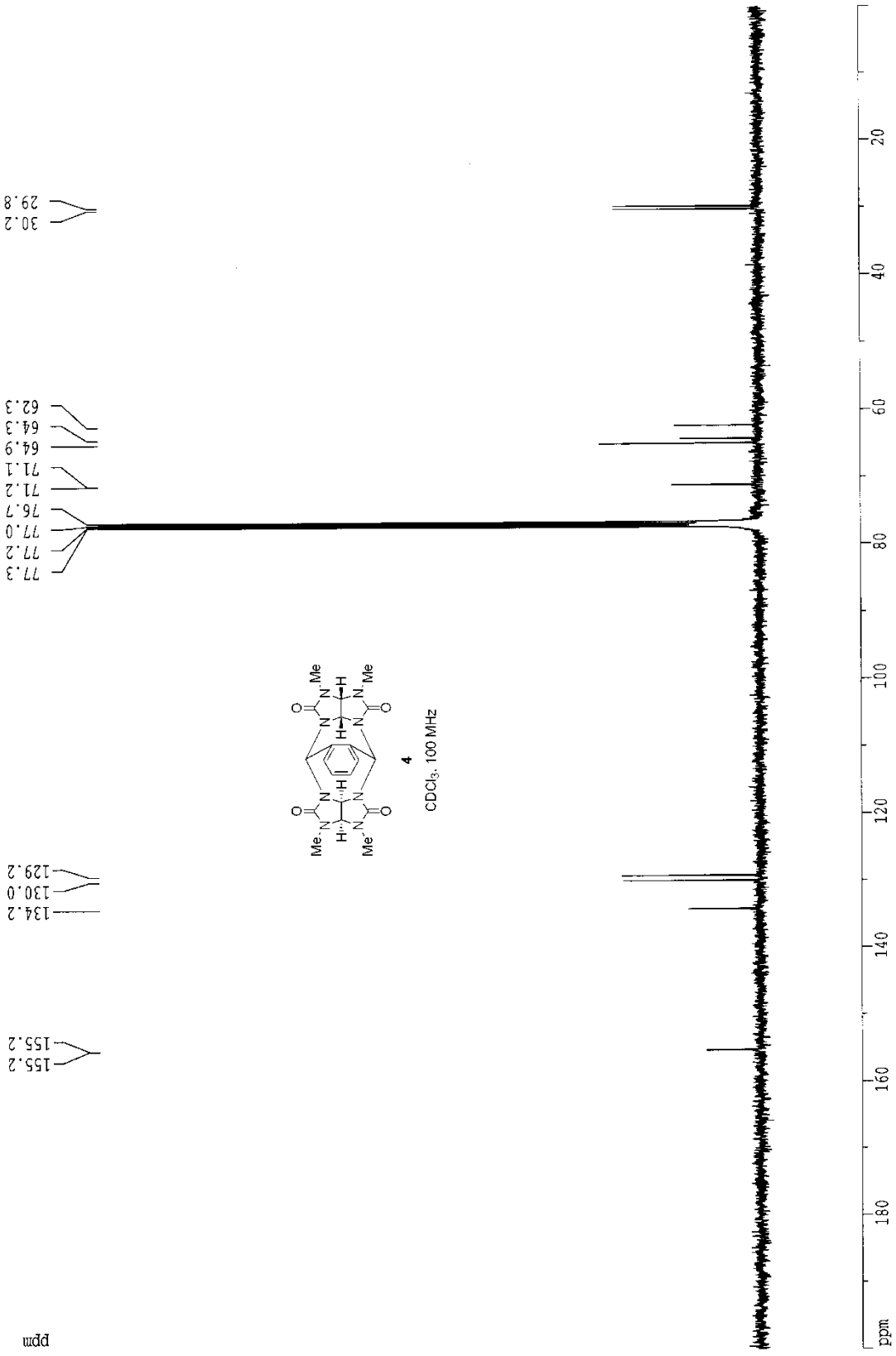

Figure III-S2. ^{13}C NMR spectra (100 MHz, $CDCl_3$) recorded for **III-16S**.

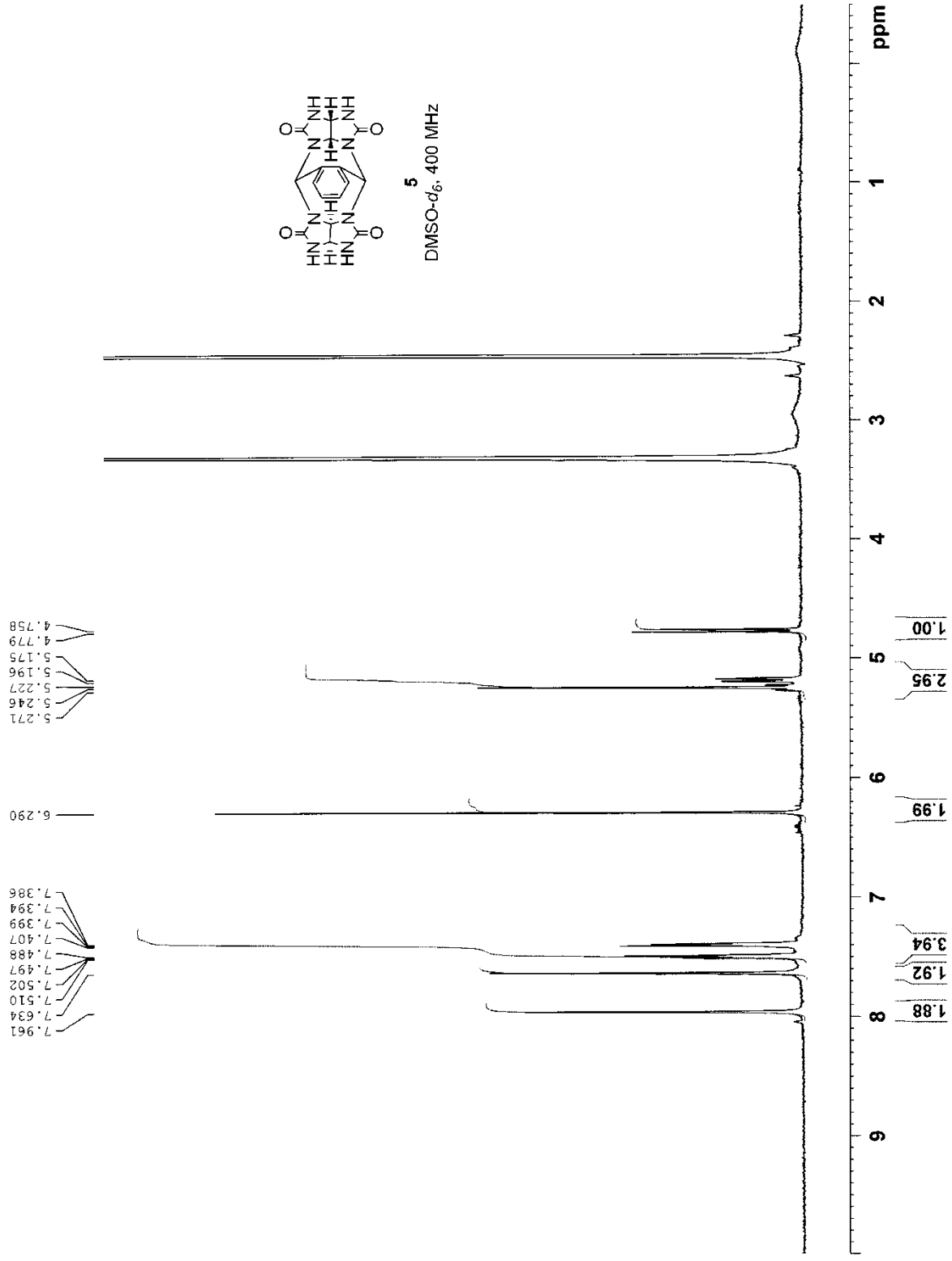

Figure III-S3. ^{1}H NMR spectra (400 MHz, DMSO-d_6) recorded for **III-15S**.

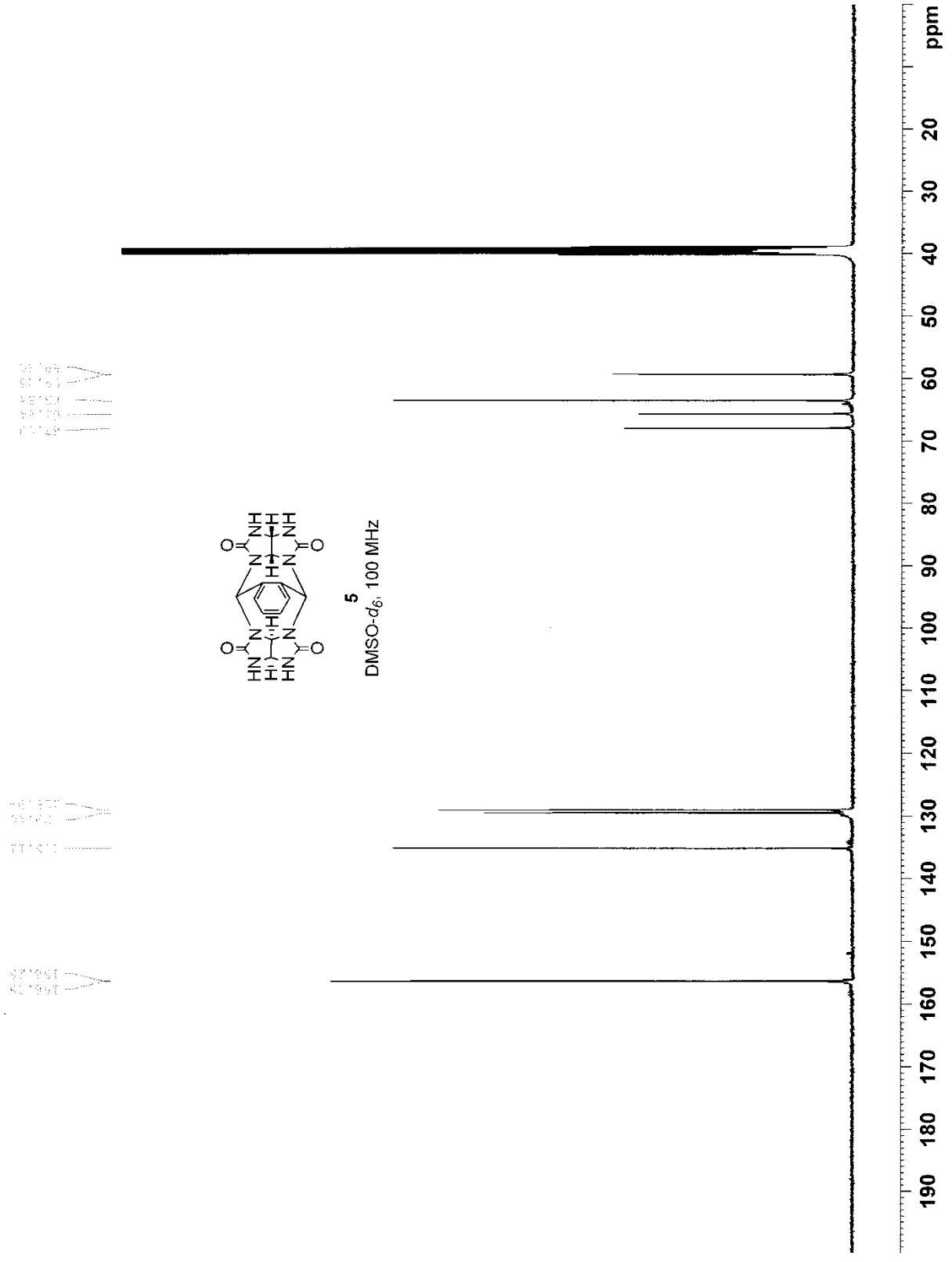

Figure III-S4. ^{13}C NMR spectra (100 MHz, DMSO-d_6) recorded for **III-15S**.

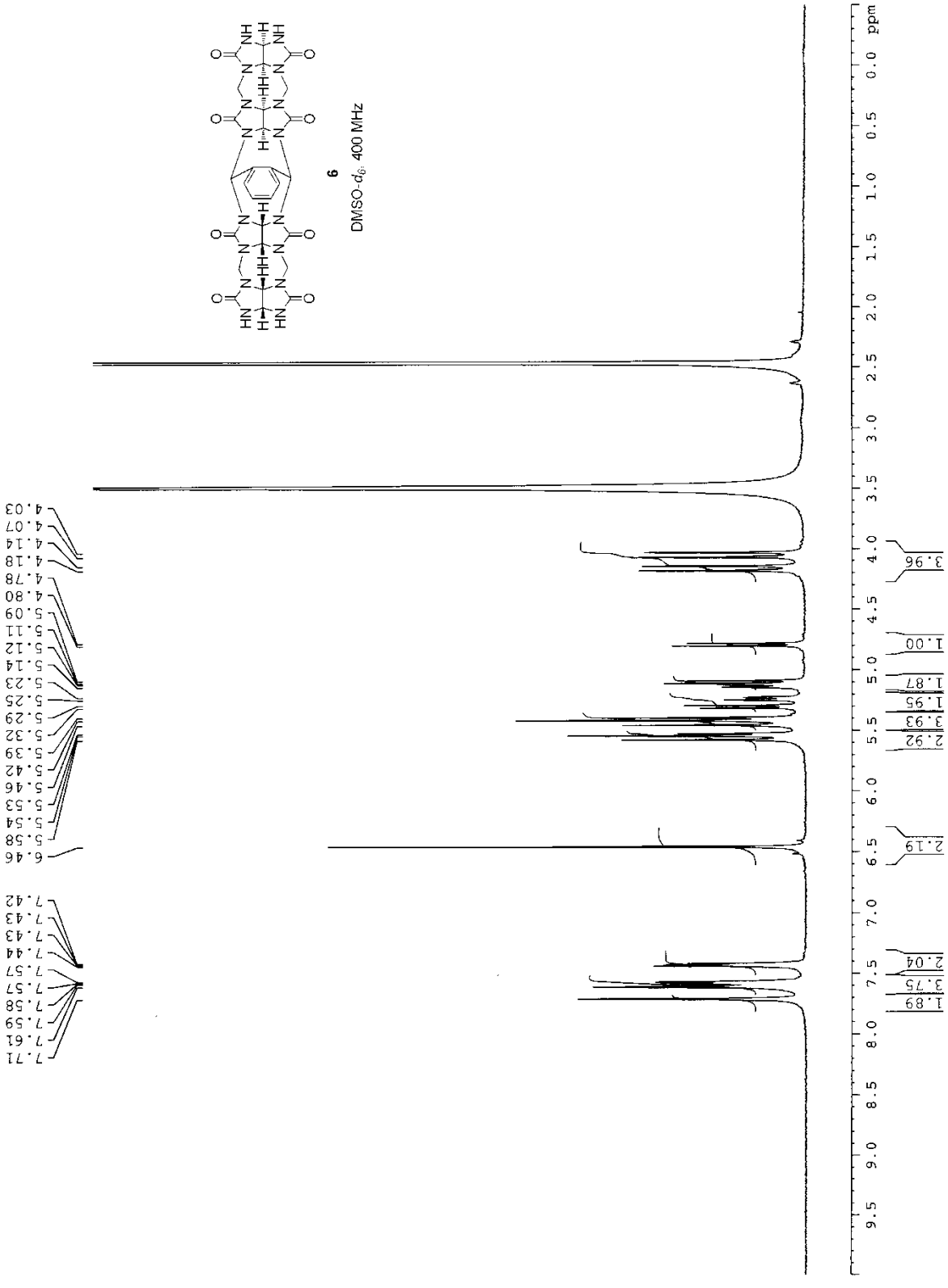

Figure III-S5. ^{1}H NMR spectrum (400 MHz, DMSO-d_6) recorded for **III-12S**.

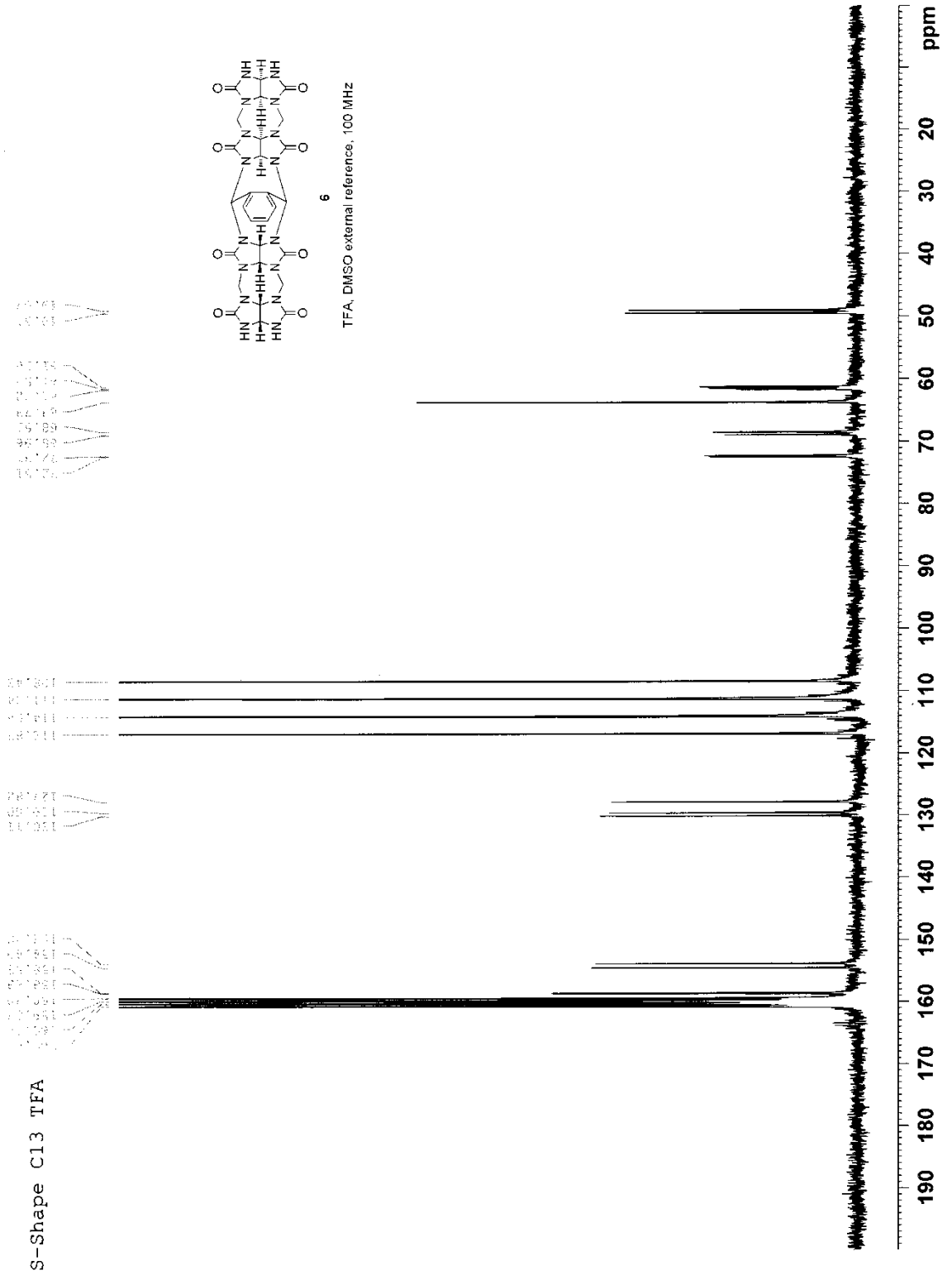

Figure III-S6. ^{13}C NMR spectrum (100 MHz, TFA, DMSO as external reference) recorded for **III-12S**.

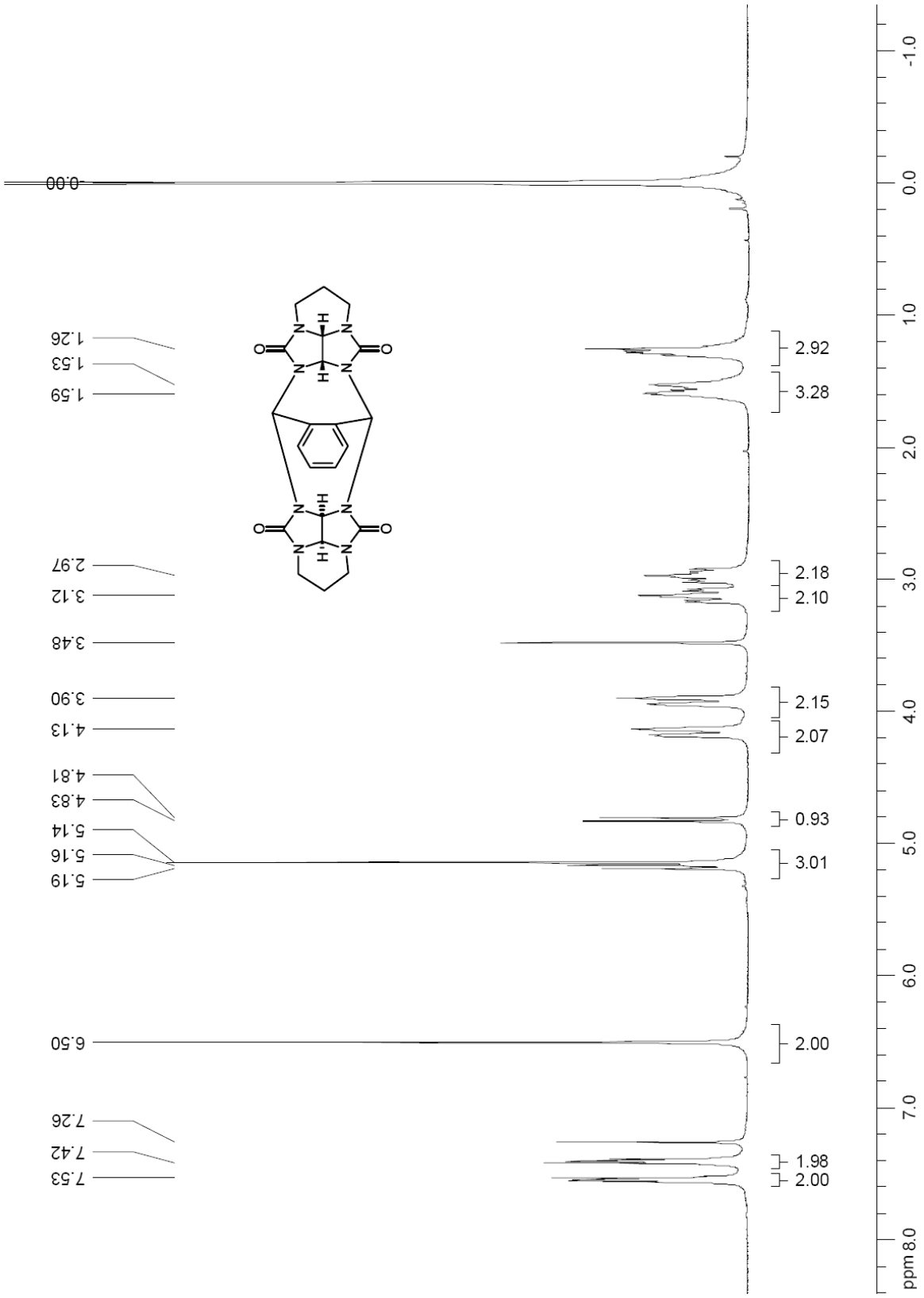

Figure III-S7. ^{1}H NMR spectrum (300 MHz, $CDCl_3$) recorded for **III-17S**.

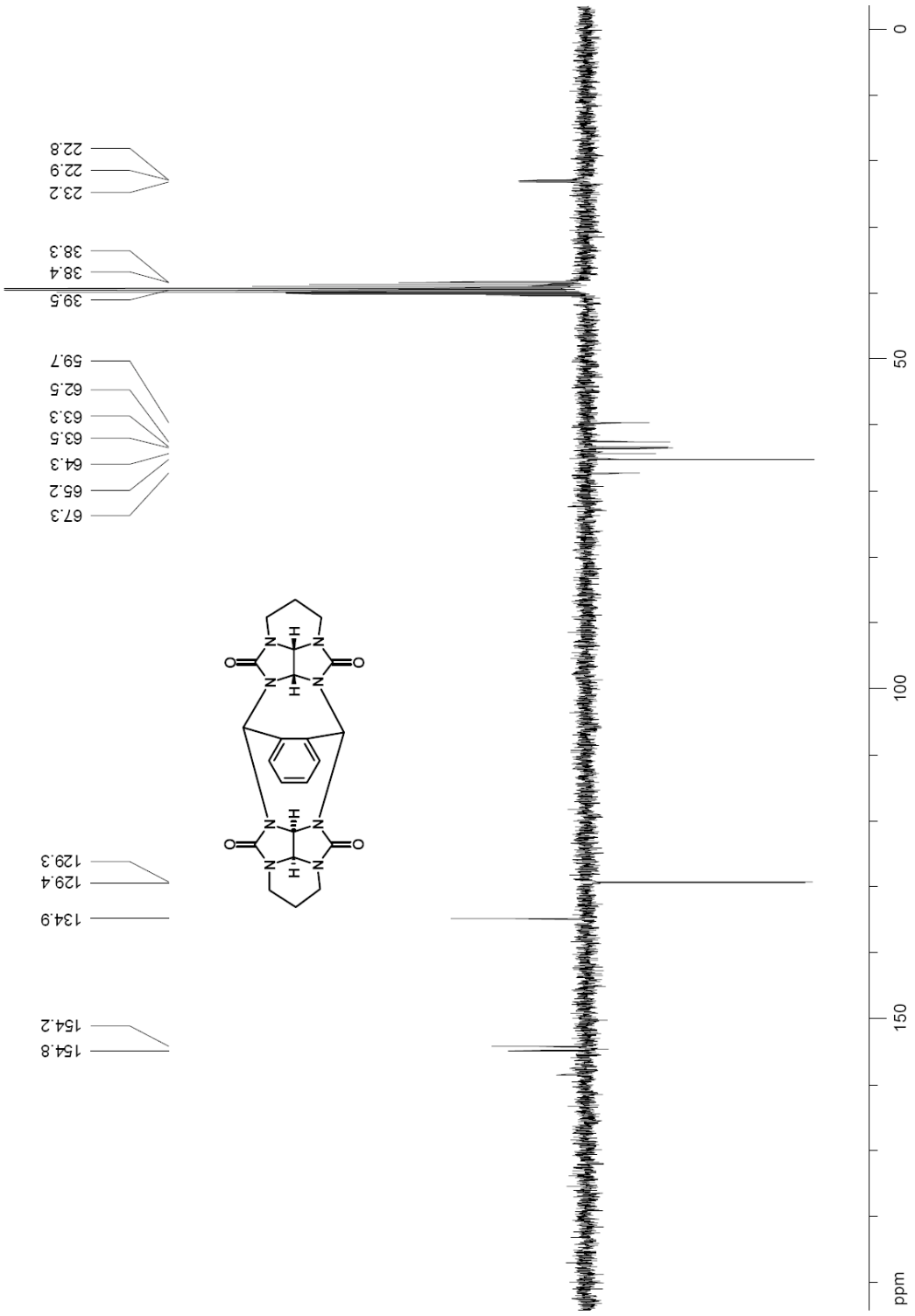

Figure III-S8. DEPT ^{13}C NMR spectrum (75 MHz, DMSO-d_6) recorded for **III-17S**.

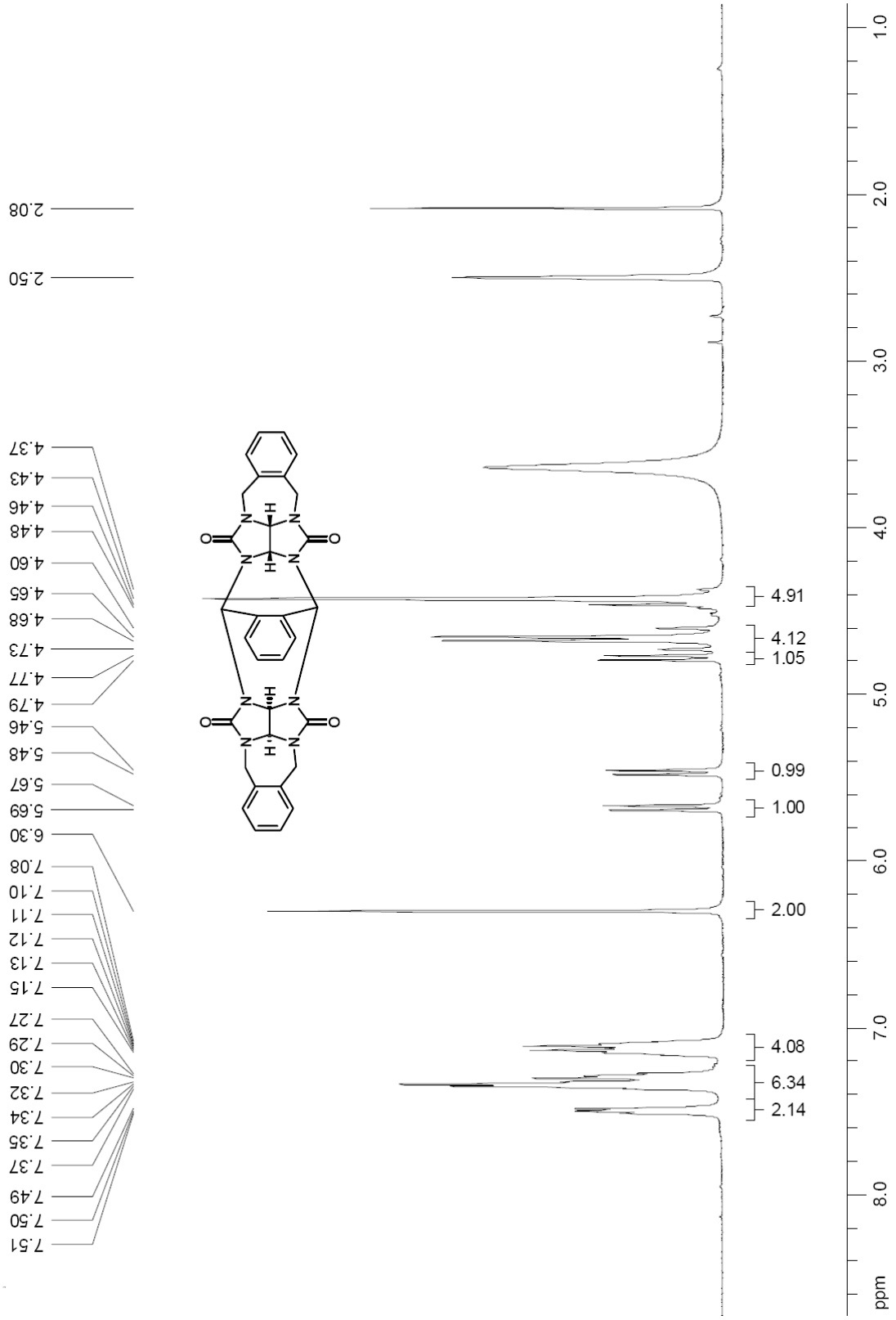

Figure III-S9. ^{1}H NMR spectrum (300 MHz, DMSO-d_6) recorded for **III-18S**.

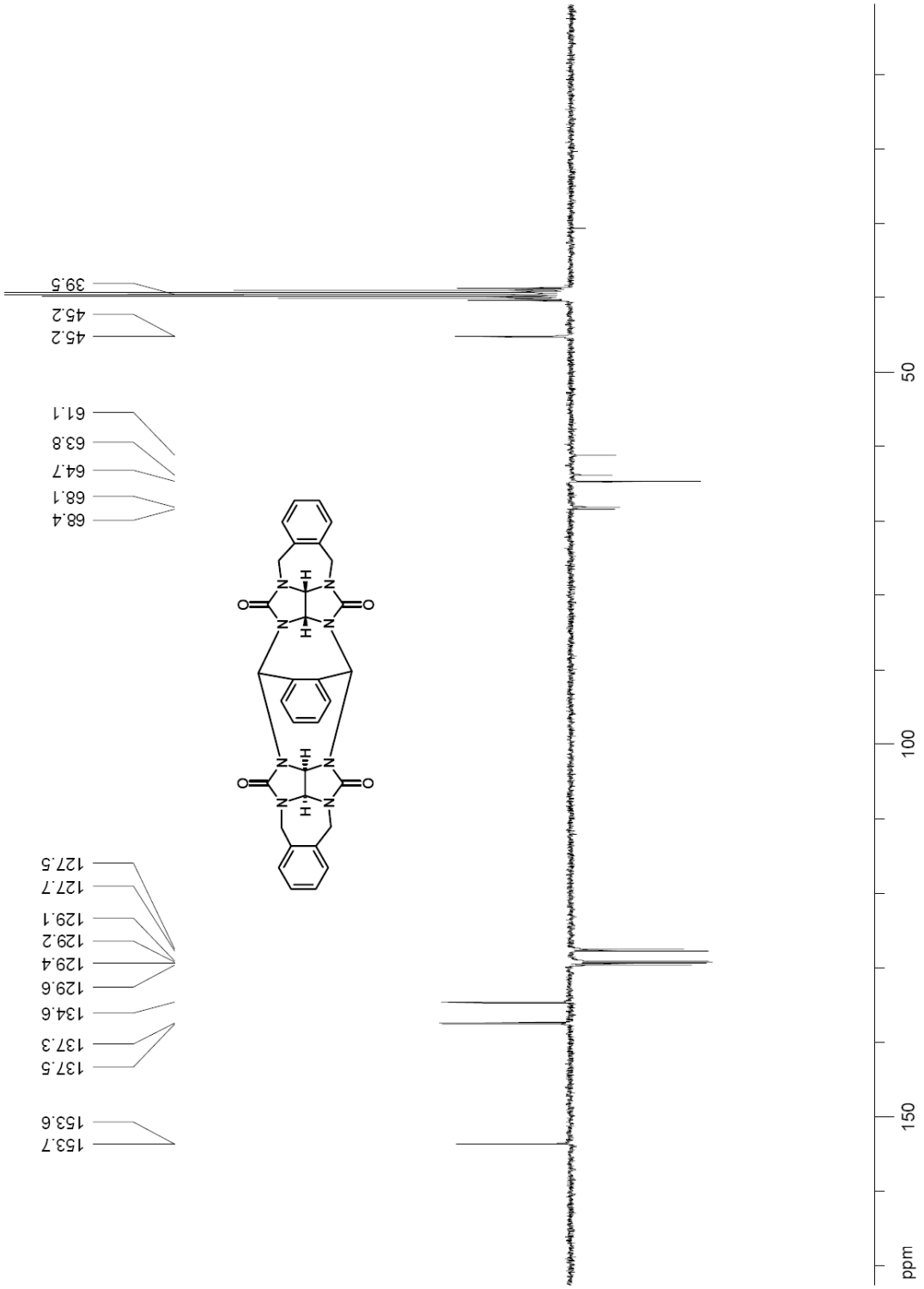

Figure III-S10. DEPT ^{13}C NMR spectrum (75 MHz, DMSO-d_6) recorded for **III-18S**.

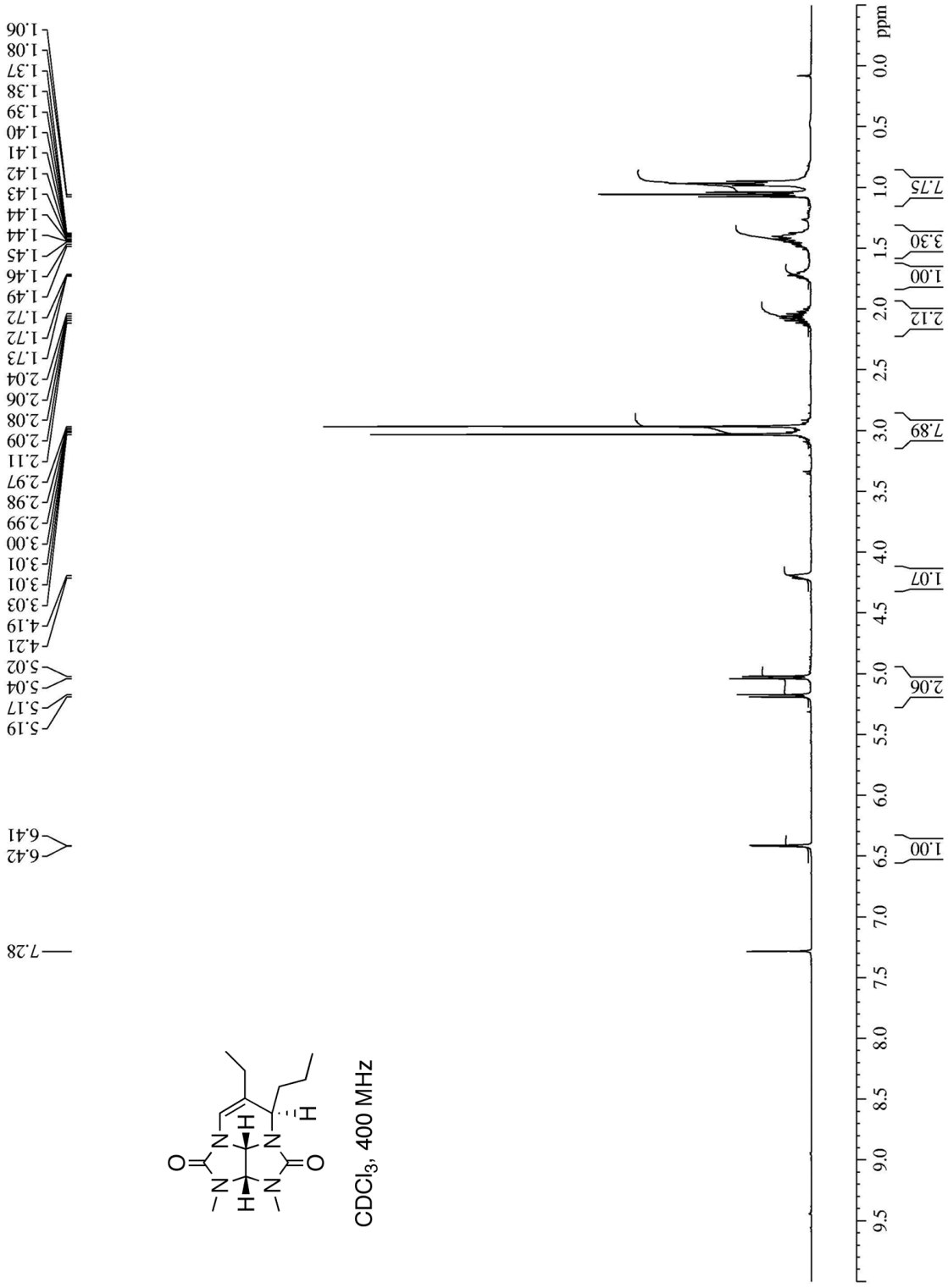

Figure III-S11. ^{1}H NMR spectrum (400 MHz, $CDCl_3$) recorded for **III-** (±)-**SP2**.

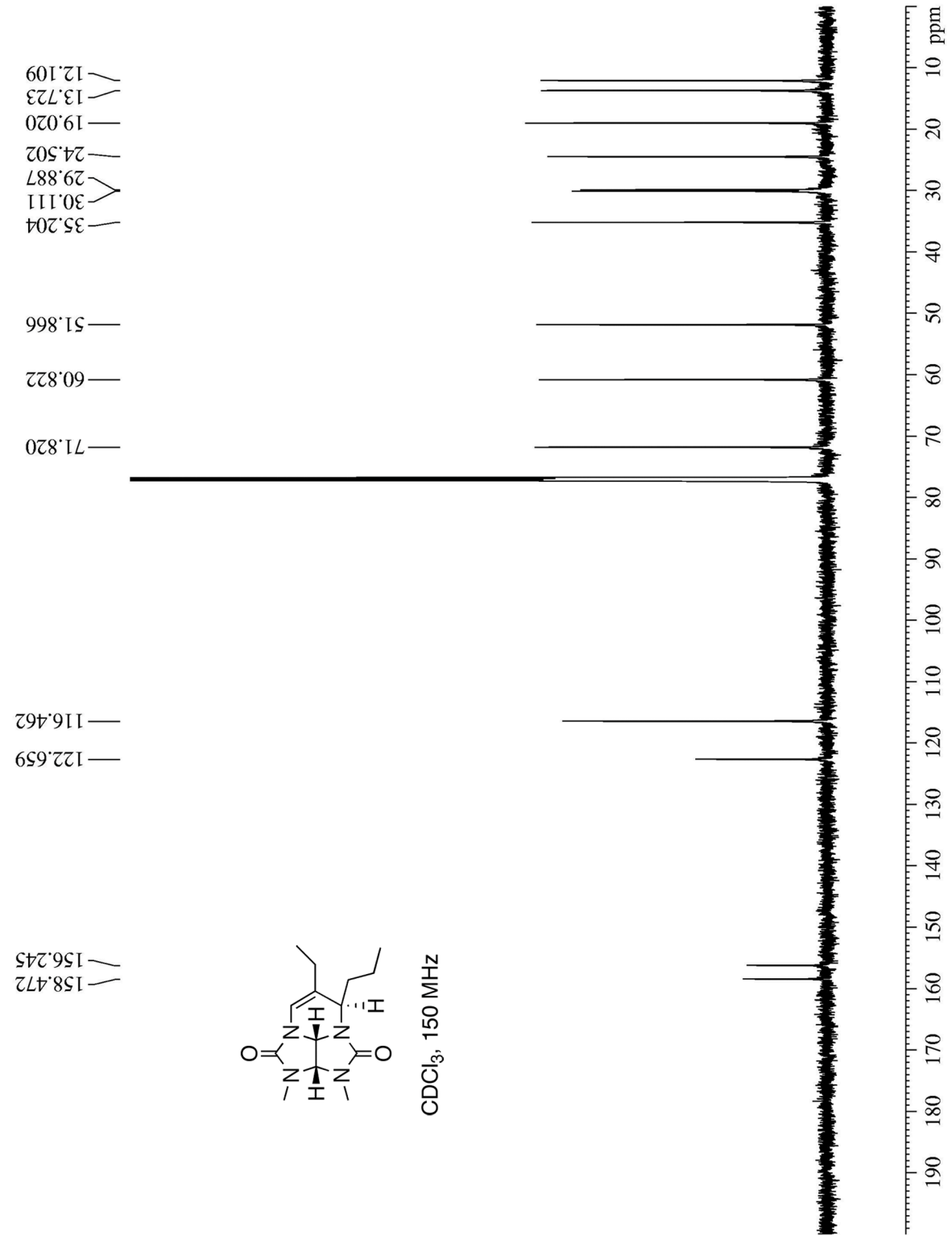

Figure III-S12. ^{13}C NMR spectrum (150 MHz, $CDCl_3$) recorded for **III-** (±)-**SP2**.

IV. Chapter 4: Summary and Future Work

4.1 Summary.

In this thesis, we discussed the work to develop new CB[*n*] type hosts and the mechanism investigation related to this study.

Supramolecular chemistry has been a very important research area. Molecular containers, especially cyclodextrin, have wide applications, both academically and in industry. Cucurbit[*n*]uril, a new generation of molecular container, is well-known for its tight and selective binding property. Yet, its poor solubility in water and difficulty to be functionalized are two significant issues which stop it from wider applications.

In order to circumvent these issues, a new type of acyclic CB[*n*] congeners has been developed (e.g. **II-5a**). It has a moderate solubility in water. It retains most of the recognition property of CB[*n*]. Due to its acyclic structure, it has fast association and dissociation kinetics. The importance of this new types of host is not limited to their own interesting property. This work also proves that it is possible to make new acyclic congener with interesting functional groups and very good recognition property. The synthesis of a new CB[*n*]-type receptors with high water solubility is a future research goal.

We also looked into the condensation reactions of glycoluril and aldehydes, which might lead to functionalized CB[*n*]. But we and other researchers as well can not make this reaction work. We then carried out very careful mechanistic investigations to explain

why aldehydes usually do not participate in CB[*n*] forming reactions. The reasons include 1) the formation of S-shape intermediate; 2) a reversible reaction with the equilibrium prefers to the reactant side; and 3) the formation of side products.

We believe our research expands the scope of CB[*n*] research area. By making new molecular container and studying the mechanism of CB[*n*] forming reactions, we are able to achieve more applications and develop more novel molecular containers.

4.2 Future Work.

As mentioned above, one of the issues for CB[*n*] application is its poor solubility in water. If we can prepare CB[*n*] type receptors that are highly soluble in water, applications, especially medicinal applications, will be possible. As shown in Scheme IV-1, this water soluble molecular container would be able to encapsulate hydrophobic drugs, and if the complex is water soluble, the drugs will be solubilized. This strategy is very important in drug delivery area. We believe it will be a very useful technology if we can make this water soluble host. Its solubility might be not limited to hydrophobic drugs. Other compounds with poor aqueous solubility, such as nanotubes and polymers, are also candidates to be solubilized by such a water soluble CB[*n*]-type molecular container.

Another possibility is to introduce fluorescence groups into the structure. Biological sensing is a research area that has attracts wide attention. Biological sensing enables researchers to 'see' where the agents are located. Fluorescence active groups are

most widely probes for biological sensing purposes. If we can attach a fluorescence active group to a CB[*n*] type receptor, we will be able to monitor the locations of the guest molecules (Scheme IV-2). There are a number of biological compounds that are able to form tight complex with CB[*n*], such as ammonium salts and some neutral compounds. This technology may be very useful to easily track the exact locations of the compounds in the cell or animal body and visualize their distribution. This technology utilizes non-covalent interactions, instead of forming covalent bonds, which means it poses less influence on the guest molecules and thus can reflect the real behavior of the guest molecules.

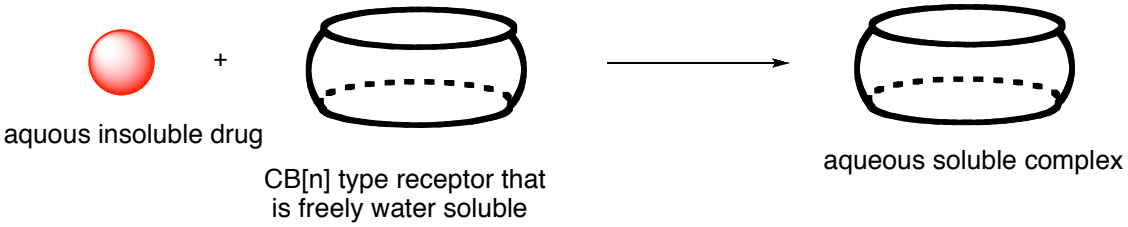

Scheme IV-1. Water soluble CB[*n*] molecular container and its capability to solubilize hydrophobic drugs.

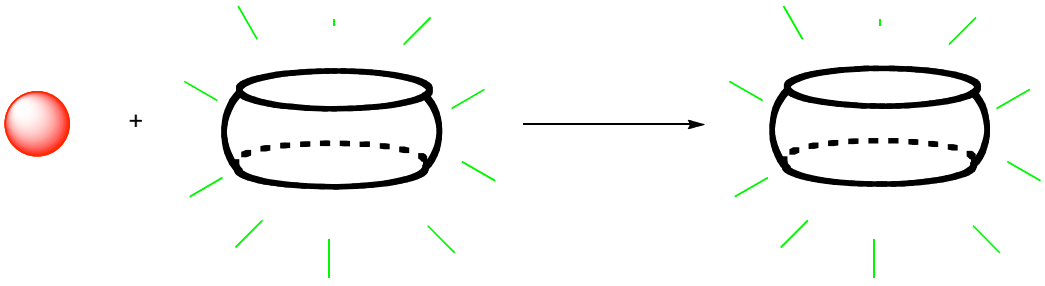

Scheme IV-2. Fluorescence active CB[*n*] molecular container which acts as a biological sensor.

List of References:

(1) Pedersen, C. J. *J. Am. Chem. Soc.* **1967**, *89*, 7017-7036.

(2) Villiers, A. *Compt. Rend.* **1891**, *112*, 536-538.

(3) Freudenberg, K.; Cramer, F. *Z. Naturforsch. B* **1948**, *3*, 464-467.

(4) French, D. *Adv. Carbohydr. Chem* **1957**, *12*, 189-260.

(5) Cramer, F. *Einschlussverbindungen (Inclusion Compounds)* Springer-Verlag: Berlin, 1954.

(6) Szejtli, J.; Sebestyen, G. *Starch/Starke* **1979**, *31*, 385-389.

(7) Müller, B. W.; Brauns, U. *Int. J. Pharm.* **1985**, *26*, 77-88.

(8) Uekama, K.; Fujinaga, T.; Hirayama, F.; Otagiri, M.; Kurono, Y.; Ikeda, K. *J. Pharm. Pharmacol.* **1982**, *34*, 627-630.

(9) Higuchi, T.; Connors, K. *Adv. Anal. Chem. Instrum.* **1965**, *4*, 117-212.

(10) Shiotani, K.; Uehata, K.; Hirayama, F.; Uekama, K. *Chem. Pharm. Bull.* **1994**, *42*, 2332-2337.

(11) Zia, V.; Rajewski, R. A.; Bornancini, E. R.; Luna, E. A.; Stella, V. J. *J. Pharm. Sci.* **1997**, *86*, 220-222.

(12) Thompson, D. O. *CRC Crit. Rev. Ther. Drug Carrier Syst.* **1997**, 1-67.

(13) Freeman, W. A.; Mock, W. L.; Shih, N.-Y. *J. Am. Chem. Soc.* **1981**, *103*, 7367 – 7368.

(14) Behrend, R.; Meyer, E.; Rusche, F. *Justus Liebigs Ann. Chem.* **1905**, *339*, 1-37.

(15) Kim, J.; Jung, I.-S.; Kim, S.-Y.; Lee, E.; Kang, J.-K.; Sakamoto, S.; Yamaguchi, K.; Kim, K. *J. Am. Chem. Soc.* **2000**, 540-541.

(16) Day, A.; Arnold, I. A. P.; Blanch, R. J.; Snushall, B. *J. Org. Chem.* **2001**, *66*, 8094 – 8100.

(17) Isaacs, L.; Park, S.-K.; Liu, S.; Ko, Y. H.; Selvapalam, N.; Kim, Y.; Kim, H.; Zavalij, P. Y.; Kim, G.-H.; Lee, H.-S.; Kim, K. *J. Am. Chem. Soc.* **2005**, *127*, 18000-18001.

(18) Liu, S.; Zavalij, P. Y.; Isaacs, L. *J. Am. Chem. Soc.* **2005**, *127*, 16798-16799.

(19) Day, A. I.; Blanch, R. J.; Arnold, A. P.; Lorenzo, S.; Lewis, G.; Dance, R. I. *Angew. Chem. Int. Ed.* **2002**, *41*, 275-277.

(20) Huang, W.-H.; Liu, S.; Zavalij, P. Y.; Isaacs, L. *J. Am. Chem. Soc.* **2006**, *128*, 14744-14745.

(21) Huang, W.-H.; Zavalij, P. Y.; Isaacs, L. *Angew. Chem. Int. Ed.* **2007**, *46*, 7425-7427.

(22) Huang, W.-H.; Zavalij, P. Y.; Isaacs, L. *Org. Lett.* **2008**, *10*, 2577-2580.

(23) Flinn, A.; Hough, G. C.; Stoddart, J. F.; Williams, D. J. *Angew. Chem. Int. Ed.* **1992**, *31*, 1475-1477.

(24) Jon, S. Y.; Selvapalam, N.; Oh, D. H.; Kang, J.-K.; Kim, S.-Y.; Jeon, Y. J.; Lee, J. W.; Kim, K. *J. Am. Chem. Soc.* **2003**, *125*, 10186-10187.

(25) Lee H.-K.; Park, K. M. J., Y. J.; Kim, D.; Oh, D. H.; Kim, H. S.; Park, C. K.; Kim, K. *J. Am. Chem. Soc.* **2005**, *127*, 5006-5007.

(26) Hwang, I.; Baek, K.; Jung, M.; Kim, Y.; Park, K. M.; Lee, D.-W.; Selvapalam, N.; Kim, K. *J. Am. Chem. Soc.* **2007**, *129*, 4170-4171.

(27) Jeon, Y. J.; Kim, H.; Jon, S.; Selvapalam, N.; Oh, D. H.; Seo, I.; Park, C.-S.; Jung, R.; Koh, D.-S.; Kim, K. *J. Am. Chem. Soc.* **2004**, *126*, 15944-15945.

(28) Lagona, J.; Fettinger, J. C.; Isaacs, L. *Org. Lett.* **2003**, *5*, 3745-3747.

(29) Miyahara, Y.; Goto, K.; Oka, M.; Inazu, T. *Angew. Chem. Int. Ed.* **2004**, *43*, 5019-5022.

(30) Burnett, C. A.; Witt, D.; Fettinger, J. C.; Isaacs, L. *J. Org. Chem.* **2003**, *68*, 6184-6191.

(31) Stancl, M.; Hodan, M.; Sindelar, V. *Org. Lett.* **2009**, *11*, 4184-4187.

(32) Mock, W. L.; Pierpont, J. *J. Chem. Soc. Chem. Commun.* **1990**, *35*, 1509-1511.

(33) Kim, H.-J.; Jeon, W. S.; Ko, Y. H.; Kim, K. *Proc. Natl. Acad. Sci. USA* **2002**, *99*, 5007-5011.

(34) Jeon, W. S.; Ziganshina, A. Y.; Lee, J. W.; Ko, Y. H.; Kang, J. K.; Lee, C.; Kim, K. *Angew. Chem. Int. Ed.* **2003**, *42*, 4097-4100.

(35) Mock, W. L.; Irra, T. A.; Wepsiec, J. P.; Manimaran, T. L. *J. Org. Chem.* **1983**, *48*, 3619-3620.

(36) Jon, S. Y.; Ko, Y. H.; Park, S. H.; Kim, H.-J.; Kim, K. *Chem. Commun.* **2001**, *46*, 1938-1939.

(37) Saleh, N.; Koner, A. L.; Nau, W. M. *Angew. Chem. Int. Ed.* **2008**, *47*, 5398-5401.

(38) Kim, S. K.; Park, K. M.; Singha, K.; Kim, J.; Ahn, Y.; Kim, K.; Kim, W. J. *Chem. Commun.* **2001**, *46*, 692-694.

(39) Uzunova, V. D.; Cullinane, C.; Brix, K.; Nau, W. M.; Day, A. I. *Org. Biomol. Chem.* **2010**, *8*, 2037-2042.

(40) Hettiarachchi, G.; Nguyen, D.; Wu, J.; Lucas, D.; Ma, D.; Isaacs, L.; Briken, V. *PLoS One* **2001**, *5*, e10514.

(41) Lagona, J.; Mukhopadhyay, P.; Chakrabarti, S.; Isaacs, L. *Angew. Chem., Int. Ed.* **2005**, *44*, 4844-4870.

(42) Lee, J. W.; Samal, S.; Selvapalam, N.; Kim, H.-J.; Kim, K. *Acc. Chem. Res.* **2003**, *36*, 621-630.

(43) Mock, W. L.; Irra, T. A.; Wepsiec, J. P.; Adhya, M. *J. Org. Chem.* **1989**, *54*, 5302-5308.

(44) Mock, W. L.; Shih, N.-Y. *J. Am. Chem. Soc.* **1988**, *110*, 4706-4710.

(45) Mock, W. L.; Shih, N.-Y. *J. Org. Chem.* **1986**, *51*, 4440-4446.

(46) Liu, S.; Ruspic, C.; Mukhopadhyay, P.; Chakrabarti, S.; Zavalij, P. Y.; Isaacs, L. *J. Am. Chem. Soc.* **2005**, *127*, 15959-15967.

(47) Rekharsky, M. V.; Mori, T. Y., C.; Ko, Y. H.; Selvapalam, N.; Kim, H.; Sobransingh, D.; Kaifer, A. E.; Liu, S.; Isaacs, L.; Chen, W.; Moghaddam, S.; Gilson, M. K.; Kim, K.; Inoue, Y. *Proc. Natl. Acad. Sci. USA* **2007**, *104*, 20737-20742.

(48) Jeon, W. S.; Moon, K.; Park, S. H.; Chun, H.; Ko, Y. H.; Lee, J. Y.; Lee, E. S.; Samal, S.; Selvapalam, N.; Rekharsky, M. V.; Sindelar, V.; Sobransingh, D.; Inoue, Y.; Kaifer, A. E.; Kim, K. *J. Am. Chem. Soc.* **2005**, *127*, 12984-12989.

(49) Ko, Y. H.; Kim, E.; Hwang, I.; Kim, K. *Chem. Commun.* **2007**, 1305-1315.

(50) Hennig, A.; Bakirci, H.; Nau, W. M. *Nat. Methods* **2007**, *4*, 629-632.

(51) Praetorius, A.; Bailey, D. M.; Schwarzlose, T.; Nau, W. M. *Org. Lett.* **2008**, *10*, 4089-4092.

(52) An, Q.; Li, G.; Tao, C.; Li, Y.; Wu, Y.; Zhang, W. *Chem. Commun.* **2008**, 1989-1991.

(53) Angelos, S.; Khashab, N. M.; Yang, Y.-W.; Trabolsi, A.; Khatib, H. A.; Stoddart, J. F.; Zink, J. I. *J. Am. Chem. Soc.* **2009**, *131*, 12912-12914.

(54) Angelos, S.; Yang, Y.-W.; Patel, K.; Stoddart, J. F.; Zink, J. I. *Angew. Chem. Int. Ed.* **2008**, *47*, 2222-2226.

(55) Bali, M. S.; Buck, D. P.; Coe, A. J.; Day, A. I.; Collins, J. G. *Dalton Trans.* **2006**, 5337-5344.

(56) Baumes, L. A.; Sogo, M. B.; Montes-Navajas, P.; Corma, A.; Garcia, H. *Tetrahedron Lett.* **2009**, *50*, 7001-7004.

(57) Bush, M. E.; Bouley, N. D.; Urbach, A. R. *J. Am. Chem. Soc.* **2005**, *127*, 14511-14517.

(58) Chakrabarti, S.; Mukhopadhyay, P.; Lin, S.; Isaacs, L. *Org. Lett.* **2007**, *9*, 2349-2352.

(59) Hwang, I.; Ziganshina, A. Y.; Ko, Y.-H.; Yun, G.; Kim, K. *Chem. Commun.* **2009**, *45*, 416-418.

(60) Kemp, S.; Wheate, N. J.; Pisani, M. J.; Aldrich-Wright, J. R. *J. Med. Chem.* **2008**, *51*, 2787-2794.

(61) Lee, J. W.; Hwang, I.; Jeon, W. S.; Ko, Y. H.; Sakamoto, S.; Yamaguchi, K.; Kim, K. *Chem. Asian J.* **2008**, *3*, 1277-1283.

(62) Montes-Navajas, P.; Baumes, L. A.; Corma, A.; Garcia, H. *Tetrahedron Lett.* **2009**, *50*, 2301-2304.

(63) Nagarajan, E. R.; Oh, D. H.; Selvapalam, N.; Ko, Y. H.; Park, K. M.; Kim, K. *Tetrahedron Lett.* **2006**, *47*, 2073-2075.

(64) Park, K. M.; Suh, K.; Jung, H.; Lee, D.-W.; Ahn, Y.; Kim, J.; Baek, K.; Kim, K. *Chem. Commun.* **2009**, *45*, 71-73.

(65) Sindelar, V.; Silvi, S.; Kaifer, A. E. *Chem. Commun.* **2006**, *42*, 2185-2187.

(66) Sindelar, V.; Silvi, S.; Parker, S. E.; Sobransingh, D.; Kaifer, A. E. *Adv. Funct. Mater.* **2007**, *17*, 694-701.

(67) Sun, S.; Zhang, R.; Andersson, S.; Pan, J.; Zou, D.; Akermark, B.; Sun, L. *J. Phys. Chem. B* **2007**, *111*, 13357-13363.

(68) Tuncel, D.; Oezsar, O.; Tiftik, H. B.; Salih, B. *Chem. Commun.* **2007**, *43*, 1369-1371.

(69) Wu, J.; Isaacs, L. *Chem. Eur. J.* **2009**, *15*, 11675-11680.

(70) Zhao, Y.; Buck, D. P.; Morris, D. L.; Pourgholami, M. H.; Day, A. I.; Collins, J. G. *Org. Biomol. Chem.* **2008**, *6*, 4509-4515.

(71) Rauwald, U.; Scherman, O. A. *Angew. Chem. Int. Ed.* **2008**, *47*, 3950-3953.

(72) Ghosh, S.; Isaacs, L. *J. Am. Chem. Soc.* **2010**, *132*, 4445-4454.

(73) Lagona, J.; Fettinger, J. C.; Isaacs, L. *J. Org. Chem.* **2005**, *70*, 10381-10392.

(74) Mock, W. L.; Shih, N.-Y. *J. Am. Chem. Soc.* **1989**, *111*, 2697-2699.

(75) Marquez, C.; Nau, W. M. *Angew. Chem., Int. Ed.* **2001**, *40*, 3155-3160.

(76) Pluth, M. D.; Raymond, K. N. *Chem. Soc. Rev.* **2007**, *36*, 161-171.

(77) Quan, M. L. C.; Cram, D. J. *J. Am. Chem. Soc.* **1991**, *113*, 2754-2755.

(78) Marquez, C.; Hudgins, R. R.; Nau, W. M. *J. Am. Chem. Soc.* **2004**, *126*, 5806-5816.

(79) Wagner, B. D.; Boland, P. G.; Lagona, J.; Isaacs, L. *J. Phys. Chem. B* **2005**, *109*, 7686-7691.

(80) Huang, W.-H.; Zavalij, P. Y.; Isaacs, L. *Org. Lett.* **2009**, *11*, 3918-3921.

(81) Huang, W.-H.; Zavalij, P. Y.; Isaacs, L. *J. Am. Chem. Soc.* **2008**, *130*, 8446-8454.

(82) Witt, D.; Lagona, J.; Damkaci, F.; Fettinger, J. C.; Isaacs, L. *Org. Lett.* **2000**, *2*, 755-758.

(83) Wu, A.; Isaacs, L. *J. Am. Chem. Soc.* **2003**, *125*, 4831-4835.

(84) Hof, F.; Craig, S. L.; Nuckolls, C.; Rebek, J., Jr. *Angew. Chem., Int. Ed.* **2002**, *41*, 1488-1508.

(85) Stancl, M.; Hodan, M.; Sindelar, V. *Org. Lett.* **2009**, *11*, 4184-4187.

(86) Jansen, K.; Wego, A.; Buschmann, H.-J.; Schollmeyer, E.; Dopp, D. *Des. Monomers Polymers* **2003**, *6*, 43-55.

(87) Niele, F. G. M.; Nolte, R. J. M. *J. Am. Chem. Soc.* **1988**, *110*, 172-177.

(88) Zhao, Y.; Xue, S.; Zhu, Q.; Tao, Z.; Zhang, J.; Wei, Z.; Long, L.; Hu, M.; Xiao, H.; Day, A. I. *Chin. Sci. Bull.* **2004**, *49*, 1111-1116.

(89) Ma, D.; Gargulakova, Z.; Zavalij, P. Y.; Sindelar, V.; Isaacs, L. *J. Org. Chem.* **2010**, *75*, 2934–2941.

(90) Day, A. I.; Arnold, A. P.; Blanch, R. J. *Molecules* **2003**, *8*, 74-84.

(91) Sijbesma, R. P.; Kentgens, A. P. M.; Lutz, E. T. G.; van der Maas, J. H.; Nolte, R. J. M. *J. Am. Chem. Soc.* **1993**, *115*, 8999-9005.

(92) Sijbesma, R. P.; Wijmenga, S. S.; Nolte, R. J. M. *J. Am. Chem. Soc.* **1992**, *114*, 9807-9813.

(93) Rowan, A. E.; Elemans, J. A. A. W.; Nolte, R. J. M. *Acc. Chem. Res.* **1999**, *32*, 995-1006.

(94) Connors, K. A. *Binding Constants*; John Wiley & Sons: New York, 1987.

(95) Wiskur, S. L.; Ait-Haddou, H.; Lavigne, J. J.; Anslyn, E. V. *Acc. Chem. Res.* **2001**, *34*, 963-972.

(96) Anslyn, E. V. *J. Org. Chem.* **2007**, *72*, 687-699.

(97) Ko, Y. H.; Kim, H.; Kim, Y.; Kim, K. *Angew. Chem., Int. Ed.* **2008**, *47*, 4106-4109.

(98) Buschmann, H. J.; Cleve, E.; Schollmeyer, E. *Inorg. Chim. Acta* **1992**, *193*, 93-97.

(99) Jeon, Y.-M.; Kim, J.; Whang, D.; Kim, K. *J. Am. Chem. Soc.* **1996**, *118*, 9790-9791.

(100) Ong, W.; Kaifer, A. E. *J. Org. Chem.* **2004**, *69*, 1383-1385.

(101) Haeg, M. E.; Whitlock, B. J.; Whitlock, H. W. *J. Am. Chem. Soc.* **1989**, *111*, 692-696.

(102) Couri, M. R. C.; Vieira de Almeida, M.; Fontes, A. P. S.; Chaves, J. D. A. S.; Cesar, E. T.; Alves, R. J.; Pereira-Maia, E. C.; Garnier-Suillerot, A. *Eur. J. Inorg. Chem.* **2006**, *45*, 1868-1874.

(103) Kim, K.; Selvapalam, N.; Ko, Y. H.; Park, K. M.; Kim, D.; Kim, J. *Chem. Soc. Rev.* **2007**, *36*, 267-279.

(104) Sasmal, S.; Sinha, M. K.; Keinan, E. *Org. Lett.* **2004**, *6*, 1225-1228.

(105) Isobe, H.; Sato, S.; Nakamura, E. *Org. Lett.* **2002**, *4*, 1287-1289.

(106) Khan, M. S. A.; Heger, D.; Necas, M.; Sindelar, V. *J. Phys. Chem. B* **2009**, *113*, 11054-11057.

(107) Jon, S. Y.; Selvapalam, N.; Oh, D. H.; Kang, J.-K.; Kim, S.-Y.; Jeon, Y. J.; Lee, J. W.; Kim, K. *J. Am. Chem. Soc.* **2003**, *125*, 10186-10187.

(108) Chakraborty, A.; Wu, A.; Witt, D.; Lagona, J.; Fettinger, J. C.; Isaacs, L. *J. Am. Chem. Soc.* **2002**, *124*, 8297-8306.

(109) Liu, S.; Kim, K.; Isaacs, L. *J. Org. Chem.* **2007**, *72*, 6840-6847.

(110) Nematollah, J.; Ketcham, R. *J. Org. Chem.* **1963**, *28*, 2378-2380.

(111) Kravchenko, A. N.; Sigachev, A. S.; Maksareva, E. Y.; Gazieva, G. A.; Trunova, N. S.; Lozhkin, B. V.; Pivina, T. S.; Il′in, M. M.; Lyssenko, K. A.; Nelyubina, Y. V.; Davankov, V. A.; Lebedev, O. V.; Makhova, N. N.; Tartakovsky, V. A. *Russ. Chem. Bull., Int. Ed.* **2001**, *54*, 691-704.

(112) Stancl, M.; Necas, M.; Taraba, J.; Sindelar, V. *J. Org. Chem.* **2008**, *73*, 4671-4675.

(113) Dunnavant, W. R.; James, F. L. *J. Am. Chem. Soc.* **1956**, *78*, 2740-2743.

(114) Zuliani, V.; Carmi, C.; Rivara, M.; Fantini, M.; Lodola, A.; Vacondio, F.; Bordi, F.; Plazzi, P. V.; Cavazzoni, A.; Galetti, M.; Alfieri, R. R.; Petronini, P. G.; Mor, M. *Eur. J. Med. Chem.* **2009**, *44*, 3471-3479.

(115) Anet, F. A. L.; Basus, V. J. *J. Am. Chem. Soc.* **1973**, *95*, 4424-4426.

(116) Dorofeeva, O. V.; Mastryukov, V. S.; Allinger, N. L.; Almenningen, A. *J. Phys. Chem.* **1985**, *89*, 252-257.

(117) Pakes, P. W.; Rounds, T. C.; Strauss, H. L. *J. Phys. Chem* **1981**, *85*, 2469-2475.

(118) Calucci, L.; Zimmermann, H.; Poupko, R.; Luz, Z. *J. Phys. Chem.* **1995**, *99*, 14942-14948.

(119) Rowland, R. S.; Taylor, R. *J. Phys. Chem.* **1996**, *100*, 7384-7391.